UNCERTAINTY ANALYSIS IN SIMULATION FOR RESERVOIR MANAGEMENT: CASE STUDY FROM NIGER DELTA

A DISSERTATION

SUBMITTED TO THE DEPARTMENT OF PETROLEUM ENGINEERING

AND THE COMMITTEE ON GRADUATE STUDIES

OF AFRICAN UNIVERSITY OF SCIENCE AND TECHNOLOGY

IN PARTIAL FULFILLMENT OF THE REQUIREMENTS

FOR THE DEGREE OF

DOCTOR OF PHILOSOPHY

ARINKOOLA Akeem Olatunde

APRIL, 2016

I certify that I have read this thesis and that in my opinion it is fully adequate, in scope and in quality, as a dissertation for the

degree of Doctor of Philosophy.

_____

Prof. David. O. Ogbe
(Principal Advisor)

I certify that I have read this thesis and that in my opinion it is

fully adequate, in scope and in quality, as a dissertation for the

degree of Doctor of Philosophy.

_____

Dr. Alpheus Igbokoyi

(Committee Member)

I certify that I have read this thesis and that in my opinion it is

fully adequate, in scope and in quality, as a dissertation for the

degree of Doctor of Philosophy.

_____

Dr. Saka Matemilola

(Committee Member)

Approved for the University Committee on Graduate Studies:

_____

Vice President Academic, Prof Charles E. Chidume

Date ……………………….

Abstract

Uncertainty analysis of flow performance predictions involves identifying significant reservoir parameters impacting the flow response. Uncertainty analysis often requires conducting large number of reservoir simulation runs. In this work, experimental design theory (DoE), Response Surface Methodology (RSM) and numerical simulation were integrated to reduce the number of simulations and simplify the optimization process. Various investigators have applied DoE/RSM to approximate a complex process with regression polynomials within a certain well defined region. The application of these DoE/RSM methods is more often based on the experimenter's discretions or company practices with no attention paid to the risks involved. Hence, in this work, it is necessary to examine the basis for the various DoE/RSM methods for the purpose of developing guidelines for the construction of valid response surfaces.

First, three families of linear experimental design methodologies, the Placket-Burman, Fractional and Relative variation, are evaluated for uncertainty screening by computing sensitivity coefficients of all identified uncertainty relative to system parameters. This procedure has useful applications in simulation for the optimization of production and management of a petroleum asset.

Second, probable reservoir proxies were developed based on linear sensitivity analysis. Three-level experimental design algorithms, i.e., Box-Behnken, Central Composite, D-Optima and Full Factorial designs, and Adaptive neuro-Fuzzy Inference System were rigorously examined. The methods were analyzed for their capabilities to reproduce actual production forecasts. The best method was selected from the case study and recommendations were made on how to select best DoE methods for similar applications.

Uncertainty quantification was performed using the selected response surface model. Although the use of regular Monte Carlo simulations (MCS) has gained tremendous attention, the fundamental assumption of variables being independent and identically distributed is often not valid in petroleum reservoir problems. Methods based on Markov Chains simulations offer reasonable solution to this problem. Mathematical foundation showing the differences between regular MCS and Markov Chains methods was demonstrated in this work using a second case study from the Niger Delta involving the placement of infill wells in a reservoir.

In the second case study, the selection of optimum number, type and locations of the infill wells in the reservoir was uncertain. The objective was to optimize infill well selection and placement and quantify the associated uncertainty. To accomplish this objective, the reservoir was delineated into four sub-regions (A, B, C and D). To drain each region, a set of only vertical wells, only horizontal and combination of vertical and horizontal wells were drilled. Reservoir heterogeneity at the infill well locations, number and type of infill wells, horizontal well lengths, perforation intervals and inter-well spacing were considered as uncertainty parameters affecting cumulative oil recovery, water cut and water breakthrough time. Uncertainty quantification was performed using both the regular MCS and Markov Chains simulations. The results of this study are useful for identification and selection of effective tools in uncertainty quantification in the oil industry. The proposed uncertainty analysis methodology in both case studies saves considerable time; and is very useful when limited data is available and can serve as practical guides for effective reservoir management.

Acknowledgments

Dedication

To my wife

Bilkiss,

whose love and support

are without measure

and to my children

Zynab, Zeenat and Mahbuub

who are a source of joy

Contents

List of Tables

List of Figures

Chapter 1

1. Introduction

1.1 Research Background

Petroleum engineer can spend a lot of time to build a model and performing reservoir simulation study. His ultimate objective is to devise economic strategies to develop, manage, and operate oil and gas fields efficiently. For many petroleum fields, attainment of these objectives can be very difficult due to many factors. The chief of which are uncertainties that associated with effective management of the reservoir portfolio. For efficient reservoir management, it is important to understand the sources of uncertainty which include; petrophysical, geological, geophysical, fluid characterization, reservoir simulation, assumptions, etc. and their impact on the physical reservoir description. Given this broad spectrum of uncertainties, a systematic and simplified procedure for identification and analysis of uncertainties is desirable.

In spite of this apparent need, most production forecasts in practice are done using deterministic models that hardly can reproduce, with a high confidence, the historic production. This is what is responsible for the underperformance and disparity between the actual worth and projections from Exploration and Production (E&P). To bridge this gap, the industry has witnessed a paradigm shift from deterministic thinking to a more balanced philosophy that recognizes surface and subsurface uncertainties. This new development has greatly influenced the enormous successes recorded with the application of

experimental design methodologies. To sustain this trend, resources are increasingly expended to develop structured, simple and systematic approaches for assessing the impact of uncertainties on investment decisions.

The use of experimental design in reservoir management for uncertainty screening and modeling is becoming popular in oil and gas industry. Experimental design methodologies enable clear understanding of impact of parameters and their interactions on quantity of interest. However, adoption of various methods is more often based on experimenter discretions or company practices. This is mostly done with no or little attention been paid to the risks associated with various decisions that emanated there from. The consequence is the underperformance of the project when compared with the actual value of the project. In this study, a detail analysis of different families of available designs for screening and response surface modeling during uncertainty analysis is given. This can provide many DoE users with the best practice in selecting various DoE methods for specific applications.

On proposal of various field development programmes, the risky nature of petroleum exploration and production requires that the decisions on reservoir management must consider all uncertainties and risks associated with all proposed strategies such as infill drilling. The selection of type and placement of infill wells can however pose a serious challenge due to the presence of uncertainty. Development of straight forward and simple methodology that can be easily applied in fields for quick assessment of infill opportunity involving infill location, selection and placement as well as the associated risks would be very useful to managers of oil and gas fields.

It should be emphasized that uncertainty cannot be completely eliminated. A model, perfect or imperfect, must be built to advance a project but the ability to identify uncertainties and incorporate them to decision making will go a long way in minimizing the risk associated with investment in oil and gas. This is the pivot upon which this research rests.

1.2 Statement of the Problem

Uncertainty in reservoir model is connected to many factors. According to Corre *et al*., (2000), they are linked to geological scheme, sedimentary framework, nature of the reservoir rocks, their extent and properties as well as heterogeneities. Due to these myriad sources of uncertainties, static model is likely the source of the greatest uncertainty in reservoir simulation. Nevertheless, static models have been helpful in supporting future development activities of hydrocarbon reservoirs. A reservoir model is first developed using available data. Except for outcrop and 2-D and 3-D seismic data, most of these data are determined at the reservoir well points. Even for fully developed and matured fields these well points only account for less than 1% of the reservoir volume (Mohaghegh *et al*., 2006). Thus parameters used in estimating the hydrocarbon volumes and reserves have uncertainties associated with them.

Ignoring the uncertainties in the reservoir lithology can result to underestimation of the inter wells structural elements and ultimately the connected pore volume. Quantifying uncertainty in volumes of hydrocarbons in place has been a challenge for the oil and gas industry (Akinwumi *et al*., 2004). The challenge stems from many factors, tangible and intangible, that enters the estimation process. Among the reservoir engineers' tasks is

3

devising strategies to achieve uncertainty assessment of important quantities such as production forecast. The pre and post-reservoir performance evaluations are generally not equal. This is due to inability to identify and analyze the key uncertainties in model input parameters.

First-Order Analysis method for uncertainty assessment is simple and less time consuming. However, it works best for small uncertainties (Corre, *et al.*, 2000). Second-Order Analysis method, an improvement over the first-order, can accommodate larger uncertainties but tends to be computation intensive due to the complexity of the function as uncertainty increase in number.

Probability theory and Derivative tree have also been used to account for uncertainties in production forecasts. These methods assumed deterministic values for uncertainties at their extreme points so that a significant number of attributes are omitted. Apart from this, these methods are highly subjective. The attributes occurrence probabilities are arbitrarily assigned *a priori* or assigned based on experience with no consideration for the interaction of the attributes in the process. Monte Carlo Simulation can be computationally intensive especially when many independent variables are involved. The criticality attached to *a priori* sample size definition, *a priori* specification of probability distribution function and convergence issues are some of the limitations of this method. The assumptions of independency in the use of ordinary Monte Carlo simulation can introduce a big mismatch in forecast figures and can seriously affect project evaluation and investment decisions.

Conventional approach for quantification of uncertainty is mainly based on Geostatistics with the use of ranking measures. Typically this technique requires many realizations and

4

runs of the reservoir model. However, generating multiple realizations to manage model uncertainties can be time consuming especially large and highly complex reservoirs. Generating hundreds or sometimes thousands of simulation runs can put considerable strain on the resources of asset team. Although ranking measures are always use for selection of best realization, the idea of ranking realizations itself is limited in application depending on reservoir complexity. Ranking tools increase in complexity and required knowledge of the specific problem. Generally, there is no single ranking index that can lead to a unique reliable conclusion (Mclennan, and Deutsch, 2005, Idrobo *et al.*, 2000).

Thus, the quantification problem is both important, and, as a practical matter, unsolved. This study integrated structural map uncertainty, flow simulation, design of experiment and response surface methodology (DoE/RS) to develop three geological models for uncertainty forecast. Despite its wide applications in the petroleum industry, the DoE methods have seldom been critically examined. The Placket-Burman (PBD), Fractional (FRD) and Relative variation (RVD) designs have been used to identify the key parameters controlling the response. Then, Box-Behnken (BBD), Central Composite (CCD), D-Optima and Full Factorial designs (FFD) have been applied for response surface model. Wanton usage of these algorithms can be very risky. The goal in any design is to select best design without compromising the efficiency. All aforementioned designs are classical with foundation of application in medical sciences. To optimize its application in other fields, there is a need to critically carry out examinations on them with the view to analyzing them and revealing positive and negative implications of using them widely in

the oil and gas industry today in spite of the existence of many other modern strategies for computer experimentations such as *Latin- hypercube* and Uniform design of experiments.

1.3 Research Aim and Objectives

The aim is to perform uncertainty analysis associated with the simulation of selected development concepts for Niger Delta marginal fields.

The followings are the specific objectives:

    i. Building static model and quantify uncertainty in hydrocarbon volume

    ii. Infill well selection and placement optimization

    iii. Examination of classical experimental designs for uncertainty analysis

    iv. Development and comparison of predictive models using response surface, polynomial averaging and Adaptive Neuro-Fuzzy Inference System (ANFIS)

    v. Uncertainty quantification using regular Monte Carlo and Markov Chain approaches

1.4 Description of Case Studies and Proposed Method

There are two case studies for analysis. Both are from the Niger Delta deposition environment. The two case studies require building and calibration of geological models. Once the static models are built and history match obtained, uncertainty quantification are performed on the implementation of the proposed field development programmes using Ordinary and Markov Chain Monte Carlo simulation.

In Case 1, the problem involves a reservoir where the stock-tank oil initially in place (STOIIP) was earlier estimated as 27 million stock tank barrels. However, analysis of the production performance after fifteen years indicated a recovery factor of approximately 40% for a reservoir under primary production scheme. It was apparent from this figure that the reserves have been under estimated. In order to determine realistic figure and assess associated uncertainties, three reservoir realizations were built and uncertainties were combined using experimental design with the three models represent distinct dependent variable in the Central Composite Design (CCD) of experiment. The dynamic models were built by integrating static and dynamic parameters. Two options were considered for the uncertainty analysis. For the first option, the extreme models (low and high cases) were considered as replicates of the base case given rise to single response surface model. For second option, each model was assumed to have equal probabilities. This gives rise to three surface models. Overall, a total of four proxy models were developed using experimental design and response surface techniques. Uncertainty was quantified using Monte Carlo methods. Comparison was made of the results from the two methods and recommendations were made based on the implications of different methods to guide financial decisions and improve reservoir management.

In Case 2, the selection of type and placement of infill wells has been a challenge due to the presence of large number of uncertainty. Here, infill wells potential was evaluated and uncertainty associated with infill well placement was assessed. Numerical simulation, pressure and saturation maps were used to determine well locations and its optimal placement within the reservoir. In the proposed methodology the reservoir was delineated into four different sub-regions (A, B, C and D) bounded by faults. To drain each fault

block, a set of only vertical wells, only horizontal wells and combination of vertical and horizontal wells were drilled. Reservoir characterization of infill well locations, number and type of infill wells, horizontal well length, perforation intervals and inter-well spacing were considered as uncertainty parameters. In all the simulations, cumulative oil and gas production, water cut and water breakthrough time are the responses calculated and analyzed.

For uncertainty analysis, Placket-Burman, Fractional (FRD) and Relative variation (RVD) designs were applied for the identification of key parameters affecting the response. Then, Box-Behnken (BBD), Central Composite (CCD), D-Optima and Full Factorial designs (FFD) were applied to select the best response surface model for Markov Chain Monte Carlo (MCMC) Simulation. ANFIS-based model was developed to predict well production performance from all the infill wells. Performance comparison was made between the ANFIS and regression based models from experimental design and response surface methodology.

1.5 Outline of Dissertation

Chapter 2 is dedicated to a review of studies that have been done on uncertainties inherent in reservoir simulation models. The chapter commences with a discussion of the subject of reservoir heterogeneity which determines the quantity and quality of data needed to characterize oil and gas reservoirs. The chapter reviews sources of uncertainties, data needed for integrated reservoir studies and the uncertainties associated with them. Finally, the chapter presents current industry practice in quantifying and assessing uncertainties for field production forecast and for general reservoir management.

In chapter 3, the workflow for stochastic modeling is presented. The workflow consists of data acquisition, quality control, data analysis, petrophysical evaluation, description of geological concept adopted for the distribution of properties and hydrocarbon volume estimation. Chapter 4 presents material balance analyses for evaluation of aquifer properties. The chapter also presents model initialization; history matching and prediction of reservoir production performance. Chapter 5 presents an outline for infill placement optimization. The description of the numerical-based conceptual model to determine the optimal infill well locations is given.

In chapter 6, examination of experimental designs is presented for optimal response surface development. This chapter also describes the methodology for development of predictive model using polynomial averaging method and fuzzy-based model. Chapter 7 is dedicated to uncertainty quantification using ordinary Monte Carlo simulation and Bayesian approach (MCMC). The mathematical foundation for these approximation methods was detailed. The implications of various assumptions is clearly revealed. Chapter 8 is dedicated for the contributions of the present research to the existing knowledge including articles already published in highly refered international journals. To conclude the report, the conclusions is presented in chapter 9 and an outline of the direction for future research in chapter 10. At the end one can find the references and various appendices.

Chapter 2

2. Literature Survey

2.1 Reservoir Heterogeneity

Heterogeneity is defined as the degree of variability in reservoir properties in space and scale. It explains how the geological properties change with a change in location within the reservoir. Naturally, reservoirs are heterogeneous. However, the degree of heterogeneity varies from one reservoir to another. Homogeneous reservoirs are very simple to describe. In this case a measured reservoir property at any location can be applied for full description of the entire reservoir domain. However, complexity grows as the reservoir becomes heterogeneous because reservoir properties vary as a function of spatial location. A complete heterogeneous reservoir description requires spatial prediction of the variation of the reservoir properties of rock facies, porosity, permeability, saturation, and faults and fractures (Kelkar, 2002).

In the construction of the simulation model, each cell of million grid blocks requires the assignment of values of rock and fluid properties. One way to generate the values of the rock and fluid properties to be used in the simulation model is to assume that the reservoir is homogeneous and use the same value of each property in every grid block. Such a simulation model ignores the geology of the reservoir and will consequently yield misleading and optimistic results. On the other hand, one may decide to populate the grid cells with property values from a random number generator. This model also ignores the

geology of the reservoir and the general observation that data from nearby locations tend to be similar whereas data from locations that are far apart tend to be dissimilar.

The estimation of reservoir properties at locations for which no measurements have been made can be accomplished with geostatistics. Geostatistics is the practical applications of the theory of regionalized variables developed by Georges Matheron in Fontainebleau (Ekwere Peters, 2010). The main difference between ordinary statistics and geostatistics is that ordinary statistics is typically based on random, independent and uncorrelated data whereas geostatistics is based on random and spatially correlated data. To successfully apply this statistics, understanding and consideration of the scales at which heterogeneities evolve can reduce uncertainty due to its application (Deutch *et al*., 1996).

Heterogeneity occurs at all scales from pore variation to major reservoir units within a field, and every scale in between. Scales of heterogeneities are important because different heterogeneities have a different impact on reservoir performance and oil recovery. Proper identification and knowledge of reservoir heterogeneities on various scales is necessary for an optimum production performance. The scales of heterogeneities are defined at four levels of complexity as shown in Table 2. 1.

Microscopic heterogeneities are measured on a micro level. Physical Laboratory measurements at the microscopic level include pores and pore throat size distributions, grain shape and size distributions, throat openings, rock lithology, packing arrangements, pore wall roughness, and clay lining of pore throats. The major controls on these parameters are the deposition of sediments and accompany compaction, cementation, and dissolution. Due to Micro-scale pore level heterogeneities, displacing fluids may take

preferential paths leaving behind residual oil. Poor displacement efficiency results in higher residual or trapped hydrocarbon. This will directly impact quantity of recoverable oil.

Table 2. 1: The four levels of reservoir heterogeneities, the types of measurement and their effects on reservoir performance (Source: Kelkar 2002)

Type	Scale	Measurements	Effects on Performance
Microscopic (Pore Level)	10-100 μm	Pore and Throat distribution, Grain size	Displacement Efficiency (Trapped Oil)
Macroscopic (Core Level)	1-100 cm	Permeability, porosity, wettability Saturation	Sweep Efficiency (Bypassed Oil)
Megascopic (Sim Grid Level)	10-100 m	Log Properties, residual Oils, Seismic	Sweep Efficiency (Bypassed Oil)
Gigascopic (Reservoir Level)	>1000 m	Well Test, geological Description	Extraction Efficiency (Un-trapped Oil)

Macroscopic heterogeneity is measured at core level. Laboratory measurements at the macroscopic level include porosity, permeability, fluid saturation, capillary pressure, and rock wettability. Macroscopic scale rock and fluid properties are employed to calibrate logs and well tests for input into reservoir simulation models. The macro-scale heterogeneities will define the shape of the flood front of the displacing fluids, which in turn will determine the amount of bypassed oil.

Megascopic heterogeneity represents flow units, and is usually investigated through reservoir simulation. Examples of megascopic heterogeneities include: lateral discontinuity of individual strata; porosity pinch-outs; reservoir fluid contacts; vertical and lateral

permeability trends; and reservoir compartmentalization. Reservoirs are managed at this scale of interwell spacing. These heterogeneities are commonly gotten from transient pressure analysis, tracer tests, well logs correlations, and high resolution seismic. It determines the well-to-well recovery variation which could result from reservoir units' primary stratification and internal permeability trends.

One of the very important heterogeneities in reservoir engineering calculations is stratification. Many reservoirs contain layers of productive rock that can be either communicating or non-communicating. These layers can be highly permeable with considerable thickness. A good description of the layers and their respective properties is important in planning many Enhanced Oil Recovery (EOR) operations. Since mega-scale heterogeneities may be an extension of the macro-scale heterogeneities, it will have the same effect as the macro-scale heterogeneities, but on a larger reservoir scale.

Areal heterogeneities affect sweep efficiency aerially, while the vertical heterogeneities affect vertical sweep efficiency. Macro- and mega-scale heterogeneities may result in variations in the areal and vertical reservoir properties which may cause the displacing fluids to reach the producing well without reaching all parts of the reservoir. This may leave behind large quantities of bypassed oil.

The whole field is encompassed in the gigascopic scale of heterogeneities. Reservoirs are explored for, discovered, and delineated at this level. Characterization at this level begins from inter-well spacing and extends up to the field dimensions. Field-wide regional variation in reservoir architecture is caused by either the original depositional settings or subsequent structural deformation and modification due to tectonic activity. Lack of

understanding of reservoir heterogeneities, in their gigascopic scale, means that some of the oil source remains uncontacted. It is well established that understanding and capturing reservoir heterogeneity in reservoir simulation models, would help us devise the proper field development to optimize production performance and maximize the hydrocarbon reserves from oil and gas reservoirs. This will depend, however, on the availability of reservoir data, as the availability of reservoir data determines our understanding of reservoir heterogeneity.

2.2 Measures of Variability

(i). Variance

The most useful measure of variability around the central value is the variance

$$\text{Var}\,(\emptyset_1 \ldots \ldots \emptyset_N) = S^2 = \frac{1}{N-1}\Sigma_{i=1}^{N}\left(\emptyset_i - \overline{\emptyset}\right)^2 \qquad\qquad 2.1$$

(ii). Dykstra-Parsons Coefficient of Variation

A measure of permeability variability that is widely used in the petroleum industry is the Dykstra-Parsons (1950) coefficient of variation. This coefficient of variation is determined based on the assumption that permeability data are drawn from a log normal distribution. The calculation of the Dykstra-Parsons coefficient of permeability variation involves plotting the frequency distribution of the permeability data on a log-normal probability graph paper. This is done by arranging the permeability values in descending order and then calculating the percent of the samples with permeabilities greater than or equal to that value for each permeability.

$$V = \frac{K_{50} - K_{84.1}}{K_{50}} \qquad\qquad 2.2$$

14

Where k_{50} is the permeability value at ($\% \geq 50$), which is the log mean permeability and $k_{84.1}$ is the permeability value at ($\% \geq 84.1$).

A homogeneous reservoir has a coefficient of permeability variation that approaches 0 whereas an extremely heterogeneous reservoir has a coefficient of permeability variation that approaches 1. Petroleum reservoirs typically have Dykstra-Parsons coefficients of permeability variation between 0.5 and 0.9.

Figure 2.1 shows theoretical log normal permeability distributions and their corresponding Dykstra-Parsons coefficients.

(iii). Lorenz Coefficient

Another measure of heterogeneity used in the petroleum industry is the Lorenz coefficient. The Lorenz coefficient of variation is obtained by plotting a graph of cumulative kh versus cumulative φh, sometimes called a flow capacity plot. Figure 2.2 shows a typical flow capacity plot for determining the Lorenz coefficient. The Lorenz coefficient is defined from Figure 2.2 as

$$\text{Lorenz Coefficient} = \frac{\text{area ABCA}}{\text{area ADCA}} \qquad\qquad 2.3$$

The Lorenz coefficient of variation also varies from 0 to 1. Unfortunately, the Lorenz coefficient is not a unique measure of reservoir heterogeneity.

Several different permeability distributions can give the same value of Lorenz coefficient. For log-normal permeability distributions, the Lorenz coefficient is very similar to the Dykstra- Parsons coefficient of permeability variation.

2.3 Sources of Uncertainty

Reservoir engineers' goal in reservoir characterization is not to seek the truth about reservoir; instead, to integrate data from various sources to build a reasonable reservoir model which is adequate to predict the future performance.
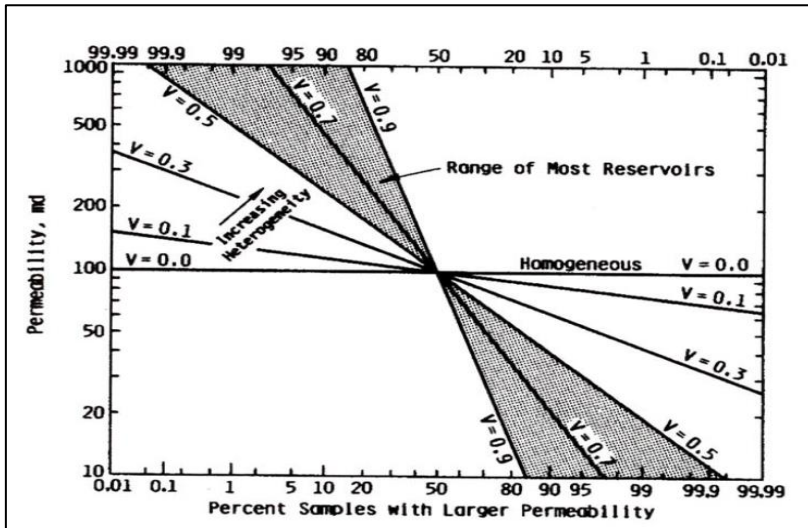
Figure 2. 1: Theoretical log normal permeability distributions and their corresponding Dykstra-Parsons coefficients (Carlson, 2003)
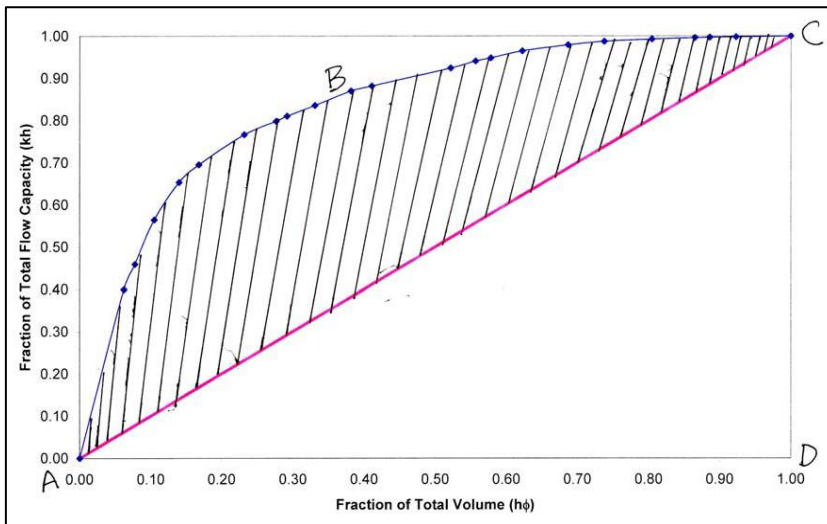
Figure 2. 2: Flow capacity distribution (Ekwere Peters, 2010)

This helps to determine the most accurate estimation of hydrocarbon reserves and production profiles for a given recovery mechanism. The three major stages involved in integrated studies are shown in Table 2.2. Integrated reservoir studies combine several types of data, including geological, seismic, petrophysical, well, and production data as shown in Table 2.2. Static data provide information on the reservoir architecture and fluid saturation at well positions, but no information on the way the fluids will move during production. Dynamic reservoir data, on the other hand, provide information on fluid dynamics during the production. All these data present specific uncertainties and are grouped as presented in the sub-sections that follows.

Table 2. 2: Three major stages involved in integrated reservoir studies (Source: Schulze-Riegert and Shawket Ghedan, (2007))

Components	Reservoir Characterization	Static Geological Model	Dynamic Simulation Model
Tasks	Regional Geological Model	Reservoir Structural Model	Upscaling of Static Geological
	Reservoir Depositional Model	Reservoir Facies Model	Design of Wells/ Facilities
	Reservoir Pore System Model	Reservoir Rock Typing Model	Intial Resevoir Fluids Distribution
	Reservoir Rock Type Scheme	Reservoir Flow Units Model	Near Wellbore Performance
		Reservoir Property Model	Validation of Simulation Model
		Defining Fluids Contacts	Optimisation Development Plans
			Economic Model & Risk Analysis

Table 2. 3: Required simulation data and their source

Data Type	Descriptions
Pressure Data	Initial reservoir pressures, Datum, pressure history, static pressure flowing bottom hole pressure, tubing head pressure, RFT/MDT Pressure transient result
Deviation Survey Data	Kelly bushing depth, well coordinate, Total depth, MD and TVD/ TVDss
Production Data	Production History, Injection history, drainage points
Completion report	Wireline history, intervention/workover history, well status, latest well test, Choke/ bean history, API
Well Test history	Oil / liquid rate, GOR, FBHP,BSW, Drainage points
Core Data (SCAL)	Relative Permeability, Capillary pressure, Cross plot, Core depth/ sample interval/ core type
PVT Data	FVF, viscosity, Bubble point pressure, Fluid composition, fluid experimental results, reservoir temperature
Petrophysical Data	Well Logs (hard copies), Porosity,Permeability, Top/Base depth Fluid contacts, NTG, sand thickness, GRV, water saturation
Well Schematic diagrams	Bottom hole location and orientation, Perforation interval, Wellbore radius, Casing string size, Tubing string, current completion
Maps	Surface Depth maps (Hard copies), Well location, Fluid definition
Economic Production prediction limit	Abandonment rates, GOR, BSW
Available Reports	Literature review / previous studies report

2.3.1 Uncertainty due to petrophysical data

Most reservoir data are determined at the reservoir well points except for outcrop and 2-D and 3-D seismic data. Even for fully developed and matured fields these well points only

account for less than 1% of the reservoir volume. Because of this and the fact that most reservoirs are highly heterogeneous, reservoir data are highly uncertain, especially at reservoir locations between wells. The degree of uncertainty may vary from one variable to another. The uncertainty of a parameter may result from difficulty in directly and accurately measuring the quantity. This is particularly true of the physical reservoir parameters which, at best, can only be sampled at various points, and are subject to errors caused by presence of the borehole and borehole fluid or by changes that occur during the transfer of rock and its fluids to laboratory temperature and pressure conditions (Walstrom, 1967).

2.3.2 Uncertainty in geophysical data

In the geophysical domain, uncertainties are linked to the acquisition, processing, and interpretation of seismic data (Vincent, 1999 and Corre, 2000). Some of these uncertainties, according to Sandsdalen *et al*., (1996) and Tyler, (1996)**,** are:

i. Uncertainties and errors in picking horizons

ii. The difference between several interpretations

iii. Uncertainties and errors in depth conversion

iv. Uncertainties in seismic-to-well-tie

v. Uncertainties in pre-processing and migration

vi. Uncertainties in the amplitude map of the top reservoir

2.3.3 Uncertainty due to geological data

In the geological domain, the uncertainties are linked to the geological scheme, to the sedimentary concept, to the nature of the reservoir rocks, their extent, and to their properties (Corre, 2000). Uncertainty in any geological model is unavoidable given the sparse well data and the difficulty in accurately relating geophysical measurements to reservoir scale heterogeneities. Some of the known geological uncertainties are:

i.   Uncertainties in gross rock volume

ii. Uncertainties in the extension and orientation of sedimentary bodies

iii. Uncertainties in the distribution, shape, and limits of reservoir rock types

iv. Uncertainties in the porosity values and their distribution

v.   Uncertainties in the horizontal permeability values and their distribution

vi. Uncertainties in the layers Net-to-Gross Ratio

vii. Uncertainties in the reservoir fluids contacts

2.3.4 Uncertainty due to dynamic reservoir data

In the production area, there are uncertainties linked to any parameter that affects flow within the reservoir, such as absolute and relative permeability, vertical to horizontal permeability ratio (Verbruggen, 2002), fault transmissibilities, horizontal barriers, thermodynamics, injectivity, and productivity index, well skin (Corre, 2000) and the extension of horizontal and vertical barriers.

2.3.5 Uncertainty of reservoir fluids data

Uncertainties in the description of reservoir fluid composition and properties are of special importance for the optimization of the processing capacities of oil and gas, as well as for planning the transport and marketing of the products from the field (Azuka *et al*., 2009, Meisingset, 1999). Some of the reservoir fluids uncertainties are:

  i.   Uncertainty in reservoir fluid samples which arises due to lack of representative samples from the reservoir.

  ii. Uncertainty in reservoir samples from different reservoir zones. Possible variations in fluid properties in different parts of the field may introduce uncertainty in the reservoir fluids description

  iii. Uncertainty in the compositional analyses

  iv. Uncertainty in volumetric measurements in the PVT laboratory. This is considered to be of less importance compared with having representative fluid samples

  v.   Uncertainties in the reservoir fluids' interfacial tension. This may be of importance due to its effect on the capillary pressure, and/or compositional effects like re-vaporization of oil into injection gas (Meisingset, 1999).

2.4 Reservoir Simulation Uncertainty

There is existence of varying degree of uncertainty associated with all data used in reservoir modeling and simulation studies. Figure 2. 3 summarizes several uncertainty sources associated with reservoir performance.

2.4.1 Mathematical model

Reservoir simulators are important tools for oil reservoir management. They are computer implementations of high-dimensional mathematical models of reservoirs. The mathematical model used in numerical simulation is derived by integration of three fundamental equations which are conservation of mass, transport equation (Darcy's equation) and equation of state (Dake, L.P, 1978, Ahmed, T. and Mckinney, D.P. 2005).
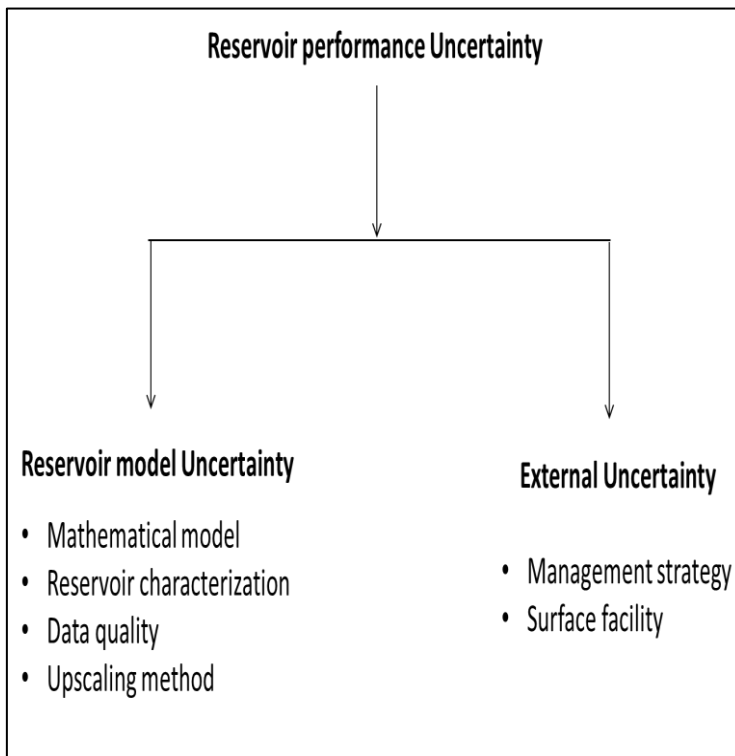
Figure 2. 3: Sources of uncertainties associated with reservoir performance.

For a 3-Dimensional, single-phase flow, the resulting mathematical model equation is:

$$\frac{\partial}{\partial x}\left(\frac{ck\beta}{\mu}\frac{\partial P}{\partial x}\right) + \frac{\partial}{\partial}\left(\frac{ck\beta}{\mu}\frac{\partial P}{\partial y}\right) + \frac{\partial}{\partial}\left(\frac{ck\beta}{\mu}\frac{\partial P}{\partial Z}\right) + Q = \frac{\partial}{\partial t}(\varphi\beta) \qquad 2.4$$

The following are the boundary conditions for solving the partial differential equation (PDE) given in equation 1.

23

$P(x, y, z, 0) = P_i$

$$\frac{\partial P}{\partial x}(0, y, z, t) = 0, \qquad\qquad \frac{\partial P}{\partial x}(L_x, y, z, t) = 0$$

$$\frac{\partial P}{\partial y}(x, 0, z, t) = 0, \qquad\qquad \frac{\partial P}{\partial y}(x, L_y, z, t) = 0$$

$$\frac{\partial P}{\partial z}(x, y, 0, t) = 0, \qquad\qquad \frac{\partial P}{\partial z}(x, y, L_z, t) = 0$$

Equation 2.4 is a non-linear partial differential equation (PDE) which can not be easily solved using analytical approach. Consequently, the PDE is converted to a numerical model using Taylor series approximation briefly discussed below:

If we consider the function p(x) shown in Figure 2. 4, suppose we know the value of p(x) at the point x and we know all the derivatives of p(x) at the point x. If we want to approximate the value of p(x+Δx) at the point (x+Δx), we can do this with a Taylor series as follows,

$$p(x + \Delta x) = p(x) + \Delta x p'(x) + \frac{\Delta x^2}{2!} p''(x) + \frac{\Delta x^3}{3!} p'''(x) + \bullet\bullet\bullet + \frac{\Delta x^n}{n!} p^n(x) + \bullet\bullet\bullet \quad 2.5$$

Where p^n is the nth derivative of p. This is an infinite series which is theoretically exact for an infinite number of terms. However, if we truncate the series after n terms, then we introduce a *truncation error*, e_t, (the remaining higher order terms which are not included).

24
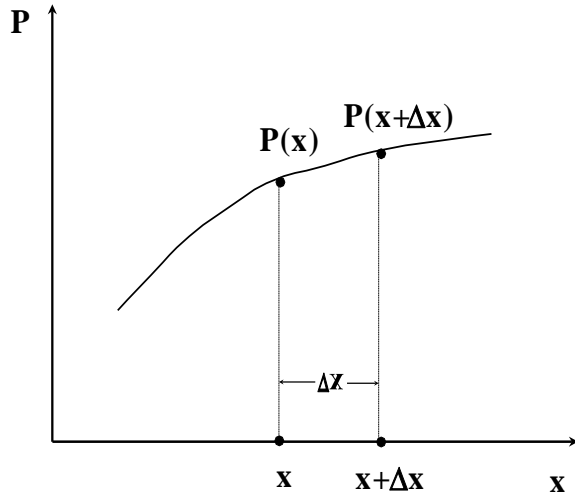
Figure 2. 4: Illustration of Taylor series for pressure analysis

This truncation error is

$$e_t = \frac{p(x\ )^{n+1}(\Delta x)^{n+1}}{(n+1)!} + \bullet\bullet\bullet \qquad\qquad 2.6$$

and is equal to

$$e_t = \frac{p(x+\ \xi\ )^{n+1}(\Delta x)^{n+1}}{(n+1)!} \qquad (0 \le \xi \le \Delta x) \qquad\qquad 2.7$$

The function $p(x)$ and all its derivatives must be continuous throughout the interval under consideration. But, we often deal with discontinuities in both time and space. That limits the Taylor series analysis.

If we take P_i as $p(x)$, p_{i+1} as $p(x+\Delta x)$, and p_{i-1} as $p(x-\Delta x)$. We can expand Taylor series in either direction as follows:

$$p_{i+1} = p_i + \Delta x \frac{\partial p}{\partial x} + \frac{(\Delta x)^2}{2!}\frac{\partial^2 p}{\partial x^2} + \frac{(\Delta x)^3}{3!}\frac{\partial^3 p}{\partial x^3} + \frac{(\Delta x)^4}{4!}\frac{\partial^4 p}{\partial x^4} + \bullet\bullet\bullet \qquad 2.8$$

$$p_{i-1} = p_i - \Delta x \frac{\partial p}{\partial x} + \frac{(\Delta x)^2}{2!}\frac{\partial^2 p}{\partial x^2} - \frac{(\Delta x)^3}{3!}\frac{\partial^3 p}{\partial x^3} + \frac{(\Delta x)^4}{4!}\frac{\partial^4 p}{\partial x^4} - \bullet\bullet\bullet \qquad 2.9$$

25

The right-hand side now uses partial derivatives (evaluated at x_i) since p is a function of both x and t, $p(x,t)$.

We have a couple of choices of approximations to $\Delta p/\Delta x$:

Forward difference (from Eq. 2.8):

$$\frac{\partial p}{\partial x} \approx \frac{p_{i+1} - p_i}{\Delta x} \qquad\qquad 2.10$$

Backward difference (from Eq. 2.9):

$$\frac{\partial p}{\partial x} \approx \frac{p_i - p_{i-1}}{\Delta x} + \vartheta(\Delta x) \qquad\qquad 2.11$$

Central difference (from Eqs. 2.8 and 2.9):

$$\frac{\partial^2 p}{\partial x^2} \approx \frac{p_{i-1} - 2 p_i + p_{i+1}}{(\Delta x)^2} + \vartheta(\Delta x^2) \qquad\qquad 2.12$$

The derivation of the numerical model is done by replacing the partial derivatives in the PDE with finite differences in equations 2.10 and 2.11 and evaluated at specific values of x, y, z, and t. With this approximation the differential equation is transformed into an algebraic equation that can be easily solved using matrix. The resulting finite difference formulation is given in equation 2.13 and the numerical model can be represented in three directions as shown in Figure 2. 5.

$$AP_{i-1,j,k} + EP_{i,j-1,k} + GP_{i,j,k-1} + BP_{i,j,k} + CP_{i+1,j,k} + FP_{i,j+1,k} + HP_{i,j,k+1} = D \quad 2.13$$

The resulting numerical equation includes pressure terms evaluated at two different points in time. These times are the initial time, $t = t_0$ and at a selected future time called time step, $t = t_1$. Knowing the pressure at the initial time, we have to solve the numerical equation for pressure at the given time step. At subsequent time steps, pressure will be calculated at

26

multiple points in a three dimensional model. The resulting numerical equation coefficient is solved using n x n matrix.
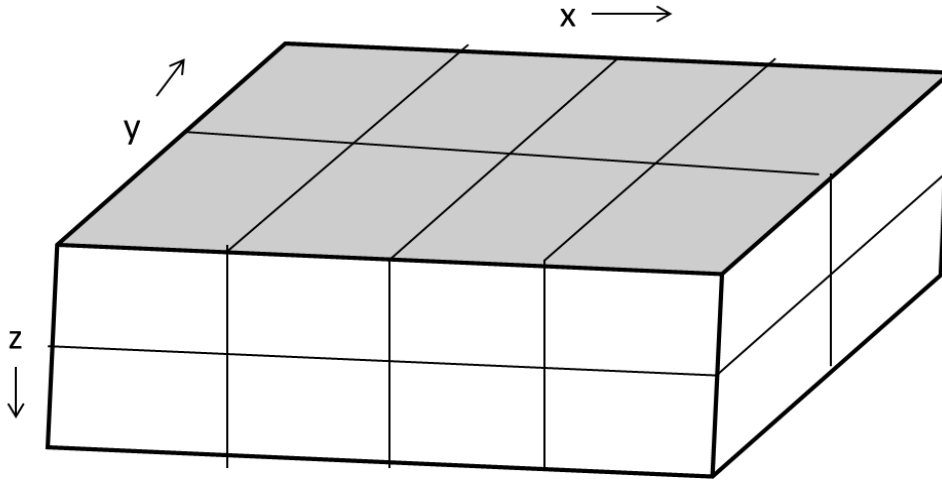
Figure 2. 5: 3-Dimensional Discretized Model

For one dimensional, single phase numerical model, a tri-diagonal matrix is formed. In a four-cell system, the matrix is depicted as in equation 2.14:

$$
\begin{pmatrix}
b_1 & c_1 & & & \\
a_2 & b_2 & c_2 & & \\
 & a_3 & b_3 & c_3 & \\
 & & a_4 & b_4 & c_4 \\
 & & & a_5 & b_5
\end{pmatrix}
\begin{pmatrix}
p_1 \\ p_2 \\ p_3 \\ p_4 \\ p_5
\end{pmatrix}
=
\begin{pmatrix}
d_1 \\ d_2 \\ d_3 \\ d_4 \\ d_5
\end{pmatrix}
\qquad 2.14
$$

This matrix representation consists of three non-zero diagonals and is easily solved.

General Implicit Methods: This is also a mixed explicit/implicit method, but is more flexible than the Crank-Nicolson (C-N) method.

$$
(1-\sigma)\frac{1}{(\Delta x)^2}(p_{i-1}^{n} - 2 p_{i}^{n} + p_{i+1}^{n}) + \sigma\frac{1}{(\Delta x)^2}(p_{i-1}^{n+1} - 2 p_{i}^{n+1} + p_{i+1}^{n+1}) = \frac{1}{\Delta t}(p_{i}^{n+1} - p_{i}^{n}) \qquad 2.15
$$

Weighting factor: $(0 \leq \sigma \leq 1)$

For:

$\sigma = 1$ (Implicit)

$\sigma = 0$ (Explicit)

$\sigma = 1/2$ (C-N)

Truncation Error: $\vartheta\,((\varDelta x)^{2},\,(\varDelta t))$ (generally)

Only the implicit method is unconditionally stable (for any time step size). The explicit method is stable only for sufficiently small time steps, which are generally impractical. Although the Crank-Nicholson method has higher order accuracy, it is on the borderline of instability and is conditionally stable for practical purposes. Therefore, the implicit method is the standard in reservoir simulation. If more accuracy is required, smaller time steps are used.

The computation time needed to obtain pressure solution (P_{n+1}) for the implicit approximation is more than that for the explicit method. The problem complexity increases with increased number of dimensions and for multiple phases present. For two phases, the fluid flow equation applies to each flowing phase individually such that at each time step there are two unknowns to be solved, P_o, and S_w in each grid block.

Three errors that are inherent in numerical model as a result of PDE discretization include:

    i.   Truncation errors

    ii.   Round-off errors

    iii.   Stability errors

The truncation error results from the substitution of the partial derivatives in the differential equation with approximate finite differences (Peaceman, D.W, 2003). As a

28

result, it is an approximate solution which does not mimic the actual reservoir exactly. Round-off error, on the other hand, is a result of using a computer to solve the numerical model because the computer cannot represent real numbers accurately. Stability error consists of the approximation method used in transforming the PDE into a numerical model and the PDE itself. Instability in numerical solution leads to one error translating to another error (truncation or round-off errors, respectively). As the error increases, the rate of error growth increases so that the error growth gets so large that the solution is lost.

Apart from the algorithms used to generate the numerical model, model uncertainties can also arise from the type of reservoir simulator used. The simulator used can either be mass balance or streamline, finite difference or finite element. The inherent uncertainty results from the inadequacy to completely translate the continuous mass balance and flow equations into discrete approximates and the use of a computer to solve the equation. Due to all these, the numerical model that is used in reservoir simulation contains uncertainty which need to be quantified.

2.4.2 Up-scaling Uncertainty

A variety of papers was published that address specific aspect of how best to capture critical geological heterogeneities in earth models *prior* to and during upscaling for dynamic simulation (Castellini *et al*., 2003, Apaydin *et al*., 2005, Stern, 2005). After acquisition and interpretation of the seismic volume, the geologist builds the static model. Because the model built is usually a fine scale level it is computationally expensive to investigate reservoir flow behavior using such model. Consequently, the geological model

is upscaled into a coarse scale model generally called a reservoir simulation model in order to evaluate the reservoir flow behavior.

Upscaling technique is needed to transform the fine grid into coarse grid model (see Figure 2. 6). During Upscaling, reservoir properties are upscaled so as to reduce the number of grid blocks and facilitating simulation runs (Durlofsky, L.J, 2003, Hui, M., 2004, Ates, H *et al*., 2005, Lambers, J. and Gerritsen, M, 2005, Sablok, R. and Aziz, K, 2005). The fine grid model is employed to characterize a reservoir although in most modeling the model areal resolution is still coarse due to computational costs for the finer grids. On the other hand, the coarse grid model is used to evaluate reservoir performance prediction because of time constraints and available resources. To evaluate reservoir performance using fine grid model can also be limited by available computer capability and costs. As a result, upscaled/coarse grid model of the fine-scale model is required. A number of upscaling techniques are available in the literature. The different approaches can be classified according to two broad methods (Durlofsky, 2003).

    i.   the type of parameter to be upscaled, and

    ii.   the method of computing the parameter
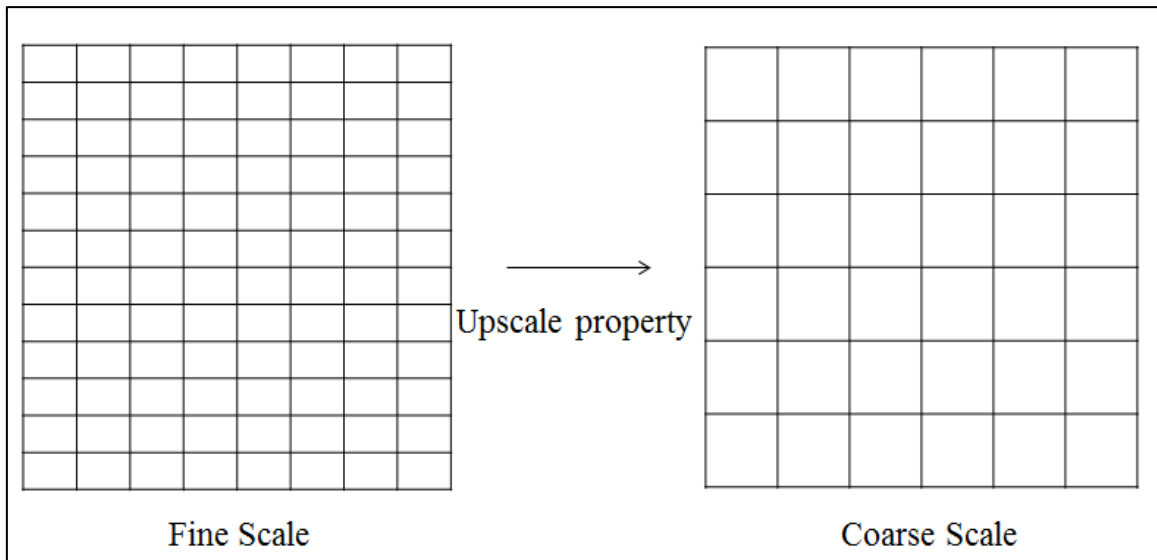
Figure 2. 6: Process in upscaling

These methods have various degrees of limitations in the ability to translate a fine-scale model into a coarse-scale model. Irrespective of the particular upscaling technique employed to generate the coarse model, utmost care should be taken to ensure that the upscaled model input parameter(s) is equivalent to the fine scale model parameter. For example, accurate upscaling of residual oil saturation and initial water saturation are vital because these two parameters determine the amount of oil that can be recovered from the reservoir. Some parameters such as porosity and saturation are accurately upscaled using simple volume averaging techniques. While absolute and relative permeability have varied upscaling algorithms. As a result, significant amount of uncertainties exist when permeabilities are upscaled from fine scale into coarse grid. Recognizing the fact that upscaling uncertainty exists, there is a need for proper quantification of upscaling uncertainty, which is important for better reservoir performance prediction.

Upscaling of fine scale model into a coarse scale model is conducted in both black oil and compositional simulation. See the work by Durlofsky, (2003) for detailed literature on upscaling of black oil model. Less work has been done on upscaling of compositional simulation; most of the work done so far on compositional upscaling (Ballin *et al*., 2001 and Hui *et al*., 2004) has been the adjustment of K-value flash calculation in order to account for using coarse grid to represent fine scale. This K-value adjustment resulted in Alpha factor method which serves as modifiers (Li and Johns, 2005). The modifiers are introduced into numerical simulation flow equation to relate fluid composition flowing out of the grid to the fluid composition within the grid.

2.4.3 Uncertainty due to Geostatistics

Estimation is one of the major applications of geostatistics, the other being conditional simulation. The objective is to estimate the variable of interest at a location X_o for which no datum has been measured, using the data measured at other locations X_i distributed in space. The major limitation of linear estimation methods stems from the fact that the structure of the heterogeneity as represented by the Variogram, the covariance function or the correlation coefficient function has not been taken into account and uncertainty is introduced to the estimation. Geostatistics uses a probabilistic framework to make estimations and in so doing provides estimates that honor the correlation structure of the heterogeneity (Ratchkoviski *et al*., 1999). It also provides quantitative assessment of the reliability of the estimates by providing both the estimate and its confidence limits. The common methods include the Variogram and Kriging.

2.4.3.1 Kriging

Kriging is a 3-D estimation program for variables defined on a constant volume support. Estimation can either be performed by simple Kriging (SK), ordinary Kriging (OK), Kriging with a polynomial trend (KT) or simple Kriging with a locally varying mean (LVM). LVM is a variant of Kriging, in which it is assumed that the mean m (U) is not constant but is known for every U. In all geostatistical estimation, the variable of interest is treated as a stationary random function with a normal probability distribution. If the measured data do not exhibit a normal distribution, they must first be transformed into a normal distribution before proceeding further. Such a transformation can always be done by using the cumulative distribution function of the data and the cumulative distribution function of a standard normal distribution with a mean of zero and a standard deviation of 1. The criteria used in ordinary Kriging to obtain the best estimate are (1) the estimate should be unbiased and (2) the estimation error should have minimum variance.

Ordinary Kriging is a Best Linear Unbiased Estimator (BLUE) which can be derivation in terms of the covariance function or Variogram function. The estimation is a classical problem of optimization, which can be solved by the method of Lagrange multipliers.

The objective function is to minimize

$$\sigma_e{}^2 = \sigma^2 + \sum_{i=1}^{N}\sum_{i=1}^{N} \lambda_i \lambda_j C(h_{ij}) - 2\sum_{i=1}^{N} \lambda_i C(h_{io}) \qquad\qquad 2.16$$

or

$$\sigma_e{}^2 = \sum_{i=1}^{N} \sum_{j=1}^{N} \lambda_i \lambda_j \gamma(h_{ij}) + 2 \sum_{i=1}^{N} \lambda_i \gamma(h_{io}) \qquad\qquad 2.17$$

Subject to

$$\sum_{i=1}^{N} \lambda_i = 1 \qquad\qquad 2.18$$

2.4.3.2 Variogram

The Variogram is used to quantify the correlation structure of the variable of interest for the purpose of estimation and conditional simulation. The Variogram of the sample data is known as the experimental Variogram. After computing the experimental Variogram, a smooth theoretical Variogram model is usually fitted to the experimental Variogram and the model is then used for estimation. The estimation process involves the solution of a set of linear simultaneous algebraic equations, whose coefficients are derived from the Variogram. Unless the Variogram is well behaved, the simultaneous equations may not have a solution. Hence, the need to fit a smooth and well behaved theoretical model to the rough experimental Variogram for the purpose of estimation.

The Variogram increases as the values of properties measured on a set of samples become more dissimilar. The formula for the "semivariogram" is written conventionally in terms of a "lag" h, and a set of observations z, known as attributes, made at a number of locations, s. The difference in attributes for pairs of spatially separated samples is compared for increasing values of the lag using;

$$\gamma(h) = \frac{1}{2N(h)} \sum_{i=1}^{N(h)} \left(z(x_i + h) - z(x_i) \right)^2 \qquad\qquad 2.19$$

Where the *N(h)* is a count of the possible pairing at each lag used to compute the function. The Variogram is truncated at the value of lag where the diminishing number of possible pairings loses statistical significance.

Figure 2.7 shows an ideal Variogram. It starts at zero and increases with increasing lag distance until a certain distance is reached at which it levels off and becomes constant. The lag distance at which the Variogram levels off (a in the figure) is defined as the correlation length, or the range of influence, and the value of the Variogram at this point is called the sill. The sill is the semivariance of the entire data set. Thus, hidden in the Variogram are the variance and standard deviation of the data set, the usual measures of heterogeneity of ordinary statistics. If the correlation length is zero, the spatial distribution of the property is fully random. With increasing correlation length, the range of influence of one value on its neighbors increases up to the correlation length. At lag distances beyond the correlation length, the data are no longer correlated. Table 2.4 summarizes the popular Variogram models.

2.4.3.3 Conditional simulation

Kriging gives a smooth estimate because the estimate is a weighted average of the sample data. Such average can never be larger than the largest sample value nor can it be smaller than the smallest sample value. Thus, Kriging eliminates local variability. If such local variability is important, then it can be incorporated into the estimated values using conditional simulation. The idea behind conditional simulation is that each of the estimates

obtained from Kriging was associated with an uncertainty in the estimated value measured by the estimation variance or the estimation standard deviation.
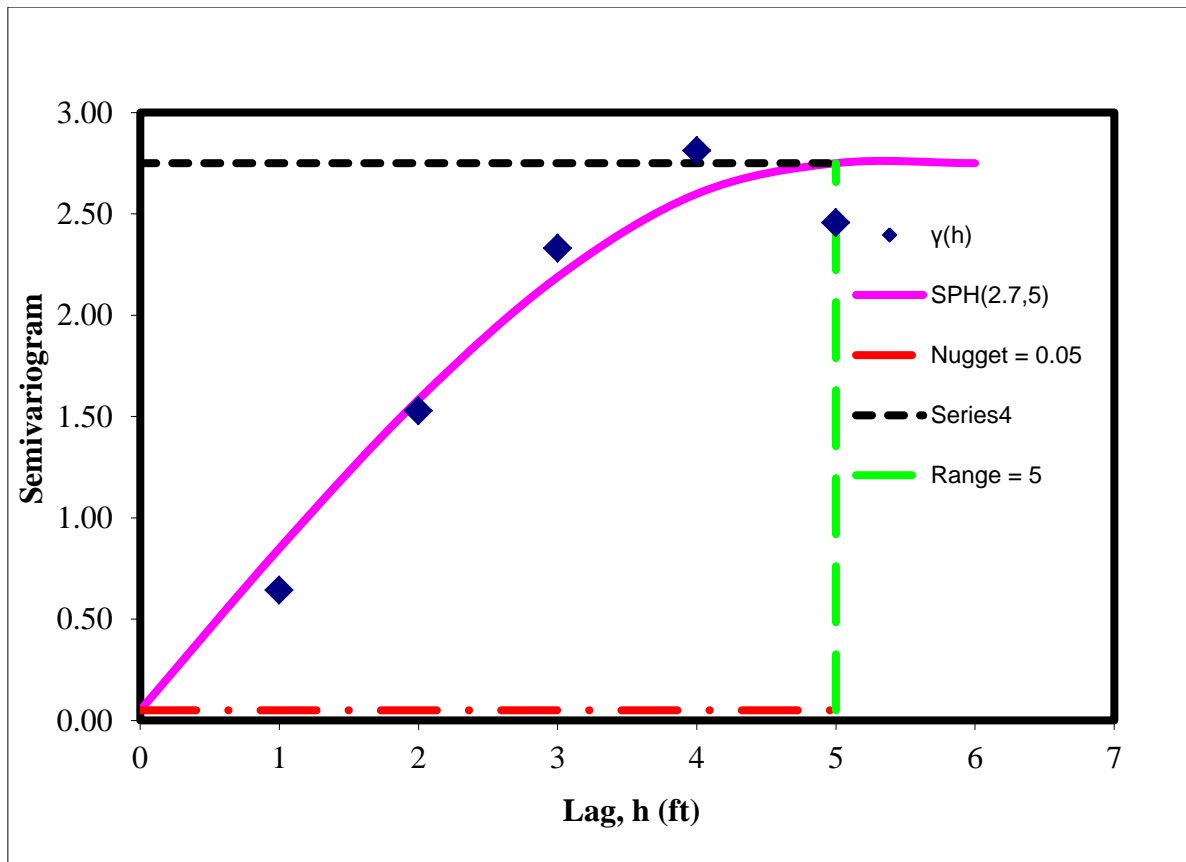
Figure 2. 7: Typical Variogram showing Variogram characteristics

Table 2. 4: Popular Variogram models

Model type	Variogram correlation
The spherical Model	$\gamma(h) = C_o + C\left[\dfrac{3}{2}\dfrac{\|h\|}{a} - \dfrac{1}{2}\dfrac{\|h\|^3}{a^3}\right]$ $\gamma(h) = C_o + C \qquad for\ \|a\| \geq a$
The Exponential Model	$\gamma(h) = C_o + C\left[1 - e^{-\left[\frac{\|h\|}{a}\right]}\right]$
The Gaussian Model	$\gamma(h) = C_o + C\left[1 - e^{\left[\frac{\|h\|^2}{a^2}\right]}\right]$
Linear Model	$\gamma(h) = C_o + m\|h\|$
Generalized Linear Model	$\gamma(h) = C_0 + m\|h\|^\alpha \quad for\ 0 < \alpha \leq 2$
Nugget Effect Model	$\gamma(h) = 0$ $\gamma(h) = C_o \ \ for\ \|h\| > 0$
Cardinal Sine Model	$\gamma(h) = C_o + C\left[1 - \dfrac{Sin(^h/_a)}{\left\|^h/_a\right\|}\right]$

*Where a is the correlation length or range, Co is the nugget effect if present, m is the slope, α is an exponent between 0 and 2 and C is the sill minus Co.

Thus, the krigged estimate is a random variable with a known variance or standard deviation. If the krigged value comes from a normal distribution, then it is possible to draw a simulated value from this distribution that is centered on the rigged value and has a variance that is equal to the estimation variance and a standard deviation that is equal to the estimation standard deviation.

In other words, conventional geostatistical estimation procedures are filtering techniques. They filter out high frequency information and capture only low frequency data. Many of the reservoir properties exhibit short scale variability (e.g., permeability), which may not be captured by conventional geostatistical techniques. Sequential simulation procedures, in contrast, capture this small scale variability (Journel and Albert, 1990). The two principal sequential simulation techniques are Sequential Indicator Simulation (SIS) (Journel and Alabert, 1990), and Sequential Gaussian Simulation (SGS) (Alabert, 1987). SIS transforms the data into discrete indicator variable before simulation, whereas, SGS transforms the data into continuous Gaussian domain before simulation. Although difficult to generalize, SIS has been found to be most useful in simulating geological facies or rock types, whereas, SGS has been found to be most useful in simulating continuous variables such as porosity, permeability, saturation, etc.

The algorithm for performing such a stochastic simulation known as Sequential Gaussian Simulation (SGS) uses estimation equation given in equation 2.20.

$$\theta_{si} = \theta_i^* + \theta_{ei}Z_i \qquad\qquad\qquad 2.20$$

Where θ_{si} is the simulated value at location i, θ_i^* is the kriged value at location i, θ_{ei} is the standard deviation or the square root of the estimation variance at location i and Z_i is a standard normal variate with $\mu = 0$ and $\sigma = 1$ drawn for location i.

The problem with geostatical modeling is that it is computationally difficult to condition the entire model with dynamic data. Also, it is difficult to utilize traditional history match process to condition all the geostatistical models (Alhuthali *et al.*, 2006). Gaussian simulation, Kriging, Kriging with external 3D drift and Collocated cokriging are some of

the techniques that have been found useful for generating multiple descriptions of the reservoir.

2.5 Management of Reservoir Uncertainties

Managing reservoir uncertainties implies reduction of uncertainties or assessment of reservoir uncertainty. Uncertainty reduction could be achieved by carefully planning a timely data acquisition campaign. Efforts should be made to guarantee that the data are acquired following best practice procedures. Assessment of reservoir uncertainties would allow asset teams to analyse the risk associated with development projects.

2.5.1 Uncertainty assessment of static reservoir parameters

Static geological modelling is associated with uncertainties in reservoir geometry and heterogeneities that have a major impact on reservoir bulk and pore volume as wells, as fluids flow in these reservoirs. The two largest static uncertainties – the reservoir geometry as defined by reservoir faults and horizons and the petrophysical property distributions – may be assessed and quantified by geostatistical methods (da Cruz, 2004). Modelling the connectivity of permeable and impermeable zones can be highly uncertain. Geostatistical methods provide means for incorporating connectivity through the indicator variograms, and help in describing the probability of lithologies at different locations resulting in different connectivity (Srivastave, 1990).

2.5.2 Uncertainty assessment of dynamic reservoir parameters

After building the most representative model, a few realizations are generated using geostatistics. These multiple realizations can be ranked to reduce the number of models for further processing with numerical simulator (Friedmann, 2003). Traditionally, the variation of one-parameter-at-a-time approach is used as a sensitivity analysis to assess effects of uncertainties in various dynamic parameters on chosen responses. The dynamic simulation model is validated by matching production history data of existing wells to simulation data by varying selected dynamic parameters such as aquifer pore volume and connectivity, relative permeability data, faults connectivity, or Kv/Kh data. Typically, one or two parameters are varied at a time (Vincent, 1999). This process is tedious and for large fields it becomes close to impossible to investigate relationships between the model responses and variations of different reservoir input parameters. A procedure that combines all uncertainty and allows transferring uncertainties through the numerical flow model up to the production forecasts is highly desired (Ballin, 1993).

2.6 Overview of History Matching

History matching is defined as an act of adjusting a model of a reservoir until it closely reproduces the past behavior of a reservoir. This is a common practice in oil and gas industry in order to have reasonable future predictions. Computation time (and cost) becomes important when we encounter problems with a large number of unknown parameters and will be even more critical when an estimation of gradients is needed. Several methods have been introduced for speeding-up optimization. One efficient way to accomplish this is to introduce a parallel or distributed computing framework (Schiozer

and Sousa 1997, Schulze-Riegert *et al*., 2003). Parallelization is common in global optimization algorithms but can be also effective for computing gradients. The gradient of the data mismatch can also be calculated by the means of using adjoints (Ruijian *et al*., 2003, Dong and Oliver 2005 and 2008).

2.6.1 Traditional history matching

Traditional history matching is performed by trial and error. Reservoir engineers analyze the difference between simulated and observed value and manually change one or a few parameters at a time in the hope of improving the match. In such an approach, reservoir parameters are updated manually and often in two steps: the pressure match and the saturation match (Mattax and Dalton 1991). The quality of this type of history matching largely depends on experience and the amount of the budget. It is important to emphasize that the key elements of traditional History Matching are viable, i.e., integration of domain knowledge and heuristics. Best practices (Selberg, 2007) are integrated into modern workflows. But the tools cannot do without them. The use of modern tools allows structuring of the History Matching workflow, and methods are adopted to interpret the reservoir simulation response and help to guide the decision process.

Since reservoirs are usually very heterogeneous, there are hundreds of thousands of grid blocks in a typical reservoir simulation model to estimate reservoir parameters in high resolution. Therefore, manual history matching is often not reliable for long periods and is always associated with many uncertainties, so computers are employed to automatically vary the parameters. This procedure is called computer aided (semi-automatic) history matching and resulted to multiple solutions. Semi-automatic history matching is defined as

construction of an initial model with an initial approximation of the reservoir parameters which then goes through a systematic process reduction of an objective function that represents the mismatch between observation and calculated response by perturbing the relevant parameters (Guohua *et al*., 2004).

One of the first studies on history matching was done by Kruger, (1961). He calculated the areal permeability distribution of the reservoir. Jacquard and Jain, (1965) developed a method to automate the history matching. Chavent *et al*., (1973) studied history matching in single phase oil reservoirs. The objective was to minimize the difference between observed and actual pressures at the wells with the permeability-thickness product and porosity-thickness product as adjustable parameters. Fasanino *et al*., (1986) studied single-phase history matching of 2D gas reservoirs using the adjoint method in combination with geostatistical information and the pilot point technique. Bi *et al*., (2000) studied the conditioning of three-dimensional stochastic channels to pressure data in single-phase reservoirs. Li *et al*., (2003) studied history matching of three-dimensional, three-phase flow production data. The objective was to minimize the mismatch in flowing wellbore pressure, producing gas oil ratio (GOR) and water oil ratio (WOR).

2.6.2 Optimization Techniques

There are several optimization methods applied in reservoir model simulation and History Matching projects. Commercial and proprietary optimization frameworks and techniques used for real full-field reservoir simulation studies include the following: evolutionary Algorithms (Williams, 2004, Schulze-Riegert, 2007), gradient techniques (Roggero, 1998), response surface modeling and optimization on the response surface (Little 2006), hybrid

schemes which couple different optimization techniques (Castellini, 2006). The most prominent techniques that are receiving a high level of attention in the research community presently are Ensemble Kalman Filter Techniques (Evensen, 2007, Evensen *et al*., 2007). Either method has advantages and limitations. An extensive review first presented in the mid 90's is given by Wen *et al*., (2005).

From various review studies, any optimization method must be transparent, and results must directly relate to verifiable workflows, in order to establish trust and confidence. For instance, the evolutionary algorithms that satisfied these requirements (Wen *et al*., (2005), can provide a methodology for challenging deployment of algorithms for an increasing number of problems which become more and more complex and require solutions in no time. The literature reports multiple implementations of Evolutionary Algorithms (Eiben, 2003). The underlying principle is derived from a population of individuals, the environmental pressure that induced natural selection (survival of the fittest), which leads to an increase in the fitness of the population. Genetic Algorithms are the most widely known type of Evolutionary Algorithm (Gen, 2000, Eiben, 2003).

2.6.3 History matching using response surface methodology

The goal is finding input variable value of the flow simulation that result in a value as near as possible of the observed data. If many observed are available, it is possible to aggregate them into an objective function:

$$OF = \frac{1}{2} \sum_{i=1}^{n} W_i (d_i^{obs} - d_i^{sim})^2 \qquad\qquad 2.21$$

In which d_i are the observed and simulated data and W_i are the weight assigned to the data.

Minimization of the OF means that to match the reservoir production history. Here, history matching process uses the following polynomial;

$$OF = \beta_0 + \beta_1 X_1 + \beta_2 X_2 + \beta_3 X_1 X_2 + \beta_4 X_1^2 + \beta_5 X_2^2 \qquad\qquad 2.22$$

Accordingly, history matching may be done by finding the minimum value for the function equation 2.22. Experimental Designs and Response Surface Modeling (RSM) are often used in diverse workflows to quantify uncertainties and to investigate the propagation of parameter uncertainties by using Monte Carlo sampling techniques. At the same time, the technique are been used to approximate complex simulation models for a number of simulated responses. The whole suite of available optimization methods can then be used to optimize responses based on surrogate models. Full field reservoir simulation results are then captured in a proxy model with a number of chosen design (uncertainty) parameters.

There is numerous response modeling techniques described in the literature (Manceau *et al*., 2001, Montgomery, 2005). Most of the available tools for response modeling generate second order polynomials that are usually, highly dimensional and may not represent a non-linear system well. In order to handle a large number of uncertainty parameters, the polynomial is typically reduced by identifying less sensitive terms, which are excluded from the calculation. Thus, for any history matching (HM) workflow, key parameters are identified based on their contributions to the objective function definition. Depending on the number of parameters, the number of terms increases rapidly. For 20 uncertainty parameters a second order polynomial will consist of 20 linear, 20 quadratic and 190 cross

terms (230 contributions). Once a response surface of acceptable quality is obtained, any optimization technique can be used to identify optimal solutions on the response surface. Identified solutions are verified through full field simulations, and update the database for recalculating an improved proxy model. In all practical application workflows this is an iterative procedure and prior information may be included in a Bayesian formulation which is used in the updating process.

2.7 Proxy Modeling

2.7.1 Experimental design

The increasing demand for systematic and consistent methodologies for analyzing uncertainty and associated effects on investment decisions is responsible for increasing usage of DoE in reservoir management (Vanegas *et al*., 2006). To be able to harness the benefits associated with Design of Experiment (DoE), users must apply it wisely failure of which causes delay in decision making process. Important areas of application of DoE in petroleum engineering include uncertainty screening and uncertainty quantification (Cotento *et al*., 2005, Peak *et al*., 2005). With DoE one can significantly reduce the number of simulations. Previous screening methodologies (Steagall and Schiozer, 2001) consider static sensitivity analysis. Though still applicable for some studies, the dynamic behavior of the sensitivity is important to observe because different uncertainty attributes may have different time of influence on reservoir performance.

Recent research and applied reservoir characterization and modeling projects have focused on the application of DoEs and Response Surface techniques (Almeida *et al*., 2003, Peng

& Gupta, 2003, Amudo *et al*., 2008). Successes recorded from their usage have been found to depend on a number of factors. These include, available time, number of uncertainty factors, the study objectives and amount of details required from integrated reservoir simulation studies. There are several types of experimental designs. Morris, (2000) classified them into fractional factorial design (FRFD), optimal design and Latin Hypercube Design (LHD). The first two classes according to Box *et al*., (2005) and Montgomery *et al*., (2005) are extensively used in the area of physical experiments for model development. LHD is efficient design that allows representation of entire parameter range in the design matrix. Its construction is based on the idea of stratified sampling which requires search algorithms and pre-specified optimality criteria (Box *et al*., (2005).

The underlying assumptions to use 2-level factorial designs are that the 3-factor interactions and higher are negligible. Consequently, most of the experiments are omitted from the analysis and therefore seldom used for construction of response surfaces especially when factors are many and interactions are envisaged. To illustrate this, if we consider 7 parameters system of $2^7=128$-runs for typical full design. Among the 127 degrees of freedom in the design, only 7 are used to estimate the linear terms and 21 to estimate the 2-factors interactions. The remaining 119 degrees of freedom are associated with three-factor interactions and higher that are supposed to be negligible. In practice, if the number of factors ranges between 2 to 15, fractional factorial can be used to screen the significant few by estimating the main effects and interactions. There are various possible fraction designs: 64-, 32- or 16-run design. The 16-run design usually is preferred since this is the cheapest design with resolution IV that is available for uncertainties higher than

eight. Two level Plackett-Burman (PB) designs have been used in the context of classical statistical experiments for screening purposes.

PB designs cannot be used when higher number of levels is required or where simulator proxies development remains the focus of the study. One variable at a time is a screening method involving varying a parameter values between its minimum (-1) and maximum (+1) range within the parameter space. The degree of the displacement from the base case of resultant response indicates the extent of influence the parameter has on the measured response. One variable at a time method is a static sensitivity common in classical laboratory experiments. However, its application for screening large number of uncertainties has been reported (Fatemeh and Nassar, (2012).

The 3-level DoE methods are high resolution algorithms for response surface construction. Central Composite Design (CCD) consists of a factorial design with the corners at +1 of the cube, augmented by additional "star" and "center" points, which allow the estimation of the second order polynomial equation (Allen *et al*., 2003). Like CCDs, Box-Behnken designs are a family of 3- level designs and can be constructed by the combination of factorial and incomplete block designs (Montgomery *et al*., 2005). The application of 3-level full factorial is limited only to four factors or lower due to the associated large number of runs for large number of uncertainty. However, 2-level factorial designs (fractional designs) have also been used where 3-level full factorial is infeasible for response surface construction (Aigbodion, *et al*., 2010 and Mu'azu *et al*., 2012).

Despite its wide applications in the petroleum industry, the DoE method has seldom been compared with MC simulations for uncertainty quantification. DoE provides a proxy of

reservoir models, and it has been used to speed up the history-matching process (Amudo *et al*., 2008; Schaaf *et al*., 2008). The DoE method is more efficient than the direct MC method. Multilevel designs increase the number of simulations significantly, and some mixed designs are more efficient (Kalla and White, 2007). However, a key disadvantage of the DoE approach is that it does not take into account the full probability distributions of the parameters consistently while creating the response surface. Further, because all samples are equally weighted for response-surface generation, there is an inherent assumption that the distributions of these parameters are uniform. As a result, the DoE method may not be appropriate when parameter distributions are arbitrary, which is common in real-world applications.

2.7.2 Analysis of variance

The analysis of variance (ANOVA) is a hypothesis test with the null hypothesis (H_o) that the factor has no effect on the simulator output. The test statistic (F) in an ANOVA is a Fisher distributed random variable with a certain number of degrees of freedom. A large value on the observed test statistic (F_{obs}) indicates that the factor has no effect. The Pr-significance value is defined as the probability of having a test statistic that is at least large as the observed test statistic:

$$P = P(F \geq F_{OBS}) \; otherwise \; the \; null \; hypothesis \; is \; true) \qquad 2.23$$

A small Pr-value means that the probability of getting the observed test statistic, given that the null hypothesis is true, is very unlikely. The null hypothesis is then rejected, and we assume that the factor has an effect.

The following equations are computed. ANOVA partitions total Sum of Squares SST into

3: SSM, SSE and SSR

$$SS_T = SS_E + SS_M + SS_R \qquad\qquad 2.24$$

Where,

$$SS_T = \sum_{I=1}^{N} [Y_I - Y_{PRED}]^2 \qquad\qquad 2.25$$

$$SS_R = \sum_{i=1}^{n} [X_i - \bar{X}]^2 \qquad\qquad 2.26$$

$$SS_E = \sum (Y_i - \bar{Y})^2 - b_i{}^2 \sum (X_i - \bar{X})^2 \qquad\qquad 2.27$$

$$F_o = \frac{SS_R/(p-1)}{SS_E/(n-p)} \qquad\qquad 2.28$$

$$R^2 = 1 - \frac{SS_E}{S_{YY}} \qquad\qquad 2.29$$

$$S_{YY} = SS_R + SS_E \qquad\qquad 2.30$$

$$R_{adj}^2 = 1 - \frac{SS_E/(1-p)}{S_{YY}/(n-1)} \qquad\qquad 2.31$$

2.7.3 Response surface methodology

RSM is one of the simplest techniques for building proxy models. It relates output
variables to input parameters over the entire parameter space. They are usually constructed

with regression method (Friedmann *et al*., 2003, Allen *et al*., 2003). The use of response surface models is detailed by Dejean and Blanc, (1999). When calibrated, the Response Surface Model is used to determine a set of design variables that optimize a response (Risso *et al*., 2007, Ogbalor and Peacock, 2010). A multi-parameter regression method is used to build regression models that link the parameters and the responses. The main interest is to save cost by using the obtained equations for response prediction in place of time costly simulation. The design selected however must have enough coverage so that all the coefficients of the model are estimated accurately and are of predictive capability. An example of the interactive model is:

$$\text{Response} = a_0 + a_1X_1 + a_2X_2 + a_3X_3 + a_{12}X_1X_2 + a_{13}X_1X_3 + a_{23}X_2X_3 \qquad 2.32$$

where X_1, X_2, and X_3 represent the main effects and X_1X_2, X_2X_3, and X_1X_3 account for interaction between the parameters. For modeling studies, where a non-linear relationship exists between the response and factors, the quadratic equation is constructed (equation 2.33).

$$\text{Response} = a_0 + a_1X_1 + a_2X_2 + a_{12}X_1X_2 + a_{11}X_1^2 + a_{22}X_2^2 \qquad 2.33$$

Where a_0, a_1... a_{22} are constant coefficients obtained by fitting a set of numerical simulations. This equation is second order. In matrix notation, the x equations obtained using the models are grouped together and expressed as:

$$y = X\beta + \varepsilon \qquad 2.34$$

X is a (n*p) matrix called the model matrix, y is the n*1 vector of observations of the response, n denotes the number of experiments, p is the number of terms in the model and

ε is any source of variability not accounted for in y. The term, β, is a vector whose elements are the unknown regression coefficients. It is estimated using the ordinary least squares method. This method estimates a vector b by minimizing the sum of the squared residuals. The errors or residual vector is defined as the difference between the observed and the fitted values,

$$e = y - \bar{y} \qquad\qquad 2.35$$

where the fitted model is written as

$$\bar{y} = Xb \qquad\qquad 2.36$$

and is obtained by minimizing L where L is given as

$$L = \sum_{i=1}^{n} \varepsilon_i^2 = \varepsilon^t \varepsilon = (y - X\beta)^t (y - X\beta) \qquad\qquad 2.37$$

b is an unbiased estimate of β. The expression for b is given by

$$b = (X^t X)^{-1} X^t y \qquad\qquad 2.38$$

The covariance of b is very important because it is directly related to the quality of the model. It is a function of the model matrix X and the standard error deviation such that

$$Cov(b) = \sigma^2 (X^t X)^{-1} \qquad\qquad 2.39$$

Where

$$\bar{\sigma} = \sqrt{\frac{\sum_{i=1}^{n}(y_i - \bar{y}_i)^2}{n - p}} \qquad\qquad 2.40$$

The use of Artificial Neural Network (ANN) and Krigging has been reported for resolving nonlinearity issues (Peng and Gupta, 2004). However, appropriate selection of experimental design and sampling techniques can significantly improve model reliability (Yeten *et al*., 2005). Yeten, (2005) studied different experimental designs and proxy-models and their capability to predict uncertainties in selected field performance. A good result was reported in application of Kriging and splines proxy-models with Latin hypercube design. But the same types of proxy-models gave worse results for traditional designs (e.g. Placket- Burman, Central Composite and D-optimal designs). Yet, traditional designs are still popular for proxy modeling in petroleum engineering. The reason is largely due to the ease of obtaining response surfaces whenever experimental design is used. The creation of proxy-models of a high quality is therefore related to the selection of appropriate experimental design algorithms, the quality of the input dataset as well as the degree of non-linearity of input-output relationship.

2.7.3 ANN and Fuzzy Inference system

Artificial Neural Network (ANN) according to Mohagheh, (2000) addresses the problem of non-linearity in the input-output relationship. ANN has been presented as an important tool that can be applied to map the response surface in the multidimensional spaces of a reservoir model (Cullick *et al*., 2006). The mapped response is then used as a substitute of reservoir simulation runs during history matching and production forecast. Some of the limitations of ANN are highlighted by Mohaghegh, (2000), and Olatunji *et al*., (2011). Recent studies have shown that these limitations can be overcome through the application of another Sensitivity Based Linear Learning Methods (SBLLM) in the conventional Feed

Forward Neural Network (FFNN) and the use of Fuzzy logic (Sampaio *et al*., 2009). According to Olatunji *et al*., (2011), SBLLM is an improvement that was able to resolve the instability problem. Fuzzy logic as pointed out by Salam *et al*., (2011), has ability to capture knowledge from data that is inherently imprecise and maintaining a high level of performance in the presence of uncertainty. The original Back-propagation method used in Nets was found to exhibit slow convergence due to large search space dimensions for learning. Fuzzy Inference System (FIS) employs hybrid-learning rules for training process.

Adaptive Neuro-Fuzzy Inference System (ANFIS) employs hybrid-learning algorithm. Hybrid algorithm is a combination of gradient descent and the least-squares method. In the forward pass of the hybrid learning algorithm, node outputs would go forward until last layer and the consequent parameters would be identified by the least-squares method (Roger, 1993). In the backward pass, the error signals propagate backwards and the premise parameters would be updated by gradient descent. The consequent parameters are optimized under the condition that the premise parameters are fixed. Thus, hybrid approach converges much faster than conventional backward propagation as applied to ANN.

2.8 Uncertainty Quantification

With the emergence of new methods for comprehensive evaluation and comparison of risk and uncertainty associated with investment choice, decision-makers are faced with challenges of making choice of methods so that they can be properly guided on the potential profitability and likelihood of achieving various levels of Return on Investment (ROI). In this section we will briefly explain different uncertainty quantification techniques and their characteristics.

2.8.1 Monte Carlo Method

Monte Carlo (MC) simulation is a powerful statistical method that has been used for more than half a century. It has been applied extensively in the petroleum industry for decades. It is employed as an alternative to numerous full-scale reservoir simulations in petroleum industry (Amudo *et al*., 2008). Other areas of its successful applications include reserves estimation, material balance analysis, work-over risk assessment and producing property estimation. MC simulation is extensively used for uncertainty quantification (Zhang, 2002). In the MC method, a large number of realizations of the random inputs are generated and solved to obtain a set of model outputs, which can be further analyzed statistically. The direct-sampling MC method is conceptually straightforward and easy to implement. However, its main disadvantage is the requirement of large computational effort because of the large number of model simulations needed to obtain statistically accurate results. It makes MC simulations prohibitive in most real applications of reservoir simulation, especially for large-scale problems.

One of the critical stages in Monte Carlo is the assignment of distribution functions to different independent parameters. There are several possibilities, different input variables might have different statistical distributions (normal, lognormal, triangular, uniform), or all input variables having the same statistical distribution but with different properties (mean and standard deviation). Those probability density functions have to be determined by trial-and-error while performing Monte Carlo simulation. This is another limitation of using this technique. There are several probability distributions in statistics, but only the

normal and log normal distributions are most commonly observed in petrophysical properties.

Normal (Gaussian) distribution function

The probability density function for a normal distribution is given by:

$$P(x) = \frac{1}{\sigma\sqrt{2\pi}}\exp\left[-\frac{(x-\mu)^2}{2\sigma^2}\right] \quad \text{for} -\infty \leq x \leq \infty \qquad 2.41$$

Where x is a random variable and μ is the mean, σ^2 is the variance and σ is the standard deviation of the distribution. The distribution is characterized by two parameters, the mean (μ) and the standard deviation (σ). The cumulative distribution function for a normal distribution is defined as

$$F(x) = \frac{1}{\sigma\sqrt{2\pi}}\int_{-\infty}^{x}\exp\left[-\frac{(x-\mu)^2}{2\sigma^2}\right]dx \qquad 2.42$$

Log normal distribution function

The probability density function for a log normal distribution is given by

$$P(x) = \frac{1}{\sigma\sqrt{2\pi}}\frac{1}{x}\exp\left[-\frac{(\ln x - \mu)^2}{2\sigma^2}\right] \qquad 2.43$$

where x is a random variable and μ is the mean, σ^2 is the variance and σ is the standard deviation of lnx. The mean, τ, and the variance, ω^2, of the log normal distribution are related to the parameters of lnx as

$$\tau = \exp\left(\mu + \frac{\sigma^2}{2}\right) \qquad 2.44$$

$$\omega^2 = \left(e^{\sigma^2} - 1\right)\exp(2\mu + \sigma^2) \qquad\qquad 2.45$$

It should be noted that x has a log normal distribution whereas lnx has a normal distribution.

To illustrate MCS method, let us consider the model equation for original gas in place (OGIP) estimation:

$$OGIP = \frac{43600\emptyset Ah(1 - S_w)}{B_{gi}} \qquad\qquad 2.46$$

Where A is the reservoir area (acres), h is the pay thickness (ft), $\emptyset$ is the average porosity (fraction), S_w is the average water saturation (fraction) and B_{gi} is the gas formation volume factor (ft^3/ scf)

A random number generator generates random numbers for all the independent variables (porosity, water saturation, and reservoir volume factor), from their user-specified probability density functions. Then the original gas in place is calculated. This process is repeated an arbitrarily large number of times. We get a lot of values of original gas in place from the process using the mathematical model. From those values, we can come up with the probability density function (PDF) and cumulative density function (CDF) for the original gas in place, from which summary statistics such as the mean, median as well as important percentiles and probabilities (P10/P50/P90) can be extracted. The quality of the generated pdf and cdf depend directly on the assumed distributions for all the input parameters. Poor distributions result in a low-quality estimation of the reserves. Selecting distributions and their character parameters is critical to the successful application of MCS.

Guideline for selecting input parameter distributions can be obtained from three sources: Fundamental principles, expert opinion, and historical data. The method has some advantages and disadvantages.

i. The results contain more information about possible outcomes than the deterministic and scenario approach.

ii. MC results are continuous distributions such as probability density and cumulative-distribution functions instead of discrete points as the case is with deterministic approach.

Thus it gives users the probability of the most likely outcomes. Users can evaluate the risks associated with the reserve estimated for the purpose of making investment decisions. The users can even obtain a confidence interval for the predicted variable–how likely the predicted value will be located within an interval. However, performing Monte Carlo simulation can be time consuming especially for large number of factors requiring knowledge of statistical distribution. The details of the mathematical foundation and implication of the associated assumptions are provided in chapter 7.

2.8.2 Decision/realization tree method

The risk analysis methodology implemented by Steagall and Schiozer, (2001) is based on the simulation of several flow models that represent the possible scenarios of the reservoir, through the combination of the uncertain attributes. The simulation models are built automatically through the decision tree technique. Each final branch of the decision tree corresponds to a complete simulation model. The probability of each resulting model is

equivalent to the product of the conditional probability of the attributes that composes it. Schiozer *et al*., (2004) used this technique. The objective function is the root of the multiple realization trees. The most significant parameter is placed at the first level consists of pessimistic, most likely and optimistic. The next significant factor is located next level and so on.

This is illustrated as shown in Figure 2. 8. The probabilities for the pessimistic, the most likely, and the optimistic value are assigned based on experience and from the insight gained from similar studies. Suppose that there are n reservoir parameters in the multiple realization tree, the tree will have n levels (excluding the Objective function), resulted to 3^n leaves (9 leaves for 2 factors), which are located at the very bottom of the tree. The probability for each leaf is the product of the probabilities of all its ancestors. For example, the probability of the left-most leaf is the product of the probabilities of pessimistic porosity, and pessimistic permeability. For each leaf, we have to conduct one simulation run to get the root.

2.8.3 Relative variation factor method

This method had been successfully used by Salomao, and Grell, 2001 to assess uncertainty in production profiles on the basis of Geostatistics characterization and flow Simulation. The methodology shares similar characteristics with the DoE and Response Surface. The starting point is the selection of the most influential reservoir parameters affecting an objective function. These factors are kept at their most likely values and are used to estimate the most likely quantities. This is followed by determination of the probability density functions for the objective function. To determine the probability density function,

one parameter is selected and varied while keeping all the other factors at their base case values. For *n* number of parameters, we will have to make $2n+1$ simulation runs, including the base case in which every reservoir parameter are set to its most likely value. The next step is to divide the resultant low, mid and high realizations quantities by the base case quantity which results in three values: a real number less than 1, 1, and a real number greater than 1. After this, we can construct a triangular distribution with these three numbers, and this gives the probability density function for the selected parameter. The probability density function of the selected objective function is the product of the reference hydrocarbon volume and the probability density functions of the most influential reservoir parameters for the objective function.
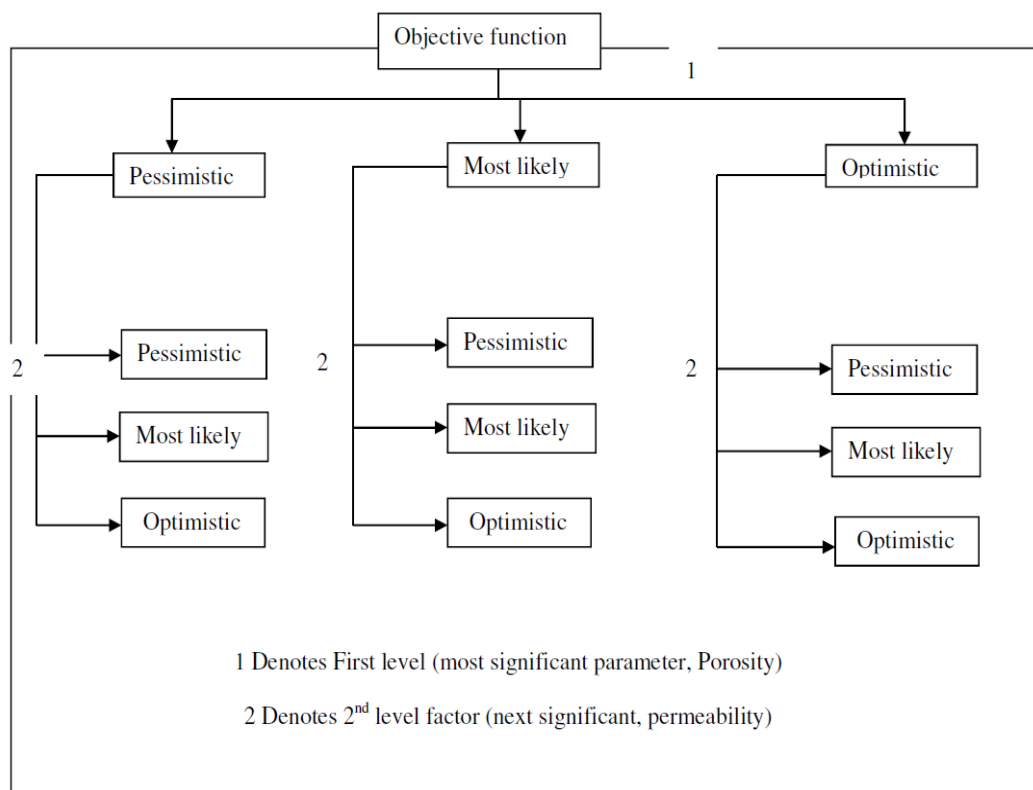
Figure 2. 8: Multiple realization tree for two key parameters (Porosity and permeability)
1 Denotes First level (most significant parameter, Porosity)
2 Denotes 2nd level factor (next significant, permeability)

This is obtained using Monte Carlo simulation. For illustration, if we consider OGIP as the objective function, using this method the expression for MCS is given as:

$$OGIP = OGIP_{base\ case} * \Delta_1 * \Delta_2 * ... * \Delta_n \qquad\qquad 2.47$$

Where n is the distribution of the hydrocarbon volume; $OGIP_{base\ case}$ is the value of the hydrocarbon volume for the base case; Δ is the distribution of the variation factors for the identified key parameters that affect the OGIP. The advantage of this method is that it requires fewer number of simulation runs for instance, if the identified number of key factors is 8, the maximum number of simulation runs to be made is 17. This is much lower when compare with experimental design or realization tree methods. The limitation of this approach is that it ignores the effect of factor interactions.

2.8.4 Bayesian approach

Bayes' theorem can be used in many applications in which we need to access the probabilities of the causes. The method has been applied in uncertainty analysis in the petroleum industry for some years (Barker *et al*., 2001). The philosophy is based on theorem from probability theory first proposed in the eighteenth-century by Thomas Bayes. A brief illustration of the theorem is to assume B_1, B_2… B_n to be n mutually exclusive outcomes of some event B. if we let A (A is not perfect information; it simply correlated to the event B, otherwise, Bayes' theorem is not needed) be an outcome of an "information" or a "symptom" related to B.

Then,

$$P\left(B_i/A\right) = \frac{P\left(A/B_i\right)P(B_i)}{\sum_{j=1}^{k} P\left(A/B_j\right)P(B_j)}$$

2.48

where $i = 1,2,3 \ldots\ldots k$

P (A / B_i) is the conditional probability of event A occurs when B_i event has happened.

P (B_i) and *P (B_j)* are respectively the probability of events B_i and B_j

P (B_i/A) is called the *probability of the causes.*

Scales and Snieder, (1997) explained the use of Bayes' theorem with this illustration thus if suppose by previous work we know something about a model before using available data (the prior knowledge and conjectures are called the *a priori* model), this knowledge is transformed into likelihoods or probabilities. Often probabilities are assumed to follow a Gaussian distribution. Suppose we then have a set of data with their variance and covariance, Bayesian approach provides a method to fine-tune the *a priori* model with the set of available data. The posterior distribution tells us how the data correct the prior knowledge.

2.9 Overview of infill drilling

Infill drilling is one of the reservoir development concept usually implemented to recover residual oil saturation. The determination of the amount of residual oil saturation after primary and secondary recovery processes has been a challenge. Locating the oil to be recovered is a difficult exercise and requires sophisticated techniques. Egbogah provided extensive review of those techniques (Egbogah, 1994). Volumetric reservoir engineering

studies and core analysis can indicate amount of the remaining oil but not the distribution of it. Tracer tests or well test methods are used to determine the location and distribution of the oil remained. Table 2. 5 shows a brief review of some of the techniques used to determine the amount of remaining oil.

The success of infill drilling as pointed out by Subbey *et al.*, (2003) and Bustamante *et al.,* (2005), is directly related to the uncertainties associated with it. Individual reservoir characteristics all add up to give a resultant total uncertainty associated with reservoir performance. Analytical models are characterized by several assumptions and are becoming less efficient in estimation and quantification of various uncertainties due to increasing complexity of petroleum reservoirs.

According to Ofoh, (1992), infill drilling can improve the recovery of hydrocarbon by accelerating the hydrocarbon productions. However, the determination of infill potential as well as selection of well type and placement has been a challenge (Thakur *et al.*, 1998). The recommended way to determine infill-drilling potential in a reservoir is to conduct a complete reservoir evaluation involving geological, geophysical, and reservoir analyses and interpretations. This approach is prohibitively time-consuming and expensive for some large hydrocarbon fields (Linhua *et al*., 2005). Infill Drilling Predictive Model (IDPM) which requires minimum amount of reservoir and geologic description has also been used (Fuller *et al*., 1992). However, IDPM requires knowledge of heterogeneity elements (pay continuity and permeability variation among layers.) which are not easily or often measured in actual fields. Voneiff and Cipolla, (1996) developed a model-based analysis method, the moving window technique, and apply it for rapid assessment of infill and re-

completion potential in the Ozona field. The method according to the author is quick but the accuracy decreases with increasing heterogeneity. Empirical correlations (Hudson *et al*., 2000) are also available to determine infill potential in a complex, low-permeability gas reservoir. These correlations are reservoir specific and therefore have gained limited applications. The use of numerical-based instead of analytical based conceptual models has been reported (Pathak *et al*., 2000).

Table 2. 5: Summary of correlations for determination of residual oil saturation

Methods	References	Correlations
Core residual oil saturation	(Kazemi, 1977)	$(\overline{S_o})_{res} = (\bar{S}_o)_{core} B_o E \dfrac{M}{1 - V^2}$
Logs	Waxman and Thomas, 1968	$S_w = \left[\dfrac{R_o}{R_t}\left(\dfrac{1 + R_w B Q_v}{1 + \dfrac{R_w B Q_v}{S_w}}\right)\right]^{\frac{1}{n}}$
Volumetric-Reservoir Engineering		$S_{or} = \dfrac{(N - N_p)B_{oWF}}{7758 A H \emptyset}$
Production data	Arps, 1995 and Fetkovich, 1987	$S_o = \dfrac{V_o}{V_p}$ $= \dfrac{(N_{foi} - N_p)B_o}{N_{foi}B_{oi}(1 - c_f \Delta P)/(1 - S_{wi})}$
Well Testing	Ramey, 1975	$S_o = \dfrac{c_t - c_w - c_f}{c_o - c_w}$
Chemical Tracer	Tomich *et al*., 1973	$V_i = \dfrac{(1 - S_o)V_W + K_i S_o V_o}{(1 - S_o) + K_i S_o}$
Log-inject-log	Verma *et al*., 1991	$SORW = \dfrac{0.06(1 - S_w)}{\emptyset}$

Conceptualized models have been used to provide answers to frequently asked questions such as the numbers of wells and their optimum placement within the reservoir (Ogbe *et al*., 2009). In this study, full field numerical simulation approach was used to evaluate infill location, selection and placement.The study utilized pressure and saturation maps to determine infill well locations within the reservoir sub-regions.

Chapter 3

3. Stochastic Modeling

3.1 Problem Description

In this case study, the STOIIP was earlier estimated as 27 million stock tank barrels. However, the analysis of production performance after fifteen years indicated a recovery factor of approximately 40% for a reservoir under primary production scheme. It is apparent from this figure that the reserve is under estimated. The main objective is to determine realistic figure by revisiting the static model and assess associated uncertainty. The Schlumberger- PETREL software was used for building the static model.

3.2 Static Modeling

To build the static model, the workflow shown in Figure 3. 1 was adopted. The methodology involves data acquisition, quality checking, petrophysical analysis, Geocellular modeling, and development of geological concept, property upscaling, Variogram modeling, properties distribution, volume calculation and uncertainty quantification.

3.2.1 Data acquisition and quality checking

Table 3. 1 shows all the available well logs in all the wells and includes lithology logs (GR-log and SP), resistivity logs, density (RHOB), sonic logs and Neutron logs. Check

shot data is also available in most of the wells. Following the depth-matching of the density and resistivity curves to reference gamma ray log, normalization of gamma ray logs was carried out out and synthetic logs [Volume of shale (V_{sh}), water saturation, effective porosity and net-to-gross (NTG) logs] were derived for all Wells. The correlations used for the synthetic log estimations are presented in the Appendix A.

Table 3. 1: Distribution of logs in the wells

	DT	DTL	GR	LLD	LLS	MSFL	NPHI	RHOB	RT	SGR	SP
1			X	X							X
2	X		X	X	X						X
3			X	X	X	X		X			X
4	X	X	X	X	X			X		X	X
5	X	X	X	X	X	X	X	X	X	X	X

The only structural map available is that generated for the most likely case (base case). In order to capture the uncertainty of interpreted surface map, a "high" and "low" realization maps was generated using a ±10 ft from the base case respectively. This assumption was made through expertise advice and by observations during the well correlation. The "Low" and "High" case structural maps were used to generate the extremes uncertainty models. The stratigraphic frameworks were constructed using the uncertainty surfaces and information from the well logs. Figure 3. 2 shows the well correlation panel with sections showing the picked horizons. The well correlation was successfully carried out and there is little or no uncertainty at the well bore. In order to manage the uncertainty away from the wells this research took the advantages of inherent uncertainties in the structural map for developing stochastic models using Geostatistics techniques.
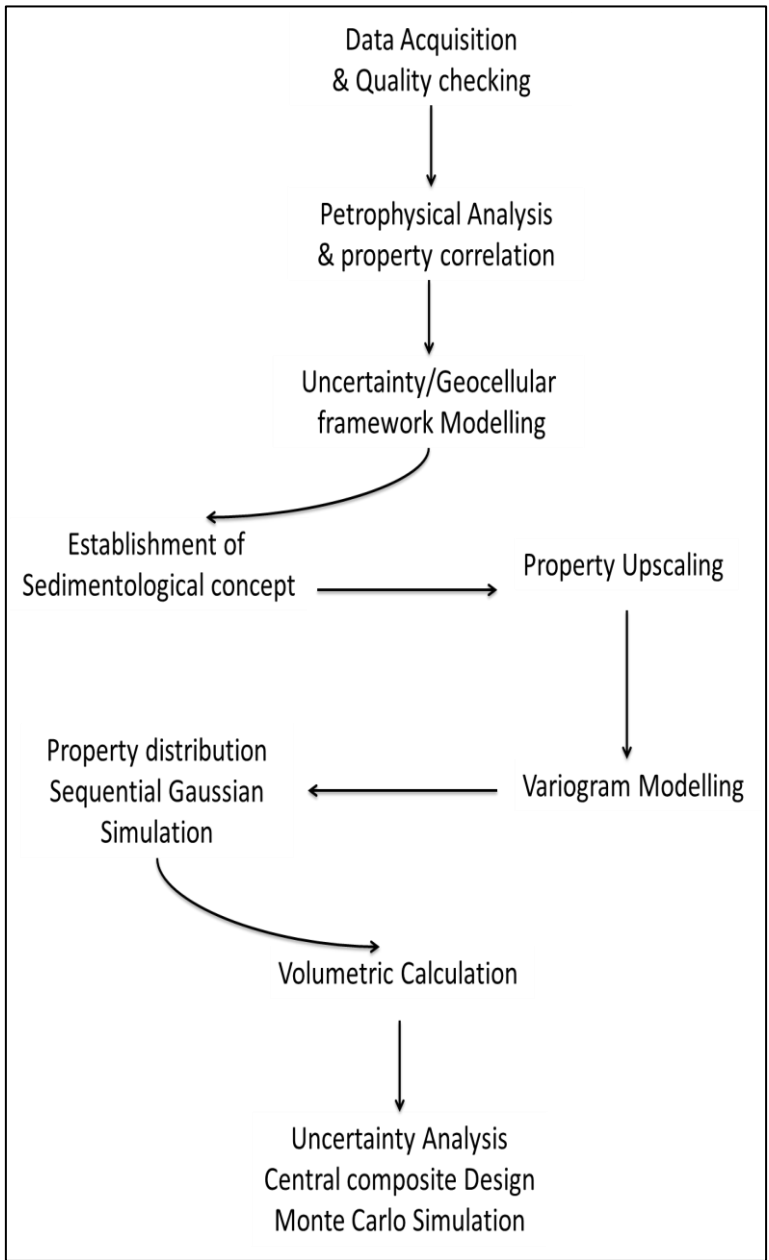
Figure 3. 1: Workflow for Static and uncertainty Analysis
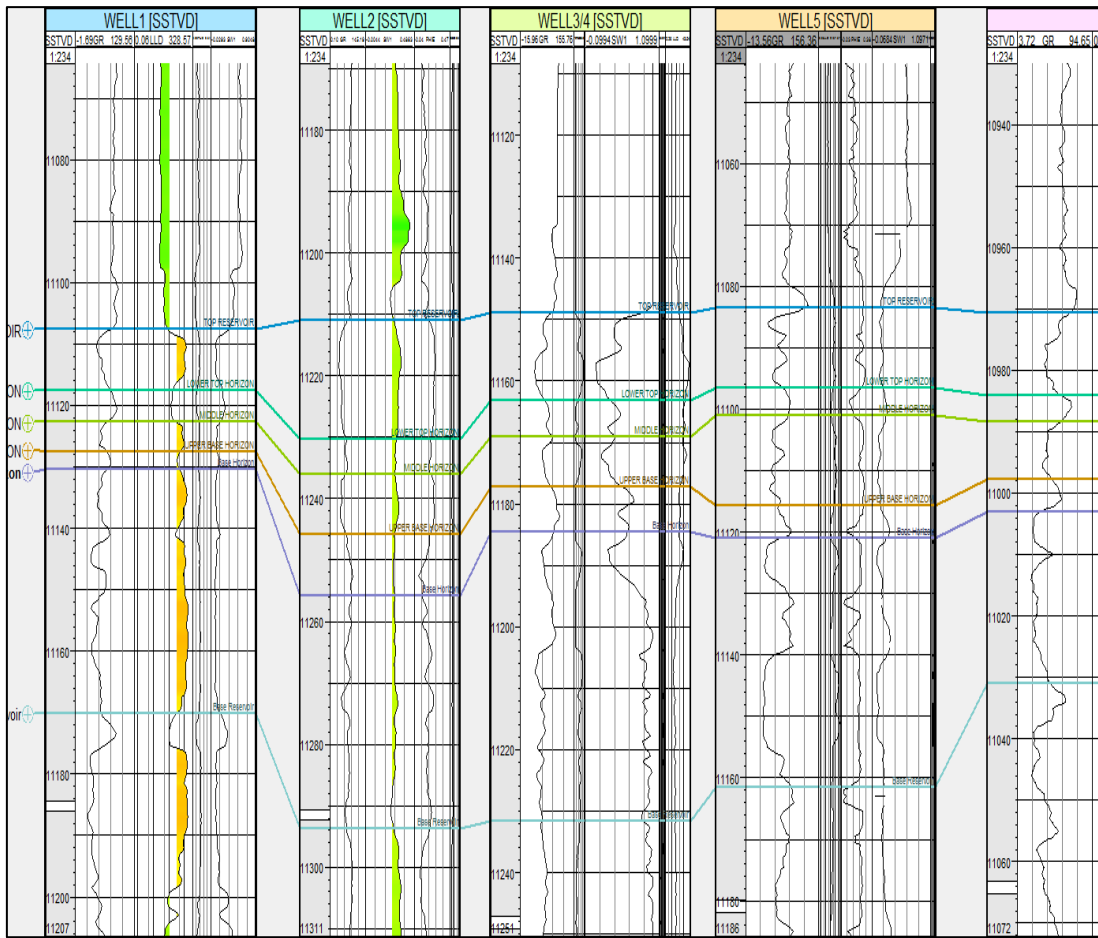
Figure 3. 2: Well section showing different picked horizons

3.2.2 Petrophysical Evaluation

The petrophysical evaluation was carried out in the six wells within the clean sand intervals. The result of the analysis shows that the porosity values from all the wells range between 19 and 27%. In all the logs, the estimated V-shale values range between 12 and 76% using a cut-off margin range from 55 to 57% across wells. Within the reservoir, the V-shale value is between 0.05 and 12%. Thus, the reservoir is relatively clean with shale intercalation. Although, these values are far below the limit of 10 to 15% that can affect

water saturation according to Hilchie, (1978), the fact that the sand is not completely clean, it could affect the water saturation model. Thus, water saturation is one of the uncertainties identified from this stage. The effective water saturation (S_w) was estimated using the Indonesian model. The need to adequately condition the saturation log estimates to V_{sh} informed the decision to select Indonesian correlation instead of Archie's model. The water resistivity was obtained using Pickett plot to be 4.2 Ωm while average shale resistivity of 0.047 Ωm was obtained from the log. The obtained S_w average value of 19% implies the occurrence of hydrocarbons within the sand intervals. The deep and shallow resistivity logs indicated the presence of hydrocarbon within the sand while neutron-density logs suggested that the fluid in the reservoir is oil.

3.2.3 Property cross-plots

Figure 3. 3 shows the graph of porosity versus V_{sh}. It is evident the existence of a strong correlation between the porosity and V_{sh}. Porosity fitted well with V_{sh} using a polynomial model with high correlation coefficient (R-square = 0.9). This value of R-square indicates that the polynomial correlation can be used in the property distribution process with high confidence. The downward sloping of the graph from left to right indicated that porosity is negatively correlated with V_{sh}. This is expected within a hydrocarbon interval. It is also evident from Figure 3. 3 that porosity values are more concentrated where the V_{sh} values are smaller. Such interval could be very good for hydrocarbon storage if the water saturation is small. This is generally true as shale formations are characterized by a low porosity values. The scatter plot of porosity and permeability in Figure 3. 4 shows non-linear correlation between the two properties.
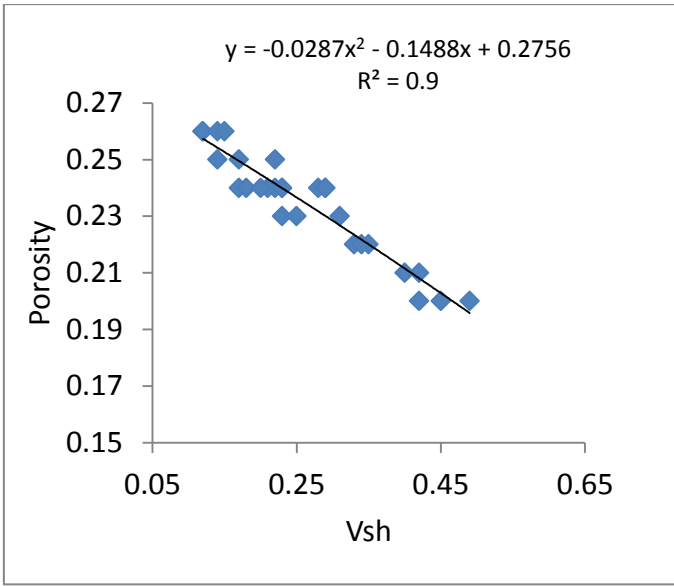
Figure 3. 3: Scatter plot of Porosity versus Volume of shale (V_{sh})
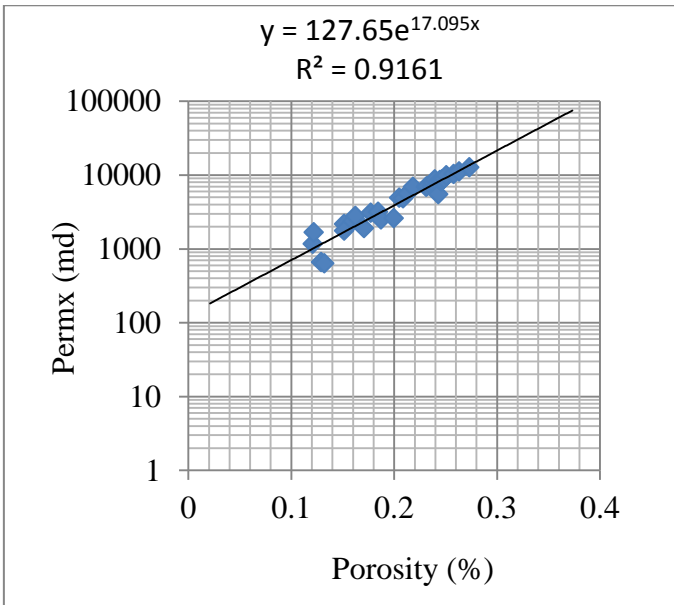
Figure 3. 4: Scatter plot of permeability versus porosity

However, porosity varied positively with logarithm of permeability. As the porosity increases, the permeability also increases. The model equation is displayed on the graph with high correlation coefficient of correlation (R-square = 0.92). The coefficient as high as this value indicated that such model equation can be employed for property distribution if adequately constrained with other properties.

3.3 Construction of Geocellular Models

The Geocellular frameworks were constructed with a commercial reservoir simulator using 32,634 grid blocks. The cell size ($\Delta X*\Delta Y*\Delta Z$) used is 50 m x 50 m x1ft which was believed to have captured all the intra-reservoir heterogeneities. In order to manage the uncertainty away from the wells, Variogram models were built for all the properties from well log. Property estimation was done using kriging and Sequential Gaussian Simulation methods as described in section 3.3.1.

3.3.1 Property distribution

The methodology adopted for the distribution of the various petrophysical properties comprises of four major steps:

Step 1: Development of a geological concept:
This involved building of horizontal trend maps for all the Para-sequences that made up the reservoir. The reason was to establish how shale volume trends within the reservoir. The ultimate reason that necessitates this was due to lack of facies model or information from where this could be modeled. It was therefore conceived that developing characteristic trends for shale volume at different layers of the reservoir, the distribution can be used to

constraint other properties. Figure 3.5 shows the porosity and Vsh trends for the Top and

Middle horizons while Figure 3.6 represents the NTG and V_{sh} trends for the Top Lower

and Base horizons.
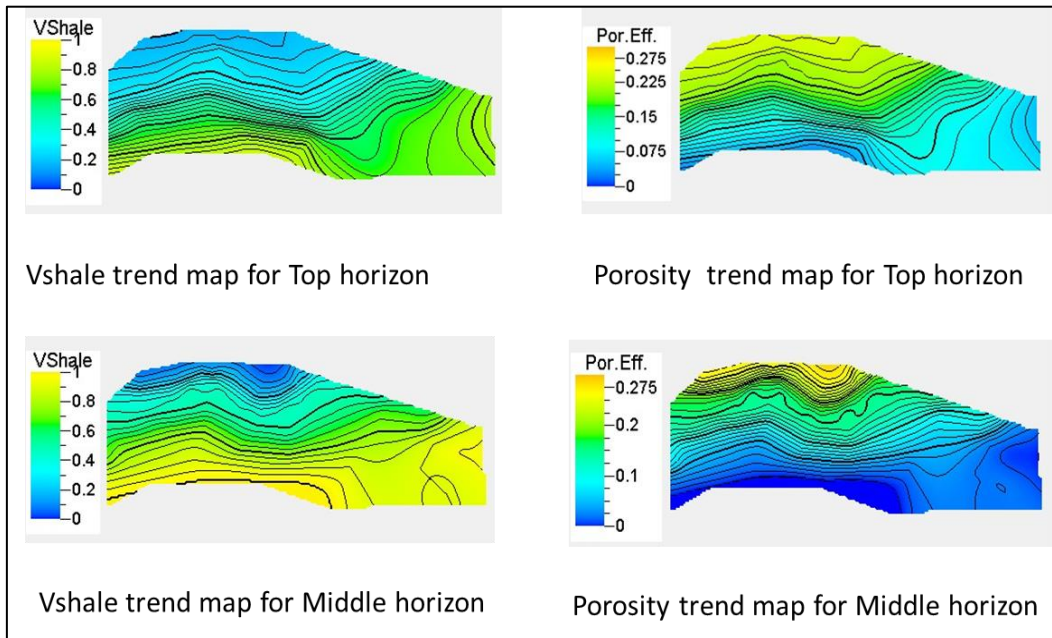
Figure 3.5: Developed horizontal trends for V_{sh} and Porosity for Top and Middle horizons

Step 2: Upscale the property to the resolution of the grid using arithmetic operations.

This was done to ensure that the properties at the wells are exact. Thus uncertainty at the

wells assumed zero since this is the only places where information is available.

Step 3: Develop Variogram models for the different properties

Variogram was developed for distribution of different properties at different zones. This

was done using the data analysis tool on the Petrel software. Different properties exhibited

different correlation structure which was used for estimating and conditioning simulation.
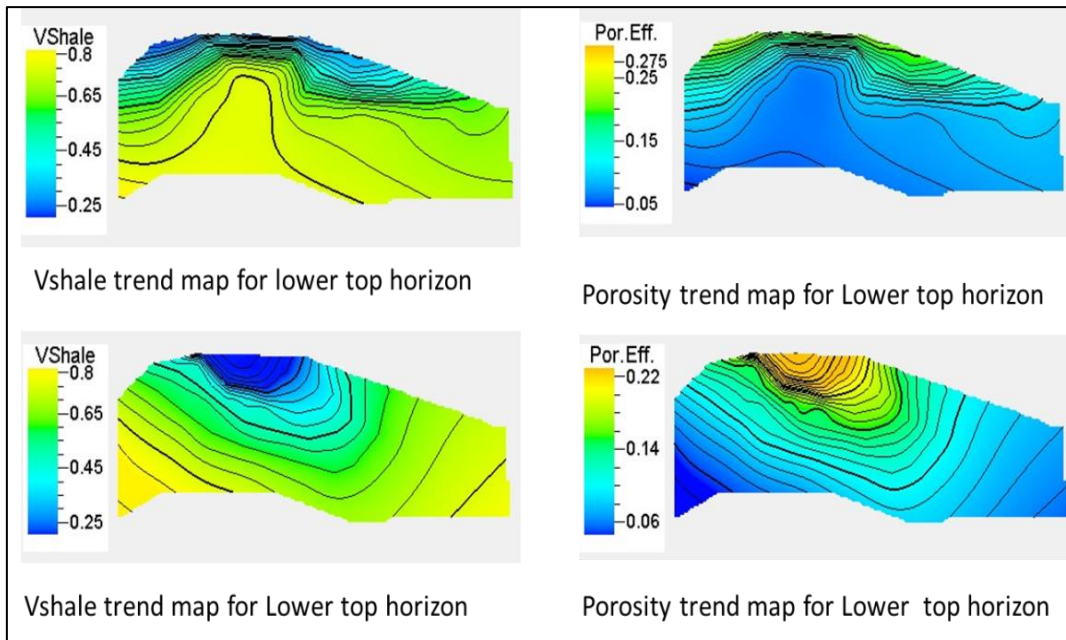
Figure 3.6: Developed horizontal trends for V_{sh} and Net-To-Gross for Lower Top and Base horizons

Step 4: Distribution of properties to the grids

The established V_{sh}, property histograms and Variogram models were used to constraint the distribution using Sequential Gaussian Simulation algorithm. Figure 3. 7 shows the histograms and cumulative density functions (CDF) for the various properties-Vsh, Porosity, NTG, and permeability. As observable from Figure 3. 7, permeability and NTG show log normal distribution. V_{sh} histogram shows skewed normal distribution with mean and standard deviation of 0.5 and 0.4. Porosity histogram also depicts a skewed normal distribution with mean and standard deviation of 18.8% and 4%. Figure 3. 8 shows Petrel template for Semivariogram model for V_{sh} correlation. This was repeated in all zonation that made up of the model architecture. Spherical Variogram model was adequate for V_{sh} with major range of 2500, minor range of 1000, vertical distant of 100 ft, Azimuth of 60° and sill and nugget of approximately 1 and 0 respectively.

73
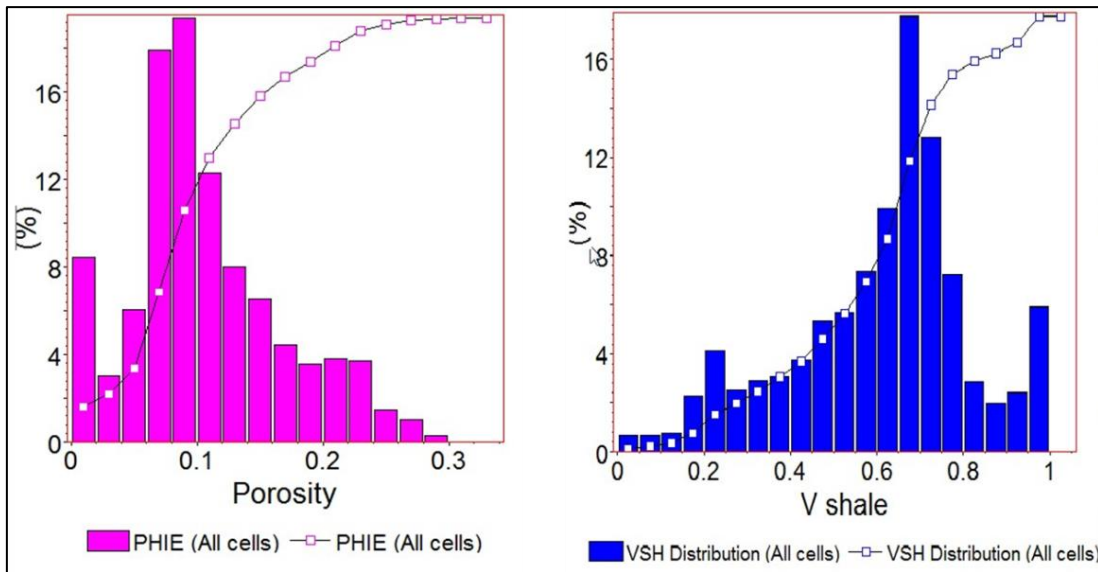
Figure 3. 7: Property histogram and cumulative density function

Similar Variogram models were developed for porosity and NTG. Sequential Gaussian simulation and Kriging with external drift were tested for the distribution of porosity and NTG. Sequential Gaussian simulation gave the best match with the well data. Spherical Variogram with major range of 800, minor range of 400, dip angle of 60°, sill of approximately 1 and nugget of 0.1 were considered adequate for the distribution of NTG. To have good control over the distribution, porosity and NTG were co-kriged with the V_{sh} property. The cross plot of porosity versus V_{sh} was used to further constrain porosity distribution in each zones. Collocated co-Kriging method was used to build the permeability model. The high value of polynomial correlation coefficient (R-square = 0.92) between permeability and porosity shows that the model is suitable to condition the distribution of permeability. Property distribution used an Exponential Variogram model having major range of 5000, minor range of 2500, dip angle of 60°, sill of 1 with nugget of 0.
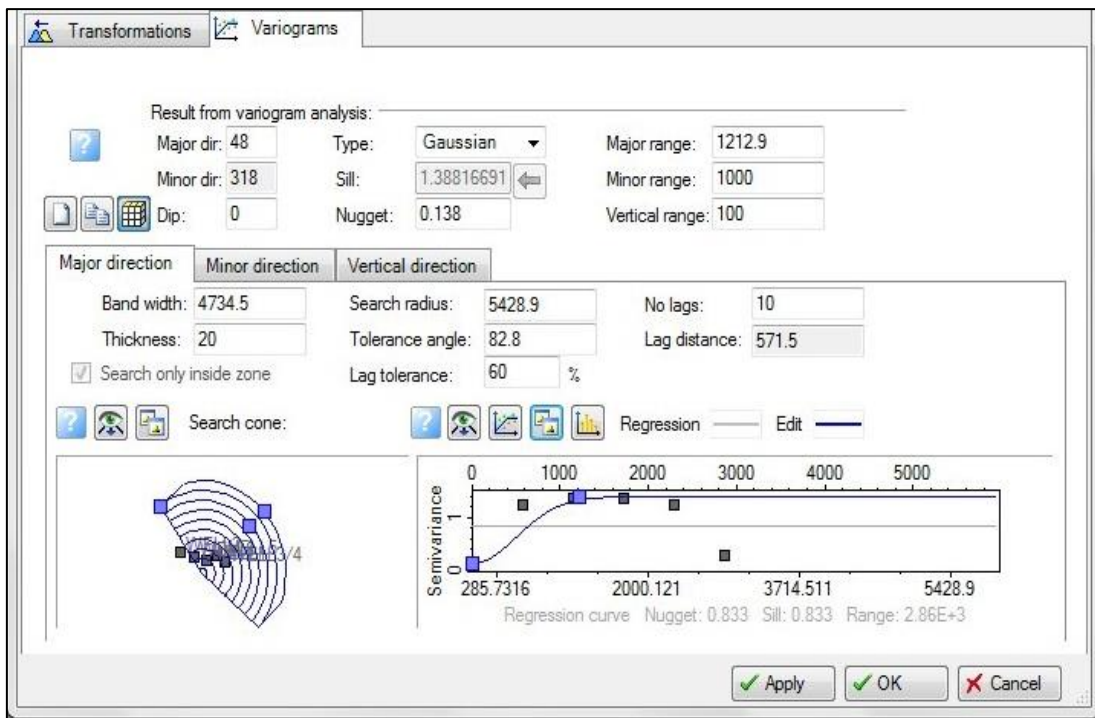
Figure 3. 8: Settings panel for Variogram Modeling in PETREL

Water saturation was estimated from well logs using the Indonesian correlation due to the heterolithic nature of the sands and to properly account for the shaliness of the hydrocarbon intervals. To populate the water saturation into the grid cells, a number of algorithms was tested. Collocated co-Kriging conditioned with V_{sh} gave the satisfactory result for water saturation. Using cross plot of water saturation versus porosity, bivariate distribution which gives full control of the distribution within the models is possible. Both primary (S_w) and secondary property (porosity) were specified.

Figure 3. 9 depicts the isometric views of the reservoir properties. One important observation common to all the properties is that they exhibit heterogeneity laterally. This could be attributed to their depositional history. Figure 3. 10 shows average property maps illustrating the variability of the properties within the reservoir. From the V_{sh} map, the V_{sh}

distribution shows that shale volume increases from North to South. At the crest of the structure where the wells are located, the V_{sh} ranges between 0 and 10% which justified the location of the drainage points. This value increases down the structure both to the East and West up to a maximum V_{sh} value of 75%.
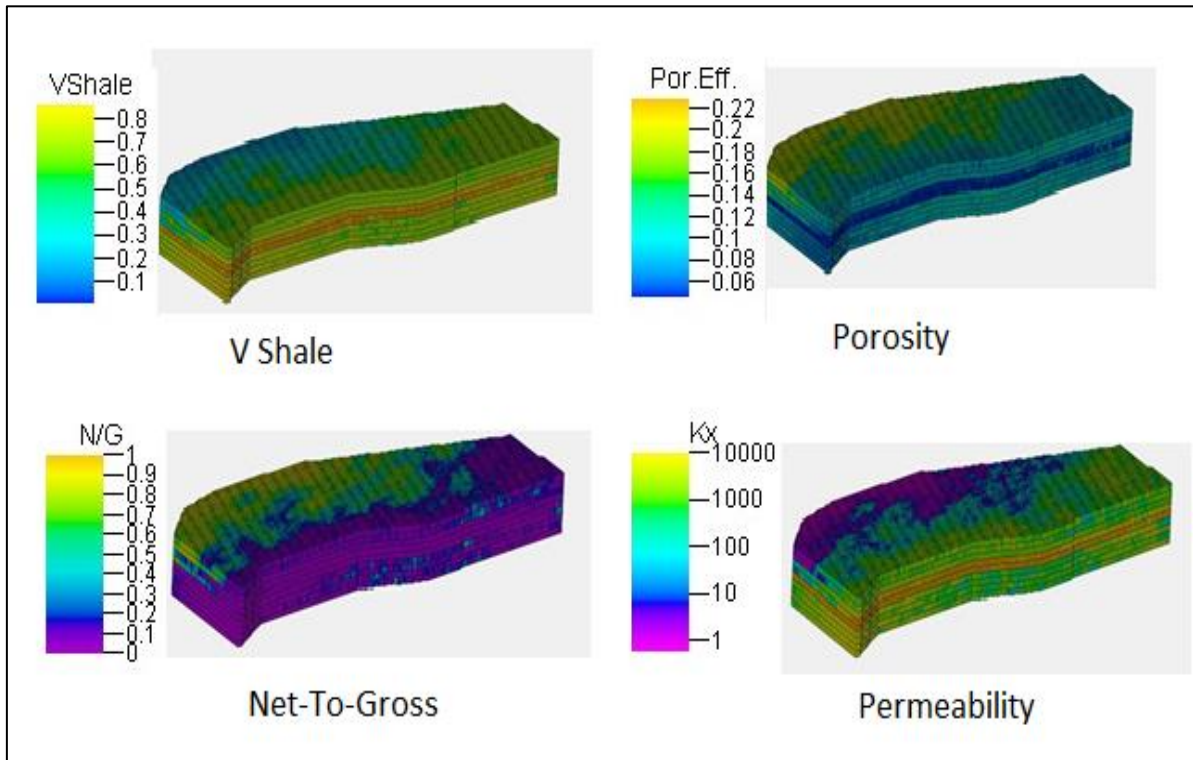
Figure 3. 9: Isometric View of the Reservoir Properties

The water saturation map shows increasing water saturation from the North towards the South. The minimum water saturation of 19.2%   was found at the crest of the structure while saturation as high as 67% occurs in the South. Both porosity and Net-To-Gross properties show high values in the upper structure and decrease from North to South. Permeability distribution is similar to the porosity distribution with minimum and maximum values of 13 mD and 2154 mD, respectively in the models.

76
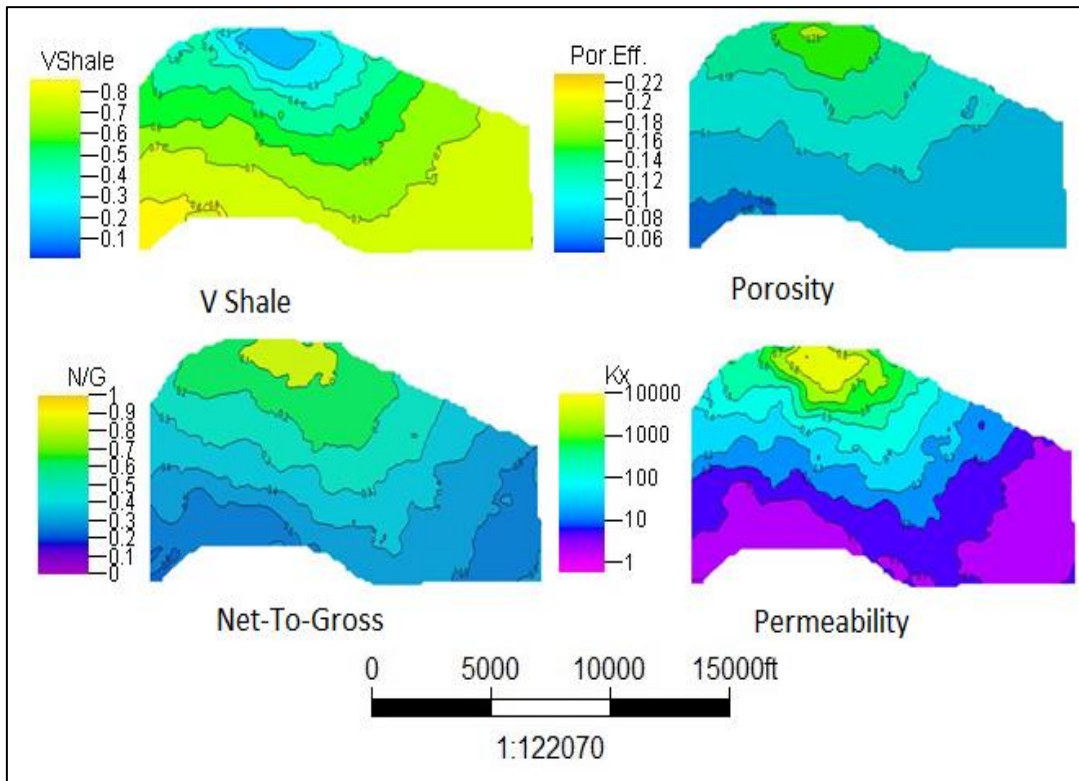
Figure 3. 10: Average Property Maps

Figure 3. 11, Figure 3. 12 and Figure 3. 13 show the distribution of V_{sh}, porosity, Net-To-Gross and horizontal permeability in Layers 1, 3 and 5, respectively. All the properties exhibit high level of variability across the layers. A lateral continuity that can be attributed to the presence of stacked sandstone beds that are laterally continuous typical of a shore face environment was observed. Although, Facies model was not generated for this study, owing to the fact that core information was not available for supervision of the facies distribution as at the time of carrying out this study, all distributions were conditioned to V_{sh} following our developed sedimentological concept.

77
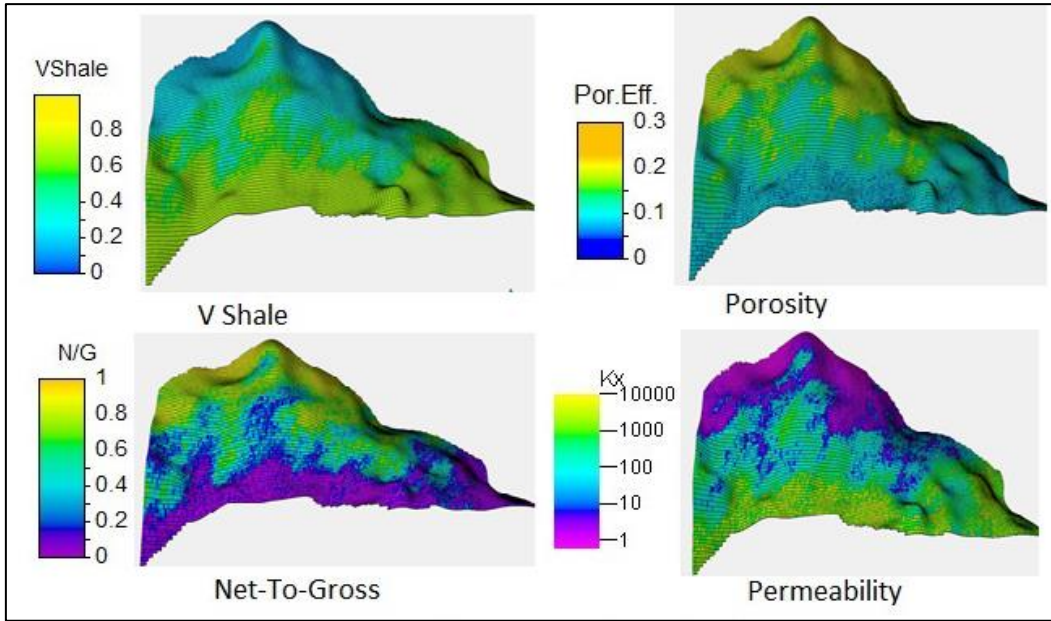
Figure 3. 11: Property distribution in the Layer 1
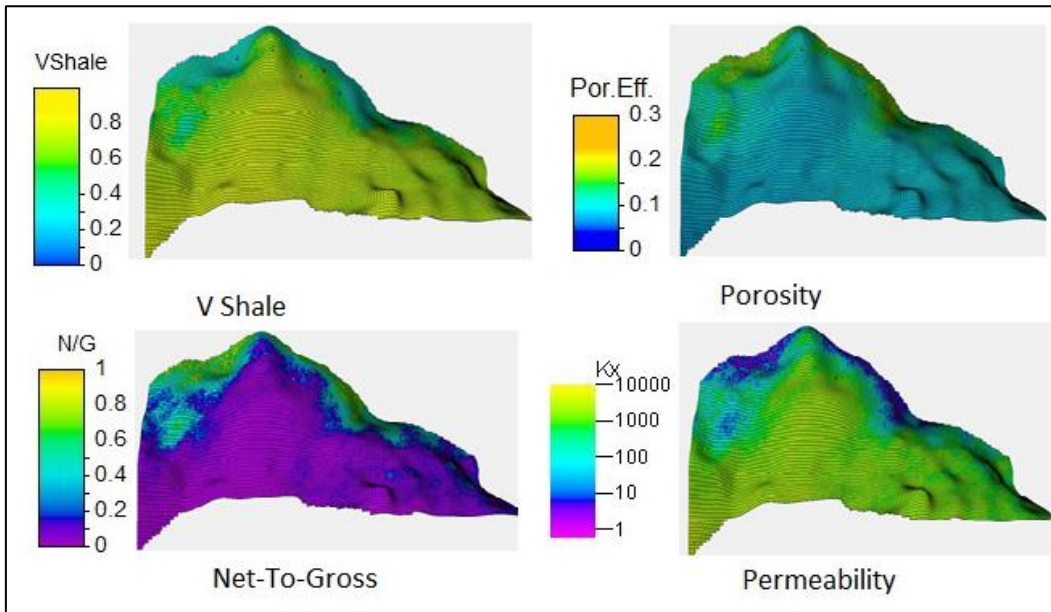
Figure 3. 12: Property distribution in the Layer 3
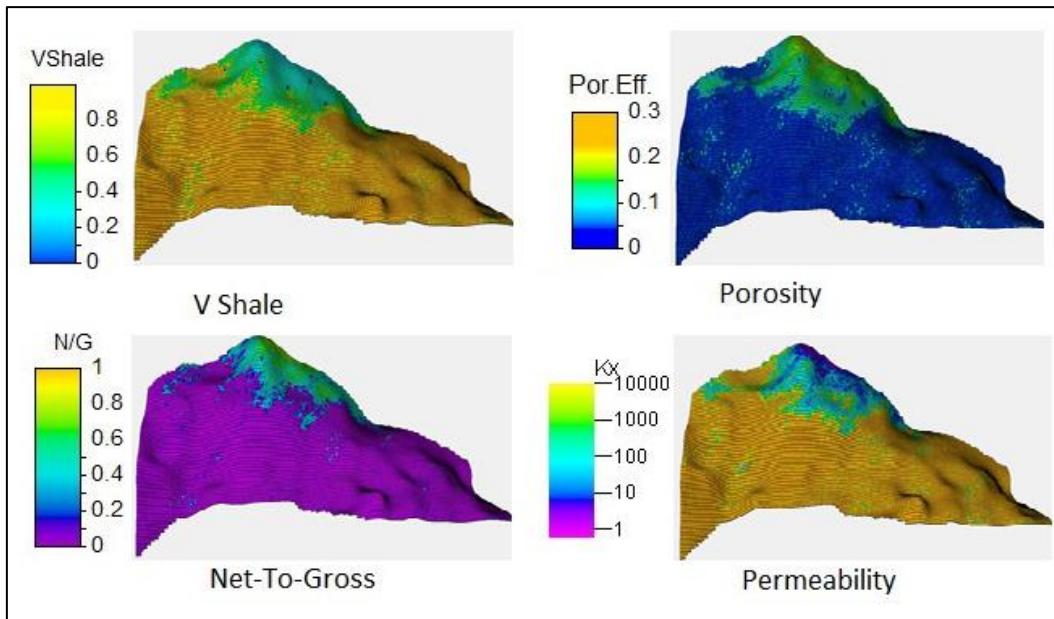
Figure 3. 13: Property distribution in the Layer 5

We recognized uncertainties in these models especially in the permeability distributions that we assumed to be horizontally isotropic which may not reflect the actual local spatial distribution of permeability. This drawback may affect the predictions as permeability has a major effect on the fluid flow according to Kupfersberger and Deutsch, 1999.

3.3.2 Oil-In-Place Estimation and Uncertainty Quantification

A set of volumetric uncertainties, "low", "mid" and "high" were calculated from the "Low", "Mid" and "High" case models. The uncertainty models were combined with the hydrocarbon contact to arrive at the volumes that captured the range of uncertainties. The formation volume factor (B_{oi}) was derived from PVT analysis to be 1.25Scf/STB. Table 3. 2 shows some important uncertainty quantities obtained from the three models which depict a marked difference in the reservoir pore volume, net volume, and bulk volume and the STOIIP.

Table 3. 2: Deterministic Volumetric Uncertainties

Cases	Pore Vol (RB)	Net Vol (bbl)	Bulk Vol (bbl)	STOIIP (STB)
High	123	742	2017	55
Mid	117	666	2015	53
Low	116	663	2017	50
Average	118.7	690.3	2016.3	54

3.4 Volumetric Uncertainty Quantification

3.4.1 Uncertainty factors and their ranges

Uncertainty analysis was quantified on STOIIP using the 'Low', 'Mid' and 'High' case static models. They were treated independently to represent low, mid and high ranges of uncertain structural factor in an experimental design. In coded form, similar to other parameters, the low, mid and high case models are denoted by (-1), (0) and (1) respectively.

The main uncertainties affecting the evaluation of STOIIP for the reservoir are as follows:

   i. Porosity

  ii. Hydrocarbon saturation

 iii. Net-to-Gross

 iv. Oil Water Contact

  v. Thickness

The selection of the multipliers for the ranges of uncertainties conforms to the practice in the Niger Delta fields. This requires using 5-10% uncertainties on the hydrocarbon saturation, 1-10% on porosity, 1-5 meters on hydrocarbon contacts, 5-10% on reservoir NTG. Table 3. 3 shows various factors and range of parameters.

Table 3. 3: Uncertainty and their range of Multipliers

Uncertainty	Units	Low	High
PHIE	fraction	0.9	1.1
Sw	fraction	0.9	1.1
NTG	fraction	0.9	1.1
OWC	ft	0.9	1.1
Thickness	ft	-10	+10

3.4.2 Design of experiment

Table 3. 4 shows the CCD matrix used to conduct the experiment in coded form. Fifty (50) experiments at various conditions were performed (see Appendix C3). The choice of CCD was based on the need for accurate proxy model for the Monte Carlo. CCD, unlike other response surface models, allows changing parameters at 5 levels (-α, -1, 0, 1, +α). The design matrix consists of 42 non center factorial designs with the corners at ±1 of the cube, augmented by additional "star" and eight rotatable "center" points (±α), which allow the estimation of the second order polynomial equation. The data set was partitioned into two, 40 data set were used for model building while the remaining data was used for validation. In order to study the effects of the main variables and possibly the interaction effects of the

identified uncertainties, the significance of the various parameters was determined using

Analysis of Variance (ANOVA). This was done by rejecting null hypothesis.

Table 3. 4: Experimental Design Matrix (CCD)

Run	PHIE	SW	NTG	OWC	Thickness	Run		PHIE	SW	NTG	OWC	Thickness
1	1	-1	1	1	-1	26		1	1	-1	1	-1
2	-1	-1	1	-1	1	27		1	-1	1	-1	1
3	0	0	0	0	0	28		-1	1	-1	-1	1
4	0	0	0	0	0	29		0	0	2	0	0
5	2	0	0	0	0	30		0	0	0	0	0
6	1	1	-1	-1	-1	31		1	1	1	1	-1
7	-1	1	1	1	1	32		1	1	1	1	1
8	-2	0	0	0	0	33		-1	-1	-1	-1	-1
9	0	0	0	0	2	34		0	0	0	0	0
10	1	-1	-1	-1	-1	35		1	1	-1	-1	1
11	1	-1	1	1	1	36		1	1	-1	1	1
12	-1	-1	1	1	1	37		-1	1	-1	-1	-1
13	-1	1	-1	1	1	38		0	2	0	0	0
14	0	-2	0	0	0	39		0	0	0	0	-2
15	0	0	0	0	0	40		-1	1	-1	1	-1
16	0	0	0	0	0	41		-1	-1	-1	-1	1
17	-1	-1	-1	1	-1	42		1	-1	-1	1	-1
18	0	0	0	0	0	43		-1	-1	-1	1	1
19	-1	1	1	-1	-1	44		1	-1	-1	1	1
20	-1	-1	1	1	-1	45		1	1	1	-1	1
21	1	-1	1	-1	-1	46		1	-1	-1	-1	1
22	0	0	0	-2	0	47		0	0	0	2	0
23	1	1	1	-1	-1	48		-1	1	1	1	-1
24	0	0	0	0	0	49		-1	1	1	-1	1
25	-1	-1	1	-1	-1	50		0	0	-2	0	0

3.4.3 Analysis of variance

To determine whether there is a linear relationship between the response and various factors, test for significance of regression was performed by Analysis of Variance. Fisher variable (F) and its associated probability (prob>F) was used to assess the model significance and to select regressors with high impact on the model. A 95% confidence level (i.e. $\alpha = 0.05$) was assumed for the analysis. Table 3. 5 is ANOVA for CCD. The Model F-value of 149.28 implies the model is significant. The p-value obtained implies that there is only a 0.01% chance that a "Model F-Value" this large could occur due to noise. Values of "Prob > F" less than 0.0500 indicate models terms are significant. In this case main factors PORO, SW, NTG, OWC and thickness are all significant model terms. Also, some significant interaction terms include PORO*OWC, PORO*NTG and NTG*OWC. With the combination of these factors, the final proxy model developed is:

$$STOIIP\ (MMSTB) = 5558.31582 - 5159.61258 * PORO - 3.01510 * SW -$$
$$3758.42013 * NTG - 0.49283 * OWC - 0.057327 * thickness + 70.78169 * PORO *$$
$$NTG + 0.45782 * PORO * OWC + 0.33282 * NTG * OWC \qquad 3.1$$

Using this model, the mean estimated STOIIP is 53.33 MMSTB. This figure approximates the experimental value of 55 MMSTB with standard deviation of 1.13, covariance of 2.1 and adequate precision of 66 (value > 4 is desirable).

Table 3. 5: Analysis of Variance for STOIIP

Source	Sum of Squares	DF	Mean Square	F Value	Prob > F
Model	1523.24	8	190.41	149.28	< 0.0001
PORO	750.79	1	750.79	588.61	< 0.0001
SW	3.56	1	3.56	2.79	0.01041
NTG	813.59	1	813.59	637.85	< 0.0001
OWC	336.16	1	336.16	263.54	< 0.0001
Thickness	10.43	1	10.43	8.18	0.0073
PORO*NTG	12.84	1	12.84	10.06	0.0033
PORO*OWC	5.37	1	5.37	4.21	0.0482
NTG*OWC	2.84	1	2.84	2.23	0.1453
Residual	42.09	33	1.28		
Lack of Fit	42.09	26	1.62		
Pure Error	0	7	0		
Cor Total	1565.33	41			

3.4.4 Model Validation

Figure 3. 14 shows the cross plot of the actual experimental values against the predicted values. Also on the same graph is the plot of the validation. The alignment of the values to the 45° line shows that the model is predictive in nature. The maximum error (equation 3.2) recorded for the validation using developed model was 6%. The high correlation coefficients obtained (R-square = 0.97, Adj. R-square = 0.97 and prediction R-square = 0.96) show that the model terms are significant and overall, the model is reliable and can be used to sample the space within the uncertainty ranges. This equation can therefore be applied for uncertainty quantification.

$$E_{max} = MAX_{I=1}^{n}|E_i| \qquad\qquad 3.2$$

Where,

$$E_i = \left|\frac{Measured - Predicted}{Predicted}\right|_i * 100$$
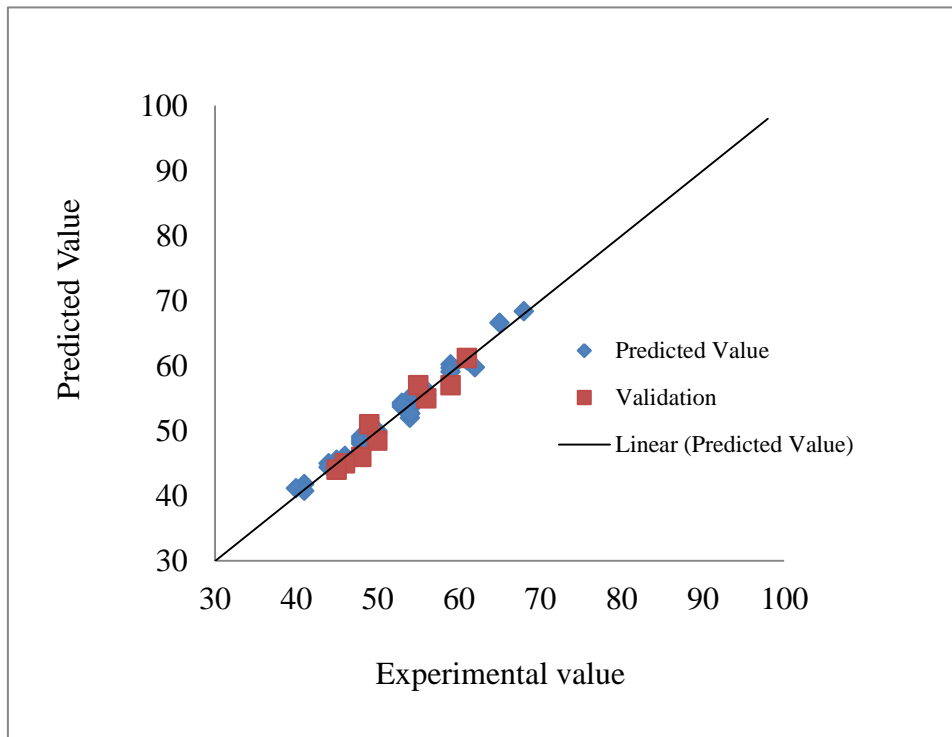
Figure 3. 14: Parity plot showing the cross actual values against the predicted value

3.5 Uncertainty Quantification

Linear, perturbation, and the scenario creation approach are some of the available methods for quantifying uncertainty. Because these methods are faster and easier for uncertainty quantification, they are commonly used. However, as these methods utilize a single reservoir description model (RDM), they often underestimate the associated uncertainty.

This study imposed probability distribution function and described the chance of obtaining a parameter value on the proxy model (Eq. 3.1) developed. An experimental probability distribution was first determined, thereafter, a theoretical distribution that would have produced such a sampling distribution were determined. After the uncertainty associated with each individual input parameter is determined by probability density function, they are treated individually and transformed into a composite uncertainty associated with the simulation model.

The relationship between the parameters was observed to be nonlinear so the interaction between the individual inputs parameters was determined by ANOVA. The choice of probability distribution for the input parameters was guided by histogram plots and experience from the neighbouring field. Most of these uncertainties do not follow normal distribution patterns. Rather, their logarithm is normally distributed and an estimation of upside potential (10%), 50%, and downside risk (90%) was determined. Figure 3.6 shows the summary of the simulation statistics. Figure 3. 15 is the Tornado chart showing the degree to which various uncertainties impact the response (STOIIP). The impacts of the main attributes on the response were observed with porosity having the maximum influence. Porosity, NTG and OWC have positive influence on the response (STOIIP) with porosity the biggest driver. Both water saturation and structural map have a negative influence on the response. The combined effect of structural map on the estimated volume is a negative one. The probability density function and the STOIIP cumulative distribution curve are shown in Figure 3.15b. The results show that there exists 10% probability of having mostly 59 MMbll, 50% chance of equalling or exceeding 53 MMbll and 90% chance of having 47 MMbll of STOIIP.

Table 3. 6: Summary of Simulation Statistics

Name	STOIIP (MMSTB)	PORO	SW	NTG	OWC	Thickness
P10	47.091	0.919	0.654	0.919	11225.400	-8.501
P50	52.620	0.999	0.974	0.999	11231.000	0.000
P90	58.919	1.079	1.295	1.079	11236.500	7.999
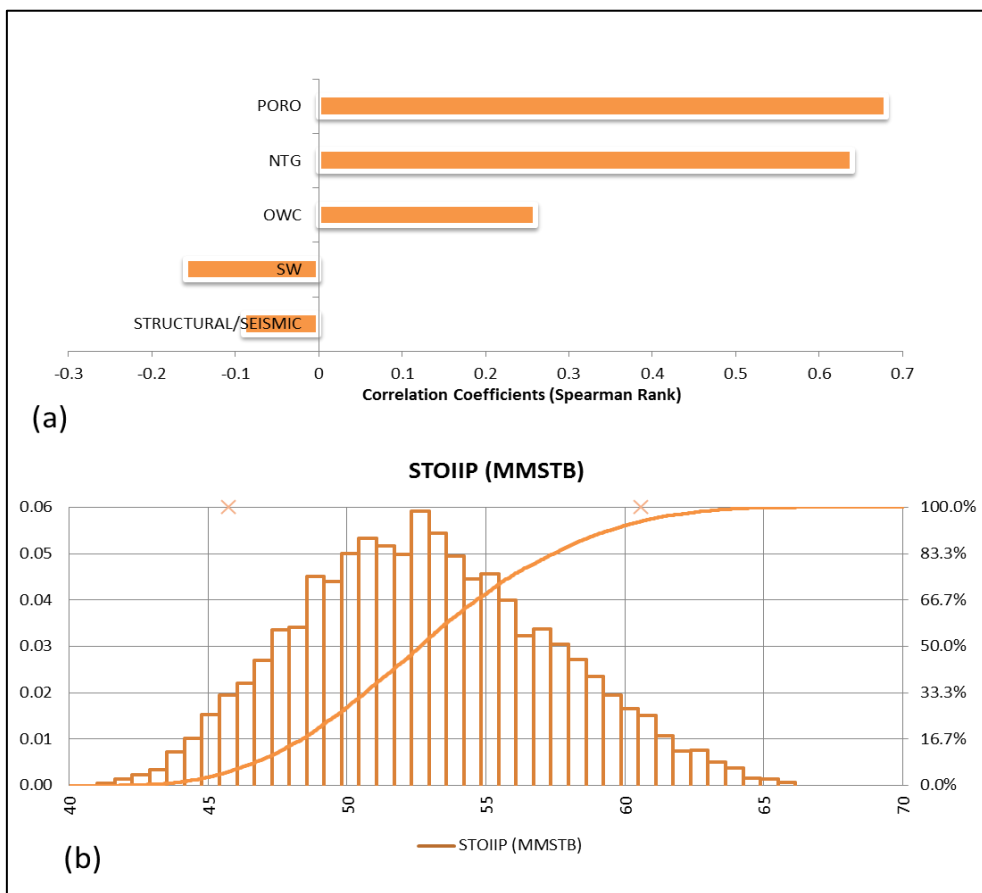
Figure 3. 15: (a) Tornado chart showing impact of various parameters on STOIIP (b) Probability and Cumulative Density for STOIIP

3.6 Summary

The objective was to develop static model and carry out the uncertainty analysis on the volumes of hydrocarbon in place. The proposed methodology can be summarised as follows:

i. Three (3) static reservoir models were built based on the uncertainty in the structural map.

ii. Before the distribution of properties in the geological models, the study developed sedimentological concept using the distribution of shale within the formation. Geostatistical method was applied for property prediction away from well. All the properties were constrained using the volume of shale, histograms and properties cross plots to ensure geological consistency aerially and vertically.

iii. To quantify uncertainty in hydrocarbon volume, CCD algorithm was used to combine all uncertainties with each model treated as uncertainty.

iv. The reliability of the model was tested before subjected to Ordinary Monte Carlo simulation. A good correlation coefficient between the actual response and prediction (R-square = 0.97) testified to the accuracy and reliability of the proxy model.

v. The result shows that the earlier estimation was underestimated and that there exists 10% probability of having at most 59 MMbll, 50% chance of equalling or

exceeding 53 MMbll and 90% probability of having at least 47 MMbll of STOIIP.

Chapter 4

4. History Matching and Uncertainty Analysis

This Chapter covers review and quality checking of available PVT and other dynamic data; material balance analysis to evaluate the aquifer properties; preparation of input data to initialize the simulation model; history matching to calibrate the dynamic model to field production history; and prediction of reservoir production performance. The dynamic model was built using exported properties from the static models in the chapter 3. Static and dynamic properties were integrated then the model initialized to equilibrate to the initial pressure and saturation conditions. The static models were validated by matching historical pressures and saturations observed from the reservoir. The available production data span between 1993 and 2006. The simulation of pressure and water cut was used as the basis for validating the quality of the history match. Prediction runs were performed to estimate reserves and generate production forecasts uncertainties for the three model cases in order to estimate the ultimate oil recovery from the reservoir and provide proper management concept for its optimum recovery.

4.1 Review of reservoir data

The reservoir was completed with four wells, all deviated; AK-01, AK-02, AK-03 and AK-04. The oil is characterized by average API gravity of 35 ^{o}API and viscosity ranges between 1-1.3cp. The initial pressure was given to be 4951 psia at reference depth of 11142 ft and reservoir average temperature is 170°F. Within the reservoir, porosity

averaged at 26% and average water saturation observed is 19.6%. None of the wells encountered an oil-water contact. However, the deepest oil-down-to (ODT) was seen by AK-02 at 11231 feet. Production started from the reservoir from AK-01 in November 1993 with an average oil rate of 1500 stb/day, GOR of 500 scf/stb, and a BS&W of 0.05%. AK-02 was opened to production in May 1995, both AK-03 and AK-04 was completed in August, 1995. A peak oil production of 5000 stb/d with a GOR of 620 Mscf/stb and a BS&W of 0.13% was attained in the reservoir in November 1998. Subsequently, the reservoir experienced a production decline with increasing BS&W and GOR. Due to inactive water drive, pressure decline of approximately 28% was recorded at the end of December 1998. Cumulative production from this reservoir as of December 2006 is 26 MMstb of oil, 30 Mscf of gas, and 2.1 MMstb of water.

Figure 4. 1 and Figure 4. 2 show the reservoir production performance and the cumulative oil, water and gas production in the reservoir. The production performance indicates a realistic trend in oil and water production. Due to gas metering issues in the facilities, it was assumed that the gas volumes recorded had inherent errors. Hence, apart from the primary phase (oil rate) that will be constrained in the saturation match, preference was given to matching the water cut. The workflow adopted for history matching follows that from Almeida *et al*., (2003). Saturation match took place after matching the pressure. This involves changing one parameter-at-a-time. Uncertainty attributes were identified in the course of sensitivity study and field water-cut and cumulative water production for the period of 15 years was matched.
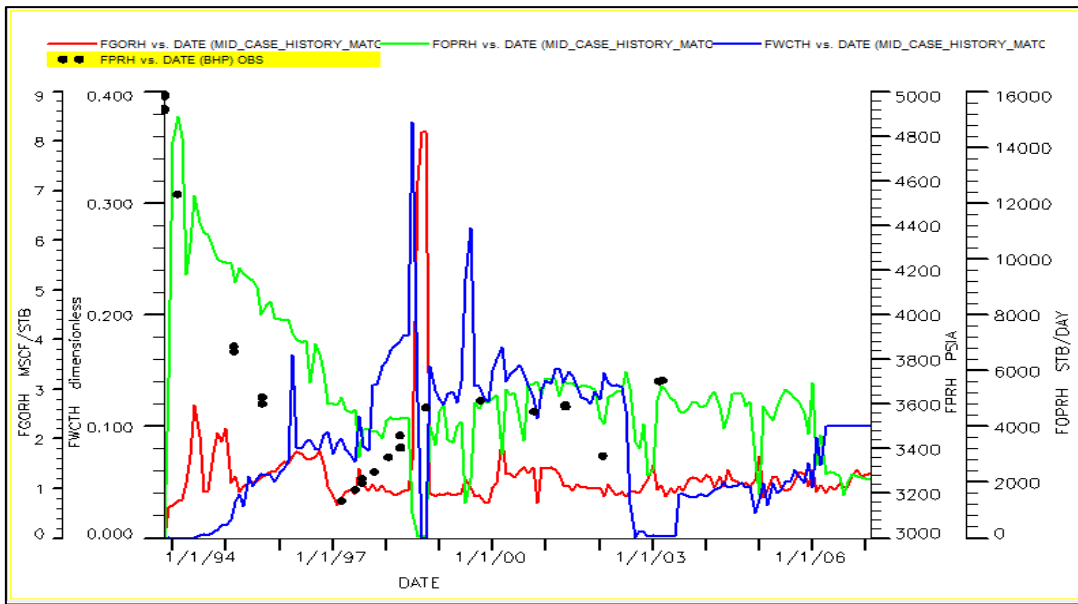
Figure 4. 1: Performance plots showing oil rate, GOR, pressure & BSW versus time.

Water cut (Blue color), reservoir pressure (black colour), Field oil rate (Green colour), and GOR (Red Colour)
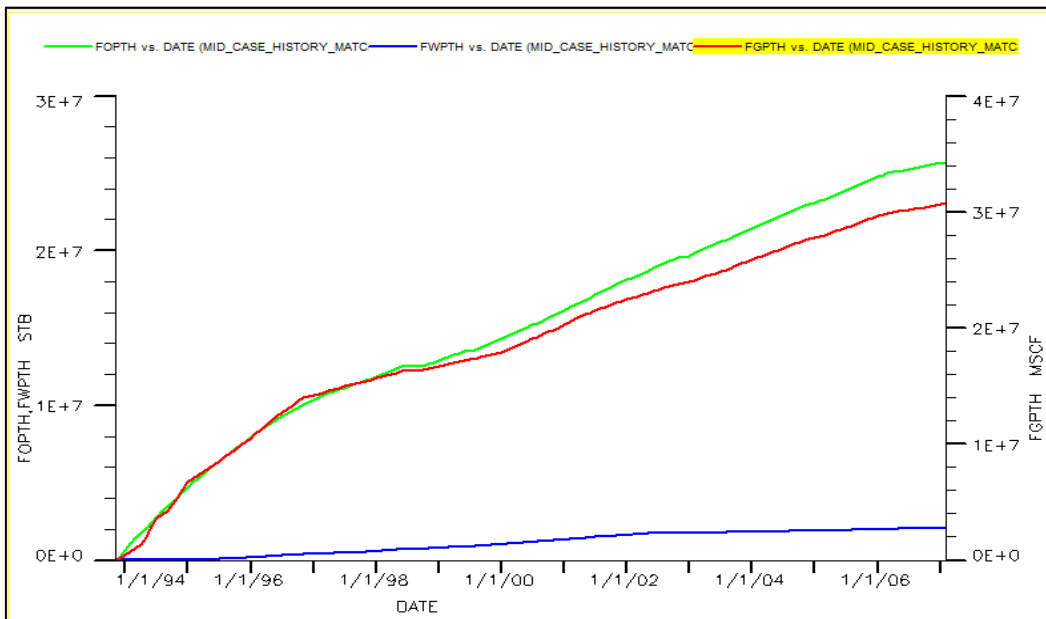
Figure 4. 2: Cumulative production of oil, gas and water production in the reservoir.

Historical oil production (Green Colour), Total gas production (Red colour) and cumulative water (Blue colour)

4.2 Material Balance Analysis

4.2.1 Reservoir cross-sectional view

Figure 4. 3 is a cross section of the reservoir and shows the direction from where water encroaches the reservoir. The direction of water influx was visualized and determined by the relative positions of the oil water contact at different time. The positions of the OWC at the start (November, 1993) and at the end (November, 2008) of the simulation have shown that the left and right regions of the reservoir sections experienced water encroachment earlier than the bottom, so the wells at the flanks experienced water influx earlier than others. This shows the predominant of edge aquifer over the bottom.

4.2.2 Aquifer modelling

To model the aquifer and its characteristics, material balance calculation was made. The aquifer was modelled using the Fetkovich analytical model. The choice of Fetkovich is because it contains fewer parameters than others analytical models. The parameters in the Fetkovich model are given in equations 4.1 through 4.3.

$$W_i = \frac{\pi(r_a^2 - r_r^2)}{5.615} \left[\frac{\emptyset}{360} \right] \qquad 4.1$$

$$r_a = \sqrt{\frac{43510 A_a}{\pi} \left(\frac{360}{\emptyset} \right)} \qquad 4.2$$

$$J = \frac{0.00708 kh \left(\emptyset / 360 \right)}{\pi \left[ln \left(\frac{r_a}{r_r} \right) - 0.75 \right]} \qquad 4.3$$
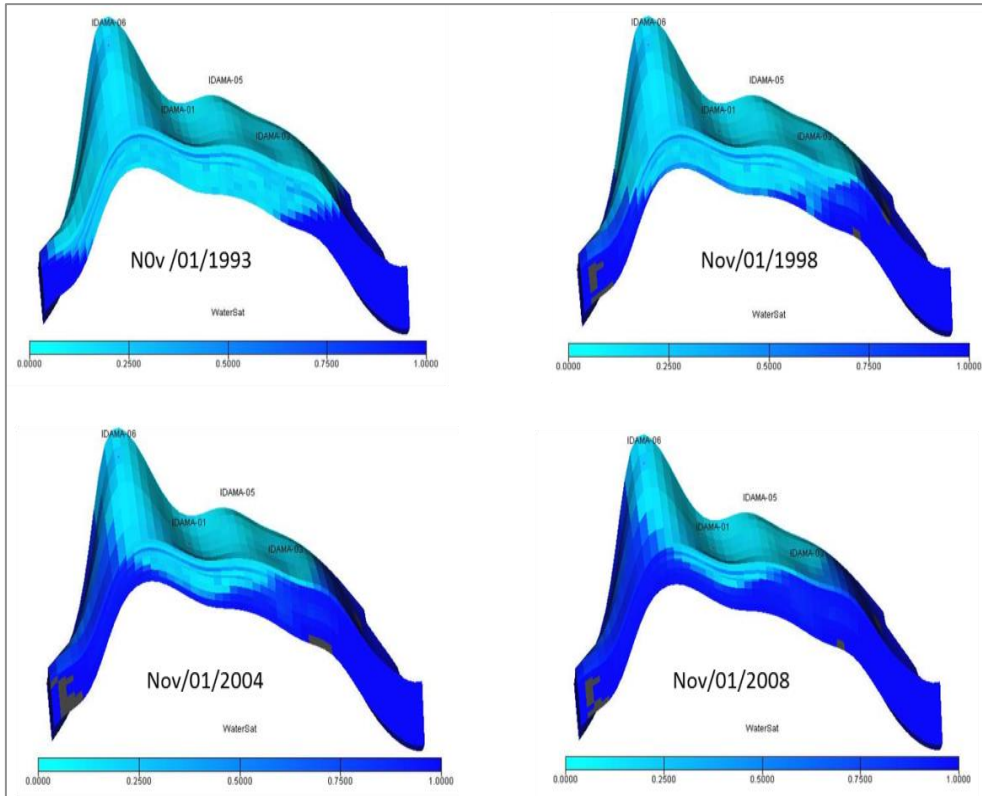
Figure 4. 3: Reservoir Cross section showing the aquifer movement

4.2.3 The analytical plot

The amount of the energy required to match the observed production was estimated through the analytical plot by constraining the material balance model to produce the observed pressure and the non-primary phases (gas and water) and then calculating the oil production. As shown in Figure 4. 4, it is evident that without the presence of aquifer it is impossible to match the observed pressure and then production.
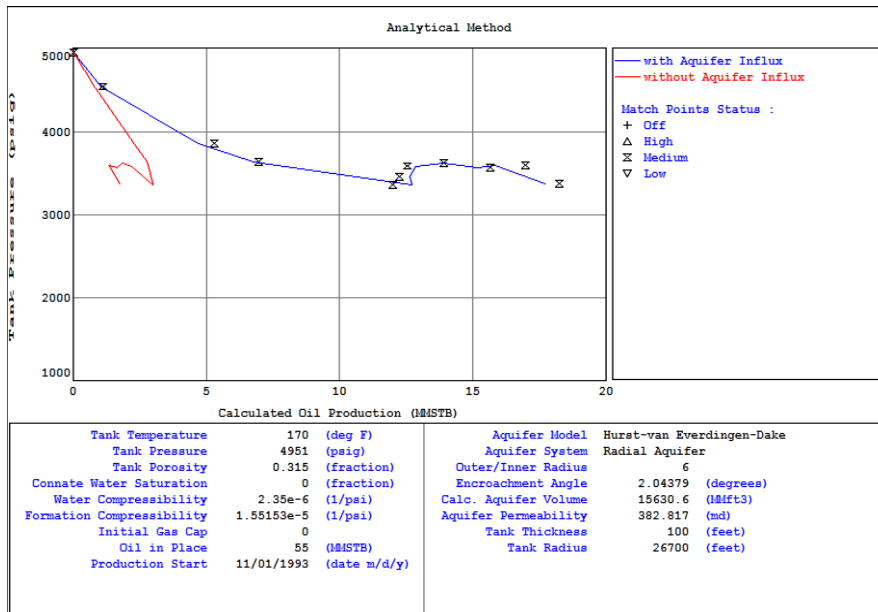
Figure 4. 4: Analytical plot.

The red line represents material balance without aquifer while the blue trend line represents that with the aquifer in place. With aquifer however, the energy was captured. The discrete points represent the pressure history while the continuous lines (red and blue) represent material balance results. To establish the aquifer properties, regression was done and a match (blue line) was achieved in the analytical plot (reservoir pressure versus cumulative oil production) as shown in Figure 4. 4.

With these details an estimate of the hydrocarbon zone to aquifer ratio was determined. The aquifer estimated pore volume is approximately 3 MMMbbl and productivity index of 450 bll/psia/day. Other aquifer characteristics such as permeability, encroachment angle and tank radius were also obtained. Below is the description of other important plots made from the material balance calculations.

95

4.2.4 The aquifer influence functions (W_d)

The aquifer influence function is shown in Figure 4. 5. W_d plot is used to determine the time the aquifer will respond to voidage due to fluid removal. It helps to determine the ratio of the aquifer radius to the reservoir radius (aquifer size). For this reservoir, the aquifer influence function revealed the ratio of the aquifer radius to the reservoir radius (aquifer size) to be 6 which is an indication of appreciable aquifer which is likely to react later to voidage caused by oil, water and gas production through the wells.
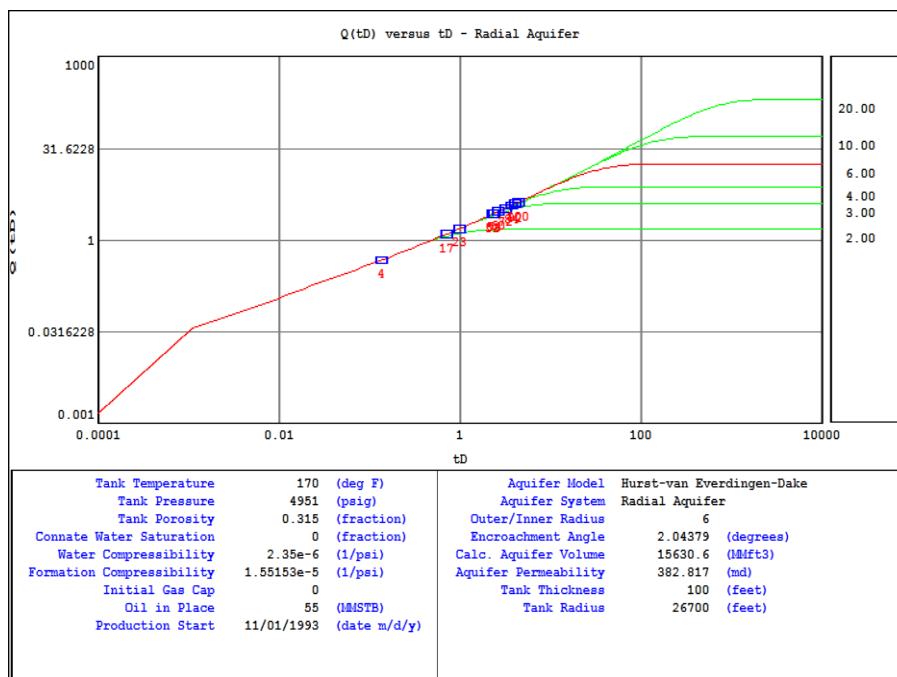
Figure 4. 5: Material balance Wd function plot

4.2.5 The reservoir drive mechanisms

Figure 4. 6 is the energy plot and it shows that the reservoir energy is majorly a combination of water influx and pore volume expansion from the aquifer. Initially the fluid expansion is the dominant energy source, but as reservoir depletion continuing, pore volume expansion from the aquifer becomes more significant drive. Usually, with these

96

energy characteristics, recovery ranges from 25 to 35% is possible. The pressure behavior reveals strong active aquifer. The aquifer influence function, the analytical plot and energy plots all indicated that Fetkovich model was adequate for modeling the reservoir aquifer. The properties of the Fetkovich aquifer model are summarized as shown in Figure 4. 1.
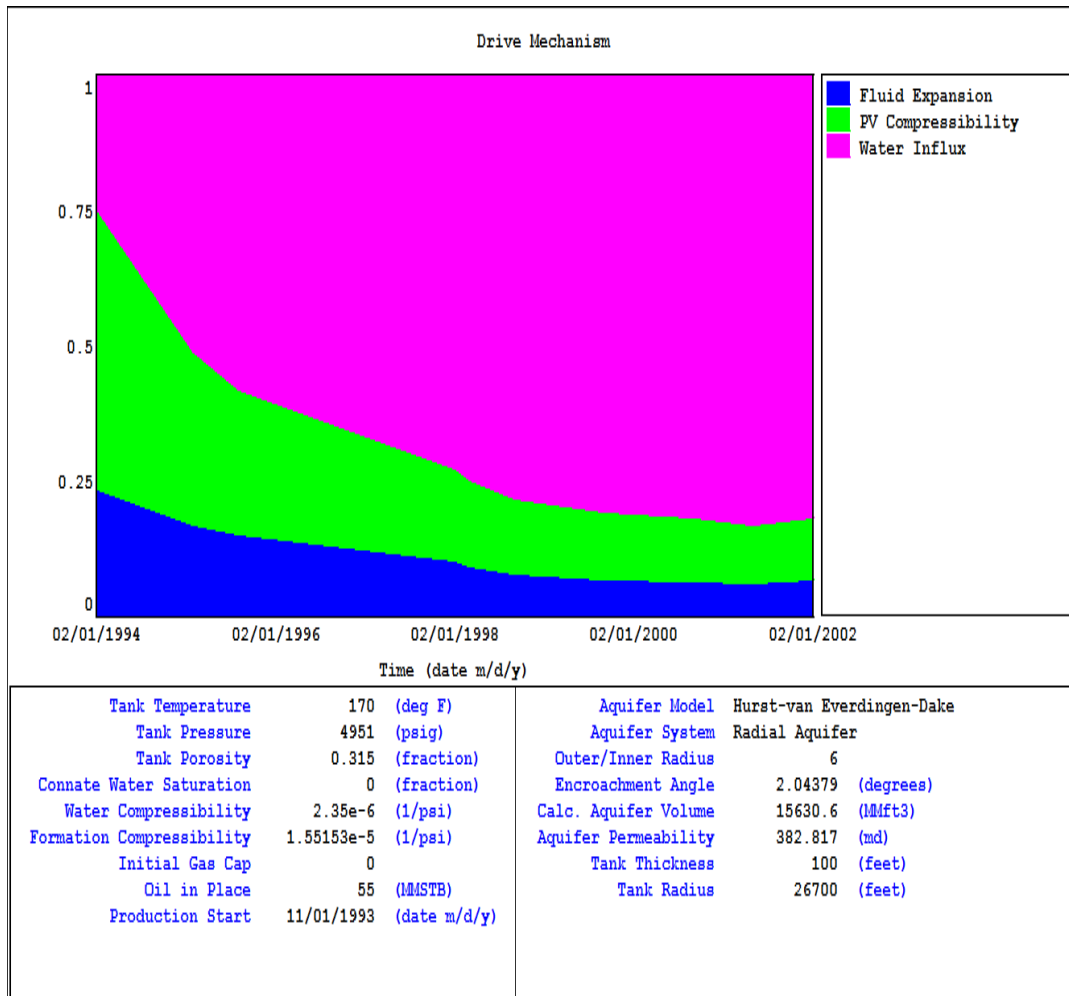
Figure 4. 6: Drive mechanism plot from material balance analysis

Table 4. 1: Aquifer properties for field pressure history match

Parameters	Estimated values
Reservoir Outer/Inner radius	6
Permeability	382.817mD
Porosity	0.315
Compressibility	2.35E-06/psi
Aquifer Thickness	100ft

4.3 Dynamic Simulation

4.3.1 Model dimensions

The reservoir model was constructed using the data obtained from the static model, material balance analysis and pertinent rock and fluid properties, SCAL, well completions and production data. The model dimensions in the X-, Y- and Z-direction are 197, 75 and 9, respectively. This amounts to 132,975 active cells on a fine scale equivalent to 98*37*9 grid dimension (32,634 3D grid blocks) on a coarse scale. This was able to preserve certain geologic features like thin shale streaks captured in certain layers of the geologic model.

4.3.2 Model properties

Properties used to build the dynamic model are as follows:

    i.   Permeability in the X and Y direction for all the cells (PERMX, PERMY)

    ii.   Permeability in the Z direction (PERMZ)

    iii.   Porosity (PHIE)

    iv.   Saturation model

    v.   Net to gross (NTG).

vi.   SCAL data comprising the relative permeabilities for oil/water and gas/oil systems

vii.   PVT data.

4.3.3 Schedule

The production history and deviation survey for the wells were loaded into the simulation model using ECLIPSE schedule. The program calculates the well connection factors using the reservoir properties. In addition, the program outputs the production data in a format that can be included directly into an ECLIPSE model.

4.4 Sensitivity Analysis

Traditional history match can be time consuming especially when huge uncertainties influence reservoir performance of interest. Accurate identification of factors and their interactions are difficult to achieve when parameters are changed one-at-a-time. Linear experiments were therefore designed for screening 11 reservoir factors in order to identify most impactful ones for the purpose of saturation match and uncertainty analysis.

The following factors were considered for sensitivity study on the 3 models:

i.   Critical water saturation, (SWCR)

ii. Critical gas saturation (Sgc)

iii. Irreducible water saturation (SWI)

iv. Porosity (PORO)

v. Water relative permeability (KRW)

vi. Aquifer volume, (AQPV)

vii. Aquifer productivity index (AQUIPI)

viii. Vertical permeability, (KZ)

ix. Horizontal permeability, (KX)

x. Global fluid contact, (OWC)

xi. Oil viscosity, (μo)

4.4.1 Placket-Burman Design

Placket-Burman was chosen because it permits screening relatively large number of parameters with minimum number of simulations. PB has a limitation of not been able to account for higher order and interaction effects that may at times be significant. Nevertheless, the objective at this stage is not seeking for "detail" nor for the development of credible reservoir proxy, rather it is employed to identify major factors to focus attention on while performing traditional history matching. This was performed on "High", "Mid" and "Low" case models. In all cases, cumulative oil produced was the response. Twelve experiments were performed at various settings.

Table 4.2Table 4.2: shows the design levels for different parameters. All entries in the third and fourth columns represent multiplier on the base case model. The definition of these multipliers was based on expert advice and experience gained from the neighbouring fields.

100

Table 4.3 shows the design matrix for linear experiment. Analysis of variance (ANOVA) of the main effects was carried out on the simulated response after 13 years to establish the contributions of different factors on the objective function. The result is presented as multiple bar charts as shown in Figure 4.7.

Table 4.2: Statistical design of the Parameters as range of multipliers

Parameters	Description	Min	Max
Swcr	Critical water saturation	0.8	1.2
Poro	Porosity	0.9	1.1
Permx	Horizontal permeability	0.6	1.4
Permz	Vertical permeability	0.3	1.7
WaterRperm	Relative permeability to water	0.25	1.1
AQUIPV	Aquifer pore volume	0.9	1.2
OWC	Oil water contact	0.9	1.1
Sgcr	Critical gas saturation	0.3	1.7
OVISC	Oil viscosity	0.8	1.1
SWI	Initial water saturation	0.74	1.26
AQUIPI	Aquifer productivity index	0.8	1.2

Table 4.3: Placket-Burman design for sensitivity analysis

Run	Φ	KX	KZ	KRW	SWI	SWCR	SGCR	μ_o	OWC	AQUPV	AQUPI
1	-1	-1	-1	-1	-1	-1	-1	-1	-1	-1	-1
2	-1	1	-1	-1	-1	1	1	1	-1	1	1
3	-1	1	1	1	-1	1	1	-1	1	-1	-1
4	1	-1	-1	-1	1	1	1	-1	1	1	-1
5	1	-1	1	1	-1	1	-1	-1	-1	1	1
6	-1	-1	1	1	1	-1	1	1	-1	1	-1
7	-1	1	1	-1	1	-1	-1	-1	1	1	1
8	1	1	-1	1	1	-1	1	-1	-1	-1	1
9	-1	-1	-1	1	1	1	-1	1	1	-1	1
10	1	1	-1	1	-1	-1	-1	1	1	1	-1
11	1	1	1	-1	1	1	-1	1	-1	-1	-1
12	1	-1	1	-1	-1	-1	1	1	1	-1	1

* "+1" denotes high level of parameter
* "-1" denotes the low level of parameter

The Bar chart shown in Figure 4.7 highlights the most influential parameters in the three models. The analysis confirms that the oil viscosity (OVISC), oil water contact, porosity (PORO), relative permeability (RELPERM), vertical permeability (PERMZ), critical water saturation (SWCR) and aquifer pore volume (AQUIPV) are significant factors on the response.
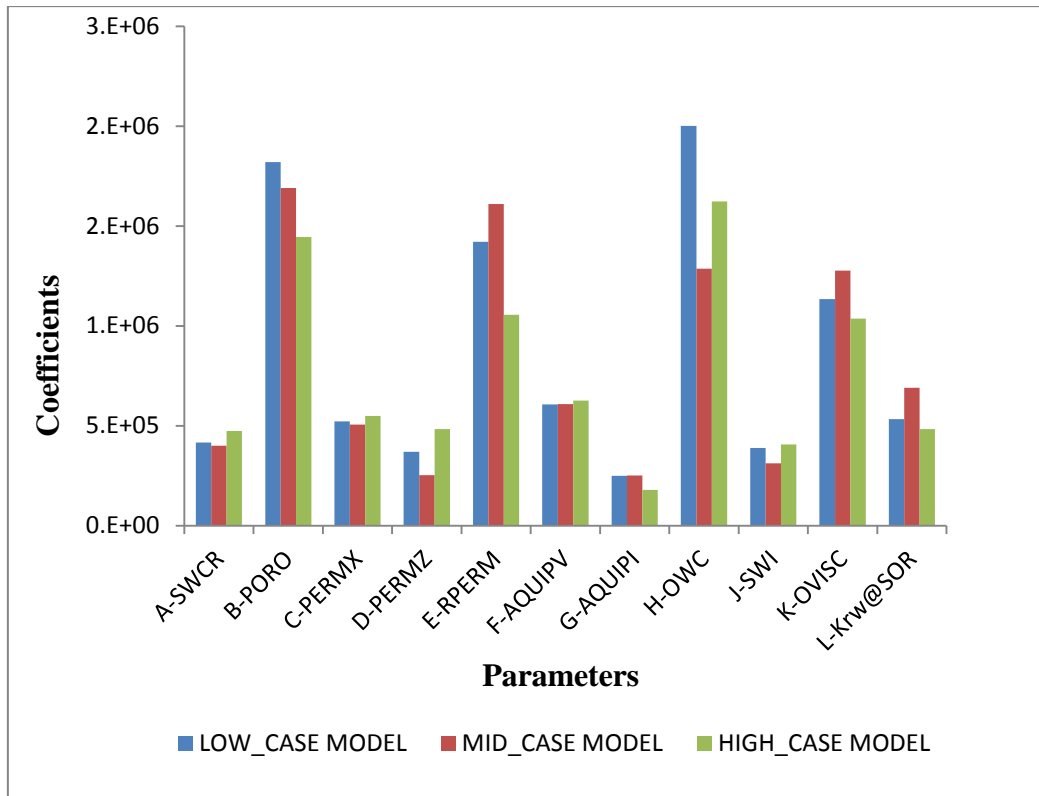
Figure 4. 7: Bar chart showing degree of significance of uncertainties from the three models on response

4.5 Saturation Match

The simulator was constrained to produce the historical oil rates and then the water cut, GOR and reservoir pressure were estimated. These were then compared to historical data to validate the dynamic model. The following changes were made to the simulation model to obtain a good history match of the pressure and production profiles:

Relative permeability to water

There was no relative permeability measurement available. The measurement from analogous reservoir was utilized after modification. Keeping end points constant, a low and high cases water relative permeability were derived from the initial assumed curves (mid

case) using some multipliers. By so doing the rock wettability become altered until satisfactory match is obtained. The relative permeability plots for oil-water and gas-oil systems used in this study are shown in Figure 4. 8 and Figure 4. 9. The connate water saturations obtained from the static model were relatively low. Critical water saturation was globally increased by 25% to match the water breakthrough time.
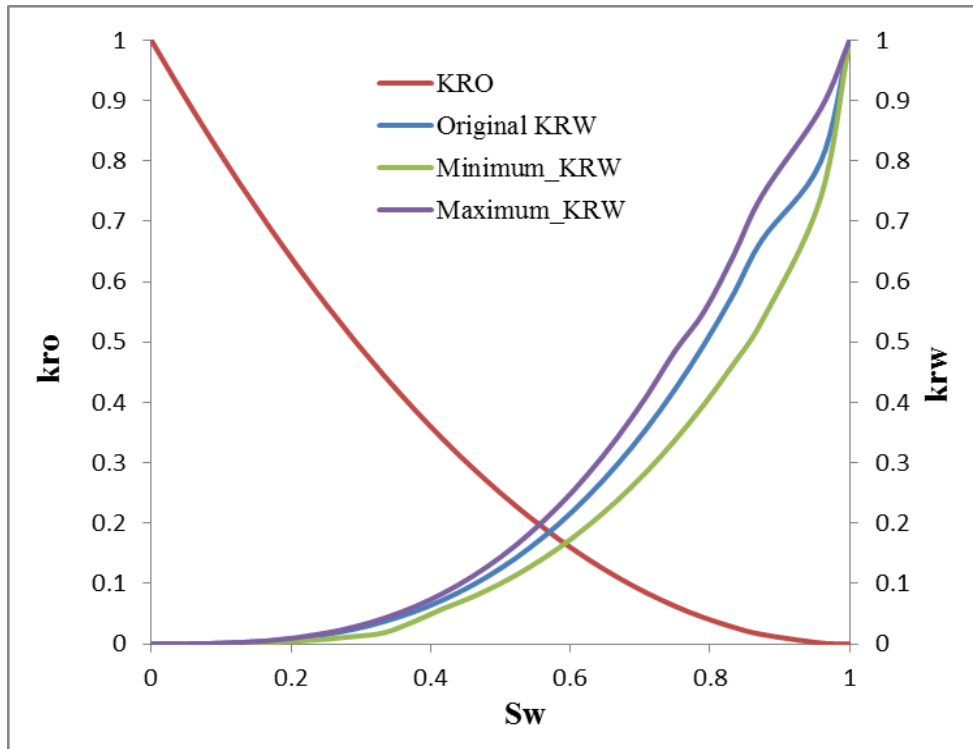
Figure 4. 8: Oil-water relative permeability curves

Oil Viscosity

The key oil properties available after carefully reviewed the PVT and sampling depth data for this reservoir include; gas-oil-ratio (GOR), gas gravity, oil API gravity and oil formation volume factor (FVF). Empirical correlation was used for oil viscosity and other PVT properties estimation. So, uncertainty of ±10% was assumed for the resulted single

black oil viscosity property. This gives rise to three viscosity models, minimum viscosity model, base case and maximum viscosity model. These were used during the history matching and while performing uncertainty analysis.
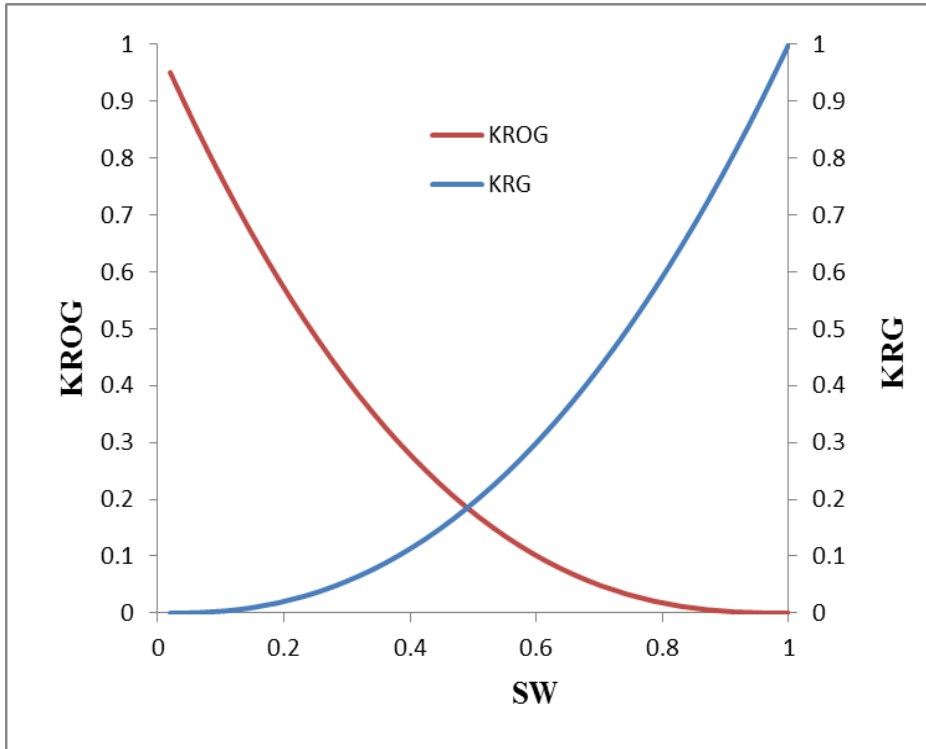
Figure 4. 9: Gas-oil relative permeability curves

Vertical/horizontal permeability (KV/KH)

KV/KH is one of the major uncertainties since there is no core measurement for kv/kh ratio supervision. At the beginning, the vertical permeability (PERMZ) was calculated using the ratio of 0.1 from PERMX model. This was guided from the information from a neighboring field with KV/KH ratio ranges from 0 – 0.25. However, the minimum KV/KH that preserves history matching ranges between 0.02 and 0.055.

Original Oil-Water Contact (OWC

The first well drilled in 1973 penetrated the sand without encountered the water-up-to (WUP) depth. However, the water-up-to from two simultaneously drilled wells indicated slightly varying depths. The average Oil-Down-To (ODT) from these wells is approximately 11239 TVD ftss. The base case match was obtained using 11240.5TVD ftss, for the low case model, a good match was obtained with ODT at 11245.5TVD ftss while for the high case, the ODT at 11238TVD ftss was adequate to obtain a good pressure and saturation matches.

A good match on water cut and pressure was obtained at reservoir level. Figure 4. 10, Figure 4. 11 and Figure 4. 12 show the outcome of the history match. This results in complimentary good match in the oil volume and oil rate. Although the water breakthrough time for high case was early than actual observed, the overall water cut match, though characterized with little variation in levels for the three cases, are relatively good.

4.5 Prediction

The objective of the prediction runs is to generate production forecasts uncertainties from the models and evaluate possible field development cases in order to optimize oil recovery from the reservoir. The current potential of the wells was evaluated and this formed the basis for defining the individual well production rate constraints. Forecast period assumed is 15 years.

Table 4.4 shows the operational and economic constraints applied to the producing wells during the prediction runs.
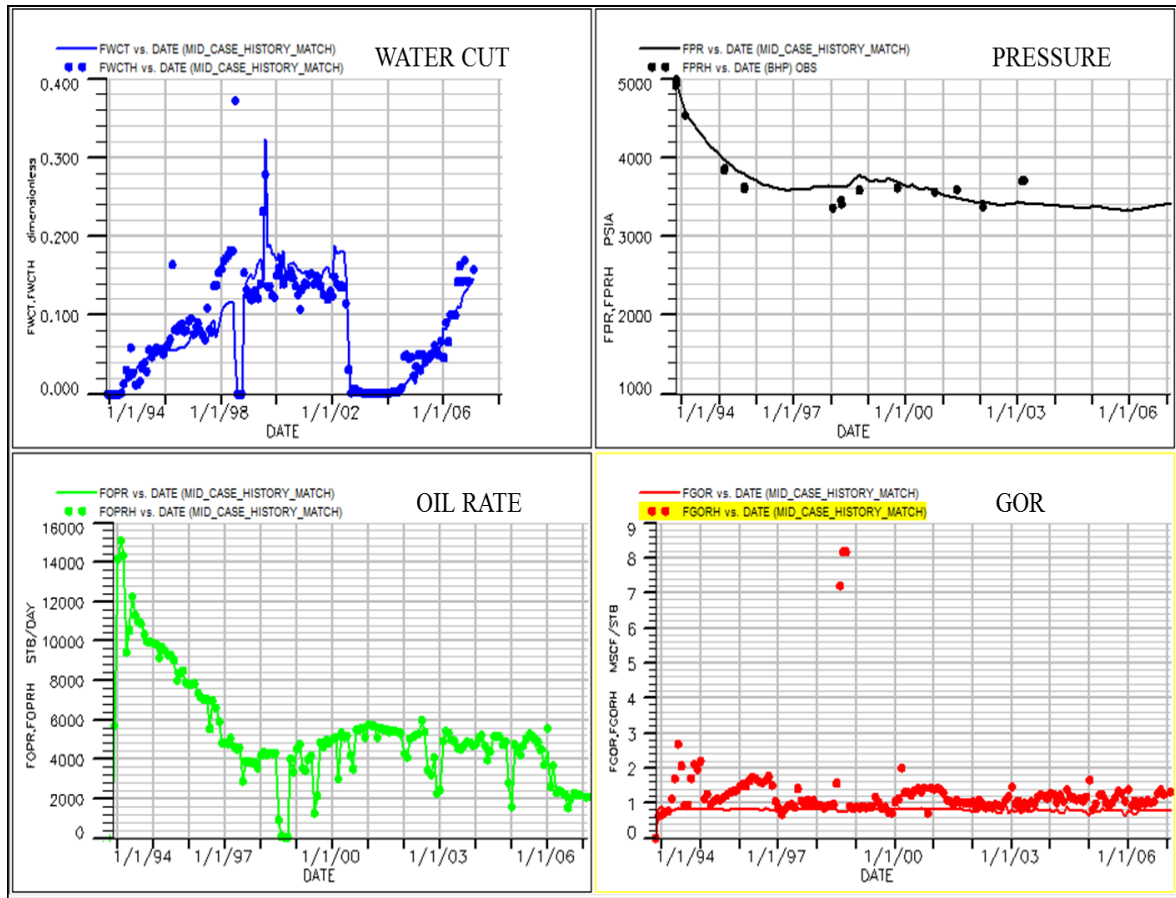
Figure 4. 10: History match plots Reservoir pressure, GOR, oil rate and water cut for Base case model
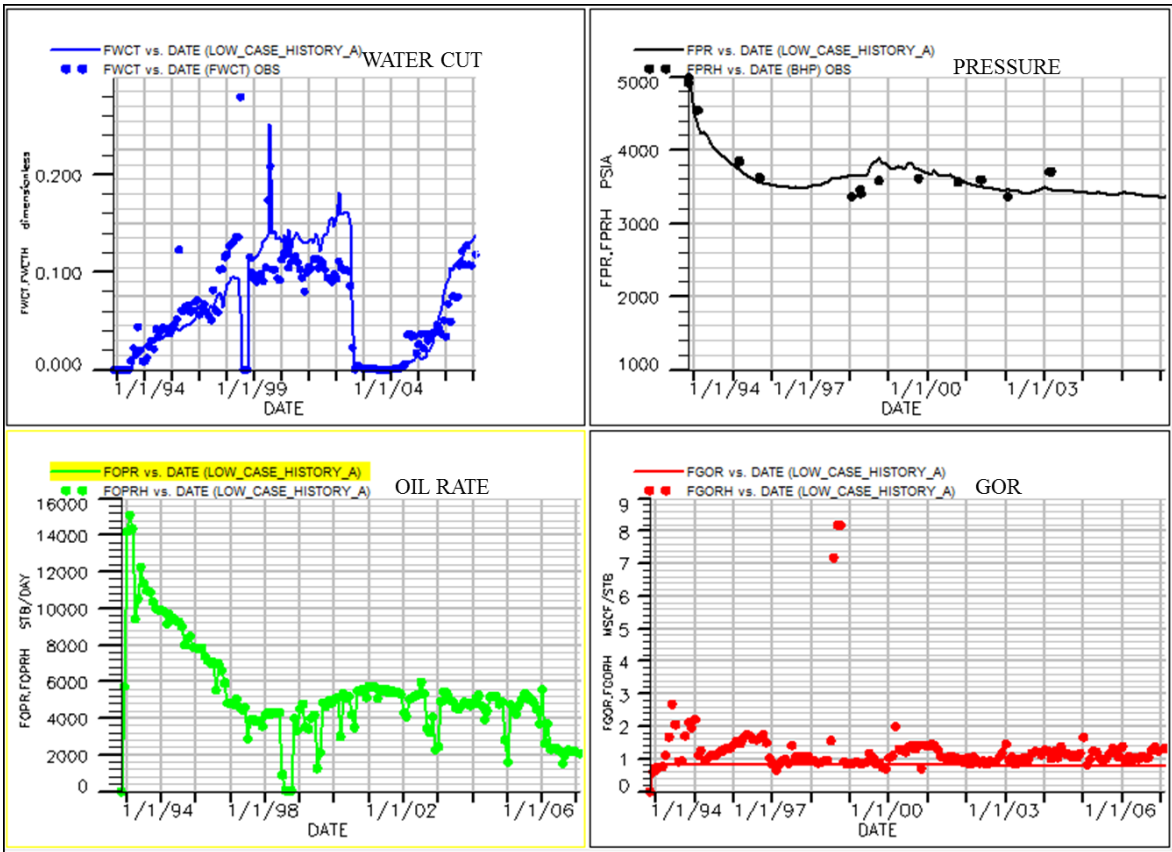
Figure 4. 11: History match plots Reservoir pressure, GOR, oil rate and water cut for Low case model
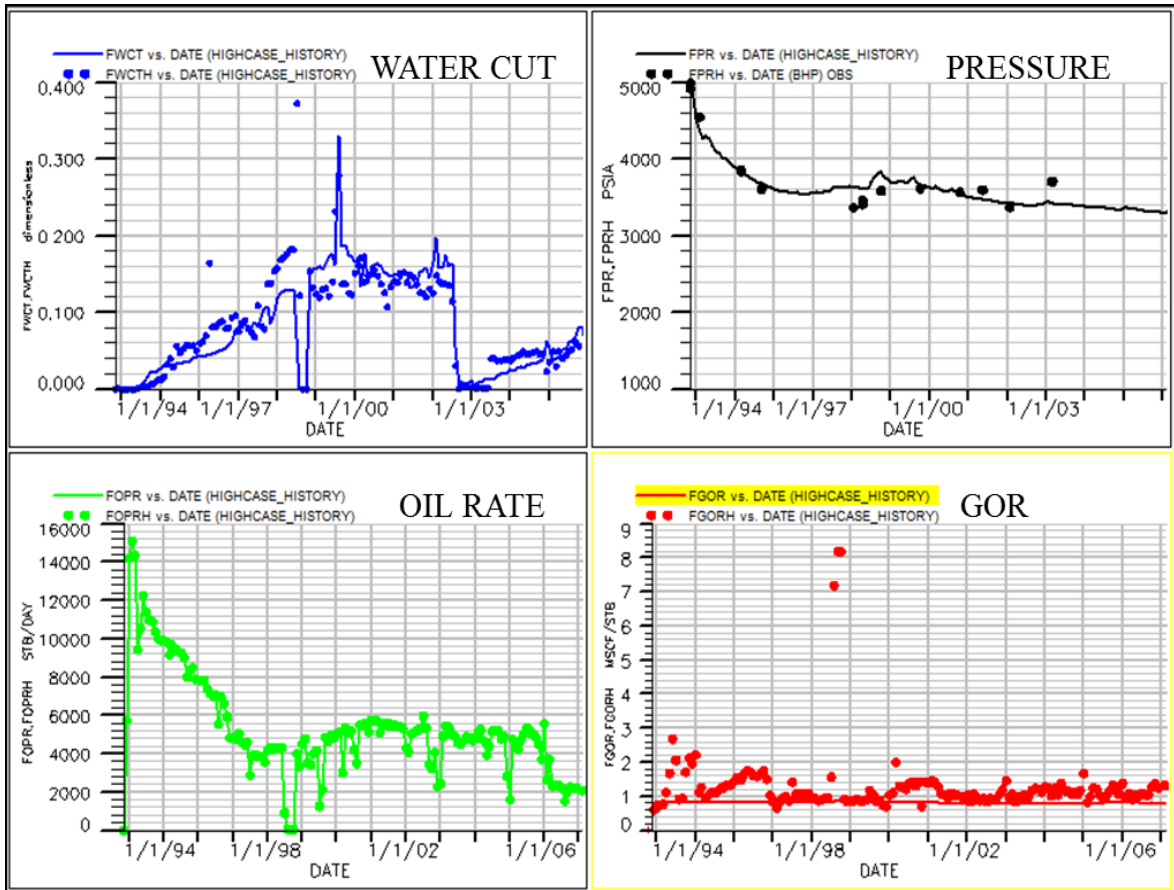
Figure 4. 12: History match plots Reservoir pressure, GOR, oil rate and water cut for High case model

109

Table 4.4: Producing constraints

Constraints	Low case	Base case	High case
Minimum oil rate (stb/d)	500	500	500
Maximum GOR (scf/ stb)	850	850	850
Maximum BS&W (Percent)	90	90	90
Maximum oil rate (stb/d)	2000	2000	2000

The following case scenario was evaluated:

CASE 1: Do nothing Case

Prediction for do nothing cases using "high", "low" and "mid" case models were performed assuming that the existing wells AK-01, AK-03, AK-05 and AK-06 will continue to produce without any intervention. Two of the wells, AK-01 and AK-03, stopped production prior to the end of history owing to excessive water production. The production performance plots for the reservoir under this condition are shown in Figure 4. 13 and Figure 4. 14. It is obvious in Figure 4. 14 that well AK-06 is making more water than AK-05. However, in all wells the high case model produced less water and hence high oil production. The base case yielded an estimated cumulative oil recovery of 31 MMstb. The well AK-06 from shuts down barely eight years into the prediction phase. Overall, the reservoir can still produce additional 6.3 MMstb of oil from July 2007 until 2020.

CASE 2: Pressure Maintenance and Well intervention

The second management case involved pressure maintenance by water injection and intervention in well AK-06 based on its completion's water production exceeding specified

water cut limits of 90%. The essence was to minimize pressure decline by water injection

and reduce the hydrostatic column in the well.
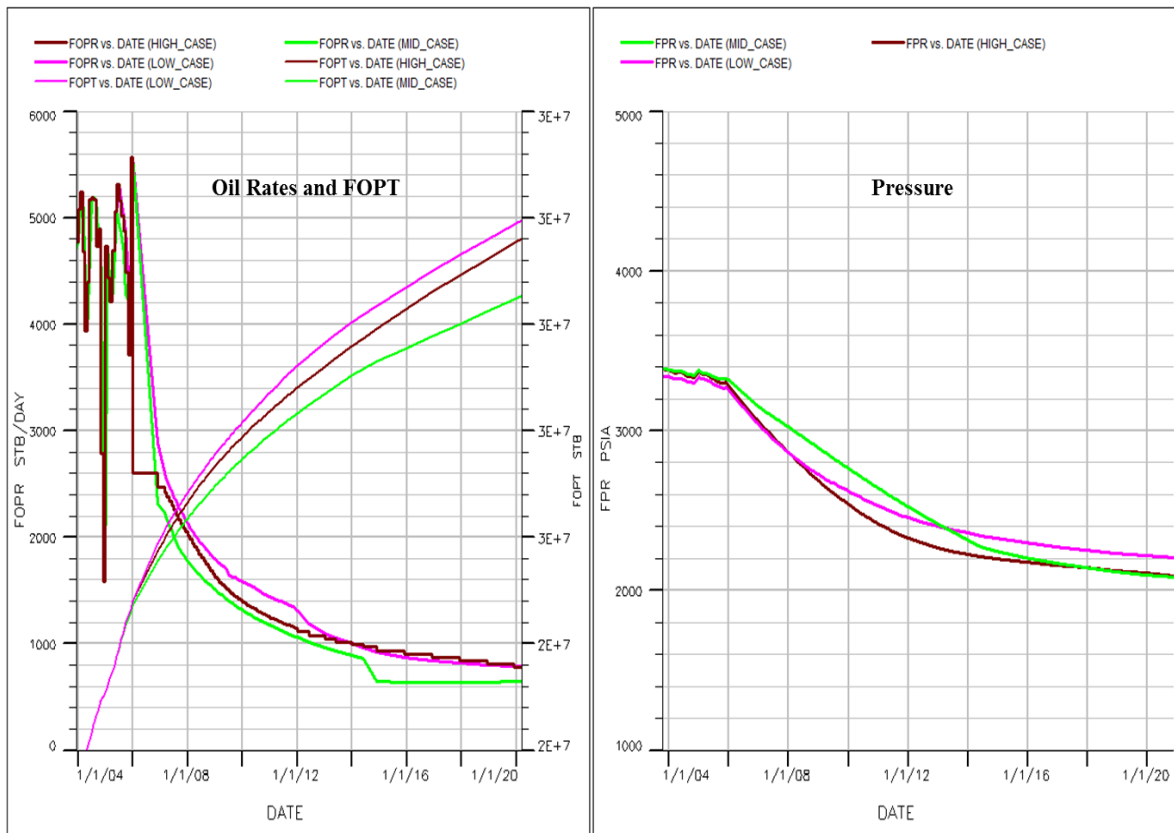
Figure 4. 13: Reservoir base case (Do nothing) production forecast oil rates and pressures from "low", "high" and "mid" case models
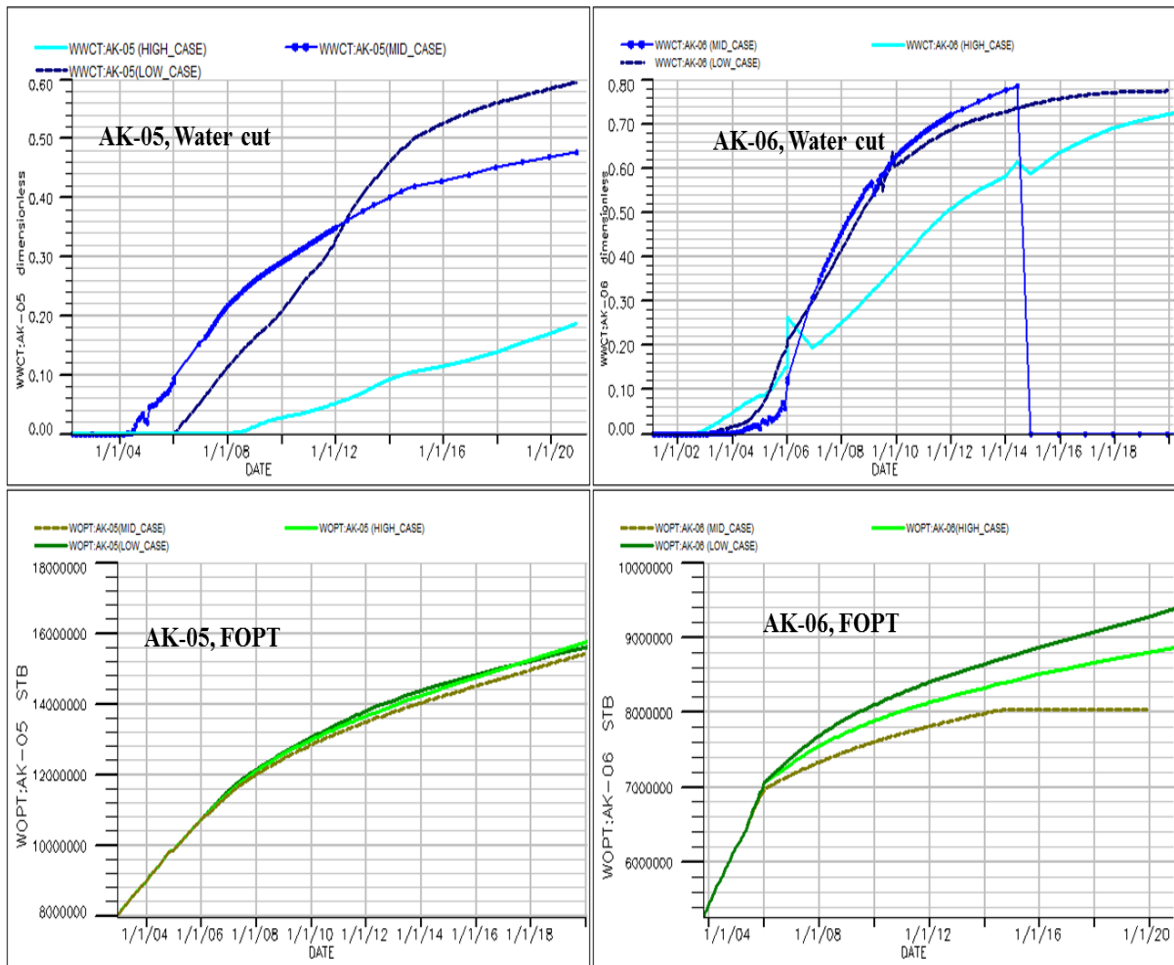
Figure 4. 14: Well performance plots for base case (Do nothing) production forecast.

This reduces the water produced which will in turn decrease the rate of decline of the tubing head pressure. The well's perforations layers closer to the OWC were plugged and other perforations opened on the basis of their water cut history prior to the prediction. The high water producing completions were shut very quickly because the completions exceeded a low maximum water cut limit and then the limit was raised to accommodate prolonged fluid production from the low water bearing completions. The wells were produced with water injection at an optimal water injection rate of 1500 bbl/d. This

optimal water injection rate was derived from sensitivity runs using injection rates between 500 bbl/d and 2500 bbl/d.

The comparison of the reservoir performance plots for the case 1 and case 2 are presented in Figure 4. 15. The plot shows the incremental production for the Case 2 when compared with the base cases. Figure 4.16 compares the water cut and oil recovery for well AK-05 and AK-06 in the water injection case versus base case.
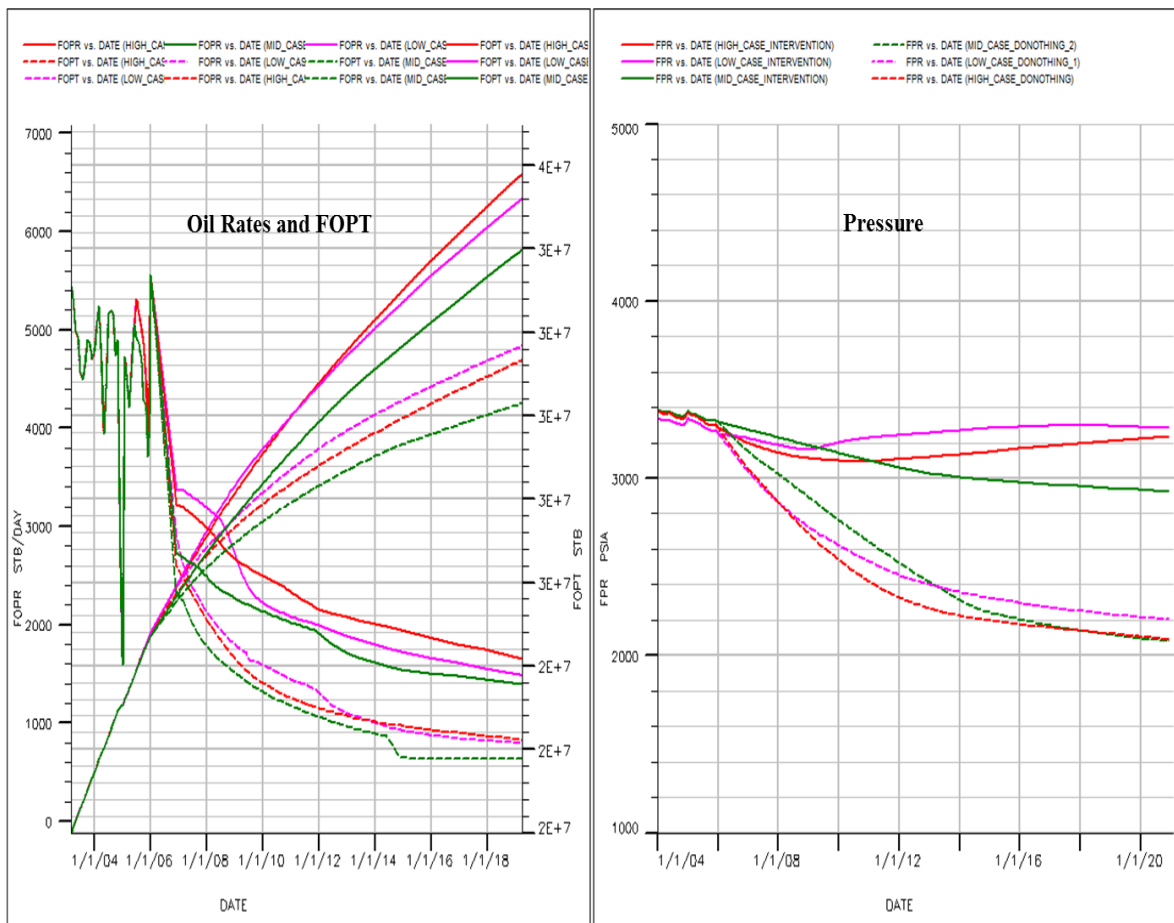
Figure 4. 15: Comparison of development Cases.

All dotted lines represent the trends for "Do nothing" rates, pressure and cumulative production. Continuous lines represent rate, pressure and cumulative recovery for well injection case.
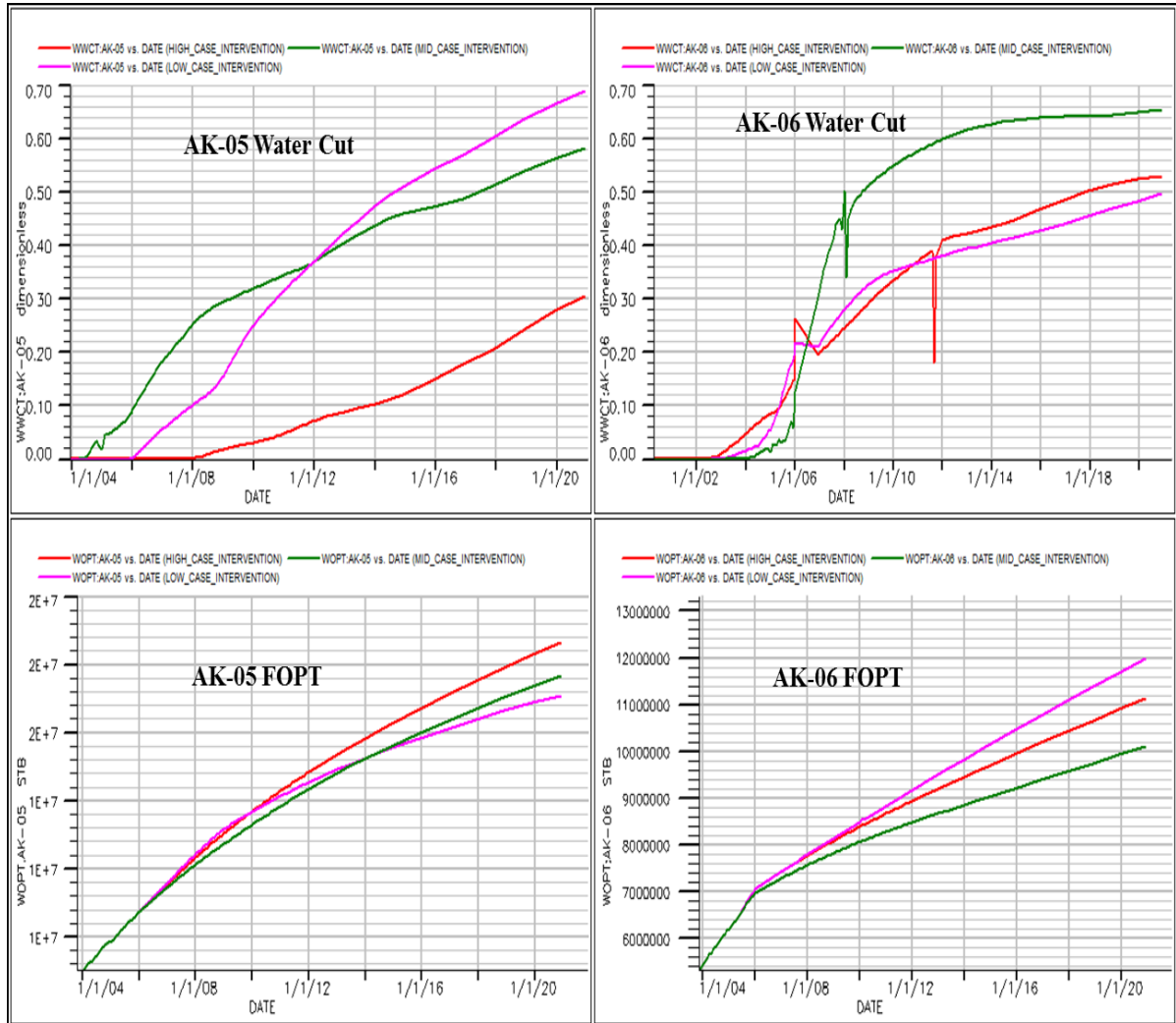
Figure 4.16: AK-05 and AK-06 water cut and oil recovery for water injection case versus base case.

The AK-05 in the high case model (Red color) exhibited delayed water breakthrough time and therefore lowest water cut (30%) and highest production when compare with the base case model (Green color). However, AK-06 of the low case (purple color) model shows minimum water cut and highest oil production. The production plots for the 2 wells show the existence and degrees of the uncertainty in the forecast figures.

4.6 Uncertainty Analysis

4.6.1 Experimental design

The following parameters were considered in the experimental design using the central composite design of the response surface methodology.

    i.   Horizontal permeability (PERMX, PERMY)

    ii.   Water injection rate (Q_{winj})

    iii.   Relative permeability to water (KRW)

    iv.   Oil Viscosity (OVISC)

    v.   Vertical permeability (PERMZ)

The analysis was performed using the "Low", "Base" and "High" case models.

4.6.2 Analysis with replication

The extreme models (low and high cases) were treated as replicates of the base case. This gives rise to a single response surface equation. Although only classical laboratory experiments are characterized by random error, the random error in numerical simulation is always assumed zero since repeating numerical simulation time without number does not

change the fundamental equation with which calculations are made except if the input data is changed. The introduction of replications as used in this analysis treated the reservoir models as uncertainty factors and believed to guarantee rigorous proxy model for uncertainty quantification.

4.6.2.1 Full Factorial Design

Conducting 3-Level full factorial experiment with 5 factors can be time-consuming. A 2-Level factorial of high resolution was chosen in that it gives a response surface of high quality comparable to other response surface designs. **Table 4.5**Table 4.5: shows the range of values of parameters for the experiments. The various combinations of the uncertain parameters were generated and their responses were derived using the history matched models in forecast mode. Thus the experiment was performed three times (with 3 models) according to design.

Table 4.5: Uncertainty factors, their descriptions and range of values as multiplier on the base case value

| | | | Multiplier Ranges | | |
| | Parameters | | Minimum | Base Case | Maximum |
S/N		Keywords	Value	Value	Value
1	Oil Viscosity	OVISC	0.9	1	1.1
2	Horizontal Permeability	PERMX	0.57	1	1.29
3	Vertical Permeability	PERMZ	0.5	1	6
4	Water relative permeability	KRW	0.36	1	1.25
5	Water injection rate	Q_{winj}	0.33	1	1.33

Table 4.6 shows the design matrix comprises of 96 (32 each for three models) experiments involving the three models. The design matrix consisted of the parameter values in coded form as well as the actual response values in stock-tank barrels after experimentation.

Figure 4. 17 shows half normal plot that shows interactively, how the factors were selected.   From Figure 4. 17, the main factors, horizontal permeability (A), vertical permeability (B), water relative permeability (C), oil viscosity (D) and water injection rate (E) were selected together with two factorial effect represented by the interaction of horizontal permeability and water injection rate (AE) and interaction of vertical permeability and water injection rate (BE).

Table 4.6: 2-Level Factorial design matrix and corresponding uncertainty recoveries for three uncertainty forecast models

						Oil Recovery		
Run	A:PERMX	B:PERMZ	C:KRW	D:OVISC	E:QWINJ	LOW CASE	MID CASE	HIGH CASE
1	1	-1	-1	1	-1	33517890	31880182	35484128
2	-1	1	-1	1	1	35227944	34433176	36092984
3	1	-1	1	-1	-1	34045084	32220234	35819788
4	1	1	-1	1	1	36892552	36028056	39617484
5	1	1	1	-1	-1	33701304	32141130	36162628
6	-1	-1	-1	-1	-1	31489326	30409224	32220530
7	1	1	-1	-1	-1	33897368	32141130	36283356
8	1	-1	-1	-1	1	36686268	36722248	40313456
9	-1	-1	1	1	-1	30384918	29864944	31976602
10	-1	-1	-1	1	-1	30893108	29913918	32071976
11	-1	1	-1	1	-1	30625454	29516720	32410822
12	1	1	-1	-1	1	37881376	37173760	40469136
13	1	1	1	1	1	37422240	36355904	39604812
14	-1	-1	1	1	1	34883624	33984920	35020244
15	1	-1	-1	-1	-1	34201168	32410058	36024780
16	1	-1	1	1	1	36098992	35553036	39321400
17	1	1	1	-1	1	38380680	37173760	35657292
18	1	1	1	1	-1	33701304	31141226	35657292
19	-1	1	1	-1	-1	31154618	30444058	32421976
20	-1	1	-1	-1	1	36606116	35360300	37171160
21	1	-1	1	-1	1	37050172	36722248	40216804
22	1	-1	1	1	-1	33322354	31671380	35298496
23	-1	-1	1	-1	-1	30958776	30409224	32152336
24	1	1	-1	1	-1	33447564	31132106	35770556
25	-1	-1	-1	1	1	34626568	33715860	35026988
26	-1	1	-1	-1	-1	31178010	30646346	32493622
27	1	-1	-1	1	1	35781336	35199272	39395696
28	-1	1	1	-1	1	36534084	35639440	37108016
29	-1	1	1	1	-1	30617418	29273420	32306050
30	-1	-1	1	-1	1	35993228	34988232	36299568
31	-1	1	1	1	1	35787588	34653404	36068340
32	-1	-1	-1	-1	1	35714748	34853836	36292076

Only these selected parameters are adequate model terms that relate the dependent and independent variables due to the deflection they exhibited for the half normal percentage

probability. In all the experiments, water cut and GOR were constrained. This implies that the adequate model that described the inter-relationship between the dependent and independent variables is the factorial model (2FI). The factorial model consists of the main factors and their interactions.
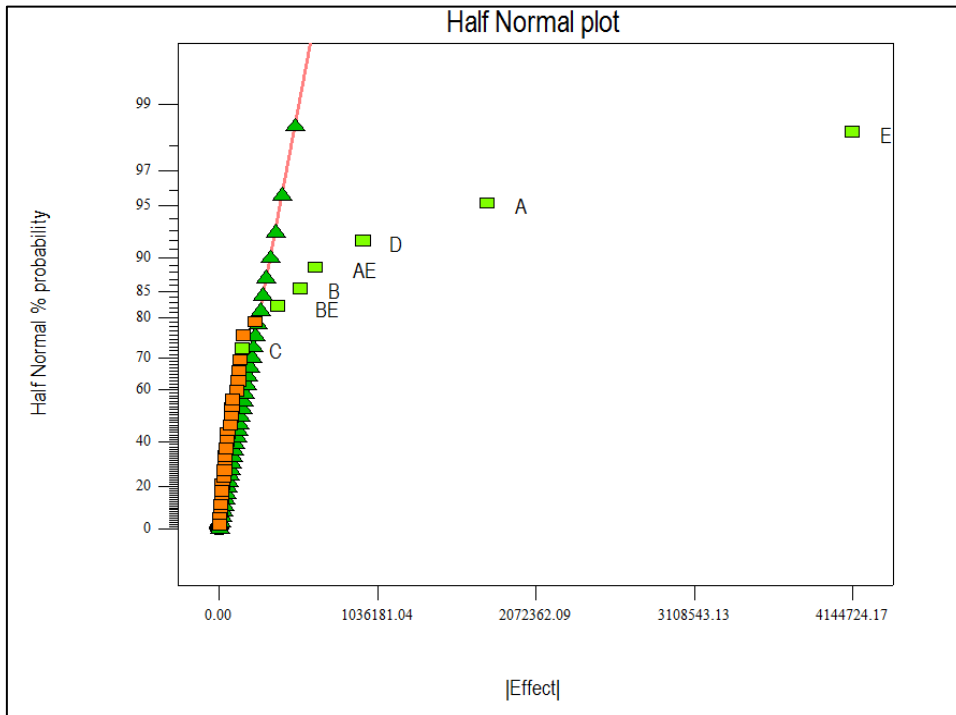
Figure 4. 17: Half normal plot depicting the manual process that led to selection of model and significant model terms. All selected terms (A, B, C, D, E, AE, and BE) have caused significant deflection of the red line away from 45° position.

4.6.2.2 Analysis of variance

In order to select the best model that fit the experimental data, linear, quadratic, polynomial and factorial models were evaluated using correlation coefficient (R-square), adjusted correlation coefficient (Adj. R-square), F-value and maximum design error criteria. Linear model augmented with the factorial model was selected. Using ANOVA,

significance of the model as well as regression parameters gave most accuracy required. The statistical indexes used include F and p statistics. From Table 4.7, the Model F-value of 116.05 implies the factorial model selected is significant. There is only a 0.01% probability that a "Model F-Value" this large could occur due to noise. For the selection of the independent variables, values of "Prob > F" less than 0.0500 indicate models terms are significant. In this case A, B, D, E, AE and BE are the only significant model terms for the construction of response surface. Thus factor C (KRW) is not signficant on the model and therefore removed from the regression process of response surface development.

Table 4.7: Analysis of variance showing significance of model terms

Factor	Sum of Squares	DF	Mean Squares	F- Value	Prob>F	
Intercept	3.60E+14	7	5.15E+13	116.05	< 0.0001	significant
A-PERMX	5.34E+13	1	5.34E+13	120.4	< 0.0001	
B-PERMZ	3.56E+12	1	3.56E+12	8.03	0.00630	
C-KRW	3.39E+11	1	3.39E+11	0.76	0.38570*	
D-OVISC	1.67E+13	1	1.67E+13	37.7	< 0.0001	
E-QWINJ	2.34E+14	1	2.34E+14	528.26	< 0.0001	
AE	6.66E+12	1	6.66E+12	15.01	0.0003	
BE	2.63E+12	1	2.63E+12	5.93	0.0179	

* not significant model term at 95% confidence interval

The regression equation relating ultimate recovery (dependent variable) and the history match variables (independent variables) is equation 4.1. The responses were transformed into logarithmic form to address non-linearity observed between the dependent and independent variables.

$$\text{Log}_{10}\text{FOPT}_{\text{Replicate}} = 7.51467 + 0.040431 * \text{PERMX} - 2.29e - 03 * \text{PERMZ} + 1.83e - 03 * \text{KRW} - 0.06368 * \text{OVISC} + 0.05981 * Q_{\text{winj}} - 0.01937 * \text{PERMX} * Q_{\text{winj}} + 9.58e - 03 * \text{PERMZ} * Q_{\text{winj}} \qquad 4.1$$

4.6.3 Analysis without replication

Each model is assumed to have equal likelihood. This approach assumed the three stochastic models are independent of one another and are deterministic. The analysis of the models will result to three (3) unique solutions and therefore three response surface equations.

4.6.4 Central Composite Design

Taking the advantage of the analyzed results gotten using the 2-Level factorial experiment, factor C (KRW) was excluded since it was found to be insignificant at assumed 95% confidence level. Table 4.8 presents the new factors and their corresponding range for performing CCD experiment. CCD is an improved algorithm due to its ability to mirror and integrate factor values outside their defined ranges. Thus, it can produce a more accurate surrogate model for optimization studies when compare with other response surface methods.

Table 4.8: Central Composite Design summary showing factors and range of values as multiplier on the base case value

Factors	-2 (-α)	-1(Low)	0 (base case)	1(High)	2(+α)
PERMX	0.21	0.57	1	1.3	1.67
PERMZ	0.04	0.54	1	1.54	2.04
OVISC	0.8	0.9	1	1.1	1.2
QWINJ	0.34	0.67	1	1.33	1.66

Table 4.9 shows the design matrix for CCD comprises of 25 experimental runs each for "high", "mid" and "low" case models. The regression equations relating dependent and

independent variables for low case (FOPT$_{\text{Low Case}}$), Mid/Base case (FOPT$_{\text{Base Case}}$) and high case (FOPT$_{\text{High Case}}$) are presented in equations 4.2 - 4.4. The responses were transformed into logarithmic form to address non-linearity observed between the dependent and independent variables.

$$\log_{10} \text{FOPT}_{\text{Low Case}} = a_0 + a_1 * \text{PERMX} + a_2 * \text{PERMZ} + a_3 * \text{OVISC} + a_4 * Q_{\text{WINJ}} + a_5 *$$

$$\text{PERMX}^2 + a_6 * \text{OVISC}^2 + a_7 * \text{PERMX} * \text{PERMZ} + a_8 * \text{PERMX} * \text{OVISC} + a_9 *$$

$$\text{PERMX} * Q_{\text{WINJ}} + a_{10} * \text{PERMZ} * Q_{\text{WINJ}} \qquad\qquad 4.2$$

$$\text{Log}_{10} \text{FOPT}_{\text{Base Case}} = b_0 + b_1 * \text{PERMX} + b_2 * \text{PERMZ} + b_3 * \text{OVISC} + b_4 * Q_{\text{WINJ}} +$$

$$b_5 * \text{PERMX}^2 + b_6 * \text{PERMZ}^2 + b_7 * \text{OVISC}^2 + b_8 * \text{PERMX} * \text{PERMZ} + b_9 * \text{PERMX} *$$

$$\text{OVISC} + b_{10} * \text{PERMX} * Q_{\text{WINJ}} + b_{11} * \text{PERMZ} * Q_{\text{WINJ}} \qquad\qquad 4.3$$

$$\text{Log}_{10} \text{FOPT}_{\text{High Case}} = c_0 + c_1 * \text{PERMX} + c_2 * \text{PERMZ} + c_3 * \text{OVISC} + c_4 * Q_{\text{WINJ}} + c_5 *$$

$$\text{PERMX}^2 + c_6 * \text{PERMZ}^2 + c_7 * \text{OVISC}^2 + c_8 * \text{PERMX} * \text{PERMZ} + c_9 * \text{PERMX} * \text{OVISC} + c_{10} *$$

$$\text{PERMX} * Q_{\text{WINJ}} + c_{11} * \text{PERMZ} * Q_{\text{WINJ}} \qquad\qquad 4.4$$

Table 4.9 Central Composite Design matrix and corresponding responses for three uncertainty forecast models

					RESPONSE		
RUN	A:PERMX	B:PERMZ	C:OVISC	D:QWINJ	HIGH	MID	LOW
1	-1	-1	-1	-1	34193700	32520500	33645400
2	1	-1	-1	-1	36245700	33670500	34439900
3	-1	1	-1	-1	34367600	32398200	33631800
4	1	1	-1	-1	36373900	33658100	35919000
5	-1	-1	1	-1	33777000	32000500	33096400
6	1	-1	1	-1	35723800	33054200	35001800
7	-1	1	1	-1	34022100	31916600	33075900
8	1	1	1	-1	35846200	33057900	35107000
9	-1	-1	-1	1	36301600	35110900	36258500
10	1	-1	-1	1	39582200	36787200	37189100
11	-1	1	-1	1	36787600	35280300	36601000
12	1	1	-1	1	39862900	36998300	37370500
13	-1	-1	1	1	35027900	34130400	35043800
14	1	-1	1	1	38374000	35733800	36292200
15	-1	1	1	1	35593400	34347700	35622000
16	1	1	1	1	38747000	36076300	36829500
17	-2	0	0	0	31031600	31356500	32666100
18	2	0	0	0	38399300	35699600	37151000
19	0	-2	0	0	36005200	34536400	35300600
20	0	2	0	0	37145600	34880500	36233800
21	0	0	-2	0	37938700	35311400	36994600
22	0	0	2	0	36426400	33955600	35290700
23	0	0	0	-2	33374200	32022000	33287700
24	0	0	0	2	38897800	36360700	36765100
25	0	0	0	0	37096600	34802800	36126900

The values of coefficients a_i, b_i, and c_i in the response surface equations are presented in Table 4.10:Table 4.10. Figure 4. 18 is the crossplots of the actual experimental values against the predicted values. If the prediction by these models were a perfect fit of the experimental data then all of the points would lie on the x=y line. On all these plots, it is clear that the dependent and independent variables are not completely linearly related.

Table 4.10: Coefficients in response surface correlation equations 4.2, 4.3 and 4. 4

	Low Case		Mid Case		High Case
a_0	8.37734	b_0	8.42247	c_0	8.54559
a_1	-0.04839	b_1	-0.05114	c_1	0.011707
a_2	0.042125	b_2	-8.96E-03	c_2	-0.02643
a_3	-1.72603	b_3	-1.7891	c_3	-2.00659
a_4	-0.06088	b_4	-0.07479	c_4	-0.11875
a_5	0.095946	b_5	0.090587	c_5	0.1141
a_6	0.93066	b_6	0.023388	c_6	0.025853
a_7	-0.04885	b_7	0.95619	c_7	1.12894
a_8	-0.09655	b_8	-0.05101	c_8	-0.05648
a_9	0.046751	b_9	-0.08804	c_9	-0.21314
a_{10}	0.018029	b_{10}	0.0647	c_{10}	0.09384
		b_{11}	0.017954	c_{11}	0.034316

This is responsible for some of the data points observed not to aligned completely on the straight line. There are more data points on the replicate cross plot because of larger experiments requirement for 5 factor. The variation of the data points on the remaining other cross plots however indicated some degree of uncertainty in the three models. With some degree of confidence nevertheless, the developed response surface models are excellent representation of reservoir and agreed amenable for sampling within the experimental range of parameters for further analysis.

4.7 Factors Interaction

The ANOVA shows clearly that all the selected main factors have significant effects on the ultimate recovery except the water relative permeability curve (KRW). Nevertheless, the interaction of some of these factors exhibits significant effect on the model development. Figure 4. 19 through Figure 4. 21 are the 3-dimensional diagrams showing the main effects of OVISC, PERMX, PERMZ, Q_{winj} and their interaction on the response.
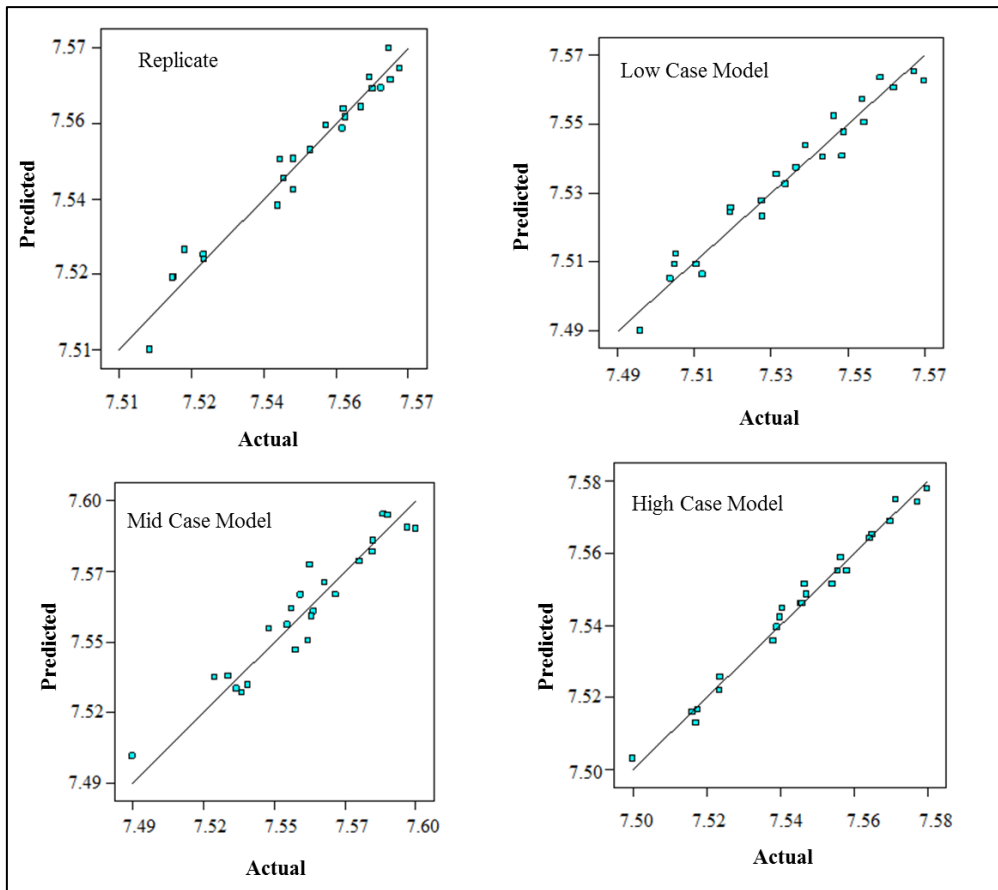
Figure 4. 18: Cross plots of actual experimental data versus predicted value for all models.

Keen observation of the base contour in all these diagrams shows that main factors OVISC, PERMZ, PERMX and Q_{winj} have influence on the recovery. For instance, as can be observed in Figure 4. 19, as the viscosity increases from minimum to its maximum value, the amount of oil recoverable was observed to be decrease. This observation is expected because viscosity controls the mobility of oil and as such as oil viscosity increases, oil mobility reduces so also the recovery. More recovery of oil was obtained while keeping Q_{winj} constant and increasing PERMX from minimum value to maximum. This observation is also true indicating the efficiency of the water flooding as Q_{winj} was set at its maximum value. Similarly, a low recovery of oil was obtained keeping PERMX

constant at minimum while Q_{winj} is at minimum. With PERMX increases to its maximum

value, a proportionate increase in recovery was observed as water injection rate increases.

This was due to preferential increase in flow of oil aerially relative to water and gas. Thus

more residual oil was contacted and swept more efficiently. Maximum recovery was

obtainable at low OVISC and moderate Q_{winj}. At high Q_{winj}, the oil recovery decreases as

the OVISC increases from minimum to maximum. This observation indicates that oil

viscosity is a huge uncertainty and the result further revealed the need to acquire more

realistic PVT data.
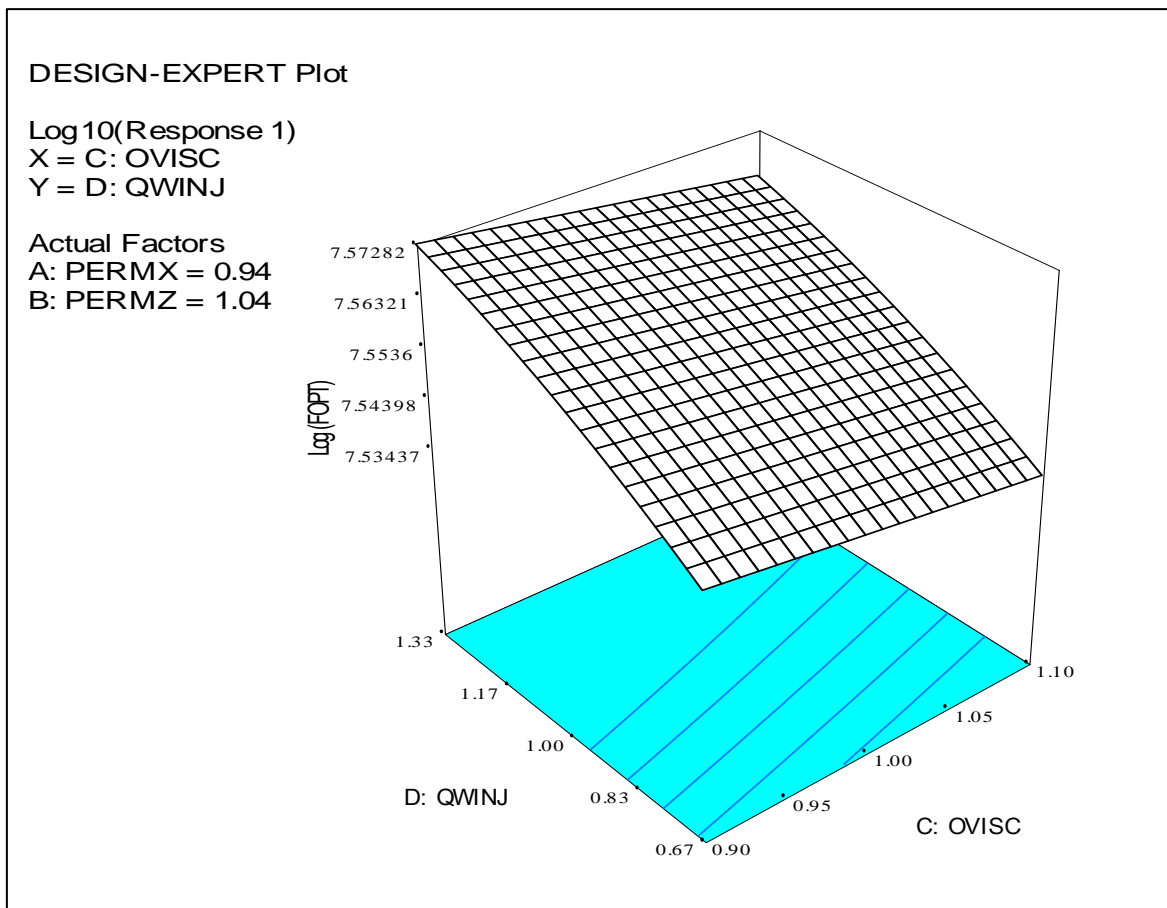
Figure 4. 19: 3-Dimensional diagram for the effect of water injection rate (Q_{winj}), oil viscosity (OVISC) and their interaction on ultimate recovery

DESIGN-EXPERT Plot

Log10(Response 1)
X = B: PERMZ
Y = D: QWINJ

Actual Factors
A: PERMX = 0.94
C: OVISC = 1.00

Log(FOPT)

7.57017

7.56188

7.5536

7.54531

7.53702

1.33

1.17

1.00

0.83

0.67 0.54

D: QWINJ

0.79

1.04

1.29

1.54
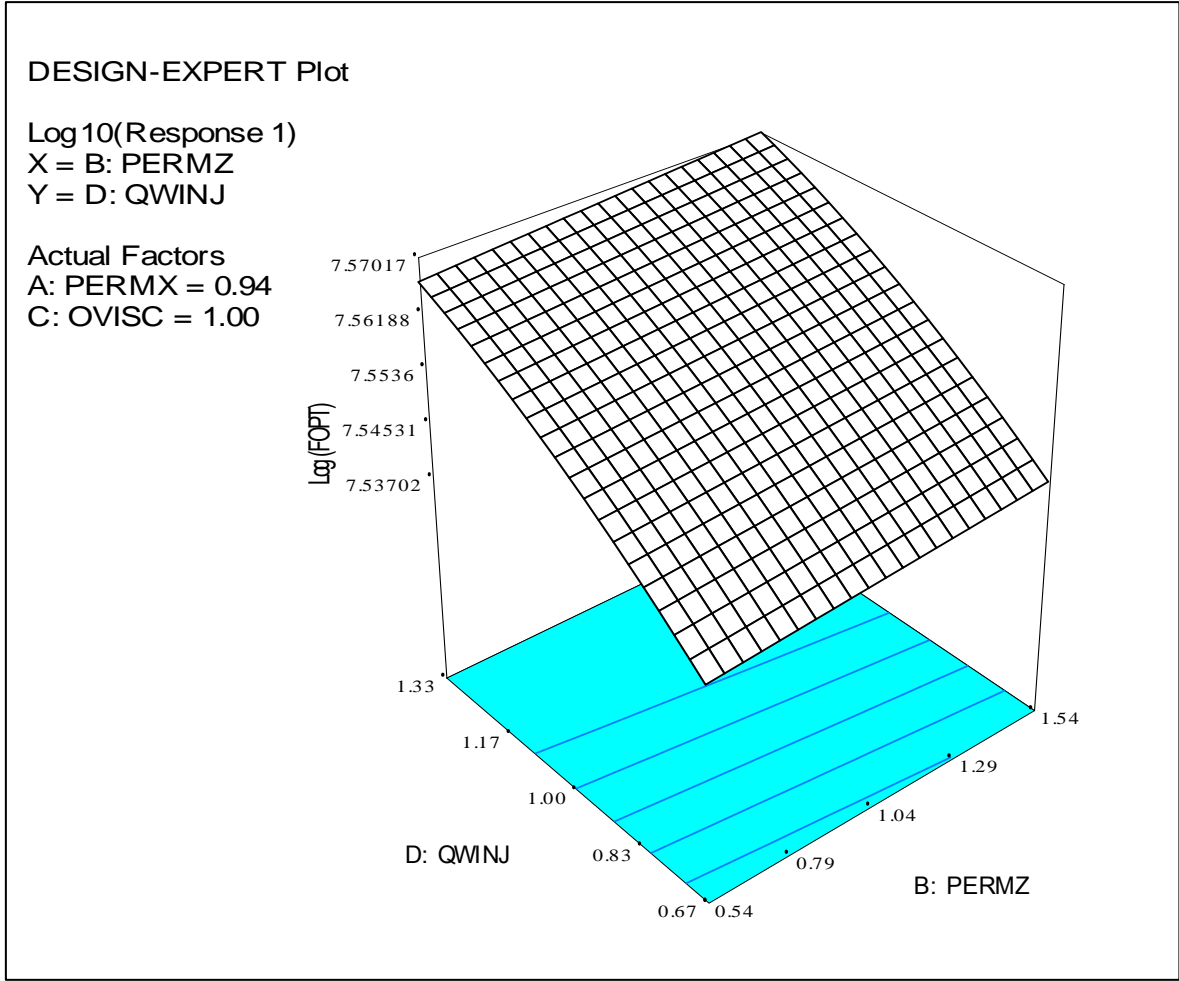
B: PERMZ

Figure 4. 20: 3-Dimensional diagram for the effect of water injection rate (Q_{winj}), PERMZ and their interaction on ultimate recovery

127

DESIGN-EXPERT Plot

Log10(Response 1)
X = A: PERMX
Y = D: QWINJ

Actual Factors
B: PERMZ = 1.04
C: OVISC = 1.00

Log(FOPT)

7.57262
7.55947
7.54632
7.53317
7.52002

1.33
1.17
1.00
0.83
0.67   0.57

D: QWINJ

1.30
1.12
0.94
0.75
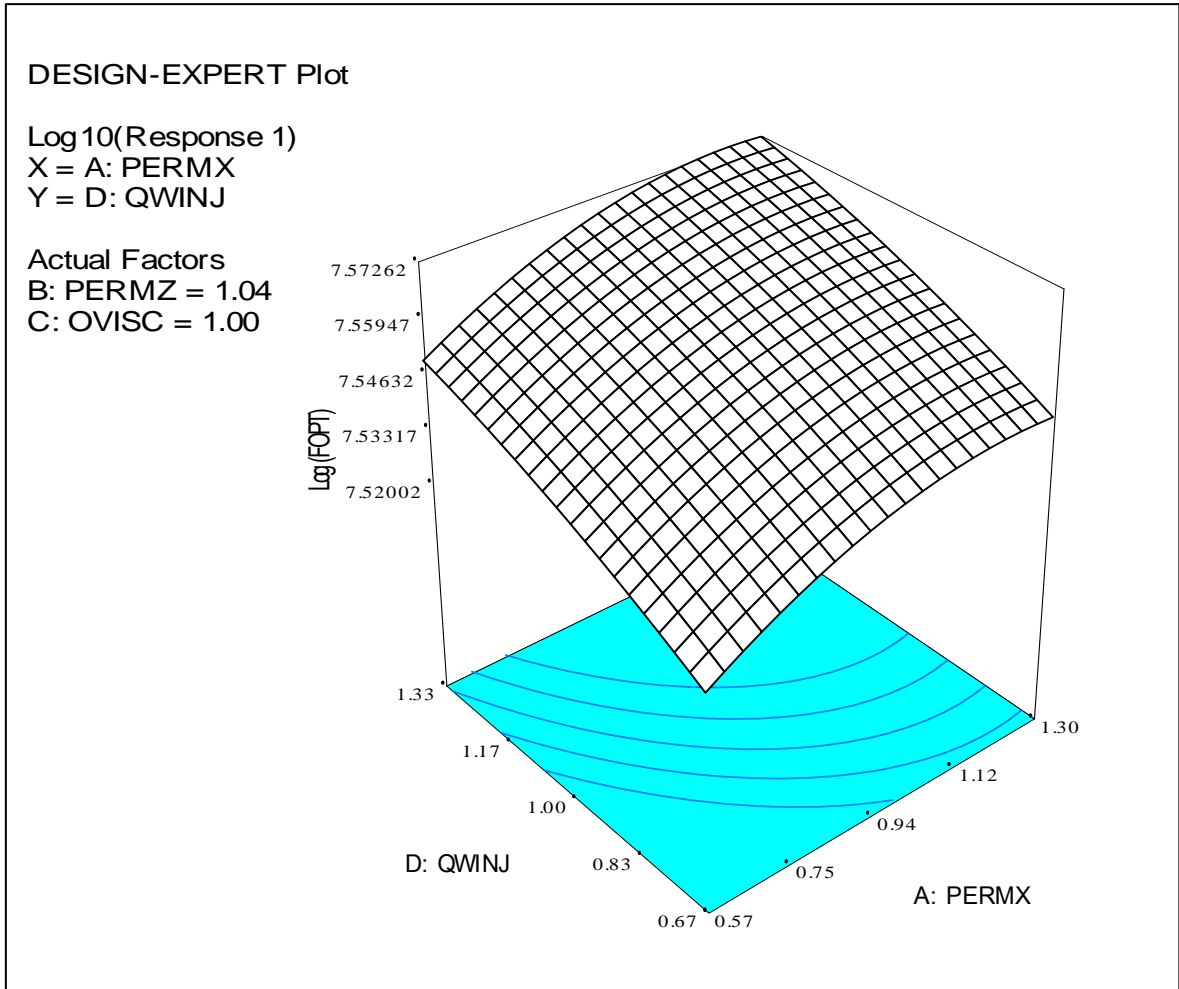
A: PERMX

Figure 4. 21: 3-Dimensional diagram for the effect of water injection rate (Qwinj), PERMX and their interaction on ultimate recovery

128

4.8 Reserves Distribution

Figure 4. 22 shows the representative distributions from the *Latin Hypercube* sampling comprises of 100,000 samples using different proxy models. Figure 4. 23 is a bar chart showing P10, P50 and P90 realizations using proxy equation 4.1, 4.2, 4.3 and 4.4 compared with when the 3 models was used directly for prediction without subjected to uncertainty analysis. The bar chart shown in Figure 4. 23 is normalized with regards to the P50 value (34.88 Mstb). This normalization was done for easy interpretation of the result. The P50 value is the total forecast reserves using the deterministic figure obtained from direct forecast assuming base case/mid case model as shown in Figure 4. 24.

The Monte carlo simulation was constrained on the mean value of reserves for all the models. In other words, the assumption of the distribution functions for different parameters was highly dependent on the P50 realization. The mean reserves was ensured approximated the deterministic figure of 34.88 Million barrels to provide a constraint on the distribution function. Therefore the base case normalized value equals one (unity). The analysis was done by considered extreme percentiles: 10-percentile (denoting a 90% probability that the normalized reserves figures will at least greater than the 10-percentile normalized figure) and 90 percentiles (denoting a 10% probability that the normalized reserves figure will at most greater than the 90-percentile figures). These figures are useful for investment decisions. To assess the degree of uncertainty and quantify them, the disparity between the normalized P10 and P90 figures can provide managers with information on weither to acquire more data for detailed study or adoption of additional

enhanced recovery techniques. Considering the Mid/base case model, the P10 and P90 normalized value are 0.93 and 1.02 respectively.
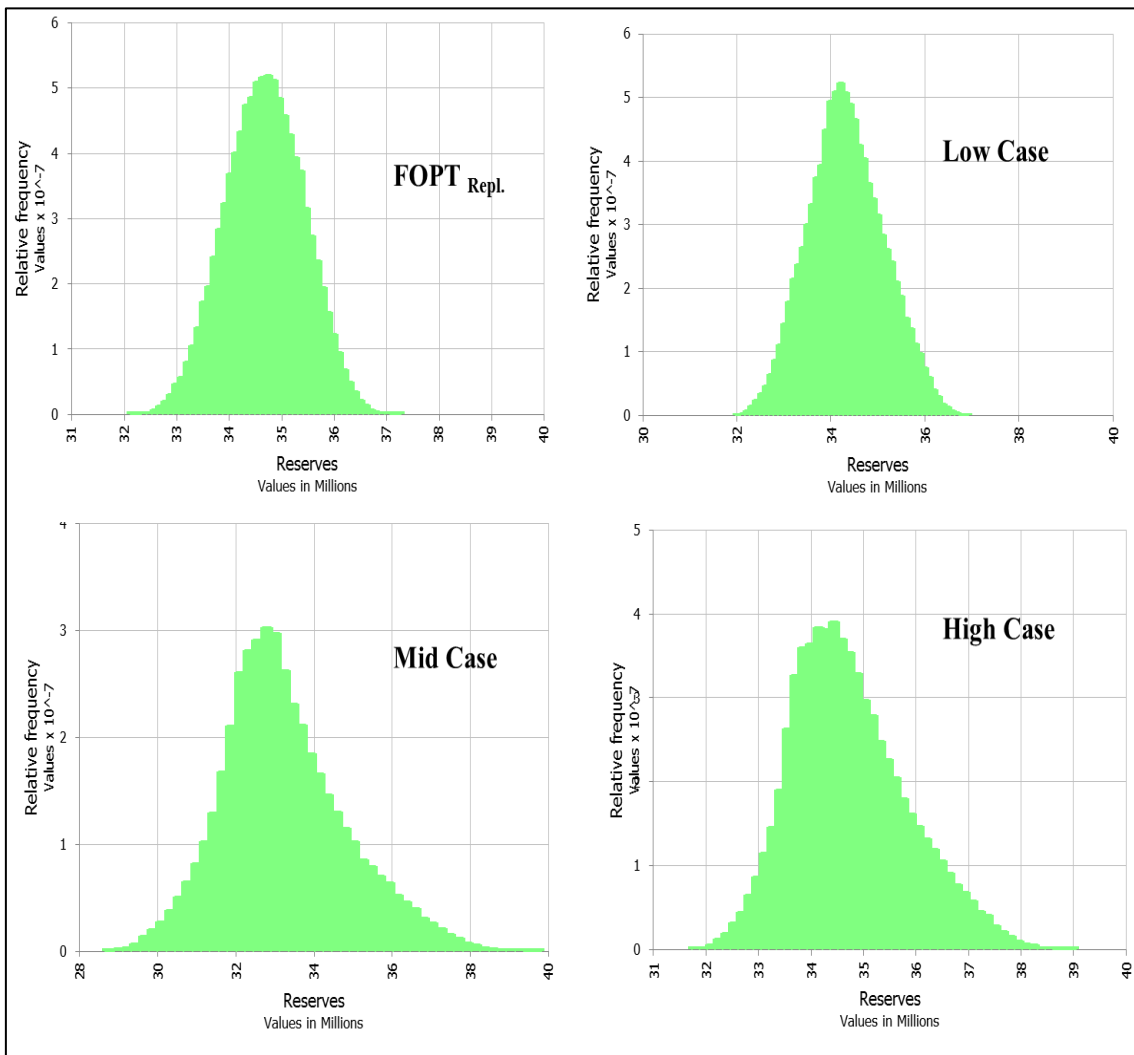
Figure 4. 22: Oil reserves histograms from Monte Carlo simulation using different proxies

This figure indicates approximately disparity of three million stock tank barrel (3.2MMstb) assuming no uncertainty in the structural map. For low case model, the P10 and P90 normalized value are 0.957 and 1.02 respectively. This figure indicates approximately disparity of 2.2 million stock tank barrel (2.2Mstb) assuming the base case

map was interpreted 10 ft below the base map (-10% uncertainty) . For high case model, the P10 and P90 normalized value are 0.961 and 1.042 respectively.
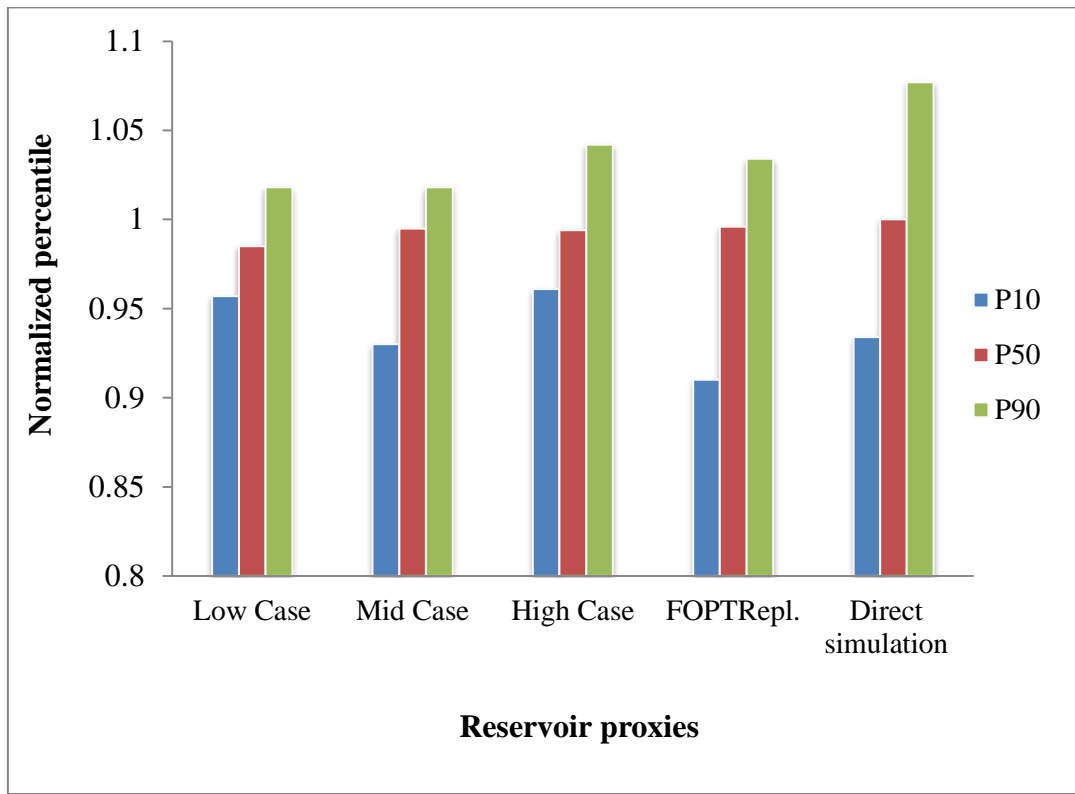
Figure 4. 23: Normalized bar chart for P10, P50 and P90 realizations from simulation and developed reservoir proxies

This figure indicates approximately disparity of 2.8 million stock tank barrel (2.8Mstb) had it been that the base case structural map was interpreted 10ft above the base map (+10% uncertainty). These figures represent uncertainty in the production forecast when compare with the base case. The top and base of the sand if not properly picked can introduce huge uncertainty. In some places, the uncertainty due to structural map can be as high as ±50 ft this can have a huge impact on economic decisions.
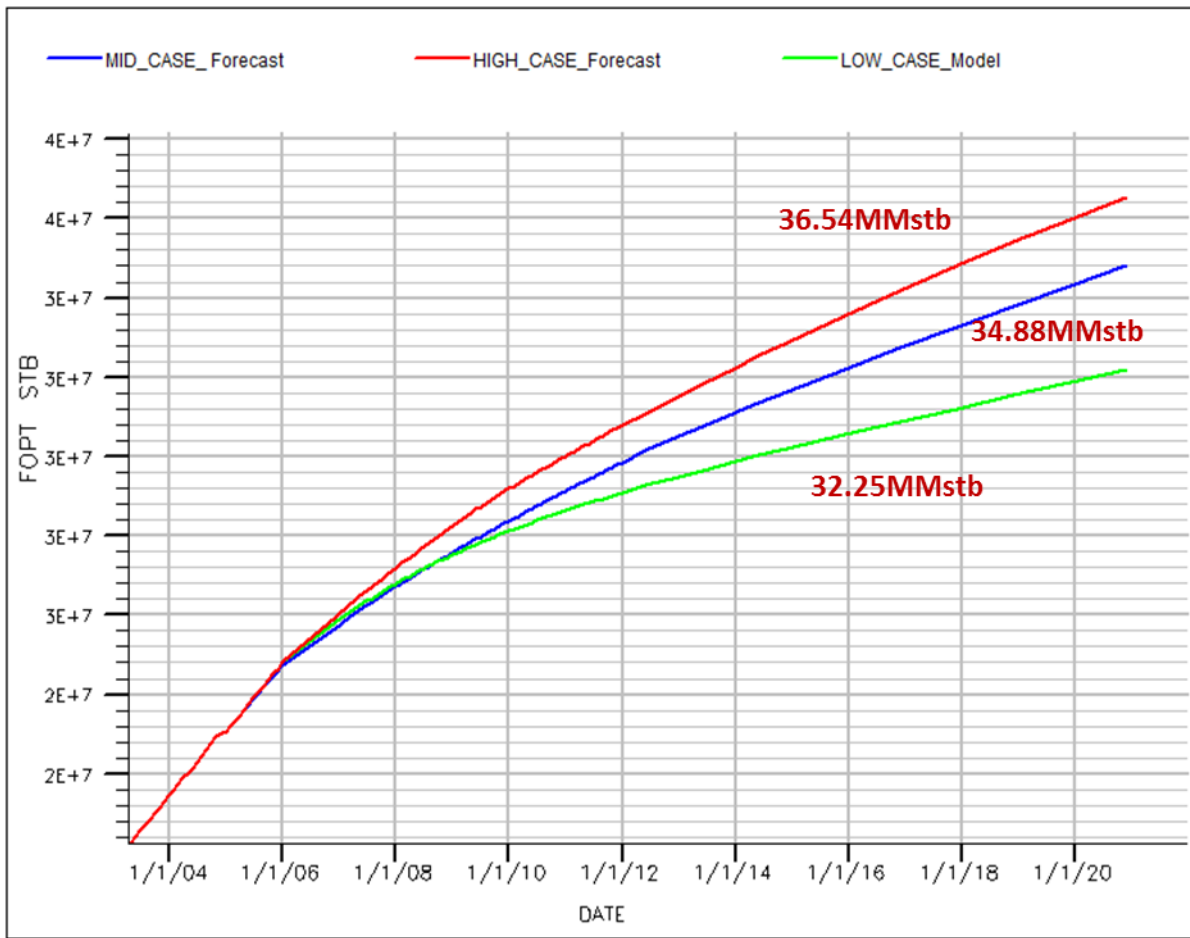
Figure 4. 24: Reprisentative models analogous to P10, P50 and P90 based on simulation approach from three history matched models

The most convention in the industry is to use the base case model then quantify uncertainty using experimental design and Monte carlo simulation. By this approach, the P10 and P90 normalized value are 0.89 and 1.077 respectively. This figure indicates approximately disparity of 6.5 million stock tank barrel (6.52MMstb). However, the proposed approach (the replicates method) which we demonstrated by the integration of the three distict uncertainty models (low, mid and high) resulted to another composite uncertainty model upon which uncertainty analysis was based. In this method, the low and the high case

models are regarded as replicates of the base case which resulted in model Equation 4.1. For FOPTRepl, the P10 and P90 normalized value are 0.91 and 1.04 respectively. This figure indicates approximately disparity of 4.5 million stock tank barrel (4.53Mstb) assuming ±10ft uncertaity in the structuiral map.

4.9 Summary

Structural maps was found to inherit huge uncertainty which affected the dynamic behaviour of the reservoir. In our study we presentat an approach for quantifying uncertainties of production forecast by incorporating uncertainty inherent in structural maps. Three static models (a "Low", "Mid" and "High" cases) were developed, history matched using DoE assisted traditional method and used for production forecast. Two (2) possible alternatives (with and without replication) were considered for uncertainty analysis. This yielded four (4) reservoir proxies using experimental design techniques. Uncertainty was quantified using validated proxies with *Latin hypercube sampling* in a Monte Carlo simulator. There is disparity in reserves figures when compare conventional and the new approach. Without replication, we assumed equal probability for the three model cases and with replication we incorporated the 3 models in the design and this offeres a more realistic answer. The result of assumption of uncertainty as small as ±10 ft on the base case map suggested that the map has inherent uncertainty. The top and base of the sand if not properly picked can introduce huge uncertainty and capable of impact decision on investment and overall management of the reservoir. From the analysis carried out, the degree of heterogeneity within the reservoir was captured by the disparity between the P10 and P90 reserves figures. In all the cases the discripancy varied between 2.2 - 6.5

million stock tank barrels with the upper extreme corresponds to the conventional method and the lower extreme the low case model. The difference suggested that the reserves figure can vary from one company to another depending on the analysis method.

The replicate method that was introduced in this study, indicates approximately the disparity of 4.5 million stock tank barrels. The analysis revealed with 90% certainty that at least a normalized reserve figure of 0.91 will be realized and 10% confidence that at most reserve figure of 1.04 will be realized. Although the conventional method overpredicted the reserves, it can be concluded that the reservoir is fairly homogeneous due to the proximity of these figures and injection of polymer instead of water injection will improve the recovery because the early water breakthrough recorded in some of the wells could actually be delayed. The method is recommendable for developing new non-complex reservoirs/fields where subsurface data acquisition is a challenge.

Chapter 5

5. Infill Placement Optimization

The original problem objective of the case study 2 was to evaluate infill drilling potentials and quantify associated uncertainty. Permeability and porosity fields are the major uncertainties identified during the static modelling phase. Other uncertainties became known during the history matching phase. Petrophysical properties were generated using existing correlations. Presently, the reservoir is producing under primary recovery with recovery factor approximate 28 %. It is desires to improve on this factor to about 35 %. It was conceived that by reducing well spacing, well connectivity can be enhanced which in turns improve oil recovery by accelerating production. Numerical simulation, pressure, and saturation maps were employed to determine well locations and its optimal placement. Evaluation and selection of infill opportunity was carried out by simulating incremental production and water breakthrough time from vertical and horizontal wells completed within the reservoir sub-regions.

5.1 Reservoir Descriptions of Porosity and Permeability

The top surface map and well location in this case study is shown in Figure 5. 1. There are seven wells penetrated the reservoir. The reservoir model was constructed using a 100 x 100 x 1ft that preserve reservoir heterogeneity and accommodate simulation runs. The grid was created using corner point geometry with dimension of 300 ft. X 300 ft. The average porosity
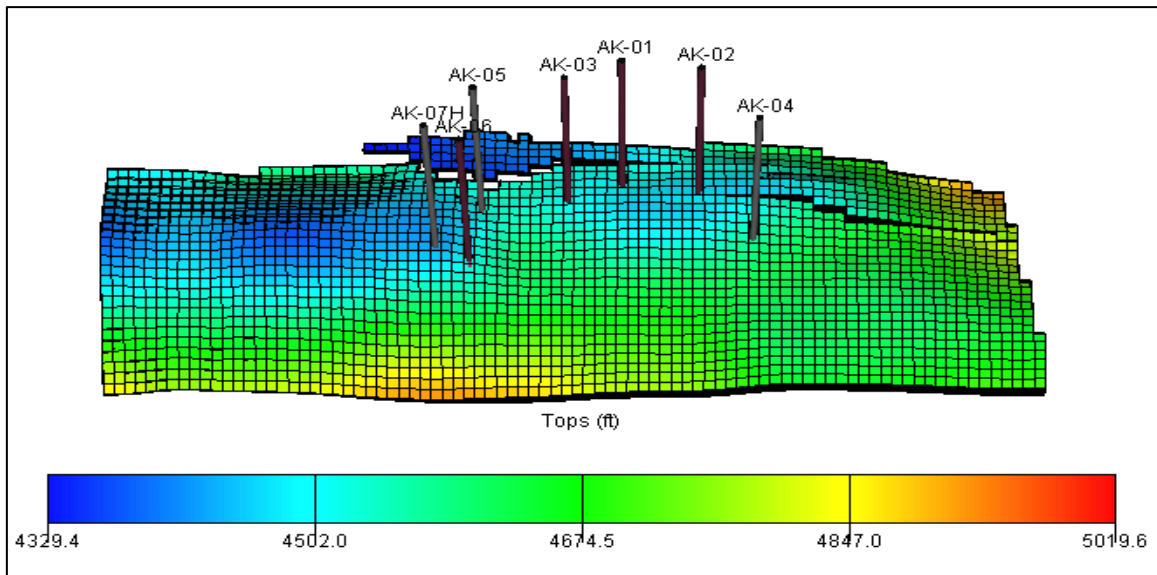
Figure 5. 1: Top surface map showing location of the drainage points

In the reservoir is 22.4% and water saturation and permeability are 27% and 700 mD respectively on the average. Figure 5. 2 shows the isometric view of the permeability distribution in fault blocks A, B, C and D. In all these regions, permeability ranges from 100 mD to 1300 mD. The vertical variation of permeability distribution is prevalent in all the regions. The lateral continuity of permeability was also observed especially in blocks A, B and C. For example, the distribution of permeability values less than 500 md in Region B is mostly laterally continuous which may be attributed to the presence of stacked beds with a high degree of lateral continuity. The permeability histograms shown in Figure 5. 3 for blocks A and C show averages of 500 and 800 mD, respectively. The permeability shows a multi-modal distribution in block A with some small peaks at the extremes of the distribution. These peaks correspond to shale bodies distributed in the reservoir. The permeability value was high at the center of the structure and becomes degraded towards the western direction.
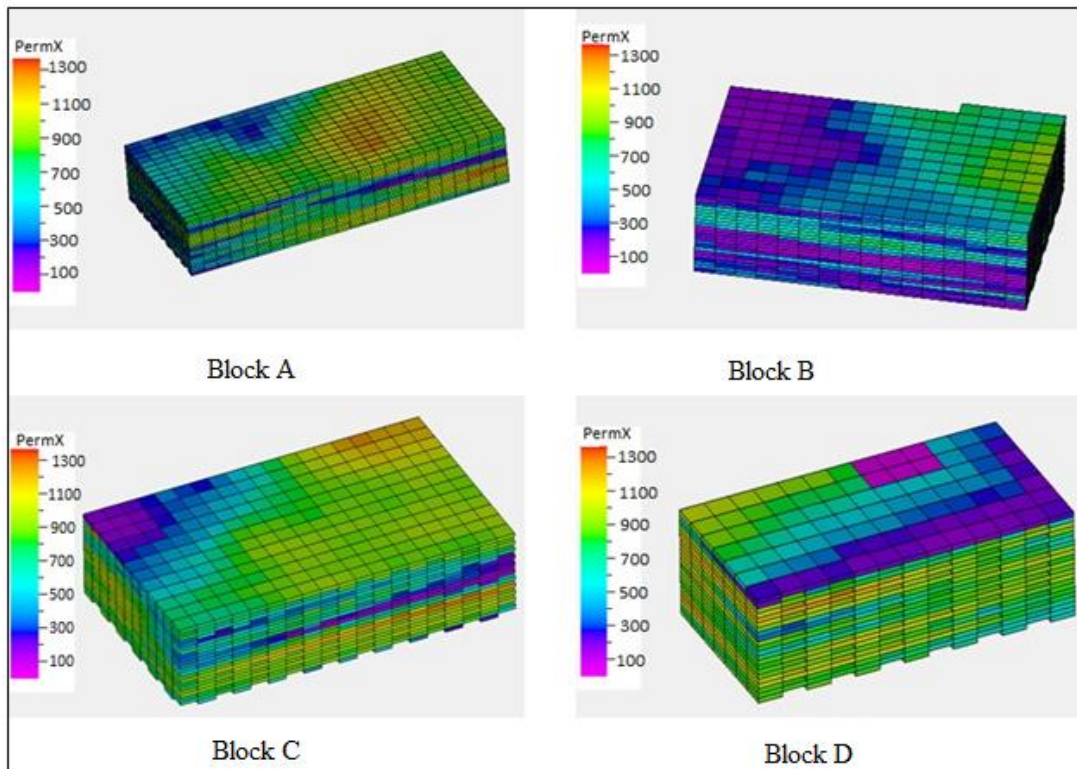
Figure 5. 2: Isometric view of regional permeability models

In block C, the distribution is fairly normal with mean permeability value of 900 mD and standard deviation of 141.4. In the fault block D the permeability is log-normal skewed to the right with mean of 500 mD with some peaks at the extreme corresponds to shale bodies distributed in the reservoir. In fault block B the distribution of permeability is fairly uniform also with peaks at the lower extreme. The average permeability in this block ranges between 500 mD and 720 mD. Porosity histograms for all the regions are shown in Figure 5. 4. Both the porosity and permeability distributions agreed geologically with high permeability found mostly in high porosity regions. Generally porosities range between 10 and 27 percent. Porosity value as high as 36 percent are found in some areas as well. Porosity distribution in

137
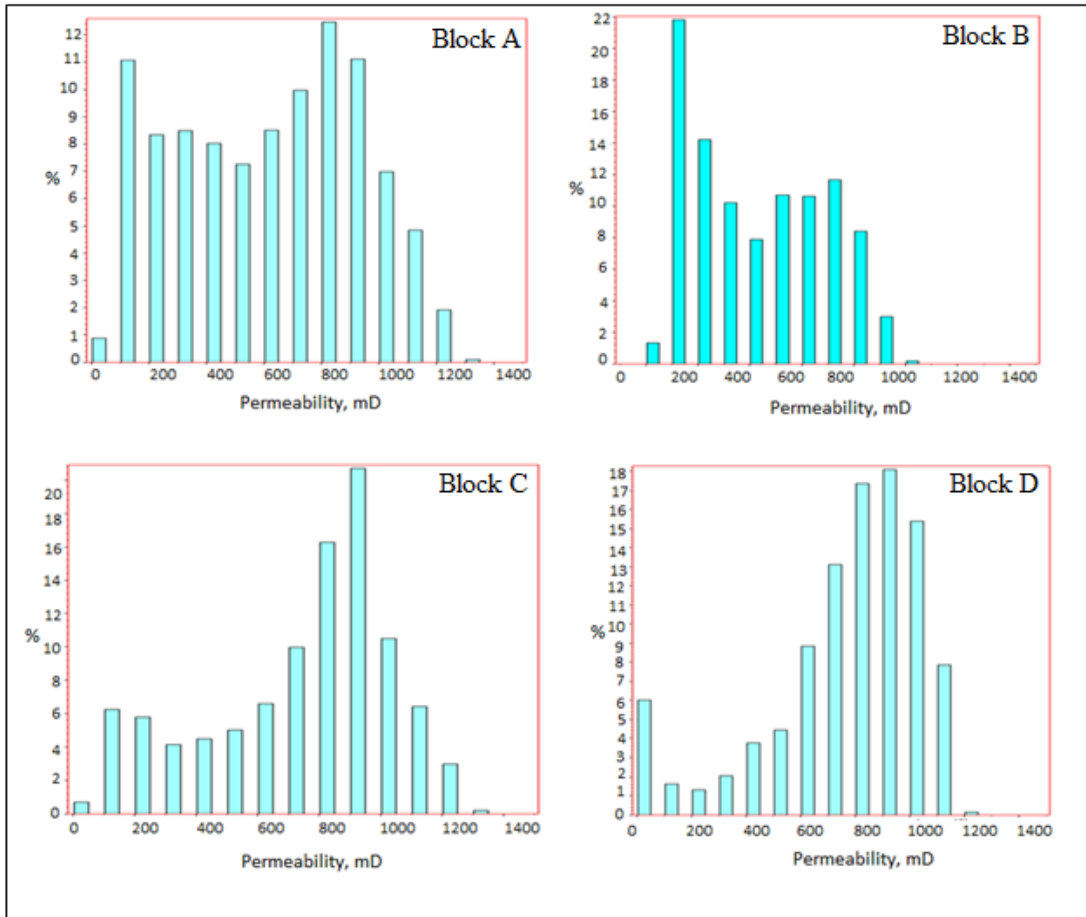
Figure 5. 3: Permeability Histograms for all the reservoir sub-regions

fault blocks A and B is multimodal while blocks C and D exhibited skewed normal distribution. Prior to the determination of infill potential and selection of well type and placement, history matching was done on well-by-well and on field levels using Rwechungura *et al.,* (2011) approach. A review of the production performance is shown in Figure 5. 5 which depicts a realistic trend in oil and water production. But due to gas metering issues in the facilities, it was observed that the gas volumes recorded had inherent errors. Hence, apart from the oil rate that was constrained in the saturation match, preference was given to matching the water cut.
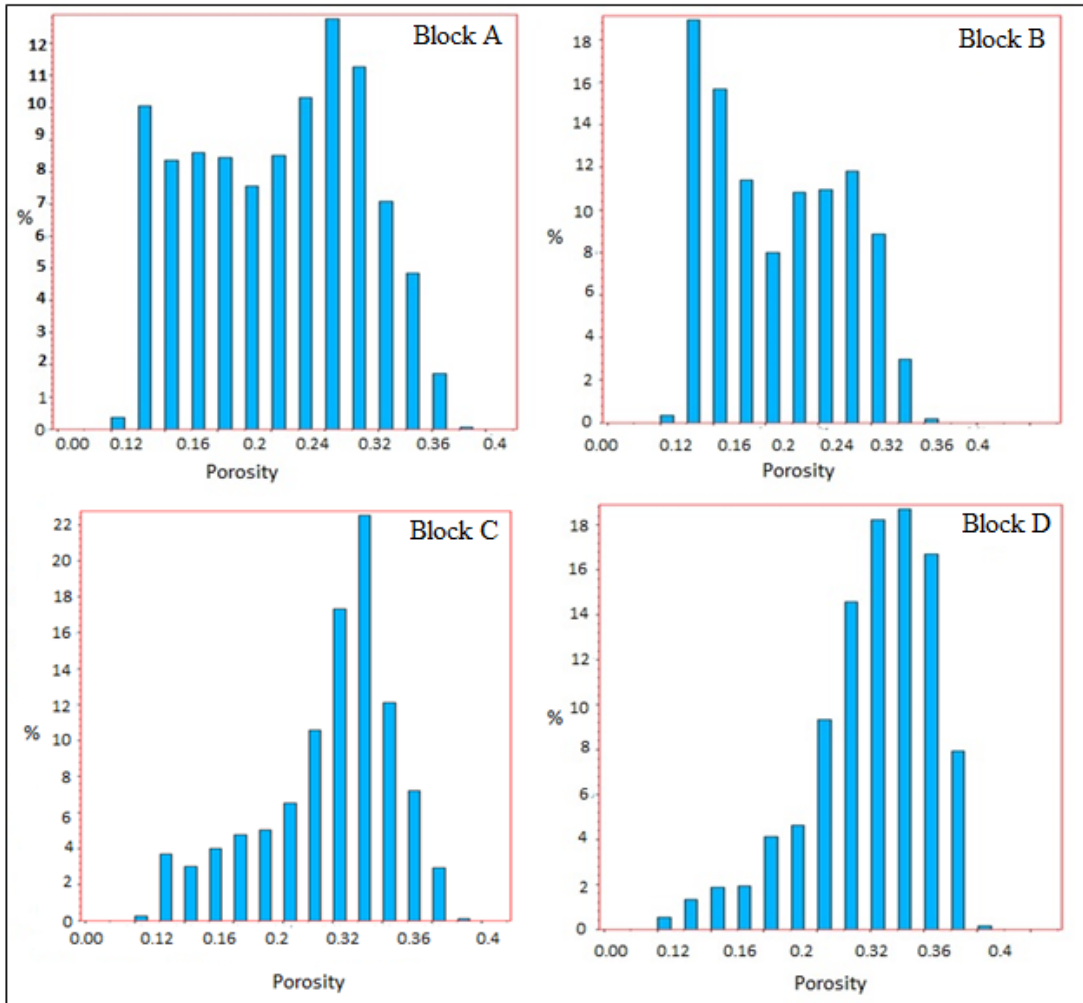
Figure 5. 4: Porosity Histograms for all the reservoir sub-regions

The methodology consists of reservoir type definition, data preparations/consistency checks, material balance calculation, pressure and saturation matching. The material balance tool (MBAL) was used for the evaluation. The three dominant drive mechanisms were fluid expansion, pore volume compressibility and water drive. As shown in Figure 5. 6a, the predominant energy is water influx. The Analytical plot in Figure 5. 6b shows clearly that the observed production cannot be matched without the aquifer in place.
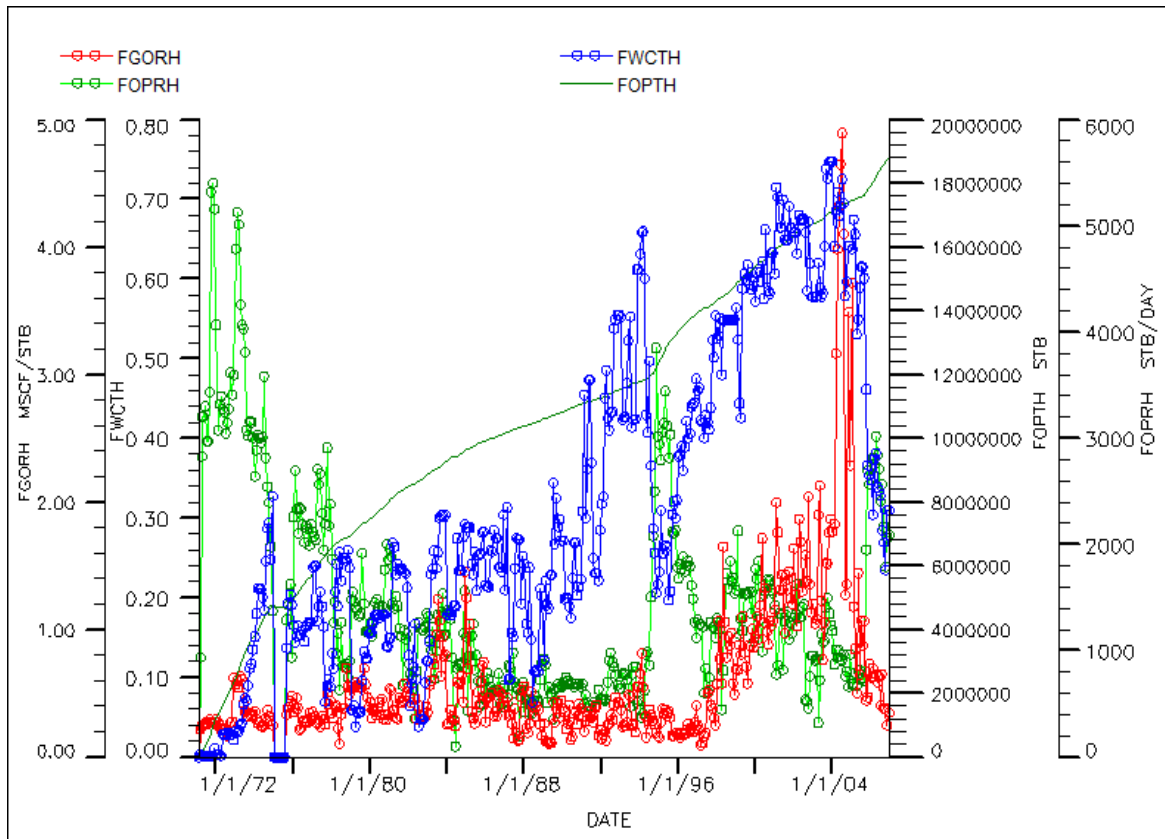
Figure 5. 5: Field Production performance profiles

A steep drop in reservoir pressure when no aquifer was included indicates insufficient energy within the reservoir. The aquifer was modelled numerically and attached to the grid. Using appropriate aquifer pore volume, a stable pressure that fairly matched the reservoir pressure was obtained. After a number of modifications to the aquifer size and its permeability, the pressure match was achieved on reservoir basis.
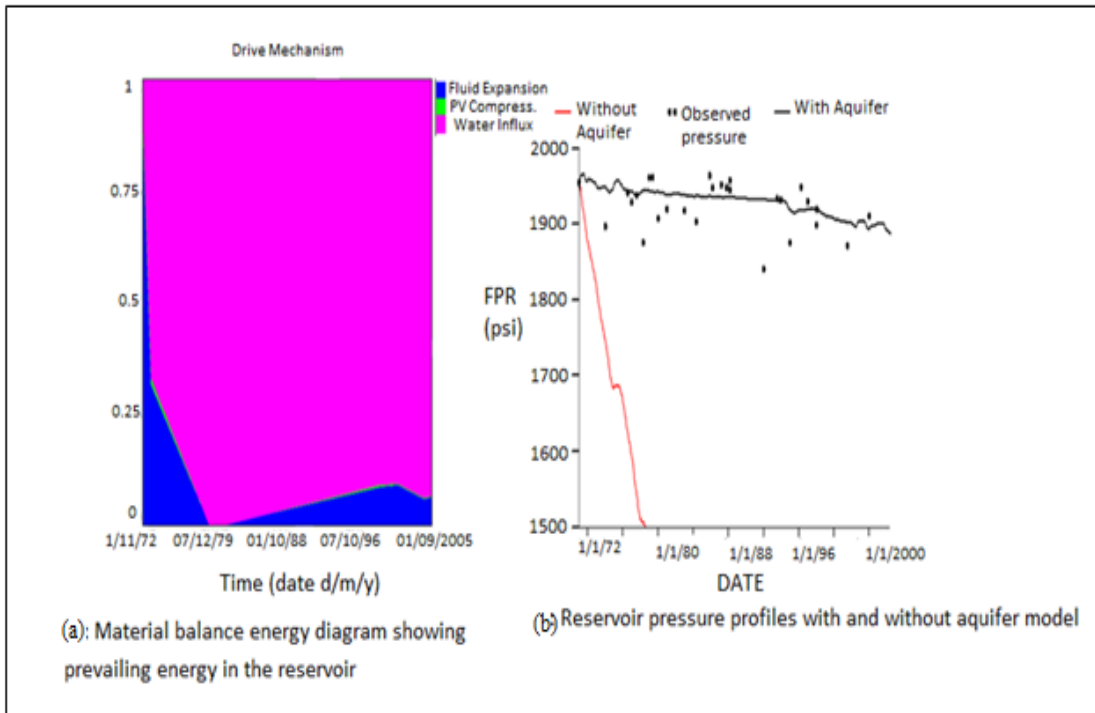
Figure 5. 6: (a) Reservoir energy diagram and (b) Pressure profile with and without aquifer model

5.2 Description of the key uncertainties

The description of the key uncertainties that were changed during the history match is given below:

Relative permeability curves and critical water

Relative permeability is highly uncertain in this study because there is no core measurement. The measurement from analogous reservoir was carefully tuned and used to obtain a history match. Initially the analog data was not favourable to the flow of water as observed in some of the wells. A multiplier of 1.25 was used on water relative permeability to match the water cut (initial water saturation of 19.5%). The reservoir appears to be mixed wet and the water saturation end point has a wide range. Critical water saturation

was increased by a factor of 2 and 1.5 around well AK-06 and AK-07 to match the water breakthrough time. The connate water saturations obtained from the static model were relatively low.

Vertical/horizontal permeability (KV/KH)

Among the parameters that remain uncertain was the ratio of vertical to horizontal permeability. Since the reservoir is undersaturated with no horizontal well penetrated, it was expected that the impact of the parameter be minimal. However, the dominant of water influx (bottom water) and proposed horizontal wells necessitates carrying this ratio further for uncertainty analysis. PERMZ was reduced globally by a multiplying factor of 0.01. This improved the water production in AK-01 by enhancing the lateral flow of water in this area that allowed matching the water cut.

Fault transmissibility

A fault multiplier of 2 was applied to the fault located between AK-01 and AK-04 to match the water influx around AK-01 well. The transmissibility of another fault towards the crest of the reservoir was reduced by 15% as a result of the excessive gas being produced in the model by well Ak-05.

Aquifer pore volume

Aquifer pore volume used for numerical aquifer model was sensitized upon until satisfactory pressure and saturation match was obtained. Figure 5. 7 shows the results of the history matching at field level. It consists of four different graphs of various responses in the vertical axis and time on the horizontal axis. The dotted points indicate the observed

data while the continuous line the simulated values. The pressure match is shown in black colour, water cut and cumulative water produced in blue and the GOR in red. Figure 5. 8 shows the water-cut match for four wells. It is clear that the breakthrough time and observed water-cut levels were matched in all the wells. However, the mismatch observed in field water breakthrough time was due to proximity of some wells to oil-water-contact. Nevertheless, the field matching was considered satisfactory and suitable to use for further evaluation.
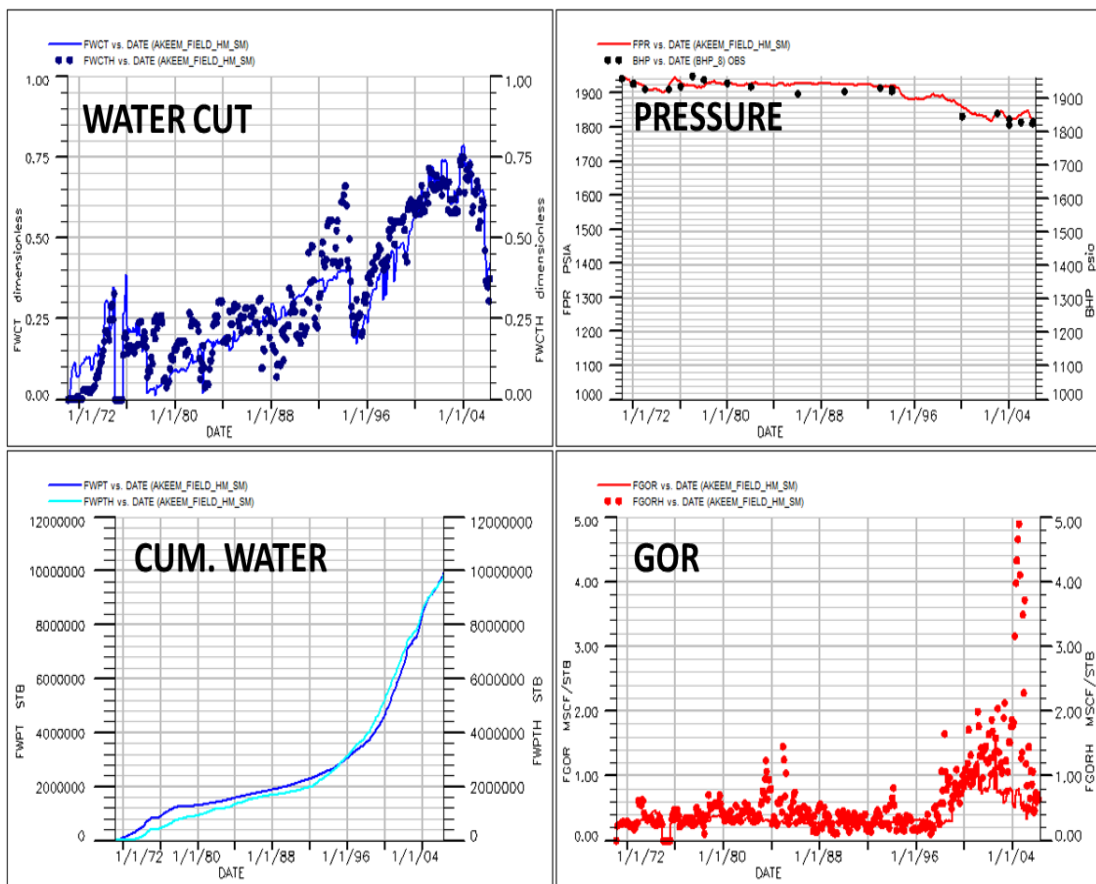
Figure 5. 7: Field pressure and saturation match

143
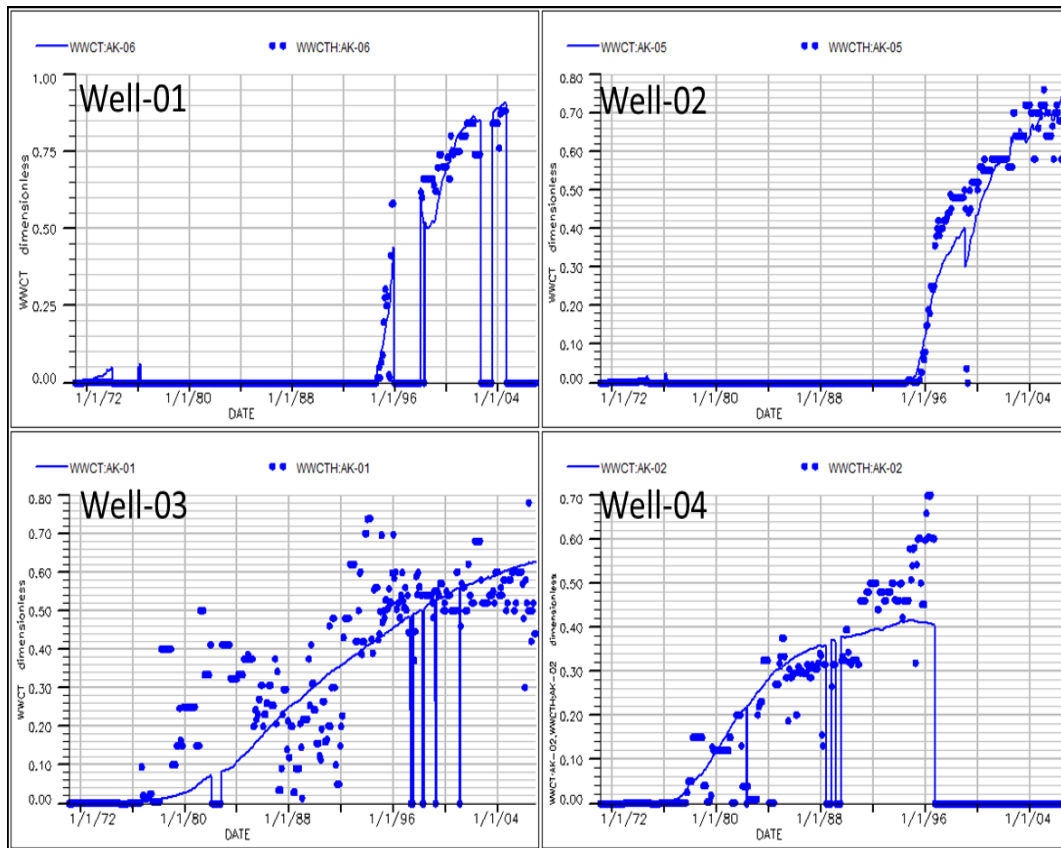
Figure 5. 8: Well saturation matches at well level. The water breakthrough time was well matched

5.3 Residual Oil Saturation

Determination of the amount and location of the remaining oil is key issue for the selection of any development concept. With the aid of saturation maps and location pressures after history match, remaining oil saturations were identified for infill well placement. Figure 5. 9 shows post-history match distribution of the residual oil saturation in some selected layers of the reservoir. It is obvious that beyond the life of the existing wells, substantial oil saturation is left behind. These are found between the existing wells as well as in the intra reservoir shale breaks. Infill drilling is a good reservoir management for this case study.

144
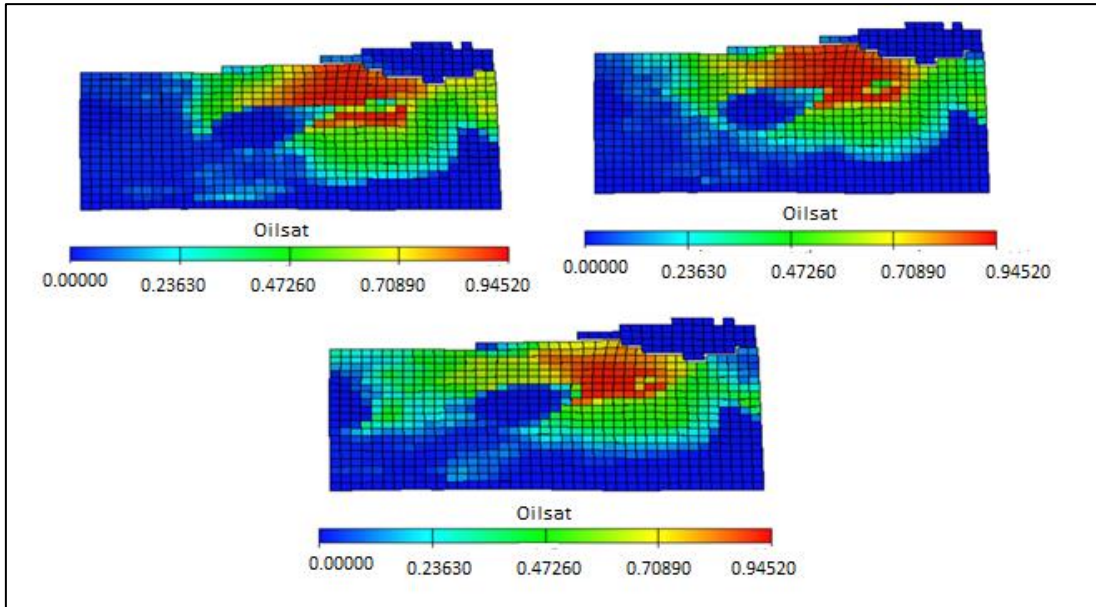
Figure 5. 9: Distribution of the residual oil saturation at the end of history match in some layers of the reservoir.

5.4 Infill Wells selection and placement

The placement of wells at different layers and the determination of optimum horizontal length to be perforated were done manually but guided well by layers oil saturation map. In order to achieve proposed 35% recovery factor, a number of production schemes were considered. This includes the use of all vertical wells or all horizontal wells, or a combination of both horizontal and vertical wells. The well placement was optimized for each scheme by placing the wells one at a time and run the simulation for 18 years. For the horizontal wells, the evaluation of the vertical placement and optimal lateral length was simulated assuming horizontal length of 700 and 1000 m. The inter-well spacing assumed was 400 m. In all the simulations, WBT and recoverable oil are the responses. Analysis was done and recommendations for vertical or horizontal well completion strategies were made based on the results. The vertical wells were always located at the center of the grid.

Analog comparison method (Obor *et al*., 2009) was used to determine the initial production rates because of uncertainties that characterized the available PVT data and also due to lack of reliable well test information. Four vertical wells were strategically located in each of the fault blocks. In each fault block, two horizontal wells were placed. The performance of the vertical wells as well as the horizontal wells was assessed by simulating 400, 600, 800 and 1000 stb/day. Figure 5. 10 and Figure 5. **11** compare production rates for horizontal and vertical wells with optimal completion strategies for the most likely reservoir characteristics. A vertical well produces at a shorter plateau period than the horizontal well for all the simulated rates. Thus vertical wells produces at a significantly lower plateau rate than horizontal wells placed in the same location. The simulation was done using bottom hole pressure of 1000 and 500 psi for vertical and horizontal wells respectively.

In all cases, the optimum rate obtained for each vertical and horizontal wells are 400 and 800 stb/day respectively.

Figure 5. 12 and Figure 5. 13 show the production performance plots for four vertical and 2 horizontal wells drilled at fault blocks B and D. It is obvious that the two horizontal well's performance is better compared with vertical wells. Apart from high cumulative production of oil, horizontal wells are associated with relatively low water cut and delayed water breakthrough time. Figure 5. 14 and Figure 5. 15 show the forecast oil and water cut for the horizontal wells at different reservoir sub-region. The wells are located at different grid blocks and are completed at different layers based on oil and water saturation distributions. The profiles give a quick screening of the possible location and completion of the wells

and therefore serve as guide for selecting appropriate grid block for optimum water cut and recovery. For the horizontal wells, the evaluation of the vertical placement and optimal lateral length was simulated assuming horizontal length of 700, 1000 and 1200 foot. In all the simulations, water breakthrough time (WBT) and recoverable oil are the reservoir responses. The simulation was performed at constant flow rate of 1500 stb/day.
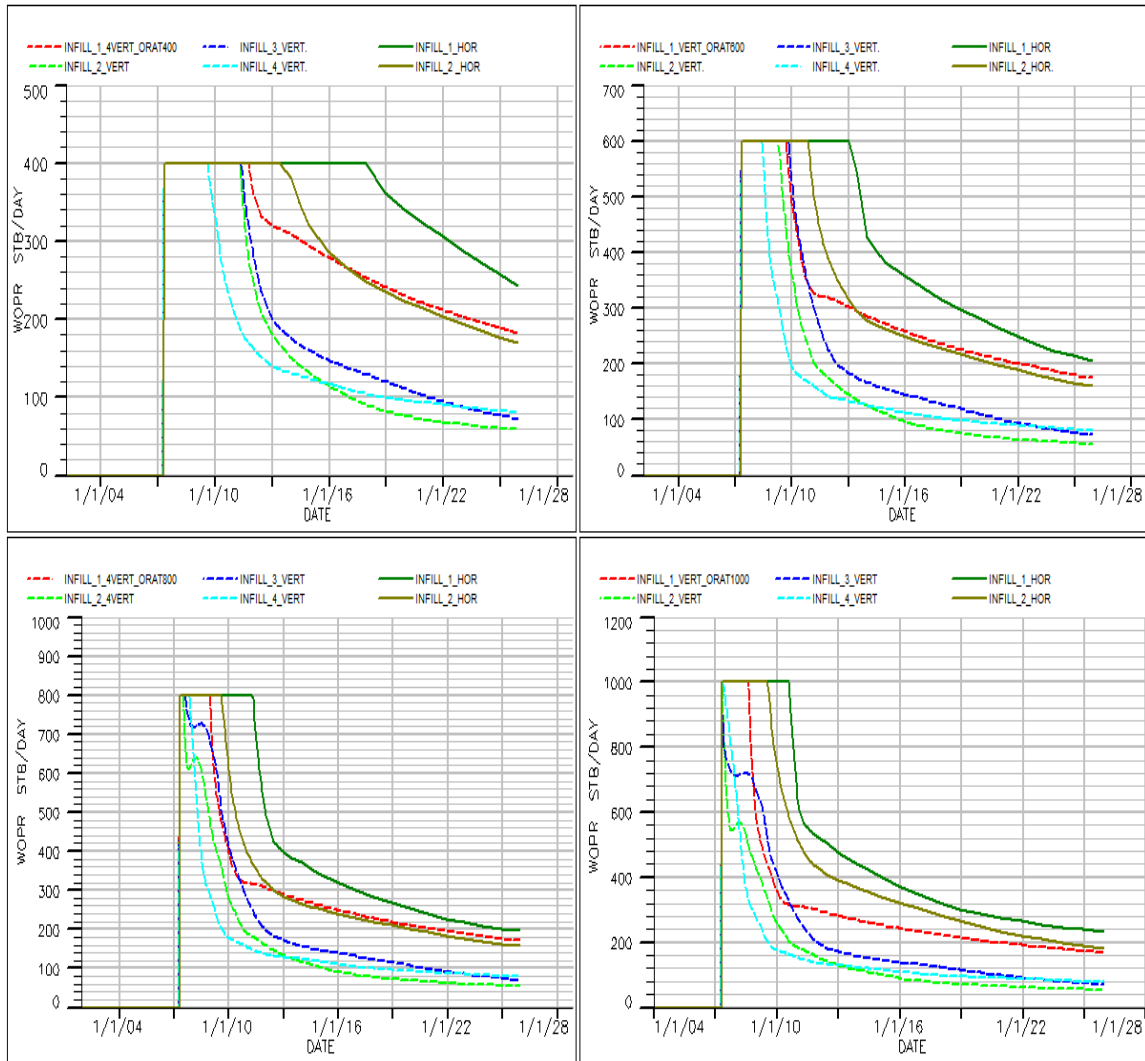
Figure 5. 10: Horizontal vs Vertical Well oil rate Performance (fault block B). Dashed trend-lines represent vertical wells, the continuous lines the horizontal wells.
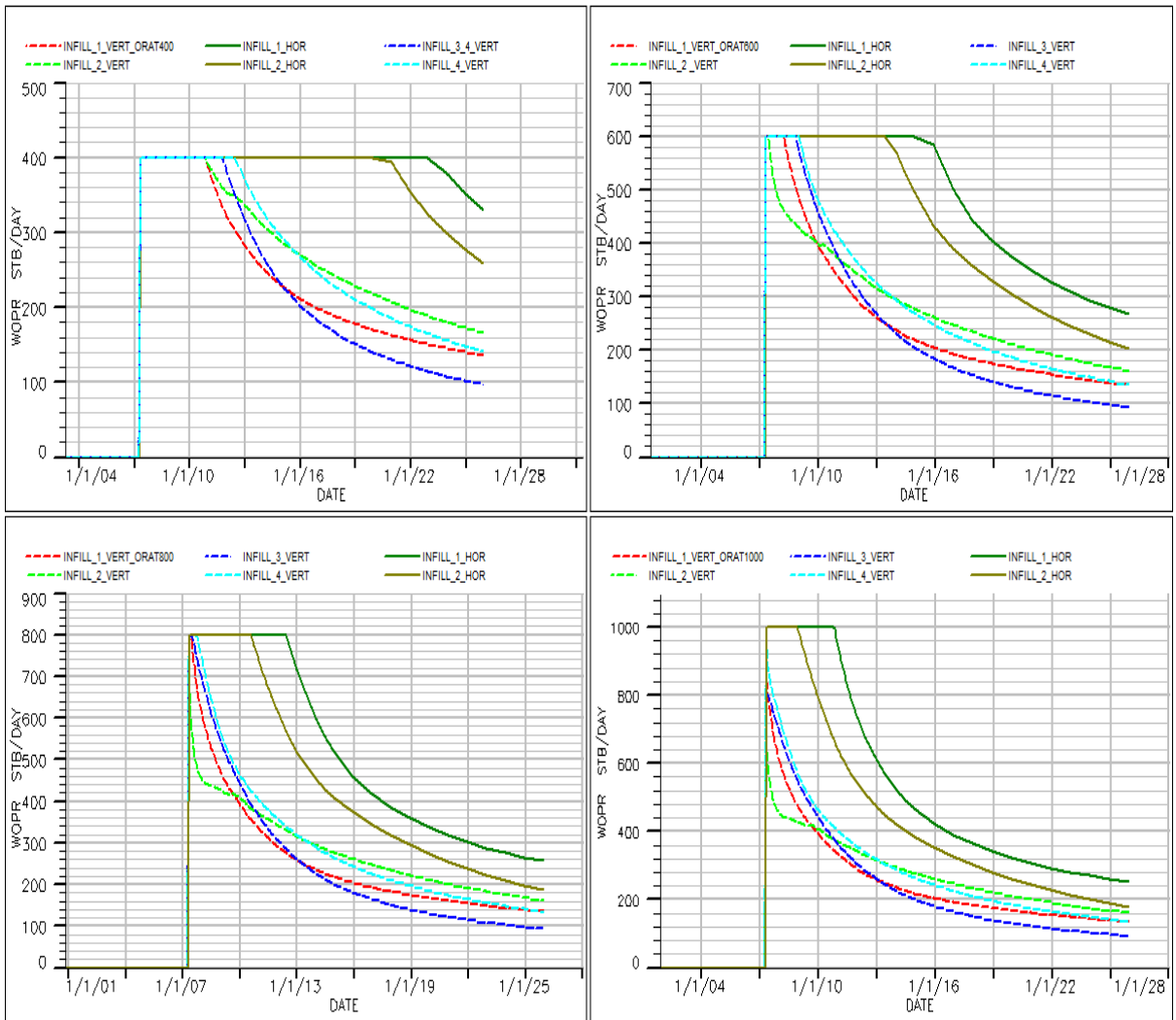
Figure 5. 11: Horizontal vs Vertical Well oil rate Performance (fault block D). Dashed trend- lines represent vertical wells, the continuous lines the horizontal wells

148
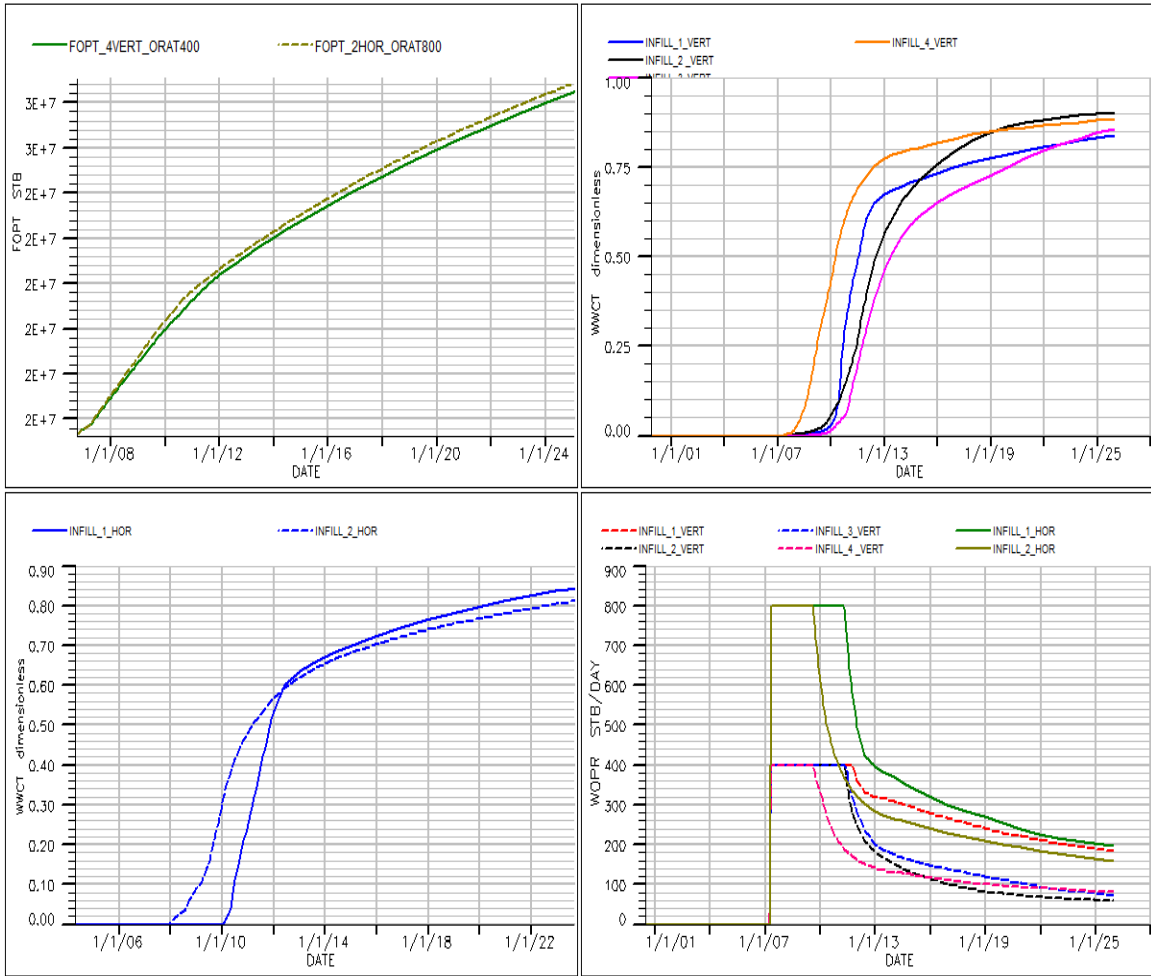
Figure 5. 12: Comparison of the performance plot (Fault block B) of 2-horizontal wells versus 4-vertical wells simulate at 400 stb/day oil rate for vertical and 800 stb/day for horizontal well.
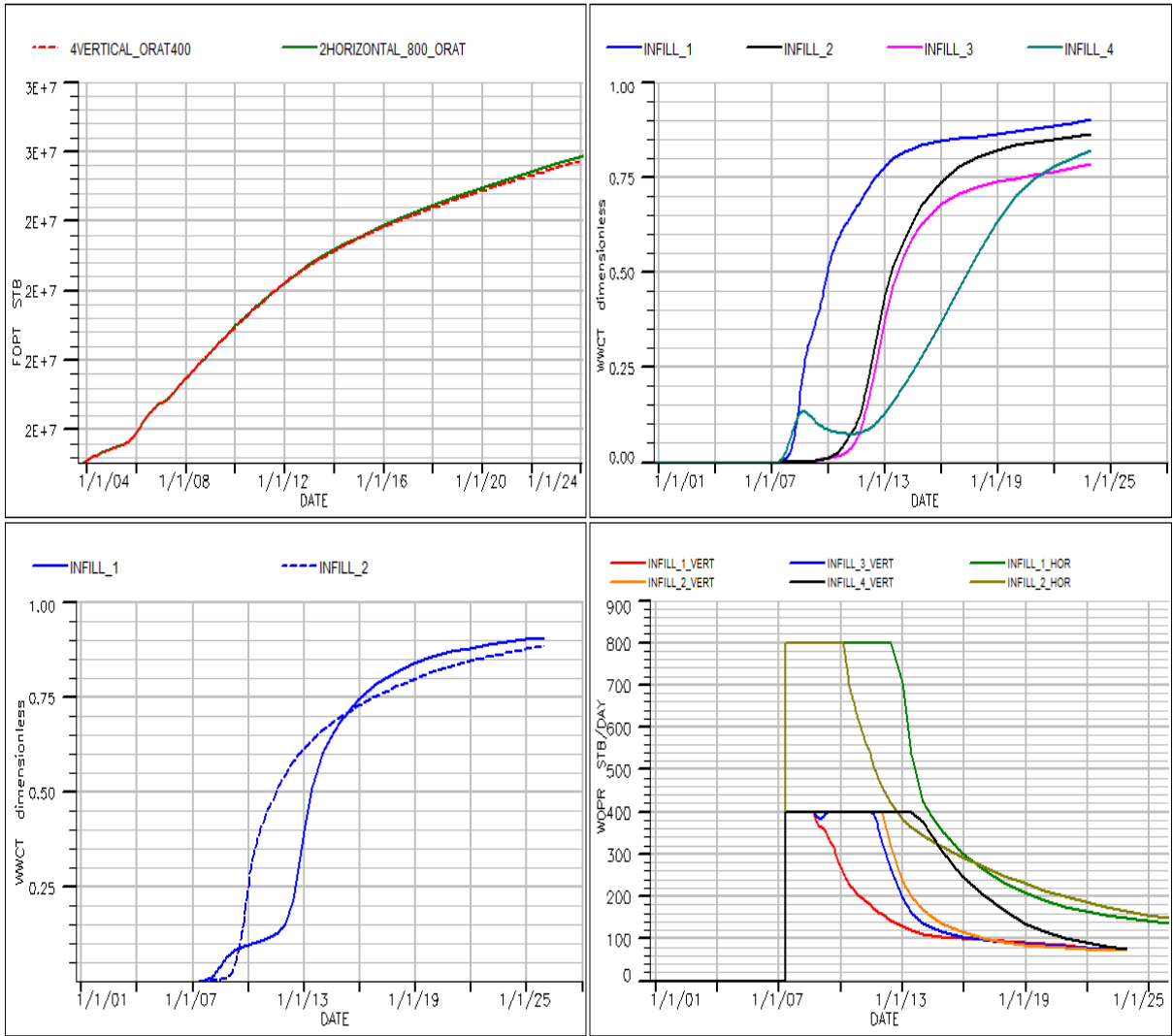
Figure 5. 13: Comparison of the performance plots (Fault block D) of 2-horizontal wells versus 4-vertical wells simulated at 400 stb/day oil rate for vertical and 800 stb/day for horizontal well
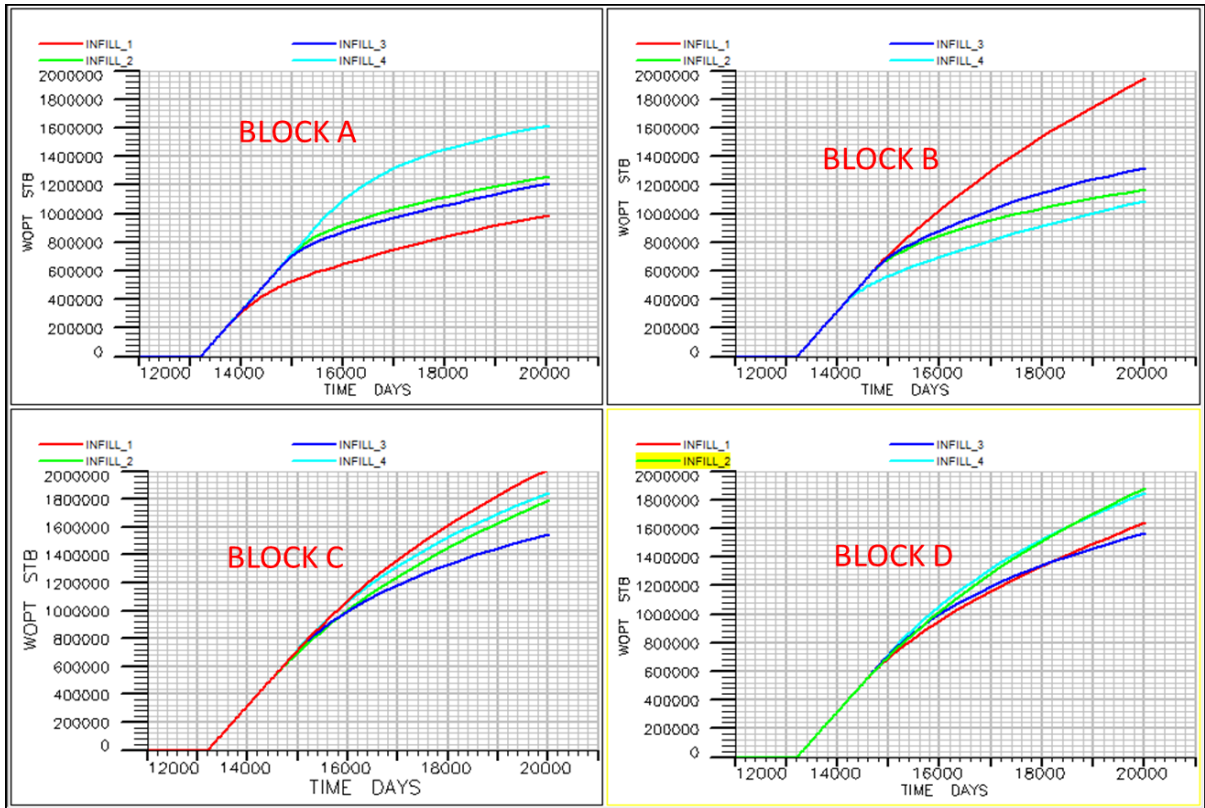
Figure 5. 14: Vertical Well Production performance plot in various reservoir sub-regions.

In Block A, it is evident that the location and completion of the well Infill_1 (red color) can be regarded non economical considering simulated oil recovery. Infill_2 (green color) and Infill_3 (blue color) exhibited higher recovery when compared with Infill_1 in this fault block. The well infill_4 (light blue) exhibited highest recovery. Similarly, in Block B, production from location of infill_1 is shows highest production forecast. Block C and D can be said to be the most prolific in-terms of oil production. Here, the placement of Infill_1 in Block C and Infill_2 and Infill_4 in Block D are potential locations for economic recovery of oil from these fault blocks.
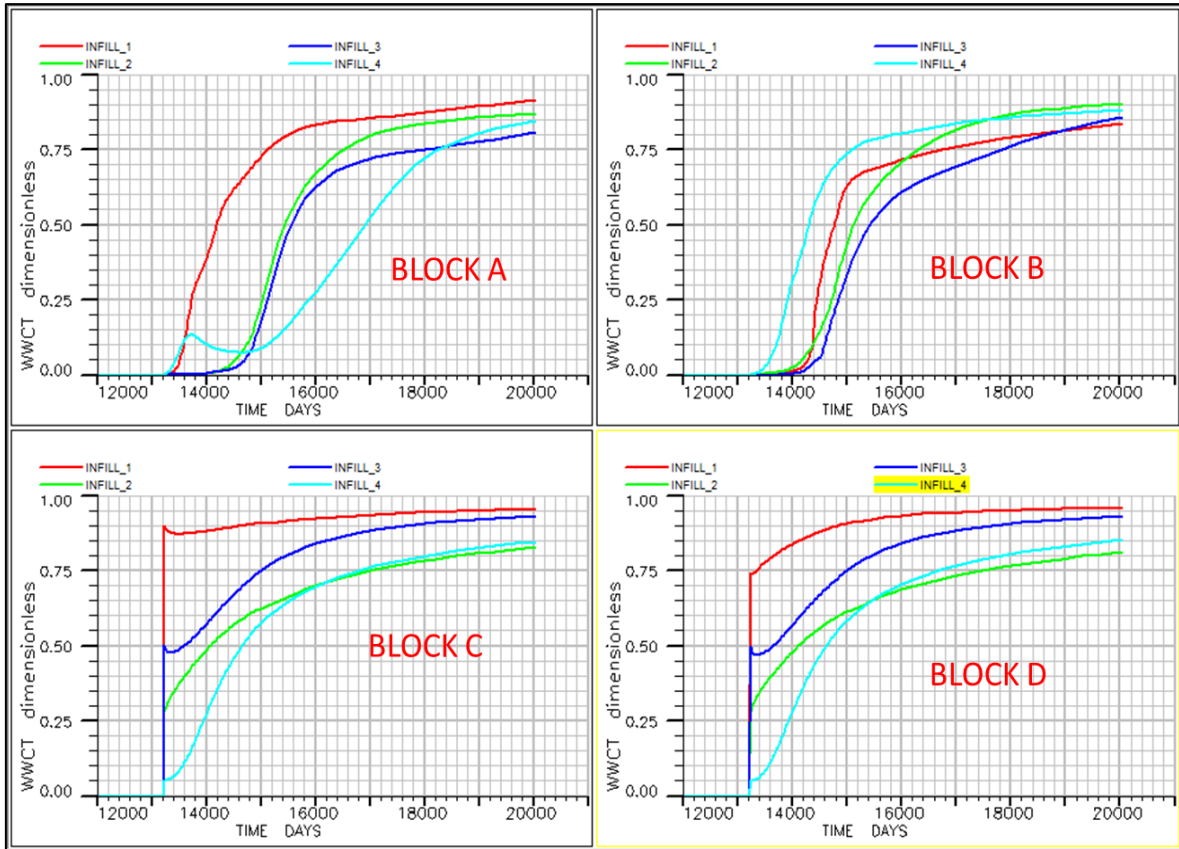
Figure 5. 15: Vertical Well water cut profiles in various reservoir sub-regions.

In Block A, the well Infill_1 shows high water cut and early WBT. In terms of WBT, Infill_2 and Infill_3 exhibited most delayed water break through time. The well infill_4 exhibits moderate water cut and recovery. In Block B, production from location of infill_1 shows minimum WBT and minimum water cut. Generally, water front reaches most wells in Blocks C and D and production was characterized by significant water conning from the top of structure and water displacement in the lower half of the reservoir. Placing horizontal well at these regions can reduce the conning effects and enhance recovery. For the vertical wells, Figure 5. 16 shows clearly that infill drilling can substantially increase the recovery. The result obtained from the simulation of 4 vertical wells drilled at each

152

fault block shows incremental production compared with the base case which is characterized by no infill well.
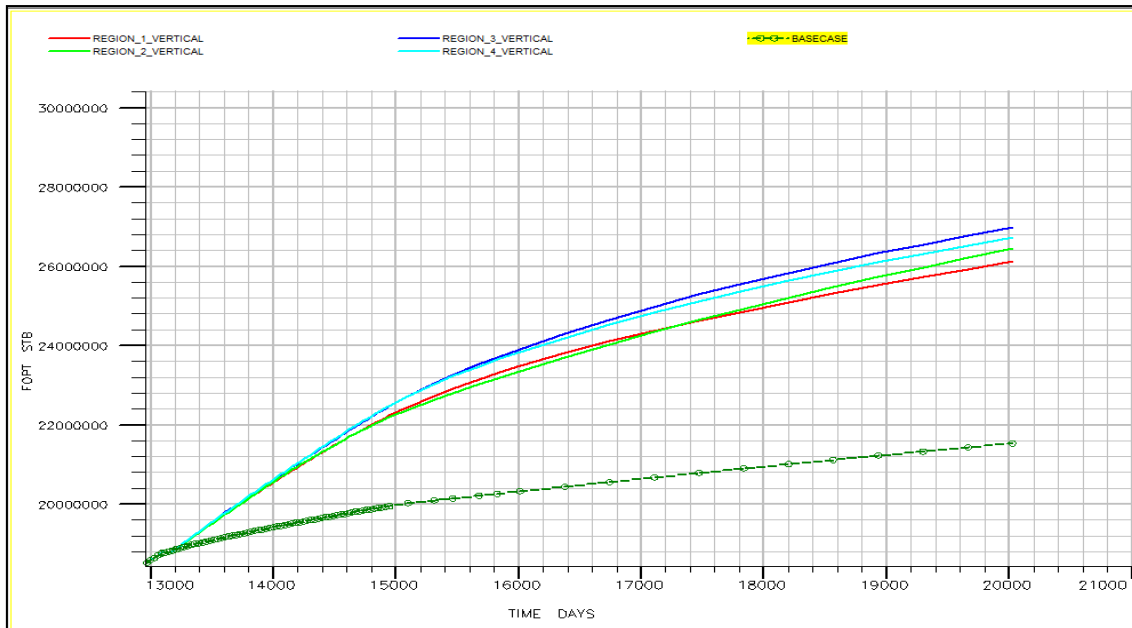
Figure 5. 16: Comparison of cumulative oil production in various reservoir sub-regions with the base forecast (no infill case), the dotted green line

5.5 Horizontal well length and oil recovery

Figure 5. 17 and Figure 5. 18 shows the sensitivity of the lateral length of the horizontal wells to incremental production from fault block B and D respectively. A strong sensitivity to the length of the horizontal well was observed between 100 to 400 meters. There is no significant difference in additional recovery when 500 meters and 600 meters horizontal length was simulated. However, a horizontal length of 400 meter shows a marked difference in additional recovery when compare with simulated 300 meter length.
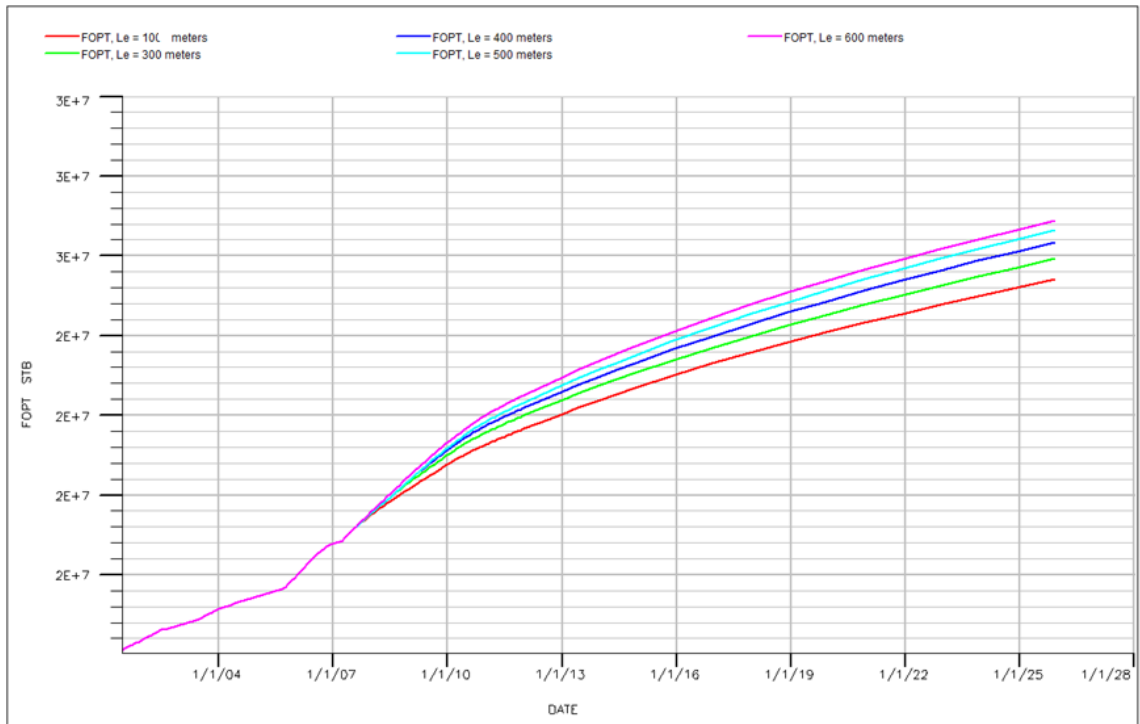
Figure 5. 17: Sensitivity of additional recovery from the fault block B to different lateral

length of the horizontal well
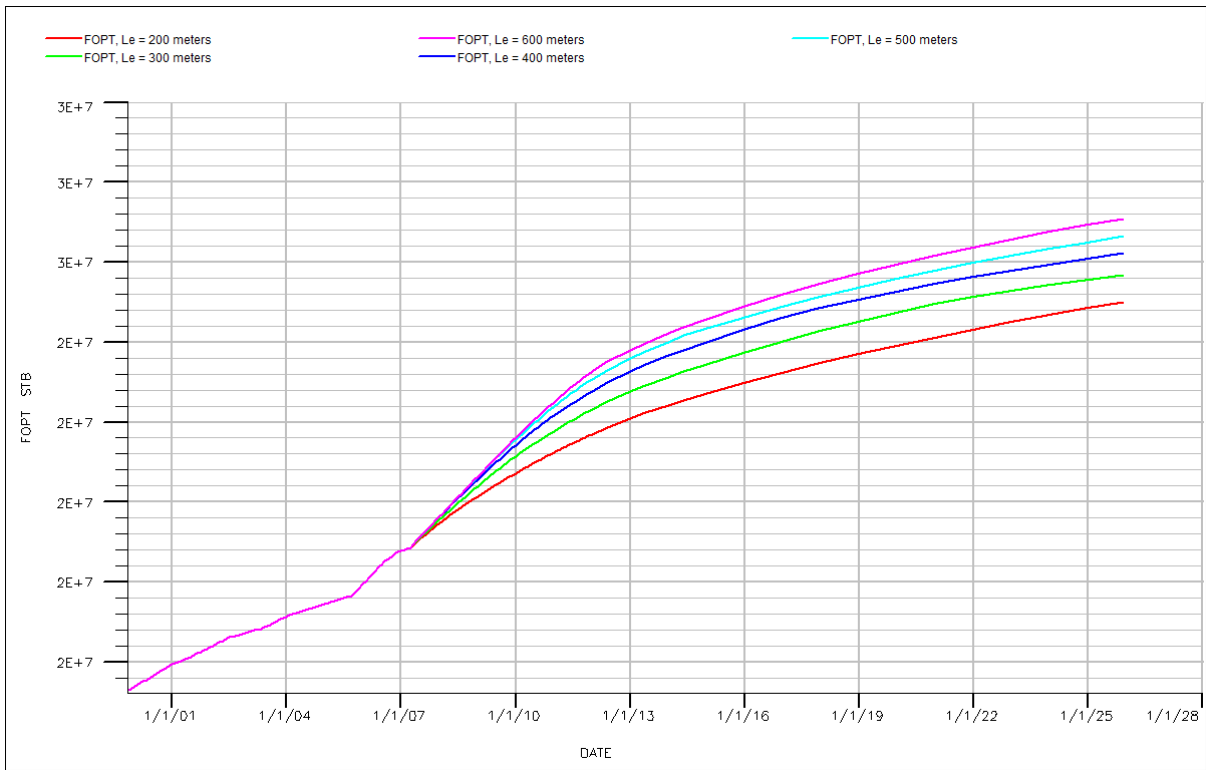
Figure 5. 18: Sensitivity of additional recovery from the fault block D to different lateral length of the horizontal well

Table 5. 1 shows the result of the analysis performed at different fault blocks for horizontal and vertical wells. It compares the performance of the horizontal and vertical wells across the reservoir sub-regions as well as the effects of the lateral length of the horizontal wells on production and water break through time. The recommendations to drill or not was based strictly on number of wells, WBT and cumulative oil recovery. The results show that in all the recommended regions for infill drilling horizontal wells with 400 meters lateral lengths give higher productivity.

155

Table 5. 1: Summary of Wells performance for optimum well selection and placement

Reservoir	Well Type	No of wells	Well length (meters)	Cum. Oil (MMSTB)	WBT (days)	Remark
	Vertical	4	6, 6, 4.5, 6	5	30	
Region1	Horizontal	2	400	5	30	No infill
			600	5.3	30	
	Vertical	4	6, 4.5, 6, 7.5	5.5	549	
Region2	Horizontal	2	400	5.3	1491	Infill
			600	6	1614	
	Vertical	4	6, 5,4.5,4.5	6.2	30	
Region3	Horizontal	2	400	6.2	30	No Infill
			600	6.5	30	
	Vertical	4	6, 4.5, 6, 6	7	30	
Region4	Horizontal	2	400	6	519	Infill
			600	7	641	

Drilling two horizontal wells each of lateral lengths of 400 meters in fault block A produced 5 MMSTB the same quantity obtained from drilling 4 vertical wells in the same block. However, using 600 meters and 400 meters horizontal well lengths, the simulation result indicated no significant difference in additional reserves. This region can be said to be almost depleted. Considering additional reserves, a horizontal well is optimum with well length of 400 meters in blocks A and C. However, it was observed that all wells (vertical and horizontal) experienced WBT a month after production hence, infill drilling in these blocks was not a viable option. The horizontal wells were observed to be more efficient producers than the vertical wells at the target rate from fault blocks B and C. Drilling two horizontal wells with lateral length of 600 meters in Blocks B and D allows more recovery and exhibited delay in WBT. Figure 5. 19 shows the incremental production and compares well performance based on well number and type. The result of the simulation show better performance with four horizontal wells compared to eight vertical wells in fault blocks B and D combined.
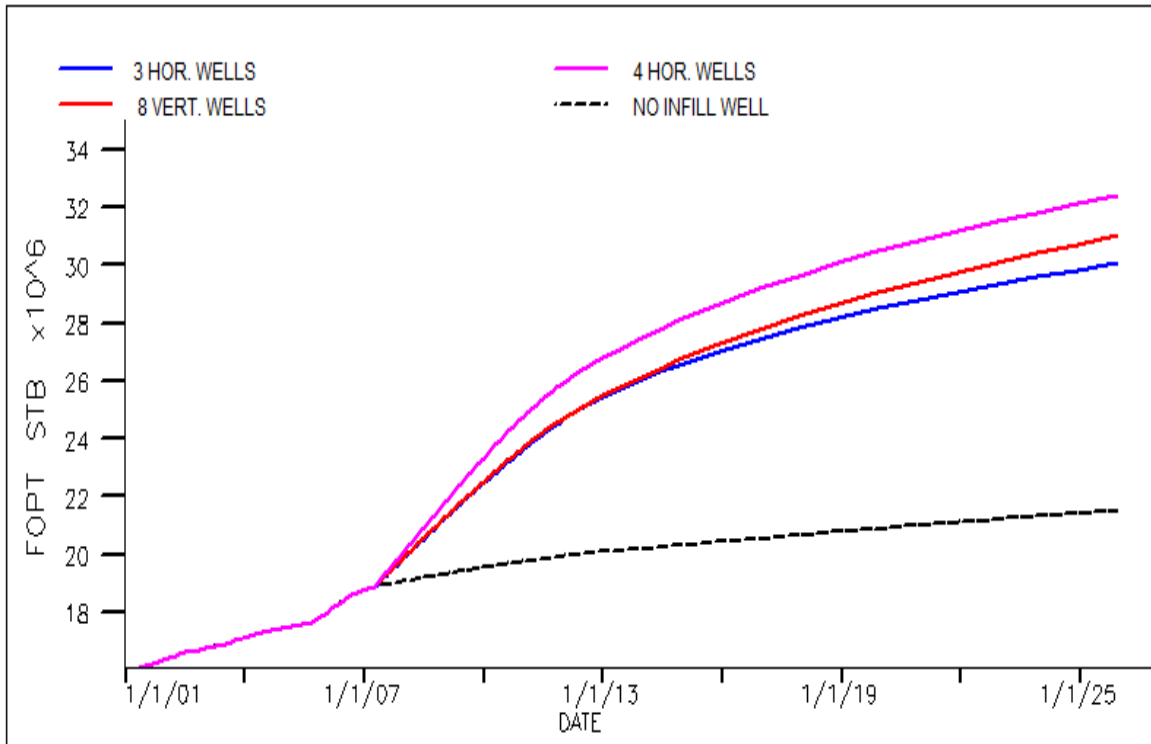
Figure 5. 19: Comparison of incremental production from vertical and horizontal wells.

The "8 vertical wells" is the total number of vertical wells drilled and completed in Blocks B and D with 4 wells drilled each to the same regions. Likewise, total number of 4 horizontal wells was drilled with two horizontal wells drilled and completed each in Blocks B and D respectively. For optimal number of infill well required, three horizontal wells were drilled and simulated. First, two wells completed in Block B and one in Block D. Then, with one horizontal well completed in Block B and two horizontal wells drilled and completed in Block D. Block D was found to be more productive than Block B and hence the ratio of horizontal wells simulated in Block B and D is 1:2. Based on this analysis, two horizontal wells of 600 meters lateral length each was recommended for drilling and evaluation in the reservoir fault blocks B and D.

Subsequent analysis therefore was performed using production results using the 4 recommended infill wells. Because it takes an average of 3 hours to run the simulation, a surrogate model of the reservoir will be constructed to facilitate further analysis.

5.6 Summary

The study objective was to evaluate infill drilling potentials and quantify uncertainty associated with infill drilling after model calibration. The active energy in the reservoir was determined by material balance calculation. The pore volume that matched reservoir pressure was modeled using Hurst–van Evaerdingen–Odeh radial model and implemented using numerical model. Saturation match was achieved at reservoir level using traditional history match approach. The major responses include field pressure and water cut. To locate infill positions, the reservoir was divided into four sub-regions and optimization of Infill Wells selection and placement was achieved using full-field numerical simulation guided by saturation and pressure depletion maps.

Chapter 6

6. Experimental Design and Response Surface Methodology

Whenever experiments are designed, response surface models are usually developed. As discussed in chapter 2, the essence is to approximate all experiments using a mathematical equation that relates dependent and independent variables. The most common regression model for approximation of computer experiments is polynomial regression. However, the construction of such models requires consideration for the time, number of experiments and variables. This chapter is dedicated to examining various DoE methods and provided alternative model using adaptive neuro-fuzzy inference system.

6.1 Examination of DoE Methods

Considering all uncertainties for experimentation and analysis can be time consuming and expensive, parameter screening are commonly done to reduce number of factors to manageable sizes.

6.1.1 Screening DoE

Several screening algorithms are available for classical experiments during reservoir management and evaluation. However, their adoption is often based on experimenter descretions. So, little attentions are paid to the risks associated with decisions that emanated from any made choices. The consequence is the underperformance of the project when compared with the actual value. For this reason, three families of experimental

designs used for parameter prioritization (Relative variation (RVD), Fractional experimental (FFD) and Placket-Burman (PBD) designs) were examined. Table 6. 1 shows the descriptions and the range of values of reservoir parameters expresses as multipliers on the base case values.

Table 6. 1: Experimental Range In terms of multipliers on the base case uncertain parameters

S/N	parameters	Keywords	Minimum Value	Base Case Value	Maximum Value
				Multiplier Ranges	
1	Oil Viscosity	OVISC	0.9	1	1.1
2	Horizontal Permeability	PERMX	0.57	1	1.29
3	Vertical Permeability	PERMZ	0.5	1	6
4	Porosity	PORO	0.9	1	1.1
5	Critical gas saturation	SGCR	0.5	1	1.5
6	Critical water saturation	SWCR	0.53	1	1.07
7	Fault transmissibility multiplier	MULTFLT	0.5	1	2
8	Water relative permeability	KRW(SORW)	0.36	1	1.25
9	Initial water saturation	SWI	0.65	1	0.9
10	Aquifer Pore volume	AQUIPV	0.85	1	1.35

6.1.2 Experimentation

Experiments were performed using history matched model integrated with proposed infill wells. The response is the cummulative oil production (FOPT) after 15 and 30 years of forecast. Simulation runs varies according to design methods and at the end of simulation, responses are available for statistical analysis. Figure 6.1 shows a typical cummulative production at the end of the history period. The profile shows the existence of uncertainty in the response. Only runs that preserved original history match were retained in design matrix for analysis.
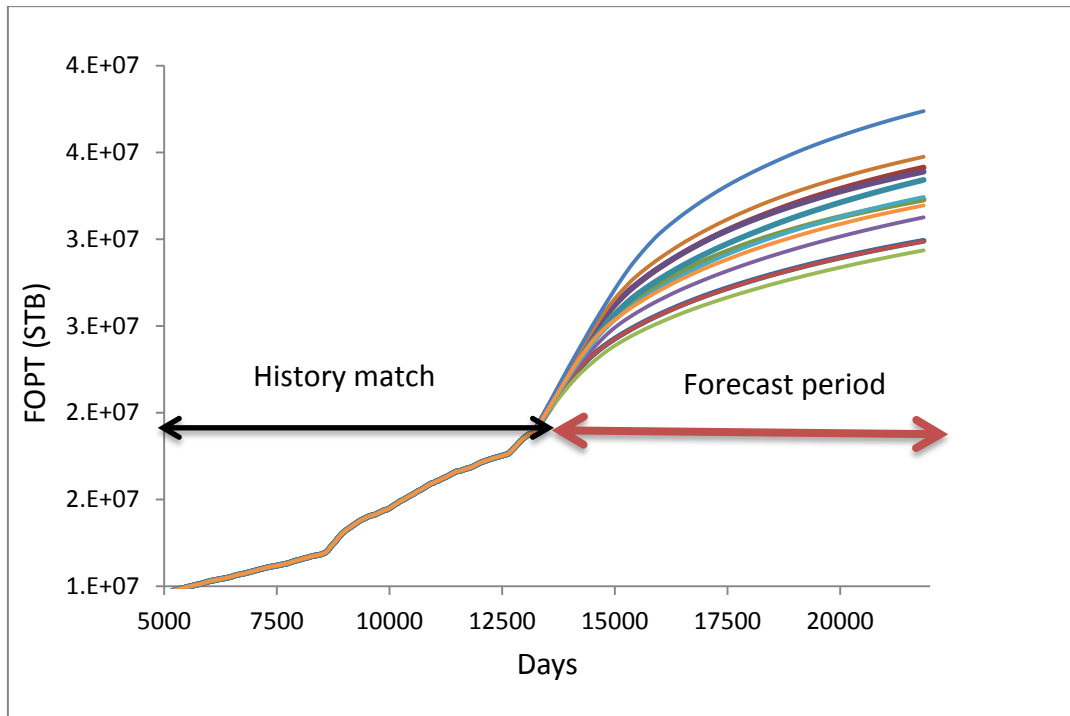
Figure 6.1: Production profile showing the end of history match and beginning of production forecast (start date for all experiments)

Using the parameters in Table 6. **1**, the design matrix containing 15 and 30 years responses for different methods are shown in Table 6. 2, Table 6.2 and Table 6. 4. The "+1", "-1" and "0" represent absolute high, low and base case values of the parameters. The contribution of each uncertainty was estimated following test of hypothesis for significance of regression using Analysis of Variance (ANOVA). The relative variation design, unlike other two techniques, does not account for the interaction of factors and as such the combined effects of parameters on reservoir performance cannot be determined. In the design matrix used for RVD, the "0" represent the base case values, "-1" represents the minimum value and "+1" the maximum value. The effects of the different attributes on the response for Table 6. **4** were estimated using Eq. 6.1.

$$\text{Attribute}_{\text{effect}} = \frac{X_{\text{max}} - X_{\text{min}}}{\sum |X_{\text{max}} - X_{\text{min}}|} \qquad\qquad 6.1$$

Where, X_{max} and X_{min} are maximum and minimum response respectively.

6.1.3 Analysis of screening experiments

All experiments were analyzed assuming 95% confidence interval for contributions of different factors on the response. The percentage contribution was determined after performing the analysis of variance. The result is presented graphically using Pareto charts as shown in Figure 6. 2, Figure 6. 3 and Figure 6. 4. The charts highlighted the impacts of the various parameters on the reserves over two different forecast periods, 15 and 30 years. The vertical black lines correspond to a 95% confidence level implying that any parameter to the right is significant ("heavy-hitter") with 95% confidence. Those to the left are insignificant.

Table 6. 2: PB design for 10 parameters

Run	A:OVISC	B:PERMX	C:PERMZ	D:PORO	E:SGCR	F:SWCR	G:MULTFL	H:KRW	J:ISW	K:AQUPV	FOPT (15yrs)	FOPT (30yrs)
1	-1	-1	-1	1	1	1	-1	1	1	-1	30848400	33479500
2	1	-1	1	1	-1	1	-1	-1	-1	1	27154800	29412400
3	1	1	1	-1	1	1	-1	1	-1	-1	28005900	29769600
4	1	1	-1	1	1	-1	1	-1	-1	-1	27889000	30076700
5	-1	-1	1	1	1	-1	1	1	-1	1	30629500	33815700
6	-1	-1	-1	-1	-1	-1	-1	-1	-1	-1	26898400	28727400
7	1	-1	1	-1	-1	-1	1	1	1	-1	28034500	29923100
8	1	-1	-1	-1	1	1	1	-1	1	1	27275300	29486200
9	-1	1	1	-1	1	-1	-1	-1	1	1	32087300	35060000
10	-1	1	-1	-1	-1	1	1	1	-1	1	30096500	32551700
11	-1	1	1	1	-1	1	1	-1	1	-1	33201400	36053900
12	1	1	-1	1	-1	-1	-1	1	1	1	30582600	33411100

Table 6. 3: DoE matrix for fractional factorial method

Run	A:OVISC	B:PERMX	C:PERMZ	D:PORO	E:SGCR	F:SWCR	G:MULTFL	H:KRW	J:ISW	K:AQUPV	15 Years	30 Years
											Response,	FOPT (STB)
1	-1	1	1	1	-1	1	-1	-1	-1	-1	29271268	33277150
2	1	-1	1	1	-1	-1	1	-1	-1	-1	25610776	28803106
3	-1	1	1	-1	-1	-1	1	1	1	-1	30558366	34219088
4	-1	-1	1	1	1	-1	-1	1	1	1	30632230	36143012
5	1	1	-1	1	-1	-1	-1	1	-1	1	27384758	31335538
6	-1	1	-1	1	1	-1	1	-1	1	-1	30327182	35035264
7	-1	1	-1	-1	1	1	-1	1	-1	-1	28117450	31376578
8	-1	-1	-1	1	-1	1	1	1	-1	1	27827028	32052148
9	1	1	1	-1	1	-1	-1	-1	-1	1	26485468	30122768
10	-1	-1	1	-1	1	1	1	-1	-1	1	27079578	31057656
11	-1	-1	-1	-1	-1	-1	-1	-1	1	1	27340390	31168096
12	1	-1	-1	-1	1	-1	1	1	-1	-1	25303208	27984070
13	1	-1	1	-1	-1	1	-1	1	1	-1	26827410	29853822
14	1	1	-1	-1	-1	1	1	-1	1	1	27344920	31090104
15	1	-1	-1	1	1	1	-1	-1	1	-1	26522916	30021116
16	1	1	1	1	1	1	1	1	1	1	30130416	35331656

Table 6. 4: Relative variation design for 10 parameters

Runs	OVISC	PERMX	PERMZ	PORO	SGCR	SWCR	MULTFL	KRW	SWI	AQUIPV	FOPT (15yrs)	FOPT (30yrs)
1	1	0	0	0	0	0	0	0	0	0	29761616	35245672
2	-1	0	0	0	0	0	0	0	0	0	29116404	34489452
3	0	1	0	0	0	0	0	0	0	0	29343824	34495768
4	0	-1	0	0	0	0	0	0	0	0	29058182	34226452
5	0	0	1	0	0	0	0	0	0	0	28566772	33322416
6	0	0	-1	0	0	0	0	0	0	0	29484880	34739616
7	0	0	0	1	0	0	0	0	0	0	29502398	35138476
8	0	0	0	-1	0	0	0	0	0	0	29016448	34228136
9	0	0	0	0	1	0	0	0	0	0	28963490	34109836
10	0	0	0	0	-1	0	0	0	0	0	28046878	32737122
11	0	0	0	0	0	1	0	0	0	0	28873100	33538296
12	0	0	0	0	0	-1	0	0	0	0	28597504	33661924
13	0	0	0	0	0	0	-1	0	0	0	28902034	34034268
14	0	0	0	0	0	0	1	0	0	0	30595368	36193200
15	0	0	0	0	0	0	0	-1	0	0	27848692	32568350
16	0	0	0	0	0	0	0	1	0	0	28692348	33769084
17	0	0	0	0	0	0	0	0	-1	0	28460282	33083528
18	0	0	0	0	0	0	0	0	1	0	28978374	33975740
19	0	0	0	0	0	0	0	0	0	-1	28928676	33991664
20	0	0	0	0	0	0	0	0	0	1	26487010	30639428
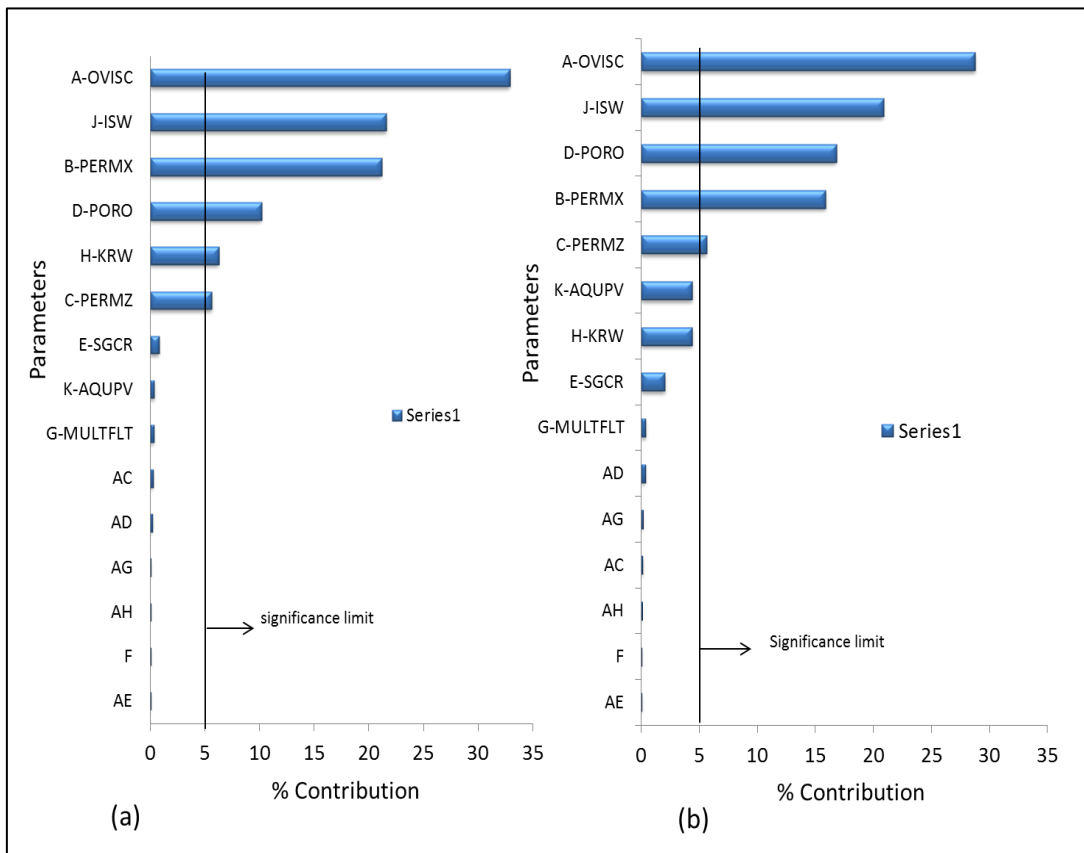
Figure 6. 2: Pareto charts from Fractional Experiment showing key parameters impacting reserves after: (a) 15 years and (b) 30 years forecasts.

Figure 6. 2 shows the six "heavy-hitters" identified for fractional experiment at the end of 15 and 30 years forecast: the OVISC, SWI, PERMX, PORO, KRW and PERMZ. The four other parameters i.e. the SGCR, the AQUIPV, MULTFLT and SWCR are insignificant on reserve forecast within these periods. However, at the end of 30 years simulation, KRW effect was insignificant this reduced the number of "heavy-hitters" to five number.
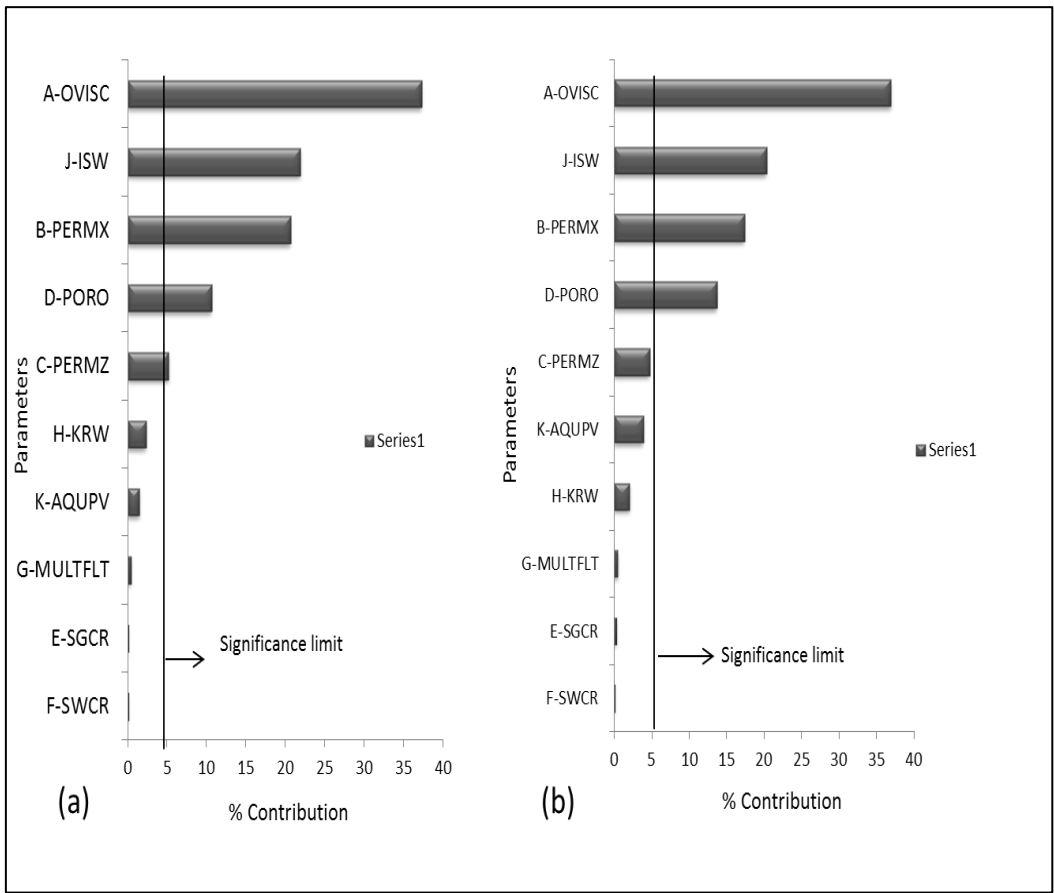
Figure 6. 3: Pareto chart from PB Experiment showing key parameters impacting reserves after (a) 15 years forecast (b) 30 years forecast

Figure 6. 3 shows the five "heavy-hitters" identified for PB experiment at the end of 15 years forecast: the OVISC, SWI, PERMX, PORO, and PERMZ. However, at the end of 30 years simulation, PERMZ became insignificant on the model. The four identified "heavy-hitters" include OVISC, SWI, PERMX, and PORO.
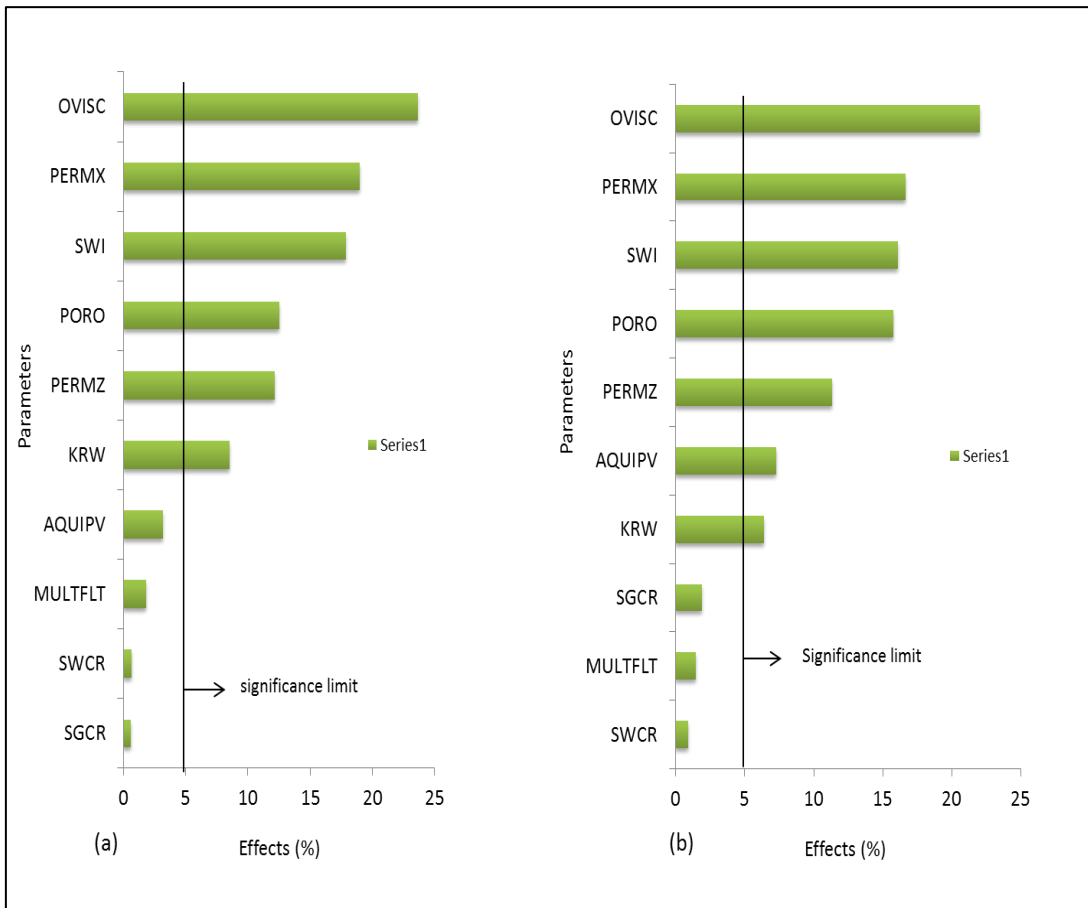
Figure 6. 4: Pareto chart from one parameter at-a-time Experiment showing key parameters impacting reserves after (a) 15 years forecast (b) 30 years forecast

Figure 6. 4 shows the "heavy-hitters" identified for relative variation at the end of 15 and 30 years forecast respectively. In both cases, OVISC, PERMX and SWI have the most influence on the response. One important observation is the time-dependent nature of the aquifer properties (AQUIPV). Six parameters namely OVISC, PERMX, SWI, PORO, PERMZ, KRW were key factors after 15 years forecast. Additional parameter AQUIPV was found significant after 30 years of forecast increasing key factors to seven.

6.2 DoE for Response surface Model

Several 3- level designs algorithms are available for the construction of response surface model. Similar to the screening designs, their adoption is often based on company practices. The four families of experimental designs used for response surface modelling considered for analysis include:

i.   Box-Behnken Design (BBD)

ii.   Central Composite Design (CCD)

iii.   Full Factorial Design (FFD)

iv.   D-Optima Design (DOD).

Table 6. 5 presents the summary of the outcome from screening analysis. The parameters from each design are listed in order of increasing order of percentage contribution to the response. Relative variation method identified with 7 factors. This is large compare with the 4 and 5 factors identified with PB and FRFD respectively. The number of significant factors dictates the number of expected experiments. The higher the number of factors the higher the numbers of simulation runs. One important assumption that was made in this study is the use of 2-level factorial design in place of full 3-Level factorial where the number of key factors is greater than four. However, design resolutions were taken into consideration. The justification for the assumption is that a 3-level full factorial design of 5 factors will require 729 experimental runs as against 32 runs by a full 2- level factorial. Running 729 experiments is not only time consuming but also highly expensive. Instead, making use of a 2-level full factorial is more economical depending on the objective and stage of the project. To use 2-

Table 6. 5: Summary of "heavy hitters" identified using different screening methods

Relative variation Design	Placket-Burman Design	Fractional Factorial Design
OVISC	OVISC	OVISC
PERMX	SWI	SWI
SWI	PERMX	PORO
PORO	PORO	PERMX
PERMZ	-	PERMZ
KRW	-	-
AQUIPV	-	-

level factorial design for developing a response surface, proper consideration must be given to design resolutions. Most useful resolutions for RSM are Resolution III, Resolution IV and Resolution V. The higher the resolution the better the design but the higher is the cost. Resolution IV designs permits freely the estimatimation of all the linear and interaction terms so that one can conclude about the influence of each of the corresponding parameters. Apart from this, it is economical. Table 6. 6 shows the statistical conditions for the experiment. In general, 10 different response surfaces were developed and examined based on the outcome from the screening methods.

Table 6. 6: Refined parameter statistics for the response surface (3-Level) experiment

S/N	parameters	Keywords	Multiplier Ranges		
			Minimum Value	Base Case Value	Maximum Value
1	Oil Viscosity	OVISC	0.9	1	1.1
2	Hor. Permeability	PERMX	0.57	1	1.29
3	Vertical Permeability	PERMZ	0.5	1	6
4	Porosity	PORO	0.9	1	1.1
5	Relative permeability	KRW(SORW)	0.36	1	1.25
6	Initial water saturation	SWI	0.65	1	0.9
7	Aquifer Pore volume	AQUIPV	0.85	1	1.35

There are 4 correlations each developed based on different factors from fractional factorial (FRFDRSMs) and Placket-Burman (PBDRSMs) methods. Only 2 feasible response surfaces were considered for the relative variation (RVDSMs) screening method. On all experiments, ANOVA was performed (see Appendix B for ANOVA) for different methods. Various design matrices are presented in the APPENDIX C. Table 6. 7 is ANOVA result for Box-Behnken experiments associated with FRFD. The Model F-value of 1031.25 implies the quadratic model selected is significant. There is only a 0.01% probability that a "Model F-Value" this large could occur due to noise. The values of "Prob > F" less than 0.0500 in Table 6. 7 indicates that all model terms are significant. In this case PORO (A), PERMX (B), PERMZ (C), Water saturation (D), Oil viscosity (E), and quadratic terms B^2, C^2, D^2 and E^2 are significant model terms.

Table 6. 7: Analysis of variance for Box-Behnken model associated with fractional factorial screening design

Source	Sum of Squares	DF	Mean Square	F Value	Prob > F	
Model	1.66E+14	9	1.85E+13	1031.25	< 0.0001	significant
A-PORO	1.58E+13	1	1.58E+13	881.42	< 0.0001	
B-PERMX	1.81E+13	1	1.81E+13	1013.13	< 0.0001	
C-PERMZ	7.53E+12	1	7.53E+12	420.69	< 0.0001	
D-ISW	1.78E+13	1	1.78E+13	994.28	< 0.0001	
E-OVISC	3.23E+13	1	3.23E+13	1806.44	< 0.0001	
B^2	1.87E+12	1	1.87E+12	104.26	< 0.0001	
C^2	1.10E+12	1	1.10E+12	61.71	< 0.0001	
D^2	5.66E+13	1	5.66E+13	3160.24	< 0.0001	
E^2	3.63E+12	1	3.63E+12	202.82	< 0.0001	
Residual	6.44E+11	36	1.79E+10			
Lack of Fit	6.44E+11	31	2.08E+10			
Pure Error	0	5	0			
Cor Total	1.67E+14	45				

The model equations developed in terms of actual experimental values for all the methods are:

A. FRFDRSMs:

$$FOPT_{Box-Behnken} = a_0 + a_1 PORO + a_2 PERMX + a_3 PERMZ + a_4 SWC + a_5 OVISC + a_6 PERX^2 + a_7 PERMZ^2 + a_8 SWC^2 + a_9 OVISC^2 \qquad 6.2$$

$$FOPT_{Central\ Composite} = a_0 + a_1 PORO + a_2 PERMX + a_3 PERMZ + a_4 SWC + a_5 OVISC + a_6 PERMX^2 \qquad 6.3$$

$$FOPT_{D-Optima} = a_0 + a_1 PORO + a_2 PERMX + a_3 PERMZ + a_4 SWC + a_5 OVISC + a_8 SWC^2 + a_9 OVISC^2 + a_{10} PORO * OVISC \qquad 6.4$$

$$FOPT_{Full\ Factorial} = a_0 + a_1 PORO + a_2 PERMX + a_3 PERMZ + a_4 SWC + a_5 OVISC + a_{10} PORO * OVISC + a_{11} PORO * PERMX \qquad 6.5$$

The coefficients in equations 6.2 ,6.3, 6.4 and 6.5 are shown in Table 6. 8.

B. PBDRSMs:

Table 6. 9 is the ANOVA result for Box-Behnken experiments associated with PB screening. The Model F-value of 710.55 implies the model is significant. There is only a 0.01% chance that a "Model F-Value" this large could occur due to noise. Values of "Prob > F" less than 0.0500 indicate models terms are significant. In this case A, B, C, D, B^2, C^2, and D^2 are significant model terms for response.

The final correlations from different methods are given in equations 6.6, 6.7, 6.8 and 6.9.

Table 6. 8: Constants in Equations (6.2), (6.3), (6.4) and (6.5)

Coefficients	Box-Behnken	Central Composite	D-Optima	Full Factorial
a_0	-6.20995	16.9659	-31.6487	17.3333
a_1	9.92838	7.37997	20.1106	18.9185
a_2	9.15993	30.8145	2.88811	0.21313
a_3	-0.044709569	0.196981	0.23518	0.214723
a_4	251.374	8.05822	214.598	8.15681
a_5	-138.295	-12.8021	-63.5763	-1.04446
a_6	-3.33886	-14.9678	0	0
a_7	0.045251129	0	0	0
a_8	-156.734	0	-132.861	0
a_9	62.0408	0	30.2034	0
a_{10}	0	0	-11.273	-12.6935
a_{11}	0	0	0	2.56571

Table 6. 9: ANOVA for Box-Behnken experiment using PB Screening method

Source	Sum of Squares	DF	Mean Square	F-Value	Prob > F	
Model	1.07E+14	7	1.52E+13	710.55	< 0.0001	significant
A-PORO	1.14E+13	1	1.14E+13	533.61	< 0.0001	
B-PERMX	1.32E+13	1	1.32E+13	614.48	< 0.0001	
C-ISW	1.31E+13	1	1.31E+13	612.73	< 0.0001	
D-OVISC	2.34E+13	1	2.34E+13	1092.08	< 0.0001	
B^2	1.20E+12	1	1.20E+12	56.1	< 0.0001	
C^2	3.76E+13	1	3.76E+13	1750.69	< 0.0001	
D^2	2.30E+12	1	2.30E+12	107.06	< 0.0001	

$$FOPT_{Box-Behnken} (MMstb) = b_0 + b_1 PORO + b_2 PERMX + b_3 SWC + b_4 OVISC +$$

$$b_5 PERMX^2 + b_6 SWC^2 + b_7 OVISC^2 \qquad\qquad 6.6$$

$$\text{FOPT}_{\text{FFD}}(\text{MMstb}) = b_0 + b_1 \text{PORO} + b_2 \text{PERMX} + b_3 \text{SWC} + b_4 \text{OVISC} + b_5 \text{PERMX}^2 +$$

$$b_6 \text{SWC}^2 + b_7 \text{OVISC}^2 + b_8 \text{PORO} * \text{PERMX} + b_9 \text{PORO} * \text{SWC} + b_{10} \text{PORO} *$$

$$\text{OVISC} \qquad 6.7$$

$$\text{FOPT}_{\text{D-Optima}}(\text{MMstb}) = b_0 + b_1 \text{PORO} + b_2 \text{PERMX} + b_3 \text{SWC} + b_4 \text{OVISC} +$$

$$b_6 \text{SWC}^2 \qquad\qquad\qquad\qquad\qquad\qquad\qquad\qquad\qquad\qquad\qquad 6.8$$

$$\text{FOPT}_{\text{CCD}}(\text{MMstb}) = b_0 + b_1 \text{PORO} + b_2 \text{PERMX} + b_3 \text{SWC} + b_4 \text{OVISC} + b_6 \text{SWC}^2 \quad 6.9$$

The coefficients of the equations are given in Table 6. 10.

Table 6. 10: Constants in Equations (6.6), (6.7), (6.8) and (6.9)

Coefficients	Box-Behnken	Central Composite	D-Optima	Full Factorial
b_0	-6.912070	-36.454900	-58.375000	-12.044100
b_1	9.765720	7.873440	10.025900	13.010900
b_2	8.956970	2.588430	2.904210	6.105920
b_3	248.646000	179.541000	235.506000	242.231000
b_4	-133.765000	-12.193800	-14.898500	-118.750000
b_5	-3.254460	-111.579000	-146.385000	-3.127380
b_6	-155.016000	0	0	-155.533000
b_7	59.897000	0	0	58.449000
b_8	0	0	0	2.572820
b_9	0	0	0	7.051630
b_{10}	0	0	0	-11.706500

C. **RVDRSMs:**

The seven "heavy hitters" identified with OVAAT screening include: PORO, PERMX, PERMZ, AQUIPV, SWI, KRW and OVISC. Response surface was limited to Box-

Behnken and D-optima methods that required 62 and 37 experimets respectively. Table 6. 11 is the ANOVA result for the Box-Behnken experiments using relative variation screening (see Appendix D for the ANOVA of correlation equations 6.10 and 6.11). The F-statistics from ANOVA indicated that quadratic model is suitable for Box-Behnken method. The final response surfaces are given in equations 6.10 and 6.11. The coefficients of the correlations are given in Table 6. 12.

$$FOPT_{D-OPT}(MMSTB) = C_0 + C_1 PORO + C_2 PERMX + C_3 PERMZ + C_4 AQUIPV + C_5 SWI + C_6 KRW + C_7 OVISC + C_8 SWI^2 \qquad 6.10$$

$$FOPT_{Box-Behnken} = C_0 + C_1 PORO + C_2 PERMX + C_3 PERMZ + C_4 AQUIPV + C_5 SWI + C_6 KRW + C_7 OVISC + C_8 SWI^2 + C_9 PERMX^2 + C_{10} PERMZ^2 + C_{11} OVISC^2 + C_{12} SWI * OVISC \qquad 6.11$$

Table 6. 11: ANOVA for the analysis of the Box-Behnken experiments using relative variation screening method

Source	Sum of Squares	DF	Mean Square	F-Value	Prob > F	
Model	2.59E+14	12	2.16E+13	212.04	< 0.0001	significant
A-PORO	1.83E+13	1	1.83E+13	180.12	< 0.0001	
B-PERMX	3.06E+13	1	3.06E+13	300.52	< 0.0001	
C-PERMZ	9.75E+12	1	9.75E+12	95.81	< 0.0001	
D-AQUIPV	5.00E+12	1	5.00E+12	49.19	< 0.0001	
E-SWI	2.94E+13	1	2.94E+13	289.48	< 0.0001	
F-KRW	4.24E+12	1	4.24E+12	41.64	< 0.0001	
G-OVISC	5.13E+13	1	5.13E+13	504.17	< 0.0001	
B^2	4.70E+12	1	4.70E+12	46.24	< 0.0001	
C^2	1.33E+12	1	1.33E+12	13.1	0.0007	
E^2	8.34E+13	1	8.34E+13	819.76	< 0.0001	
G^2	8.40E+12	1	8.40E+12	82.63	< 0.0001	
EG	1.14E+12	1	1.14E+12	11.18	0.0016	

Table 6. 12: Constants in Equations (6.10) and (6.11)

Coefficients	Box-Behnken Method	D-Optima Method
C_0	34	34.29
C_1	0.8737	0.8997
C_2	1.129	0.9811
C_3	0.6538	0.5659
C_4	0.4684	0.5926
C_5	1.108	1.153
C_6	0.4201	0.3715
C_7	-1.5	-1.431
C_8	-0.5758	-2.345
C_9	0.3101	0
C_{10}	-2.424	0
C_{11}	0.7786	0
C_{12}	-0.3769	0

6.3 Model Validation

The data used for the development of the proxy models are presented in the Appendix C4 through C12. The response surface developed would be used during the uncertainty quantification. The following criteria were used to assess their validity.

6.3.1 Correlation coefficients

The model validity was partly established using correlation coefficients: R-square, Adjusted R-Square and predicted R-square values. In all equations, the R-square and adjusted R-square values are greater than 90% which shows that the models explain at least 90% of the variability observed on the response at the points of the design. Figure 6. 5 (a, b and c) is the parity plots for the various prediction methods, each of the four methods that corresponds to different screening method is shown on a separate plot. These graphs are plots of the predicted production forecast against the experimental reserves values. If the

prediction method were a perfect fit of the experimental data then all of the points would

lie on the x = y
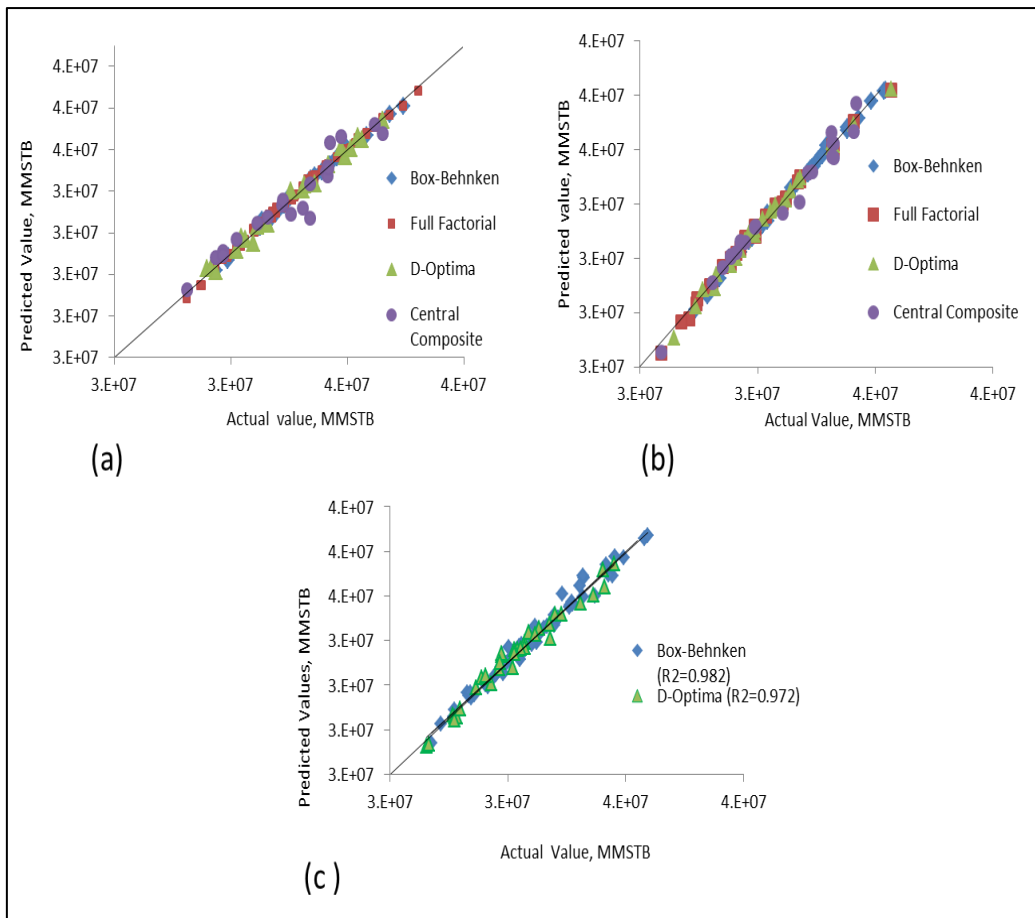
Figure 6. 5: Comparison of the actual and predicted reserves by (a) FRFRSMs, (b) PBRSMs and (c) RVDRSMs

line. By and large, the parity plots do not reveal much needed information. However, the

plots for the Box-Behnken method generally demonstrate that the method predict the actual

value more accurately. On these plots the vast majority of the points are along the x = y

line. In addition, the plots reveal that regardless of the screening method used, CCD

exhibits the least accurate prediction as this analysis revealed.

175

6.3.2 Statistical error analysis

The performance indices used for error analysis are summarized in Table 6. 13. Root Mean square Error (RMSE) is a measure of the residuals of the model and the experimental data. A good model is characterized by low RMSE value. Average absolute percentage Relative Error (AAPRE) indicates the relative absolute deviation in percent from the experimental values. A lower value implies a better correlation. In the case of a perfect match AAPRE is zero. After the absolute percent relative error for each data point was calculated, both the minimum (E_{min}) and maximum (E_{max}) values were scanned to know the range of error for each model equation. The accuracy of a correlation was examined by maximum absolute percent relative error. The lower the value of maximum absolute percent relative error, the higher is the accuracy of the correlation.

Standard deviation (SD) is a measure of dispersion. A lower value of standard deviation means a smaller degree of scatter. A small AD and a relatively large AAD indicates that the errors tend to cancel (some are positive and some negative) and indicates less bias in the prediction. If both the AD and AAD are large this indicates a bias in the prediction – a tendency to either over predict (if the AD is negative) or under predict (if the AD is positive) the experimental data. Each of the response surface developed was used to estimate the production forecast for each of the data sets.Table 6.14, Table 6.15 and Table 6.16 show the result from the error analysis. In addition to the estimated errors, the coefficients of correlations are also indicated. Box-Behnken method exhibited the least estimation error with highest values of correlation coefficients. CCD on the other hand shows maximum estimated error and least correlation coefficients.

176

Table 6. 13: Performance Indices for Model Evaluation

Name of Measure	Formula
Absolute Deviation	$AD = \dfrac{1}{N} \sum_{i=1}^{N} (Pred. - Exp)$
Average Absolute Deviation	$AAD = \dfrac{1}{N} \sum_{I=1}^{N} |(Pred. - Exp.)|$
Root Mean Square Error	$RMSE = \sqrt{\dfrac{1}{N} \sum_{i=1}^{N} (Actual - Predicted)^2}$
Average Absolute Percentage Relative Error	$AAPRE = \dfrac{1}{N} \left[\sum_{i=1}^{N} |E_i| \right]$
Maximum Error	$E_{max} = Max|E_i| \text{ and } Min|E_i|$
	$E_i = \dfrac{Pred - Exp}{Exp} * 100$
Standard Deviation	$SD = \dfrac{1}{N_d - 1} * \sum_{i=1}^{N} E_i{}^2$

Table 6. 14: Summary of the Statistical Analysis of FRFDRSMs

Performance Index	Box-Behnken	Full Factorial*	D-Optima	Central Composite
RMSE	118587.704	181420.322	181659.021	302095.247
AAD	84565.217	141333.333	153333.333	227692.308
AD	-652.174	-666.667	740.741	-1538.462
Emax	0.885	1.470	1.441	2.073
SD	0.134	0.336	0.336	0.837
AAPRE	0.256	0.443	0.477	0.685
R-Square	0.996	0.994	0.993	0.979
Adj. R-square	0.995	0.992	0.989	0.973
Pred. R-Square	0.994	0.988	0.982	0.957
Exp. Runs	46	32	31	47

* 2- level full factorial was used

Table 6. 15: Summary of the Statistical Analysis of PBRSMs

Index	Box- Behnken	Full Factorial	D-Optima	Central Composite
RMSE	125328.141	124264.503	218269.711	608581.489
AAD	90714.286	94166.667	184166.667	448571.429
AD	-714.286	-595.238	0.000	-952.381
Emax	0.829	1.147	1.453	5.148
SD	0.150	0.154	0.485	3.504
AAPRE	0.275	0.291	0.573	1.366
R-Square	0.996	0.997	0.991	0.924
Adj. R-square	0.995	0.996	0.989	0.899
Pred. R-Square	0.992	0.995	0.985	0.844
Exp. Runs	29	84	24	25

Table 6. 16: Summary of the Statistical Analysis of RVDRSMs

Performance Index	D-Optima	Box_Behnken
RMSE	345823.825	282381.558
AAD	281176.471	215245.902
AD	588.235	-819.672
E_{max}	2.130	2.303
SD	1.149	0.706
AAPRE	0.868	0.641
R-Square	0.9723	0.9815
Adj. R-square	0.9634	0.9769
Pred. R-Square	0.9509	0.9673
Exp. Runs	37	62

6.3.3 Blind test analysis

Mostly application of RSMs are limited to generating probabilistic models. This is because like other data driven models, they work better when apply to cases within the range of values with which they are developed. In order to establish model predictability outside the range of parameters, which are desired sometimes, a "blind test" is recommended to be performed using parameter values outside the range already defined in Table 6. 6. The justification for blind test is because the parameter ranges used for different experiments were gotten from analogy and experience from neighboring fields which may not be exactly the true values. Assuming more data became available and it was found that the ranges earlier utilized are less than or greater than the real extreme values, the earlier models can not predict accurately the response of interest. A good model should therefore affords to estimate important quantities such as expected reserves figures when some parameter values are changed. Such figures, if reliable, can be useful for supporting mangement decisions. This was demonstrated by simulating the decision whether to

embark on Enhance Recovery (thermal or Insitu-combustion) or stimulation using RSMs. The study selected OVISC because it is controllable insitu by combustion, steam flooding or injection of diluents.

Figure 6. 6 (a), (b) and (c) show respectively the comparison of RSMs with the actual experimental values. The simulated production upon degradation of OVISC by 30, 50 and 70% is shown in Figure 6. 6 (d). It was noticed that prediction using Full Factorial method was excellent with maximum deviation of 0.79 followed by Central Composite method with maximum deviation of 0.9 in reserves estimation. Box-behnken generally overpredicted the actual reserves volume with deviation approximately factor of 20.

6.3.4 Selection of response surface for analysis

Table 6. 17 summarizes various criteria used for the evaluation of all response surfaces developed. The idea is to rank them using these measures and select the best for uncertainty quantification. The decision to select appropriate model was based on two scenerios:
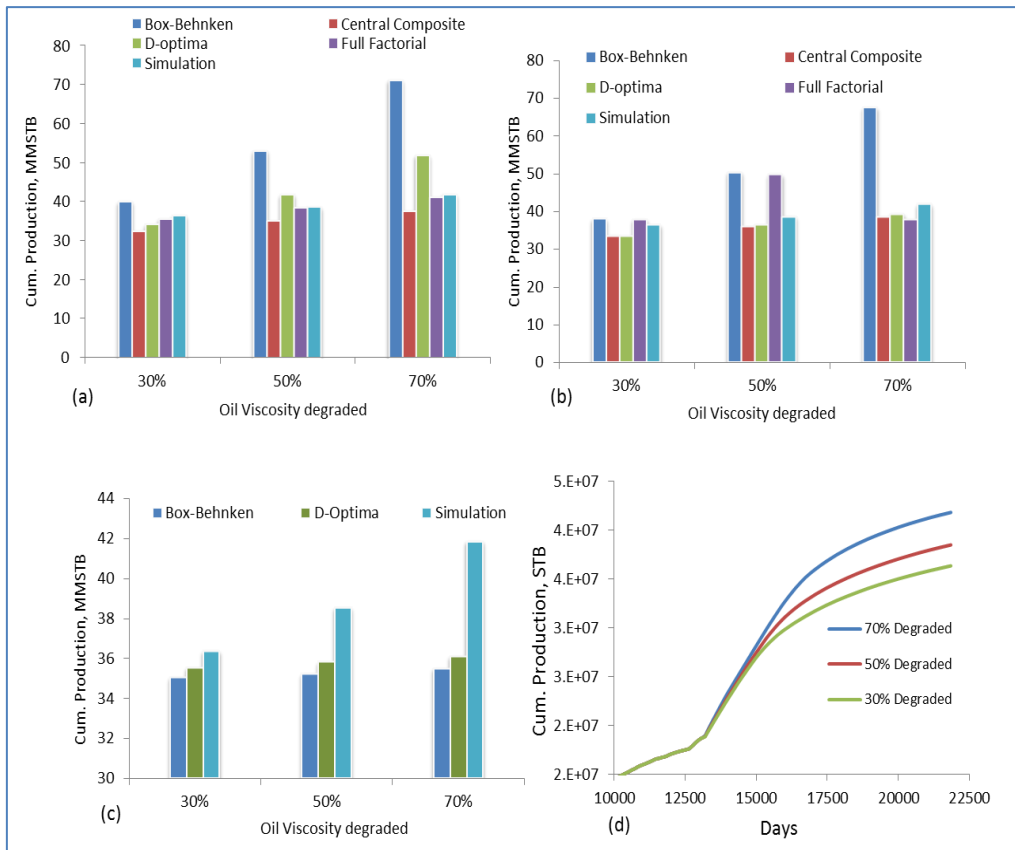
Figure 6. 6: Comparison of the predictions using (a) FRFRSMs, (b) PBRSMs and (c) RVDRSMs with the simulated reserves upon reduction of OVISC by 30, 50 and 70%.

Scenario 1:

If it is desired to develop risk curves from where only P90-P50-P10 response values and associated parameter values are to be determined. The analysis favours the selection of Box-Behnken method. There are however three possible response surfaces associated with Box-behnken depending on the screening methods. These are response surface equations 6.11 (with 5 factors, 46 runs), 6.15 (with 4 factors, 29 runs) and 6.20 (with 7 factors, 62 runs). For practical purposes, response surface equation 6.15 is desirable with fewer number of factors and experimental runs.

Scenario 2:

If it is desired to utilized the proxy equation for simulation and evaluation of future development strategies such as determination of needs for acquiring additional information, undertaking stimulation or any of EOR methods such as in-situ combustion, a more efficient model capable of extrapolating reservoir performance within an acceptable margin of error is desired.

Table 6. 17: Summary for model ranking

| | | Response Surface Methods | | |
Ranking Measures	Box-Behnken	Central Composite	D-Optima	Full factorial
Fractional Factorial Screening	✓	✓	✓	Infeasible
Placket-Burman Screening	✓	✓	✓	✓
RVD Screening	✓	Infeasible	✓	Infeasible
Error Analysis	Best	Average	Average	Better
Blind test	Fail	✓	Fail	✓
Correlation R-squares	✓	✓	✓	✓

✓ = *Pass ,* **Infeasble** *= not practicable due to large number of experimental runs*

Both Central Composite (CCD) and Full Factorial methods are adequate. However, full factorial method performed far better than the CCD. FFD tends to be impractical for large number of uncertainty. We have demonstrated in this study that a 2-level factorial experiments can be used for constructing response surface of quality comparable to that from 3-level full factorial. However, we highly recommended consideration for the stability and resolution of the factorial fractions to be used.

For the purpose of comparison, it was decided to select three response surface models for uncertainty quantification. These include those associated with the Placket-Burman and fractional factorial screening methods. They are: (a) Box-Behnken equations 6.6 (b) Central Composite equations 6.3 (c) Full Factorial equations 6.5.

6.4 Uniform Experimental Design

Unlike classical experimental designs, modern experimental designs are characterized by wider coverage of uncertainty domain and require fewer number of simulation runs. Approximation models are usually constructed using polynomial surrogate, quadratic model and kriging. With 4 factors the minimum number of experiments to construct a polynomial model is given as:

$$P = {(m + 1)(m + 2)}/{2} \qquad\qquad 6.12$$

This will require at least a total of 15 experiments. Conducting 16 experiments is common and the total of all possible combinations is $16^4 = 65,536$. Orthogonal test designs can reduce test number to $16^2 = 256$; uniform design however, can reduce it to only 16 tests. This is an advantage of modern experimental design over the conventional designs like central composite, Box-Behnken and full factorial designs. Uniform design (UD) was used to determine the locations of sample points within the design space. The design was constructed such that each of the variables is divided into 16 equal levels each comprises of only one sample point. To prevent a design that has poor space filling qualities, Translational Propagation Algorithm (Cioppa and Lucas, 2007) was modified and implemented in MATLAB.

Figure 6. 7 shows the schematics of initial 16 sample points (black spots) selected by UD for a two-dimensional problem and augmented samples (red spots) that were used to validate the model.

6.4.1 Quadratic model

The use of polynomial approximation model in surrogate modeling is common. Here, the sampled data is fitted by a least-square regression technique. The accuracy of this method depends on the highest degree of the polynomials used. However, the degree has opposite effect on the smoothness of the representative function. To maintain balance between interpolation accuracy, smoothness and computational expense, the "quadratic" polynomial model was selected.
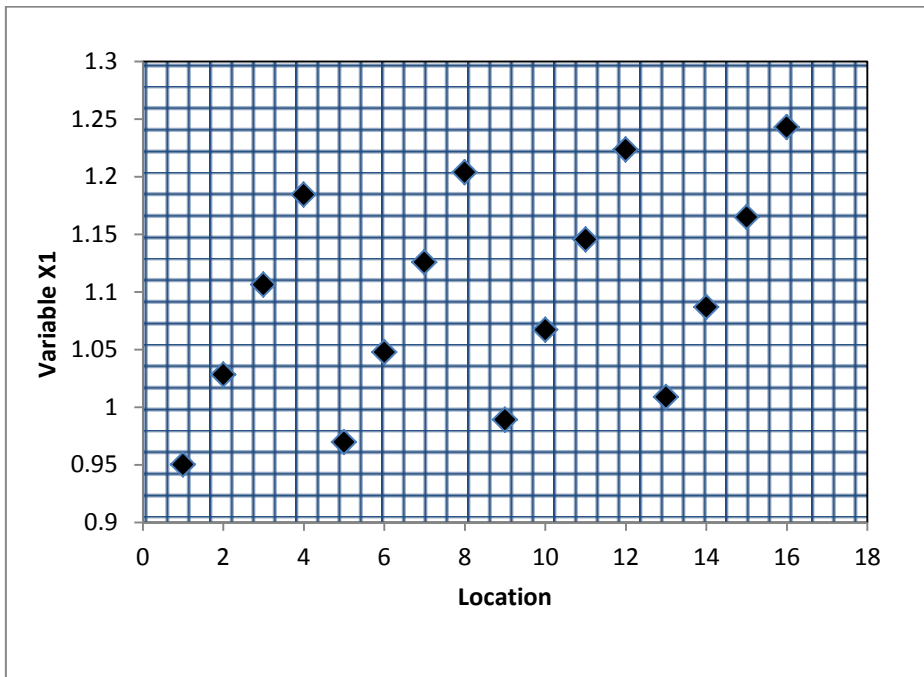
Figure 6. 7: Schematics of initial 16 sample points selected by UD for a two dimensional design problem.

The true quadratic RSM can be written in the following form:

$$y(X) = \hat{y}(X) + \varepsilon, X \in R^m \qquad\qquad 6.13$$

Where $\hat{y}(X)$ the quadratic polynomial approximation and ε is the random error which is assumed to be normally distributed with mean zero and variance σ^2. The error ε_i at each observation is supposed to be independent and identically distributed (iid).

The modeled quadratic RSM predictor $\hat{y}(X)$ is defined as:

$$\hat{y}(X) = \beta_0 + \sum_{i=1}^{m} \beta_i x_i + \sum_{i=1}^{m} \beta_{ii} x_i^2 + \sum_{i=1}^{m} \sum_{j \geq i}^{m} \beta_{ij} x_i x_j \qquad 6.14$$

Where $\beta_0, \beta_i, \beta_{ii}$ and β_{ij} are the unknown coefficients in equation 6.14. Let $\beta \epsilon R^m$ be the column vector contains these P unknown coefficients. The least square estimator of β is

$$\beta = (U^T U)^{-1} U^T y_s \qquad 6.15$$

Where

$$U = \begin{bmatrix} 1 & x_1^{(1)} & \cdots & x_m^{(1)} & x_1^{(1)} x_2^{(1)} & \cdots & x_{m-1}^{(1)} x_m^{(1)} & (x_1^{(1)})^2 & \cdots & (x_m^{(1)})^2 \\ \vdots & \vdots & \ddots & \vdots & \vdots & \ddots & \vdots & \vdots & \ddots & \vdots \\ 1 & x_1^{(n)} & \cdots & x_m^{(n)} & x_1^{(n)} x_2^{(n)} & \cdots & x_{m-1}^{(n)} x_m^{(n)} & (x_1^{(n)})^2 & \cdots & (x_m^{(n)})^2 \end{bmatrix} \in R^{nXp} \qquad 6.16$$

and y_s are observations, $\beta_0 = 2.488$, $\beta_1 = 53.0332$ and $\beta_2 = -17.2437$. The approximated response $\hat{y}(X)$ at any untried x can be efficiently predicted by Eq. (6.17).

$$\hat{y}(X)[MMstb] = \beta_0 + \beta_1 SWI + \beta_2 PERMX^2 \qquad 6.17$$

The cross plot of the model prediction against the actual experimental value is shown in Figure 6.8. On this plot the vast majority of the points are along the x = y line. This shows that the predictions were nearly a perfect fit of the experimental data.

6.4.2 Evaluation of approximation models

Relative Error (RE) and Root Mean Squared Error (RMSE) were used to evaluate the error of the approximation models at test points other than those used in building the model. The test points comprises of ten new sample points within the sample space.

The relative error is

$$\bar{e} = \frac{1}{n_t} \sum_{i=1}^{n_t} e^{(i)}, \quad \text{where,} \qquad e^{(i)} = \left\| \frac{\hat{y}_t^{(i)} - y_t^{(i)}}{y_t^{(i)}} \right\| \qquad\qquad 6.18$$

n_t is number of the test points; $y_t^{(i)}$ and $\bar{y}_t^{(i)}$ are the true value and predicted value corresponding to the ith test point, respectively.
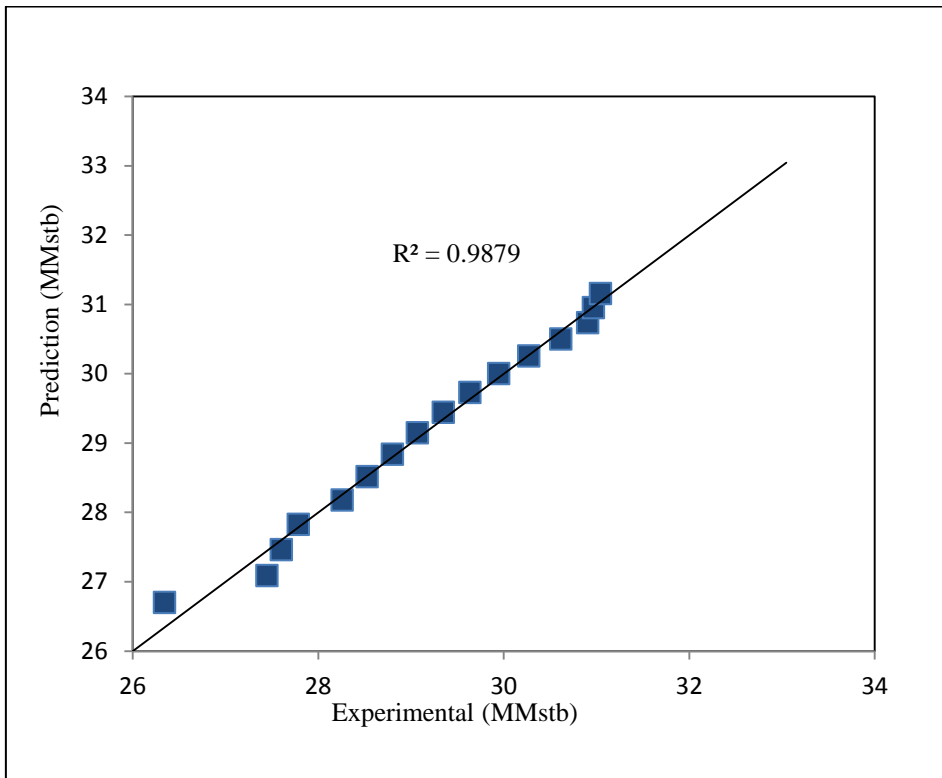
Figure 6. 8: Comparison of the actual experimental value and model predicted values

186

The root mean squared error is defined by

$$\sigma_e = \sqrt{\frac{\sum_{i=1}^{n_t}(e^{(i)})^2}{n_t}}$$

6.19

Table 6. 18 is the result obtained from statistical error analysis. The low (RMSE = 1.05) value indicates a good model. Approximately zero value of Average Absolute Percentage Relative Error (AAPRE = 0.76%) recorded indicates relative low absolute deviation in percent from the experimental values. Hence, implies a better correlation.

Table 6. 18: Statistical Error Analysis

Experimental	Prediction	Residual	AD	% Error	MSE
27.70	27.67	0.03	0.03	0.12	0.01
30.55	30.15	0.40	0.40	1.32	1.75
31.43	31.07	0.36	0.36	1.13	1.28
28.15	28.03	0.13	0.13	0.45	0.20
30.46	30.40	0.07	0.07	0.21	0.05
28.41	28.37	0.04	0.04	0.15	0.02
29.50	29.61	-0.10	0.10	-0.35	0.12
31.12	31.45	-0.33	0.33	-1.07	1.14
29.44	28.70	0.74	0.74	2.53	6.39
30.94	30.86	0.08	0.08	0.25	0.06

6.5   Adaptive Neuro-Fuzzy Inference System

Fuzzy logic has ability to maintain a high level of performance in the presence of uncertainty. The original Back-propagation method used in Nets (Artificial Neural Networks) was found to exhibit slow convergence due to large search space dimensions for learning. Fuzzy Inference System (FIS) employs hybrid-learning rules for training process which is a combination of gradient descent and the least-squares method. In this section

experimental design and Adaptive Neuro Fuzzy Inference System (ANFIS) were integrated to develop a predictive model for production forecast after infill drilling in a real Niger Delta Field. Experimental design was employed for data gathering while ANFIS technique was utilized for factor selection and predictive model development.

6.5.1 Data collection

Central Composite algorithm provides sufficient data within the design space for ANFIS modelling. An overall of 145 experiments (Appendix D) were performed considering the full factorial of CCD consisting of 128 cube points, 14 axial points, and 3 center points for the seven screened "heavy-hitters". Each factor was varied over five levels $\pm\alpha$ (axial points), ±1 (factorial points) and "0" (center-point). After data quality control, 143 valid experimental points were used.

6.5.2 Data partitioning

Out of a total of 143 input–output pairs, 72% were randomly selected and used for training. The remaining 28% of data were used for testing or validation. For training, the fuzzy rules were generated directly from the input-output data sets and the model learnt the salient features in the data and automatically adjusted the system parameters to reduce the error between the predicted output and the measured output. The training was achieved using genfis1 and the trainings of these networks were stopped after reaching the minimum error goal of 0.0001 (MATLAB 2007 run on an Intel (R) Core (TM) i5 CPU (2.5 GHz, 6 GB RAM) PC).

6.5.3 Optimization and selection of input parameters

Two optimization schemes were tested to reveal the inputs that have more impact on the output, an exhaustive and sequential optimization schemes. Sequential search scheme capable of selecting between 1 to 4 input variables from all input candidates and identifies influence of variable and its interactions on model prediction. The search began with main factor followed by 2-factors interaction, 3 factors interaction and 4 factors interaction. Table 6. 19 shows how main factors and their interactions impacted the output for one epoch number using RMSE criteria. The selection of the key factors was based on the magnitude of RMSE of the training and data checking.

Table 6. 19: SEQSRCH results of "heavy-hitters" selection used for proposed model development

Uncertainty	RMSE Training	Testing
A	0.8020	0.8397
B	0.8631	0.8514
C	0.8638	0.8348
D	0.7554	0.7471
E	0.6270	0.7001
F	0.8237	0.8552
G	0.7642	0.7407
(EA)	0.5533	0.6571
(EB)	0.534	0.6318
(EC)	0.5058	0.6121
(ED)	0.5333	0.6399
(EF)	0.5528	0.6838
(EG)	0.4774	0.5559
(EGA)	0.3264	0.6446
(EGB)	0.3719	0.5642
(EGC)	0.3082	0.514
(EGD	0.3726	0.7366
(EGF)	0.3783	0.7315
(CEGA)	0.0682	0.9566
(CEGB)	0.1344	1.5383
(CEGD)	0.0998	1.5102
(CEGF)	0.1639	1.4011

A low training RMSE and significantly high checking RMSE is a sign of over-fitting. Parameter E (training error of 0.6270 and checking error of 0.7001) is therefore selected first ahead of remaining six main effects. For 2 interaction factors, EG with lowest training and checking RMSE (0.4774 and 0.5559) was selected. The order of arrangement (EG and not GE) also indicates the degree of significance of the two parameters with E having more impact on the response than G. The selection process is similar for the other higher combination of variables. Three (3) factors searching revealed EGC as having the closest and lowest RMSE (0.3082 and 0.5140) values for training and checking errors. CEGA was selected on searching for four factors with RMSE (0.0682 and 0.9566) for the training and checking errors respectively. The selection process is similar for the other higher combination of variables. Three (3) factors searching revealed EGC as having the closest and lowest RMSE (0.3082 and 0.5140) values for training and checking errors. CEGA was selected on searching for four factors with RMSE (0.0682 and 0.9566) for the training and checking errors respectively.

6.5.4 Network architecture for ANFIS model

For the construction of ANFIS model, MATLAB toolbox was used. The training of the ANFIS network was accomplished by employing grid partitioning to generate Fuzzy-Inference System (FIS). FIS utilizes different membership functions. The membership function assigned to each input was tuned using hybrid optimization method (which is a combination of least squares method and gradient steepest descent method) for the parameters associated with the input membership function and the least squares estimation for the parameters associated with the output membership functions. A gradient vector was

used to measure how well the fuzzy system is modeling the input– output data. The fuzzy inference system generated is shown in Figure 6. 9. The neuro-fuzzy structure is shown in Figure 6. 10. Figure 6. 11 shows the rule for 4 Input Fuzzy Inference System and the output panel. Figure 6. 12 shows error propagation from checking and training processes. Figure 6. 13 shows the cross plot of actual and predicted values in ANFIS for training data sets. Figure 6. 14 depicts the cross plot for the checking data versus model prediction for the remaining 43 data set. Figure 6. 15 presents the parity plot of actual and predicted values in ANFIS for all data sets.

6.5.5 Influence of membership function

Table 6.20 shows the different membership functions tested during modeling and they influence the training and checking errors. Gaussian membership function (Gaussmf) exhibited least over-fitting with R-square value of 96 percent. Figure 6. 9 consists of three different parts: fuzzifiers, which map the crisp values of the preprocessed input of the model into suitable fuzzy sets represented by membership functions; followed by the inference mechanism or inference engine, which is the computational method to compute the extent to which each rule fires for a given fuzzified input pattern according to an active inference rule; and the last part is a defuzzifier, which maps the crisp values of the preprocessed input of the model into suitable fuzzy sets represented by membership functions and postprocessed to give the output of the fuzzy system based on the crisp signal obtained after defuzzification.
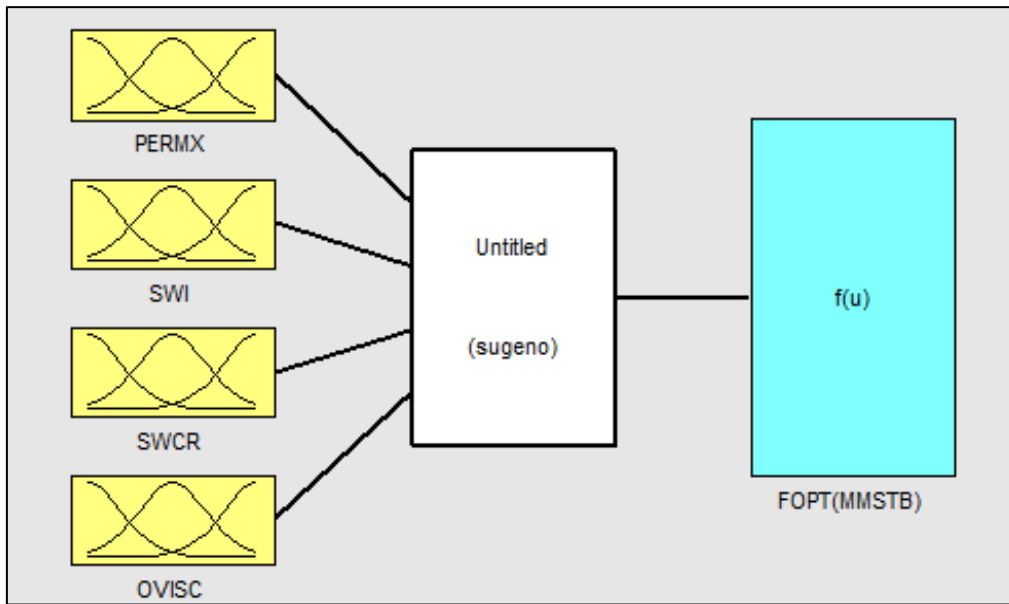
Figure 6. 9: High-level display of fuzzy inference system
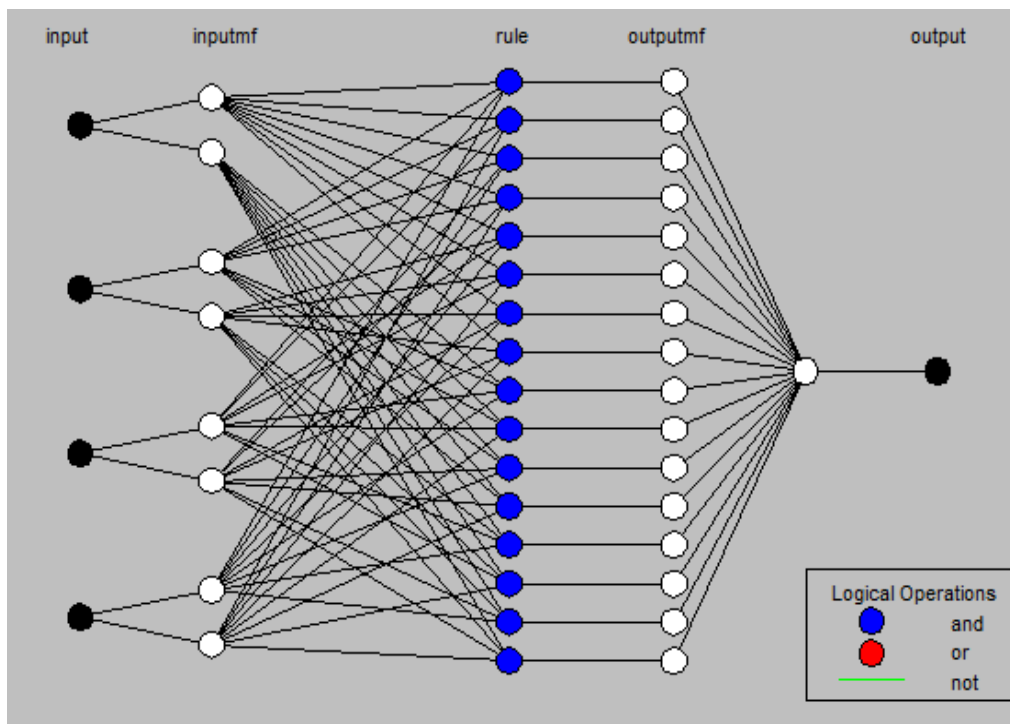
Figure 6. 10: Schematic of ANFIS network used for this study

The neuro-fuzzy structure is shown in Figure 6. 10, which consists of 4 input nodes, 8 input membership function nodes, one node for normalized rules, one output membership node, and one output node.
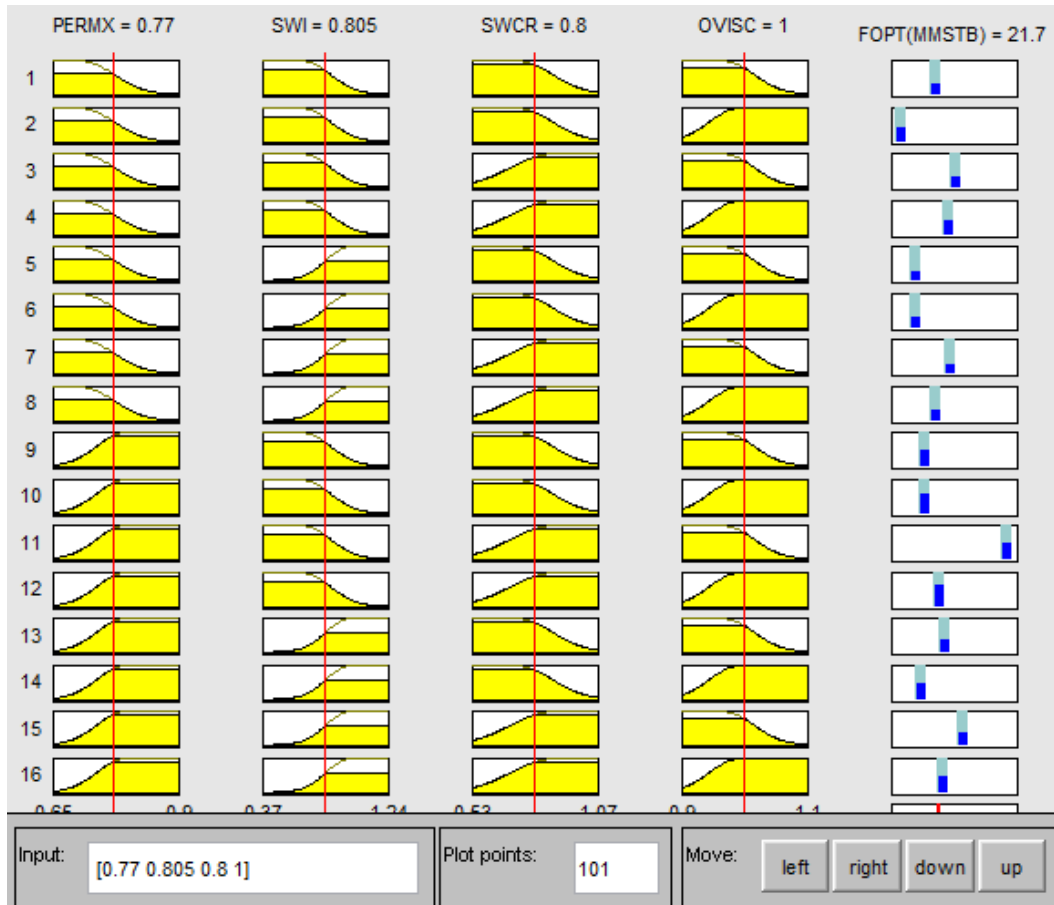
Figure 6. 11: Panel showing Rule for 4 Input Fuzzy Inference System

Table 6. 20: Influence of different Membership Function

MF	RMSE Error		R-Square Value
	Training	Checking	
Gbell	0.215383	0.324773	0.95471
Gauss	0.22372	0.304382	0.956
Gauss2	0.21318	0.323268	0.95545
Tri	0.221813	0.302415	0.95673
Pi	0.198293	0.350266	0.95415
Psig	0.223396	0.353501	0.9486
Dsig	0.223396	0.353501	0.9486
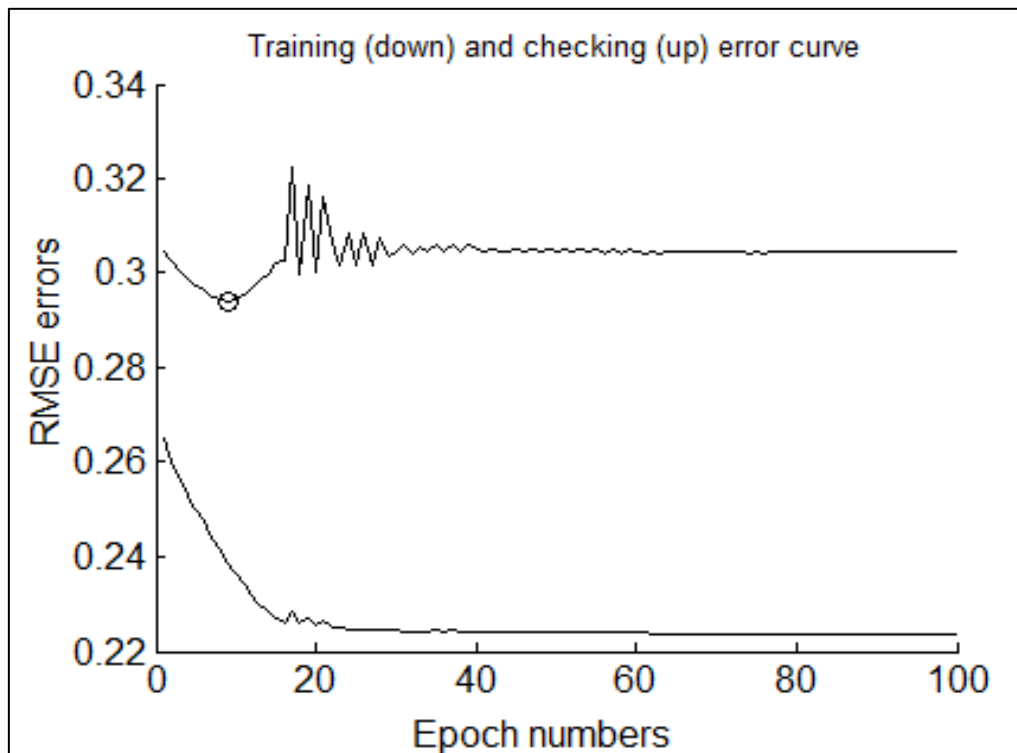
Figure 6. 12: Error propagation for checking (upper) and training (lower).

194

It is evident from Figure 6. 12 that as the training error decreased from 0.264917 to 0.22372, the checking error reduced up to epoch number of about 18 and shoot up gently indicating occurrence of minimum over-fitting before it stabilized. Over-fitting was checked by selecting appropriate membership function that associated with the minimum checking error.
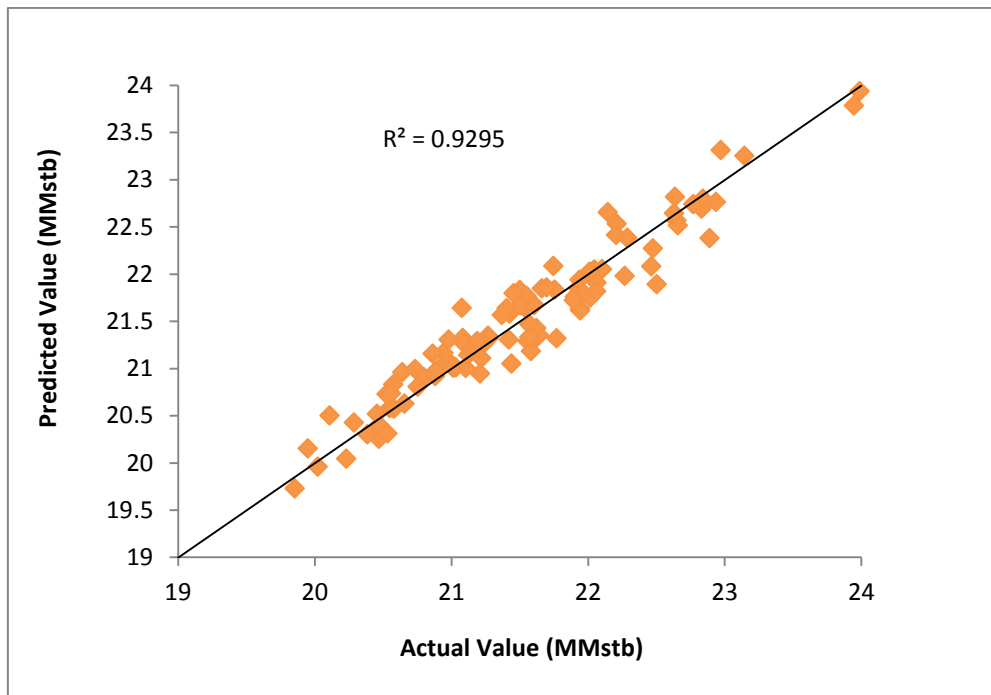
Figure 6. 13: Parity plot of Actual and predicted values in ANFIS for training data sets.

Figure 6. 13 is the cross plot of the trained 100 data set versus model prediction for the first 100 epoch number. The model intersected most of the data point with correlation coefficient of 93 percent.
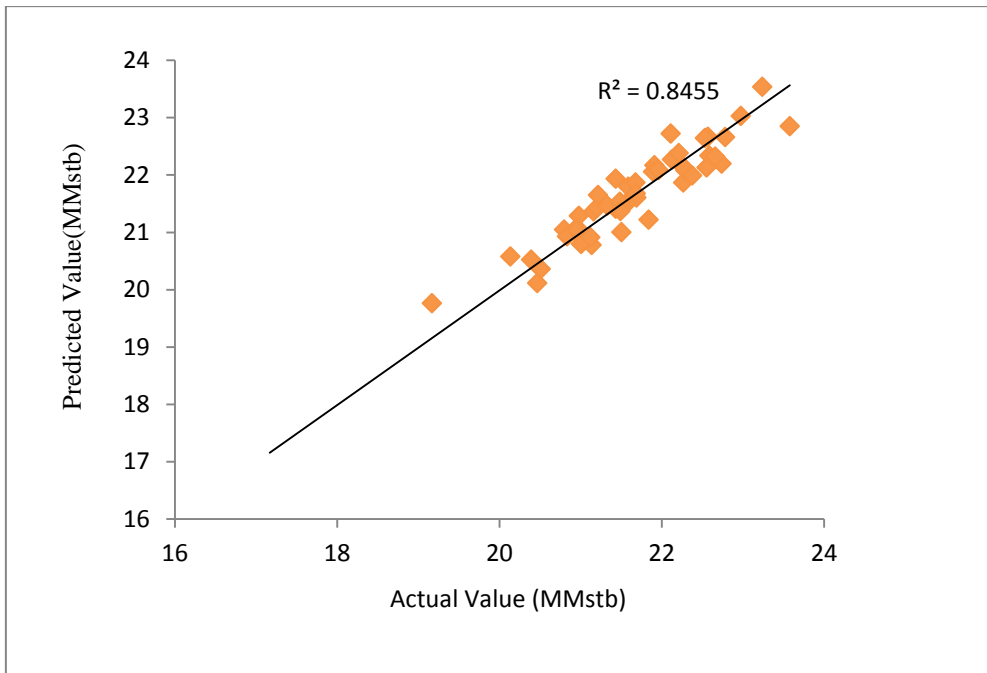
Figure 6. 14: Parity plot of Actual and predicted values in ANFIS for checking data sets.

Figure 6. 14 depicts the cross plot for the checking data versus model prediction for the remaining 43 data set. The prediction coefficient is 0.8455 and the root mean square error is 4%.
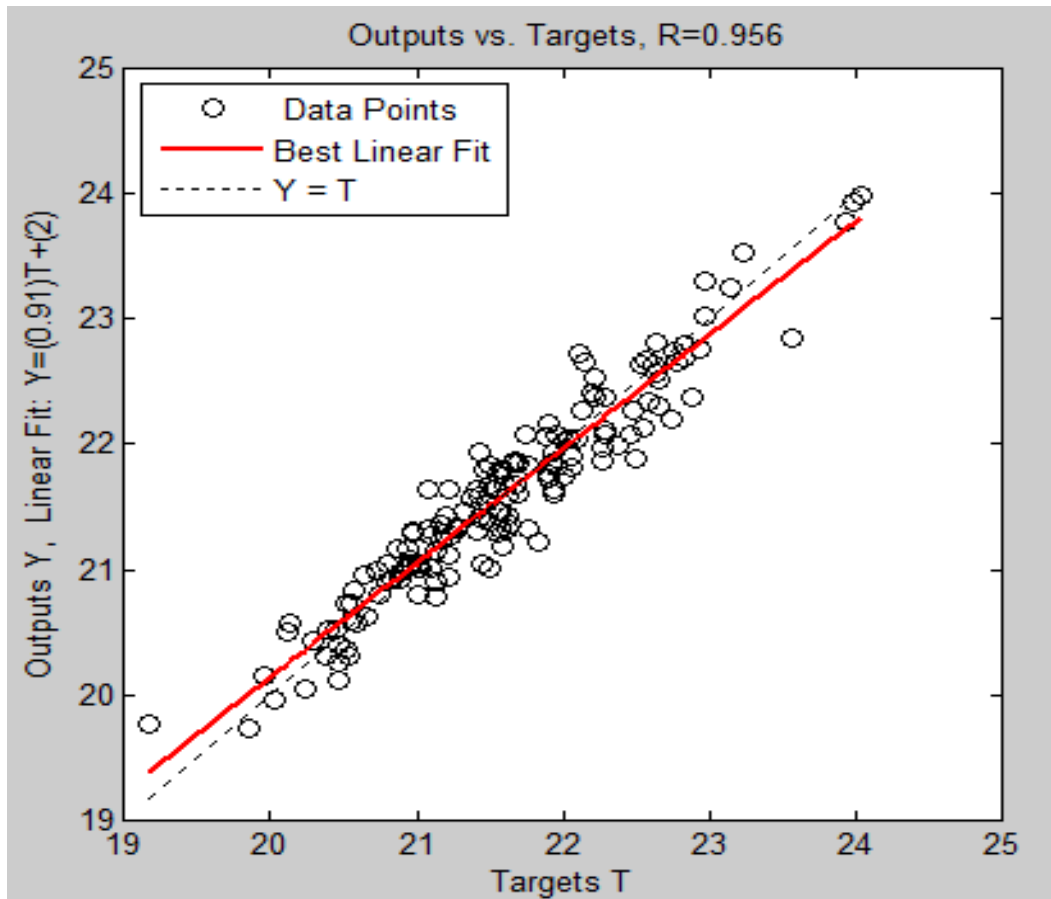
Figure 6. 15: Parity plot of Actual and predicted values in ANFIS for all data sets.

Figure 6. 15 shows the parity plot of actual reserves value versus ANFIS prediction for the whole data set used. The correlation coefficient of 95.6% is more than desired and indicates that the model is predictive.

6.6 Summary

i. The three families of screening designs considered are fractional factorial, Placket-Burman, and one variable at-a-time.

ii. The four response surface methods considered for the regression modeling are full factorial, central composite, Box-Behnken, and D-optimal.

iii. A total of 9 response surface models developed were validated and subjected to statistical error analysis.

iv. In all screening methods, years of production forecast played important role on associated number of "heavy-hitters." A full 2-level factorial or high resolution fractional factorial method was equally adequate for the construction of response surfaces for uncertainty quantification where 3-level full factorial was not feasible. Uniform design (UD) of experiment was also used to provide alternative to all conventional designs.

vi. Experimental design and Numerical simulation were integrated to develop ANFIS based proxy model for the production forecast. The prediction from the ANFIS model gives a better prediction and accuracy (AAPRE of 0.7406 and R-square of 0.956) than the response surface models (AAPRE of 2.913 and 0.8819) usually developed from the analysis of experimental design.

ANFIS model utilized fewer parameters when compare with RSM based proxy-model and therefore offers more flexibility where data availability poses serious challenge.

Chapter 7

7. Uncertainty Quantification

Two Monte Carlo methods were compared on the basis of underlying assumptions that characterizes them for quantifying uncertainty in reservoir forecast.

7.1 The Ordinary Monte Carlo simulations

The term Monte Carlo indicates all those stochastic algorithms using the central limit theorem to compute multidimensional integrals. Numerical solution of a D–dimensional integral with a relative accuracy ϵ requires a computation time proportional to ϵ^{-D}. However, with the central limit theorem, Monte Carlo methods scale as ϵ^{-2}, regardless of the dimensionality. Consequently, a surprising number of statistical problems utilize Monte Carlo techniques. Apart from this, numerical methods often give perfectly 'deterministic' results.

Whether or not the Monte Carlo method can be applied to a given problem does not depend on the stochastic nature of the system being studied, but only on our ability to formulate the problem in such a way that random numbers may be used to obtain the solution. Every application of the Monte Carlo method can be represented as a definite integral:

$$I = \int_\Omega f(x)\,dx \qquad\qquad 7.1$$

Where domain Ω is a region in multiple-dimensional space and f(x) is the integrand. The idea is to estimate the integral with an expected value using random samples. Integral I can be interpreted as the expected value of random variable f(X), where x is an independent random variable and identically distributed (iid) usually, uniformly distributed in Ω.

If we draw a set of samples, $x_1, \dots, x_n$ uniformly in Ω, then an approximation to I can be obtained by its arithmetic mean:

$$\hat{I}_N = \frac{1}{N} \sum_{i=1}^{N} f(X_i) \qquad\qquad 7.2$$

Generally, we often possess a probability distribution, π, from which we want to determine a point-estimate. However, scientific facts are usually presented in the media through the first moment, the mean, even though such an estimate rarely reflects the actual structure of π. Such an estimate can be determined through the following expression for any suitable function g:

$$\pi(g) = E_\pi[g(X)] = \int_E g(x)\pi(dx) \qquad\qquad 7.3$$

In most practical cases, analytic calculation of $\pi(g)$ in equation 7.3 is rarely possible. So, approximate answer is usually demanded. In order to determine such estimates one has to resort to an approximation.

7.1.1 Framework for integral computation

For a generic real function $f(x)$ of dimension D, we can compute the integral as follows:

$$\int f(\vec{x})d^Dx = \int \frac{f(\vec{x})}{p(\vec{x})} p(\vec{x})d^Dx \qquad\qquad 7.4$$

$$= \int g(\vec{x})p(\vec{x})d^Dx \qquad\qquad 7.5$$

200

With

$$g(\vec{x}) = \frac{f(\vec{x})}{p(\vec{x})}$$

and we can use the central limit theorem to write the estimate

$$\int f(\vec{x})d^Dx \approx S_N \pm \sigma_N$$

Central limit theorem

Let $\{\vec{x_i}\}$ be a sequence of stochastic D–dimensional independent variables distributed with a probability density $p(\vec{x})$, and $f(\vec{x})$ a real function. For the function, in accordance with the law of large number,

$$S_N \equiv \frac{1}{N}\sum_{i=1}^{N} f(\vec{x_i}) \tag{7.6}$$

Central limit theorem states that the probability density S_N in the large N limit can be written as

$$\lim_{N \to +\infty} P(S_N) = \frac{1}{\sqrt{2\pi\sigma_N^2}} e^{-\frac{(S_N - <f>)^2}{2\sigma_N^2}} \tag{7.7}$$

Where

$$< f > \equiv \int f(\vec{x})p(\vec{x})d^Dx \tag{7.8}$$

$$< f^2 > \equiv \int f^2(\vec{x})p(\vec{x})d^Dx \tag{7.9}$$

$$\sigma_N^2 = \frac{< f^2 > - < f >^2}{N} \tag{7.10}$$

In other words S_N is an estimate of $< f >$ and σ_N is its variance.

7.1.2 Naïve Bayes

Graphically, framework to explain the difference and the complexity associated with Ordinary and Markov chain simulations can be made. The graphical model for Naıve Bayes has a node for each x_d, with no edges between any of the nodes. Figure 7. 1 is a directed graphical model for the joint distribution with class variable c and feature vector $x = \{x_d\}$. This simplest multivariate distribution assumes that all of their component variables x_d are independent.
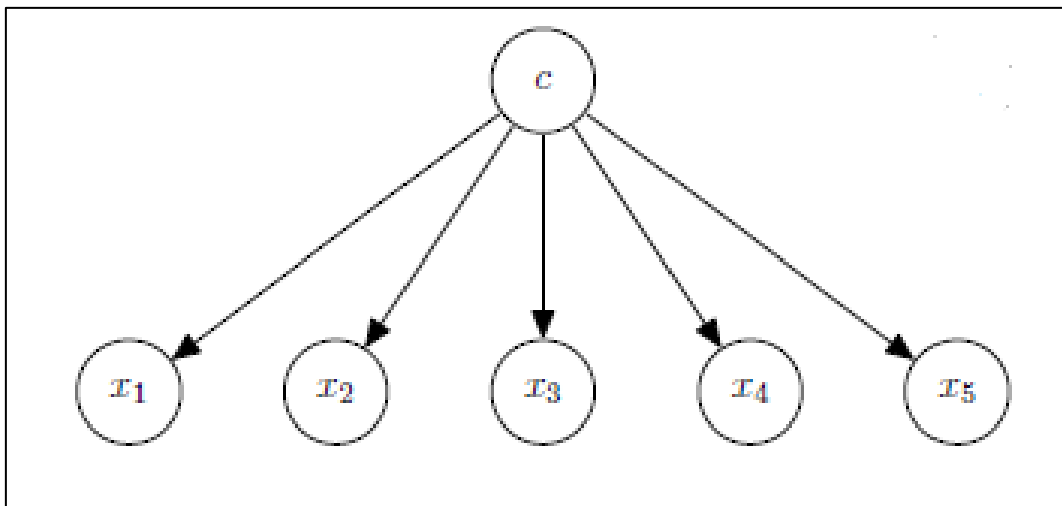
Figure 7. 1: Naïve Bayes

Mathematically:

$$P(X) = \prod_{d=1}^{D} p(x_d) \qquad\qquad 7.11$$

This assumption is generally inappropriate as it means that no relationships between any of the variables can ever be learned. The features x are dependent, but independent conditioned on the class variable c.

7.1.3 Assumption in OMCS

Independence of two measurable sets implies that any information about an event occurring in one set has no information about whether an event occurs in another set. If we let X_1 and X_2 to be two events in the sample space, then X_1 and X_2 are independent if and only if

$$Pr(X_1 \cap X_2) = Pr(X_1)Pr(X_2) \qquad\qquad 7.12$$

One immediate implication of the definition of independence is that when X_1 and X_2 independent, the conditional probability of one given the other is the same as the unconditional probability of the random variable:

$$Pr(X_1/X_2) = Pr(X_1) \qquad\qquad 7.13$$

Let us consider two random variables x and y. In order to specify completely the distribution of x and y, we now requires an approximation function of the two variables say:

$$h(x, y) = ax + b \qquad\qquad 7.14$$

This ensuing mathematics can be more complicated. However, when the function h(x, y) can be factored exactly into a product of two functions, each of the variable depends only on one variable, we say that x and y are stochastically independent since the distribution of x does not depend on the value of y and vice versa.

$$h(x, y) = p(x)q(y) \qquad\qquad 7.15$$

When more than two variables are considered, the concept of independence becomes more complicated, and it is no longer sufficient to consider only the dependence of pairs of

variables. Indeed, it is possible to have all pairs of variables independent and still have dependence among triplets or higher combinations of variables.

The solution of the integral always requires the estimation of probability and cumulative density functions (pdf and cdf). Those probability density functions have to be determined by trial-and-error while performing Monte Carlo simulation. Consider a separable multivariable function:

$$f(k, \emptyset) = g(k)h(\emptyset) \qquad\qquad 7.16$$

The probability density function as a function of one of the variables can be found by separation as shown in Equations 7.17 through 7.20.

$$P(k) = \frac{\int_{\emptyset min}^{\emptyset max} f(k, \emptyset)d\emptyset}{\int_{kmin}^{kmax} \int_{\emptyset min}^{\emptyset max} f(k, \emptyset)dkd\emptyset} \qquad\qquad 7.17$$

$$P(k) = \frac{g(k) \int_{\emptyset min}^{\emptyset max} h(\emptyset)d\emptyset}{\int_{kmin}^{kmax} g(k)dk \int_{\emptyset min}^{\emptyset max} h(\emptyset)d\emptyset} \qquad\qquad 7.18$$

$$P(k) = \frac{g(k)}{\int_{kmin}^{kmax} g(k)dk} \qquad\qquad 7.19$$

$$P(\emptyset) = \frac{h(\emptyset)}{\int_{\emptyset min}^{\emptyset max} h(\emptyset)d\emptyset} \qquad\qquad 7.20$$

For non-separable functions

$$h(k, \emptyset) = ak + b\emptyset^2 \qquad\qquad 7.21$$

The Marginal Density Functions can be found as identified in Equations 7.22.

$$R(k) = \int_{-\infty}^{k} \int_{\emptyset min}^{\emptyset max} P(k, \emptyset)d\emptyset dk \qquad\qquad 7.22$$

Suppose X is a bivariate random variable with probability density function

$$f(k, \emptyset) = ak + b\emptyset^2 \qquad\qquad 7.23$$

defined on [0, 1] x [0, 1]. Then the associated cdf is

$$F(k, \emptyset) = \int \int (ak + b\emptyset^2) dk d\emptyset \qquad\qquad 7.24$$

$$= \frac{a}{2} k^2 \emptyset + \frac{b}{3} k \emptyset^3 \qquad\qquad 7.25$$

7.1.4 Relationship between CDF and PDF

Let $f(x_1, \ldots, x_n)$ and $F(x_1, \ldots, x_n)$ represent the pdf and cdf of an $n-$ dimensional con$-$tinuous random variable X, respectively. the density function for X can be defined as

$$f(x_1, \ldots, x_n) = \frac{\partial^n F(X)}{\partial x_1 \, \partial x_2 \ldots \partial x_n} \qquad\qquad 7.26$$

wherever $f(x_1, \ldots, x_n)$ is continuous and $f(x_1, \ldots, x_n) = 0$ elsewhere.

Suppose X is a bivariate random variable with cumulative distribution function

$$F = \frac{a}{2} k^2 \emptyset + \frac{b}{3} k \emptyset^3$$

The probability density function can be determined thus:

$$f(x_1, \ldots, x_n) = \frac{\partial^2 F(k, \emptyset)}{\partial k \, \partial \emptyset}$$

$$= \frac{\partial}{\partial \emptyset} \left(ak\emptyset + \frac{b}{3} \emptyset^3 \right)$$

$$= ak + b\emptyset^2$$

7.1.5 Solution from Ordinary Monte Carlo

From the definition of a Monte Carlo, the method produces a result f which is a function of random numbers x_i. For simplicity, if we assume that the x_i are uniformly distributed between zero and one. Then the Monte Carlo result $f = f(x_1, x_2, ..., x_n)$ is an unbiased estimator of the multidimensional integral:

$$I = \int_0^1 ..... \int_0^1 f(x_1, x_2, ..., x_n) dx_1 dx_2 ... dx_n \qquad 7.27$$

For many problems, variables are continuous, not discrete. The variable could be any number within a range of values. The probability of any value being chosen could be represented by a continuous distribution (probability density function, pdf). Figure 7. 2 illustrates a continuous probability density function. Given a function f(x) the value of the associated probability density function P(x) can be found by dividing f(x) by the integral of f(x) over all values of

$$P(X) = \frac{f(X)}{\int_{-\infty}^{\infty} f(X) dX} \qquad 7.28$$

Figure 7. 3 shows the cumulative density function that corresponds to the probability density function. The value of the cumulative density function R at any value x is simply the area under the probability density function up to x. This can be represented in equation form as:

$$R(X) = \int_{-\infty}^{X} P(X) dX \qquad 7.29$$

The cumulative density function represents the probability that a value of x or less occurs.
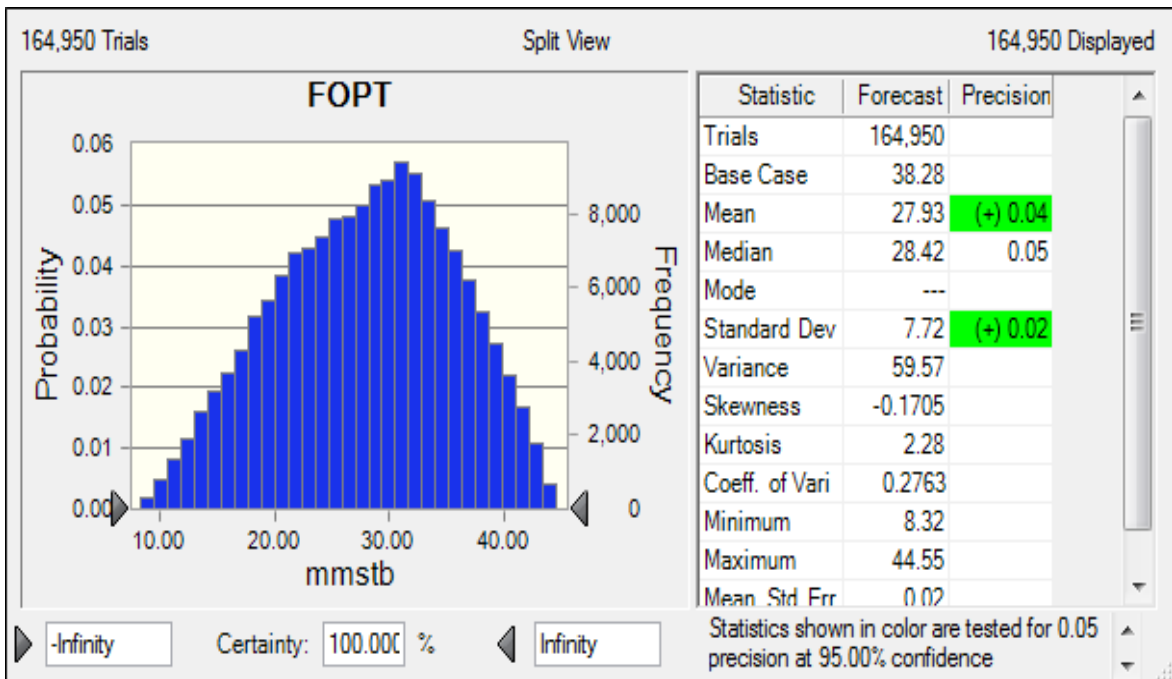
Figure 7. 2: Continuous probability density function (pdf)
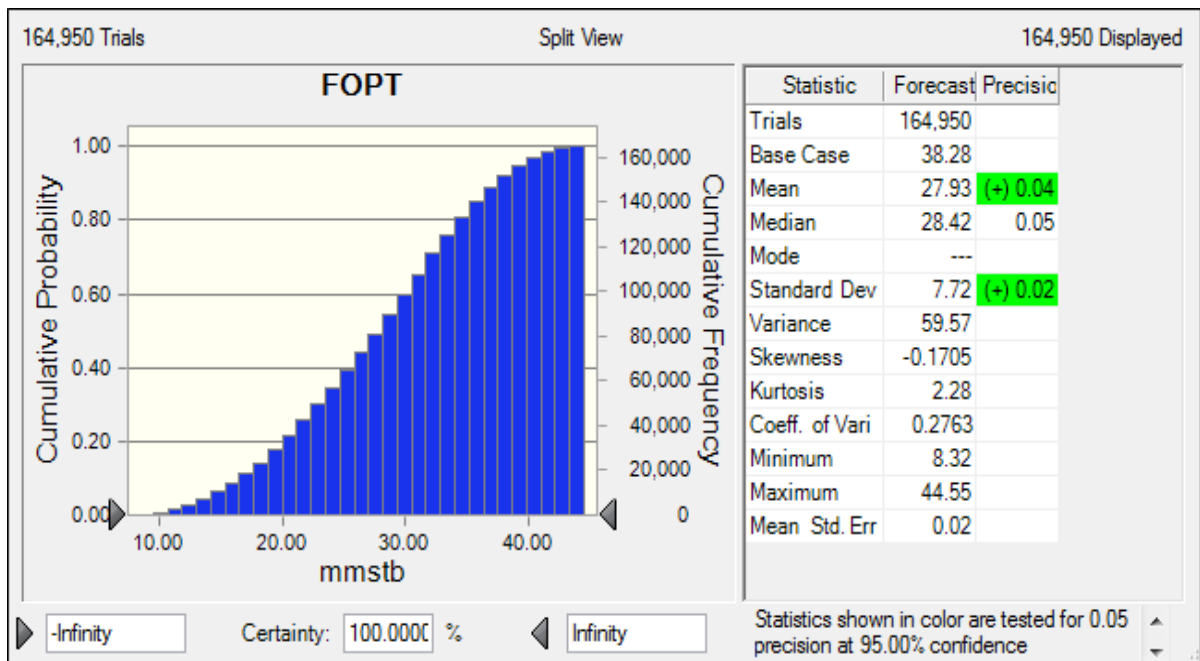
Figure 7. 3: Cumulative Density Function

7.1.6 Risk curves using OMCS

The Monte Carlo technique was used to combine the uncertain attributes using response surface equations developed in chapter 6. Two thousand (2000) iterations were made while assumed the following distribution functions: triangular for OVISC, uniform for PORO, Log normal for PERMX and PERMZ, Normal for SWC, triangular for AQUIPV and triangular for KRW.

It was found that 2000 equiprobable realisations iteratively built in Excel were enough to stabilize the resulting forecast distributions. One critical measure used to generate each realisation of the model is that the deterministic reserve value was fairly maintained at simulation base case value throughout the process. Cumulative probability distribution for the forecast reserves are shown in Figure 7. 4 through Figure 7. **6**. The impact of the major uncertain parameters was quantified.
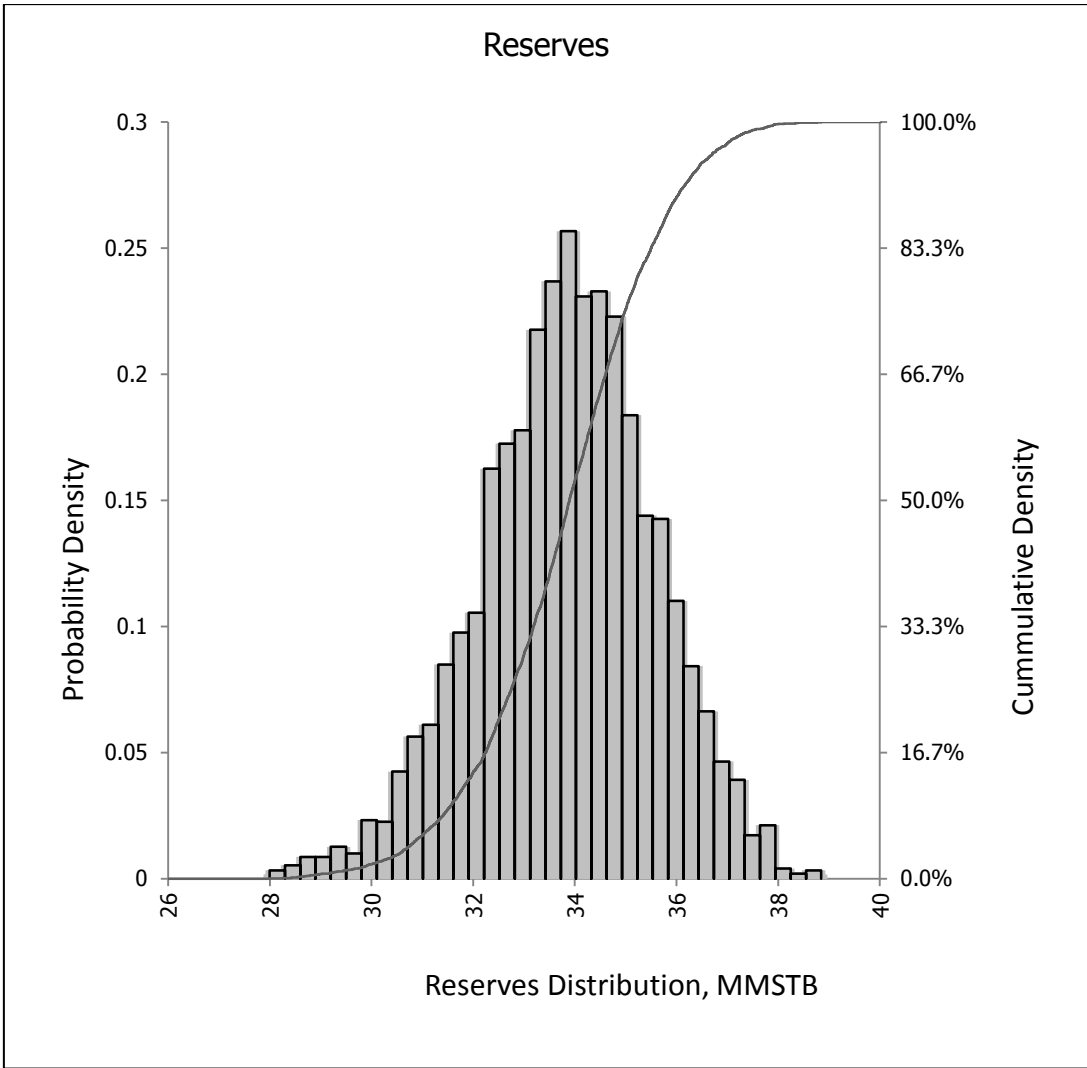
Figure 7. 4: Reserves distribution for Box-Behnken RSM equation 6
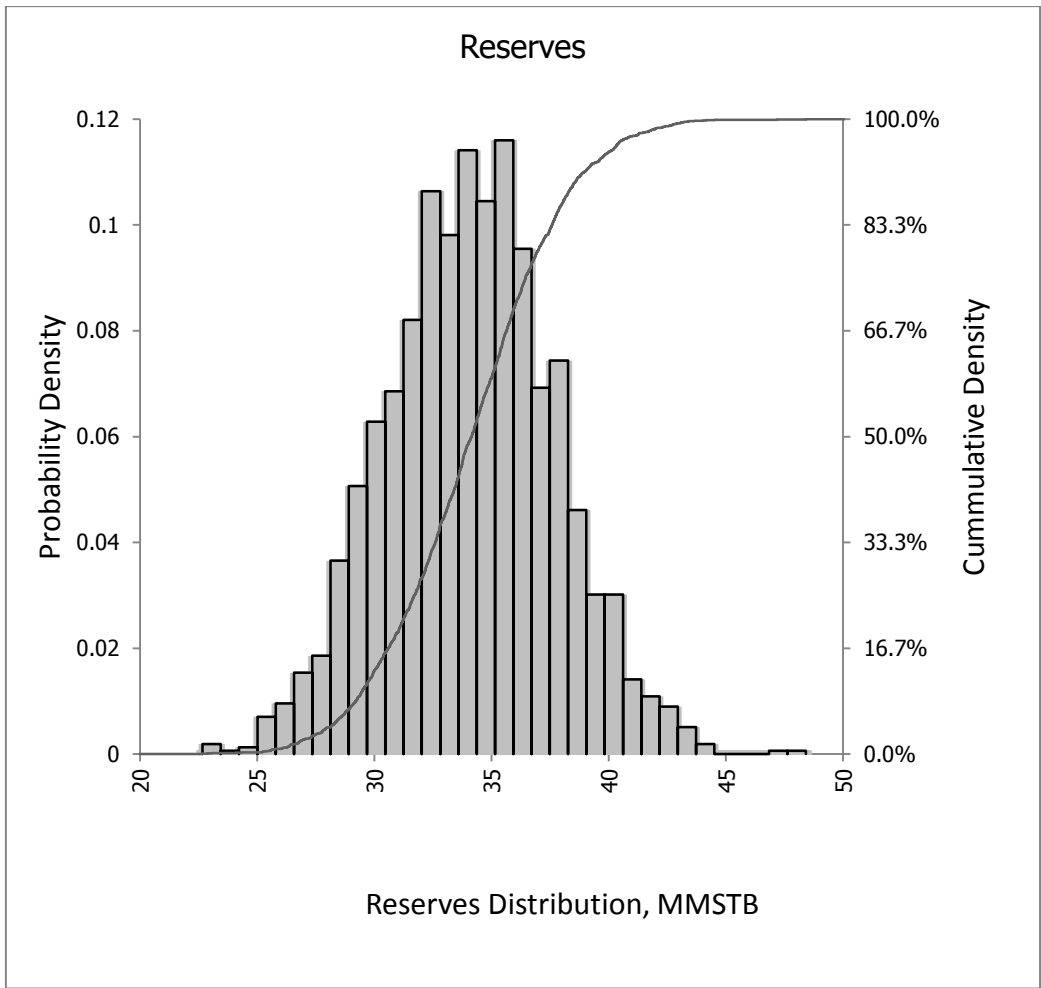
Figure 7. 5: Reserves distribution for Central Composite Response surface associated with Placket-Burman Screening method.
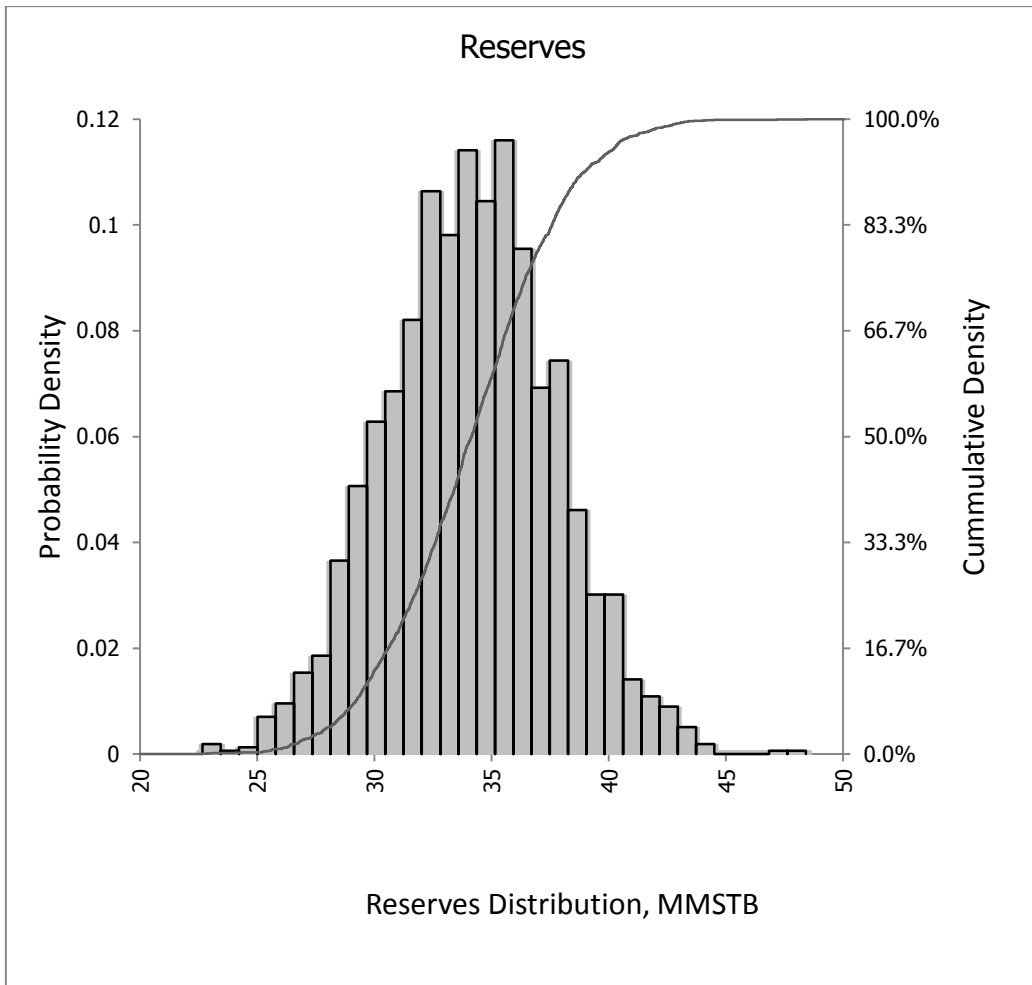
Figure 7. 6: Reserves distribution for Full Factorial Response surface associated with Placket-Burman Screening method.

The spread in production profiles (P10-P90 range) from the deterministic fotecast (P50) volume is shown in Figure 7. 7 which indicates occurrence of uncertainty in the forecast. The extreme quantities to a large extent are investment indicators.
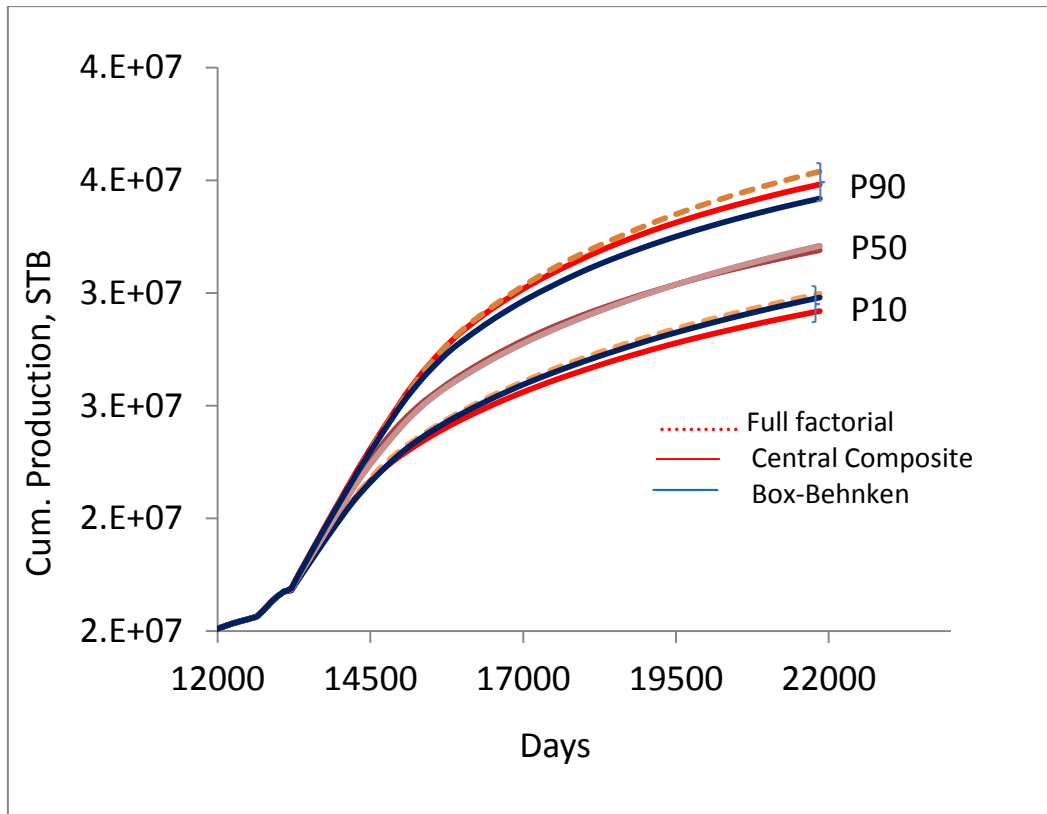
Figure 7. 7: Stochastic model profiles corresponded with P10/P50/P90 for Box-Behnken, Central Composite and Full Factorial PB associated methods.

Figure 7. 8 shows risk curves in terms of cumulative oil production obtained from various RSMs for the uncertainty assessment. It can be seen that the P10 and P90 values differ according to the assumed response surface methods. Full factorial method gives the highest P10 (38.4 MMSTB) value and minimum P90 (28 MMSTB) value. CCD is characterized by lowest P10 (35.4 MMSTB) and P90 (32 MMSTB). Both Box-Behnken and D-optima methods gives approximately equal values of P90 (36 MMSTB) and P10 (30 MMSTB). The difference between P10 andP90 values is an indication of the degree of uncertainty.
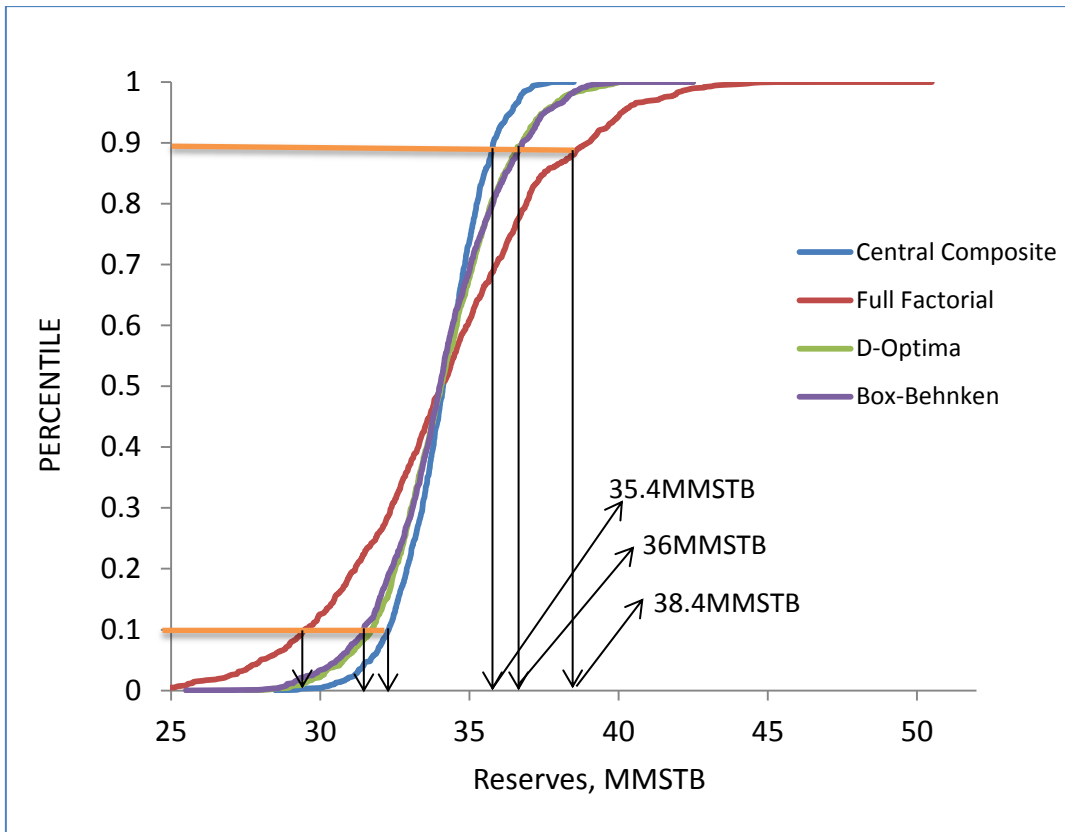
Figure 7. 8: Impact of different RSMs on Uncertainty assessment

The risk curves generated from MCS provide information on the risk associated with wanton adoption of experimental designs for response surface methodology. The figure clearly shows the uncertainties associated with the choice of percentiles for investment decision. The costs and benefits of conducting additional experiments due to preference for one design method relative to others are also highlighted in Figure 7. 8.
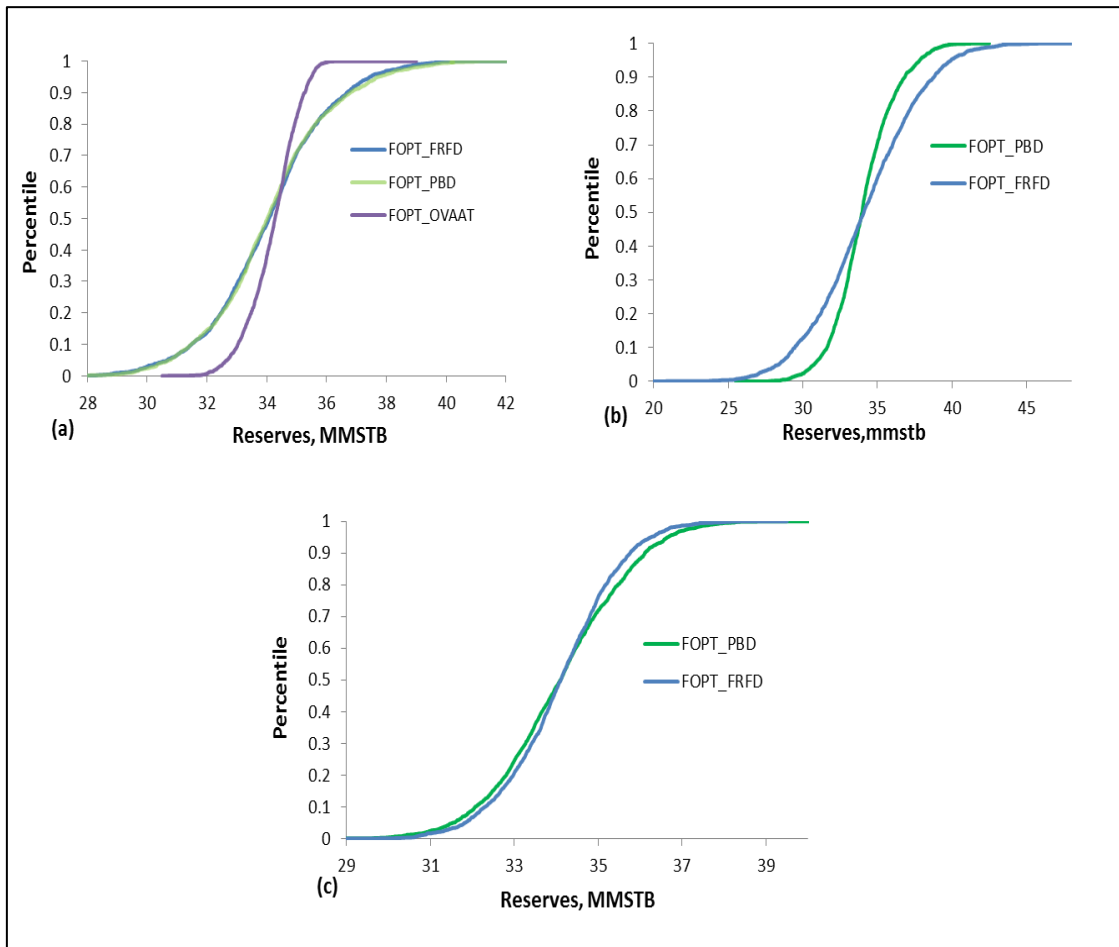
Figure 7. 9: Risk Curves for Case 1 – (a) Box-Behnken equations 6.2, 6.6 and 6.10 (b) Central Composite equations 6.3 and 6.9 (c) Full Factorial equations 6.5 and 6.7

The implication of performing 46 and 62 experiments using fractional and relative variation designs respectively instead of the 29 using PB design was examined by constructing a multiple risk curves. For the curves, P50 values are ensured equal after MCS as shown in Figure 7. 9. A good agreement of risk curves of Box-Behnken associated with Placket-Burman and fractional factorial screening designs. The same applied to full factorial risk curves shown in Figure 7. 9c. However, the risk curve associated with screening using the one variable at-a-time exhibits wider variability from others and tends

214

to be more optimistic which is perhaps due to different occurrence probability and larger number of factors involved in the regression analysis. The risk curves obtained by CCD developed from Placket-Burman and fractional factorial is a little at variance from each other due to combination that possesses dissimilar occurrence probability. In summary, both fractional screening design and PB design tend to give approximate result. Based on the analysis, there is no significant added advantage in performing 46 experiments as required by fractional factorial screening method. PB with fewer experimental runs is therefore desirable.

7.2 Markov Chains Model

The arrow directions make a big difference in Figure 7.10 compare with Figure 7.1. The x variables are independent in the generative process.
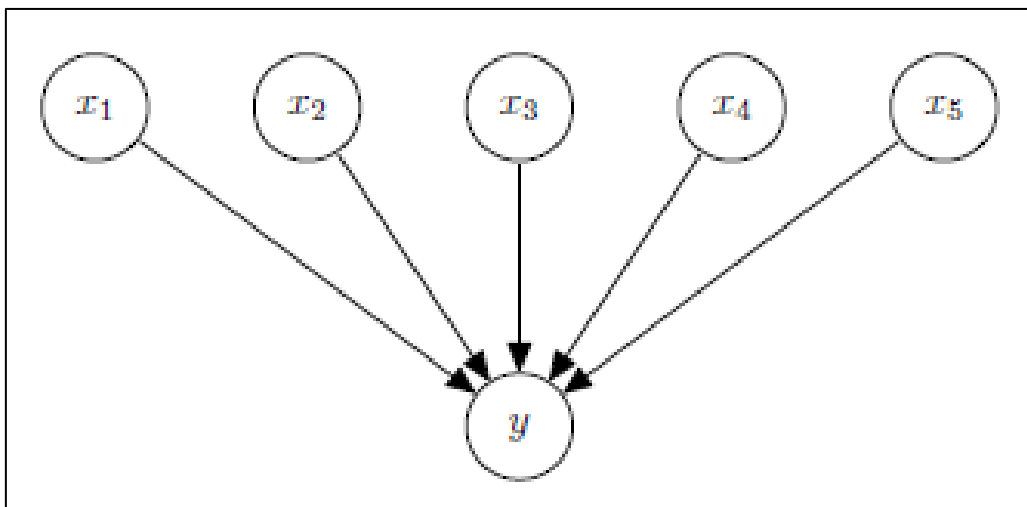
Figure 2: Hidden causes

After observing y our knowledge about x forms a potentially complex joint distribution. Ordinary Monte Carlo approach can-not be used here because we do not expect direct

sampling from $p\left(x/y\right)$ to be easy. Methods based on Markov chains will offer a solution to this problem.

Mathematically,

$$p(y, X) = p(y)p\left(X/y\right) = p(y) \prod_{d=1}^{D} p\left(x_d/y\right)$$

7.2.1 Uncertainty quantification

Bayesian approach, expresses uncertainties in the model's parameters θ in terms of probability. Parameter uncertainty is quantified first by introducing a prior probability distribution $P(\theta)$, which represents the knowledge about θ before collecting any new data, and second, by updating this prior probability on θ to account for the new data collected (D).

This updating is performed using Bayes' theorem, which can be expressed as:

$$P\left(D/\theta\right) = \frac{P(D/\theta).P(\theta)}{\int P(D/\theta).P(\theta).d\theta} \qquad\qquad 7.30$$

Where $P(\theta/D)$ is the posterior distribution of θ; $\int P(D/\theta).P(\theta)d\theta$ is a normalizing constant required so that $\int P(D/\theta).d\theta = 1$, and $P(D/\theta)$ is the conditional probability for the measured data given the parameters. $P(D/\theta)$ is often referred to as the likelihood function.

7.2.2 The advantage of Bayesian Monte Carlo method

Bayesian methods explicitly use probability distributions as a way to quantify uncertainties about the unknown quantities. The inference is carried out conditional on the observed data

and unlike OMCS, it does not rely on the assumption that a hypothetical infinite population of data exists. This quality gives certain advantages to Bayesian methods over ordinary Monte Carlo; such as that all inferences are exact and not approximated and that the results are interpretable so that one can easily answer any scientific questions directly.

However, no readily available asymptotic results (such as the central limit theorem based on an asymptotic increment of data) can be used to facilitate estimations, and Bayesian analysis usually requires a much greater amount of computational resources.

7.2.3 Markov simulation

With MCMC, we sample from the posterior directly, and obtain sample estimates of the quantities of interest, thereby performing the integration implicitly. Suppose that we have some distribution $\pi(x), x \in E \subseteq R^p$, which is known only up to some multiplicative constant. We commonly refer to this as the target distribution. If π is sufficiently complex that we cannot sample from it directly, an indirect method for obtaining samples from π is to construct an aperiodic and irreducible Markov chain with state space E, and whose stationary (or invariant) distribution is $\pi(x)$, as discussed in Smith and Roberts (1993). Then, if we run the chain for sufficiently long, simulated values from the chain, can be treated as a dependent sample from the target distribution and used as a basis for summarizing important features of π. A brief description of the implementation of MCMC algorithm in a general setting is given here. Let us define

$$X = (x_1, x_2, \ldots, x_n)^T$$

as an observed sample of size n from the univariate distribution $f(x/\theta)$. Here the parameter θ is a vector containing p elements,

$$\theta = \left(\vartheta_1, \vartheta_2, \ldots, \vartheta_p\right)^{\mathrm{T}}.$$

We assume the parameters are conditionally independent and the prior distribution of θ_j is $P_j(\theta_j)$, for $j = 1, 2, \ldots, p$. Therefore the likelihood function $L(X/\theta)$ takes the form

$$L(X/\theta) = \prod_{i=1}^{n} f(x_i/\theta) \qquad\qquad 7.31$$

The joint posterior distributions of the parameter vector up to the normalizing constant is

$$P(\theta/X) \propto \prod_{i=1}^{n} f(x_i/\theta) . \prod_{j=1}^{p} P_j(\theta_j) \qquad\qquad 7.32$$

Except in a few cases, the posterior distribution in equation 7.32 cannot be evaluated. However, the Metropolis-Hastings (MH) method prescribes a way to simulate the posterior distribution. We describe the algorithm in the following manner.

Step 1 Specify the initial guess of the parameter vector θ_0 (for example this could be the modes of each of the prior distributions).

Step 2 Specify proposal distributions, $q_j(\theta_j/\theta)$ for each of the parameters θ_j for $j = 1, 2, \ldots, p$.

Step 3 MCMC Simulation

$$\text{For } t \text{ from } 1 \text{ to } B + N \text{ do } /* B \text{ simulations are burn} - \text{in } */$$

$$\text{Let } \theta^t = \left[\theta_1^t, \theta_2^t, \ldots, \theta_p^t\right]$$

For j from 1 to p do

$$\text{Simulate } \theta_j^* \text{ from } q_j\left(\theta/\theta_j^{t-1}\right)$$

$$\text{Let } \theta_{j*}^t = \left[\theta_1^t, \theta_2^t, \ldots, \theta_j^*, \theta_{j+1}^{t-1}, \theta_{j+2}^{t-1}, \ldots, \theta_p^{t-1}\right]$$

$$\text{Let } r = \frac{P\left(\theta_{j*}^t / X\right) q_j\left(\theta_j^{t-1} / \theta_j^*\right)}{P\left(\theta^{t-1} / X\right) q_j\left(\theta_j^* / \theta_j^{t-1}\right)}$$

Simulate U from Uniform[0,1]

$$\text{Set } \theta_j^t = \left\{ \begin{array}{l} \theta_j^* \text{ if } U < \min(r, 1) \\ \theta_j^{t-1} \text{ otherwise} \end{array} \right\}$$

end do

if t > B then

Simulate x_{t-B}^{pred} from $f(x/\theta^t)$

end if

end do

Step 3 Simulate observations from the predictive distributions after a certain number of burn-ins. At the end we could construct the empirical distribution based on the simulated sample $x_1^{pred}, x_2^{pred}, \ldots, x_N^{pred}$ and this would be the predictive distribution (Gilks *et al.*, 1996).

7.2.4 Metropolis algorithm

Although the Metropolis algorithm is not the most efficient Markov Chain sampler, it is chosen in this study because of the simplicity of its implementation, and its generality. It only requires knowledge about the likelihood function to update simultaneously the parameters set for each iteration. Supposing that residuals between model and observation are N(0, σ2), the likelihood function can be written in the multiplicative form:

$$P(D/\theta) = \prod_{t=1}^{n} \frac{1}{(2.\pi.\sigma^2)^{1/2}} . e^{\frac{(Y_t - f(X_t, \theta))^2}{2.\sigma^2}} \qquad\qquad 7.33$$

Where $(Y_1 \dots Y_n)$ is the vector of the measured response Y, $(Y_1 \dots Y_n)$ is a vector of input data, $\theta = (\theta_1, \dots, \theta p)$ is the vector of p unknown parameters, and $f(\ )$ is the model's output. σ is considered, as well as θ, as a set of parameters to be estimated during calibration.

At each iteration, candidate values of parameters are drawn from a multi-normal transition probability distribution for which the variance could be tuned up in a way to increase the speed of convergence. However, updating periodically (automatically) the variance during the simulation, is difficult. This was handled by fixing a prior value of the variance according to the information about the parameters during all the simulation (Kuczera and Parent, 1998).

An interesting feature of the Metropolis algorithm is that the interaction among the model's parameters is reflected in the likelihood function, so there will be no need to incorporate correlation in the prior distributions of parameters. In order to avoid favoring any initial value, a uniform prior distribution was used over the range of parameters.

7.3 Monte Carlo Application to Case Study

7.3.1 Surrogate Model

The reservoir described in chapter 5 as case study 2 was used to illustrate the differences between the Ordinary and Bayesian Monte Carlo simulations. The first task was to develop a mathematical function that approximates the observations (cumulative production) after running the flow simulation over 25 years. The following assumptions are considered:

1. A data set $X \in R^{n,s}, y \in R^n$ is provided

2. The rows $X^i \in R^s$ of $X := (X^i, .., X^n)^T$ are independent and identically distributed (i.i.d.) realizations of a random vector with a probability density function p(x), which is non-zero everywhere on the cube $D := [X_{min}, X_{max}] = ([x_{j,min}, x_{j,max}])_{j=1,...,s}$ and zero outside.

3. The provided values of $y = (y^1, ..., y^n)^T$ are noisy observations of $f(X^i), i = 1 ..., n$ with

$$y^i = f(X^i) + \epsilon^i, \quad i = 1 ..., n$$

where ϵ^i is random with $E[\epsilon^i] = 0$, independent of X^i

4. The function $f: R^s \to R, \ f \in \beta$ has a representation:

$$f(X) = \sum_{j=1}^{\infty} a_j b_j(X), \quad X \in R^s,$$

where $b_j \in \beta, j = 1, ..., \infty$ are bounded basis functions $b_j: R^s$ of a vector space $\beta CC'$ with $\|b_j(X)\|_{\infty} = C_j < \infty, \ni X \in D: |b_j(X)| > 0, j = 1, ..., \infty$.

The final approximation equation is given as:

$$\hat{y} (SWI, PERMX)[MMstb] = \beta_0 + \beta_1 SWI + \beta_2 PERMX^2 \qquad 7.34$$

where $\beta_0 = 2.488, \beta_1 = 53.0332$ and $\beta_2 = -17.2437$. Only two of the four parameters are significant during the optimization.

Ordinary Monte Carlo Method

The probability density for f(SWI, PERMX) can be found by dividing f(SWI, PERMX) by the total area under its curve. Say that we want to know the probability of forecast landing within an acceptable value of SWI and PERMX. Applying f(SWI, PERMX) to Equation 7.35:

$$P(X, Y) = \frac{f(X, Y)}{\int_{x_1}^{x_2} \int_{y_1}^{y_2} f(X, Y) dX dY} \qquad\qquad 7.35$$

where $X = $ SWI and $Y = $ PERMX

Knowing the probability distribution, it is necessary to randomly draw uniformly distributed numbers between x_1 to x_2, and y_1 to y_2. In reality, computer programs with random number generators develop pseudorandom numbers. The pseudo-random numbers that are drawn independently are assigned as variables x_1 and y_1. These variables does not obey the intended probability density function though, it obeys a uniform distribution. To ensure that x_1 and y_1 obey the distribution identified by Equation 7.35, input x_1 and y_1 into $P(X, Y)$. This will result in a value $P(x_1, y_1)$. Now draw another pseudo-random number between 0 and 1, which will be called P_2. If $P(x_1, y_1)$ is less than P_2, then a realistic forecast is made at (x_1, y_1). If not, the value chosen for (x_1, y_1) should be rejected and another attempt at selecting (x_1, y_1) should be made. The rejections result in a distribution for (x_1, y_1) that obeys $P(X, Y)$. The obvious disadvantage of forcing (x_1, y_1) to obey the selected probability distribution is that there will be a lot of rejections at higher (x_1, y_1) resulting in longer computational time. A method of identifying (x_1, y_1) that makes more sense computationally is to utilize the cumulative distribution function.

The cumulative distribution function that corresponds to Equation 7.31 can be found by the application of Equation 7.29 extended to two variables X and Y is given as:

$$R(X, Y) = \int_{-\infty}^{\infty} \int_{-\infty}^{\infty} P(X, Y) dX dY \qquad\qquad 7.36$$

The cumulative density function given by Equation 7.36 accounts for the distribution of the probability density function over all values of x and y. Because of this, no rejections are

required in order to use the cumulative density function to generate values of (x_1, y_1). It is for this reason that most Monte Carlo codes utilize the cumulative density function rather than the probability density function to generate simulated variables. To use the cumulative density function to determine x and y, a uniformly distributed number between 0 and 1 should be drawn using a pseudo-random number generator. This value is substituted for $R(X, Y)$ independently, and x and y can then be solved for using Equation 7.36.

However, by using Equation 7.34 and substituting in, the mid values for SWI (0.65-0.9) of 0.775 and PERMX (0.57-1.3) of 0.935, the forecast is analytically determined to be 28.54MMstb by direct substitution.

Assuming uniform parameter distribution, the 500, 1000, 2500, 3500, 5000 and 10000 trials, for the Monte Carlo using Crystal Ball produces the mean forecast shown in Table 7.1.

Because the results for the forecasts are determined based on a number of trials and have some variability, 10 trials for each sample size were performed so as to be able to assess the mean and variance. The means, standard deviations, and variances are also reported in Table 7.1 along with the forecasts for each sample size. It is possible to make some observations from the data. Note that as the sample size increases, the standard deviation and variance are reduced. Additionally, larger sample sizes tend to result in mean forecast that are closer than for smaller sample sizes. The results compare well with the deterministic value of 28.54MMstb. Even for 1000 trials, the difference between the deterministic forecast and the mean Monte Carlo determined forecast value was only 1.92%.

223

The cumulative and density functions from the Crystal ball are presented as shown in Figure 7.10 and Figure 7.11 as cdf and pdf respectively. The distribution of forecast at 5% increment with corresponding values of parameter is also presented in Table 7. 2.

Table 7. 1: Results for uncertainty quantification for forecast problem

Size Run	500	1000	2500	3500	5000	10000
1	28.23	28.02	27.91	27.76	27.82	27.95
2	28.16	28.13	27.86	27.93	28	27.96
3	27.72	28.34	27.67	28.02	27.9	27.93
4	27.3	27.53	28.01	27.85	28.05	27.95
5	28.16	28.01	27.85	27.79	27.92	27.99
6	27.95	28.33	27.88	27.77	27.99	27.95
7	27.91	27.34	27.78	27.86	27.86	27.95
8	27.24	28.13	27.71	27.93	27.89	27.96
9	27.93	27.98	27.82	28.04	27.92	27.96
10	27.85	28.1	27.76	27.81	27.9	27.98
Mean	27.845	27.991	27.825	27.876	27.925	27.958
St. Dev	0.341215149	0.320570672	0.099916632	0.100465583	0.069322114	0.016865481
Variance	0.104785	0.092489	0.008985	0.009084	0.004325	0.000256
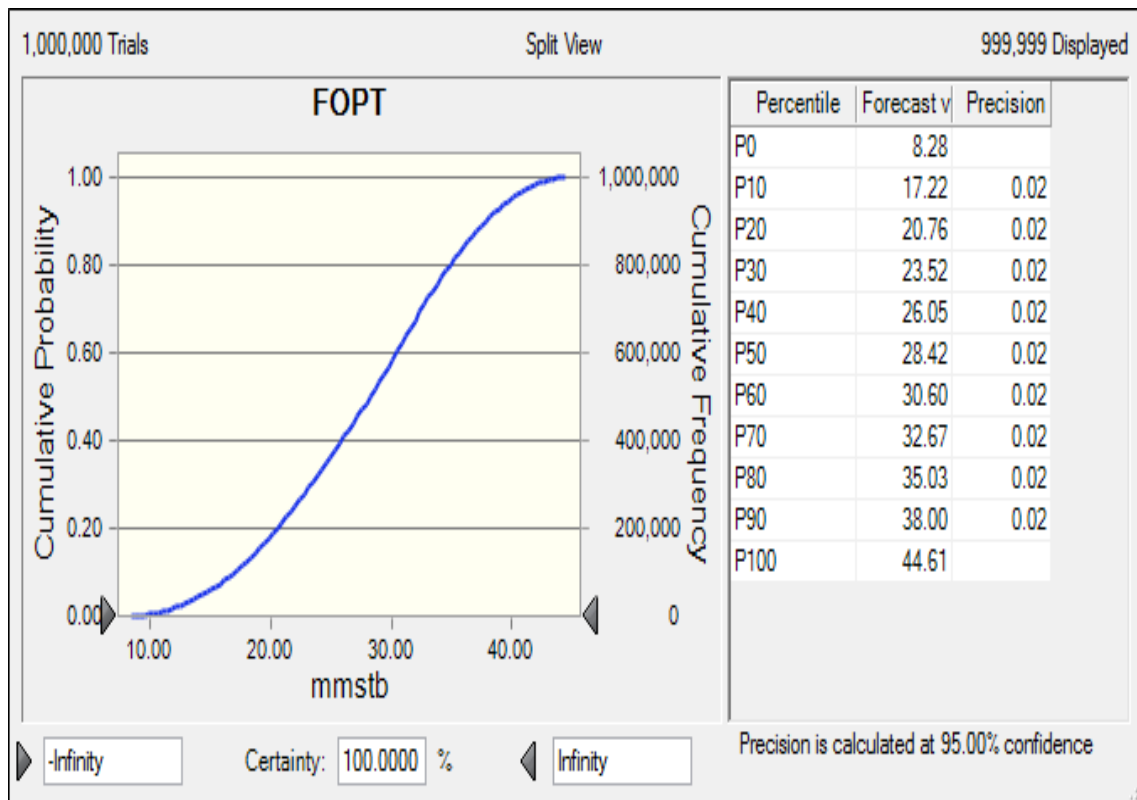
Figure 7. 10: The cumulative density function of forecast distribution
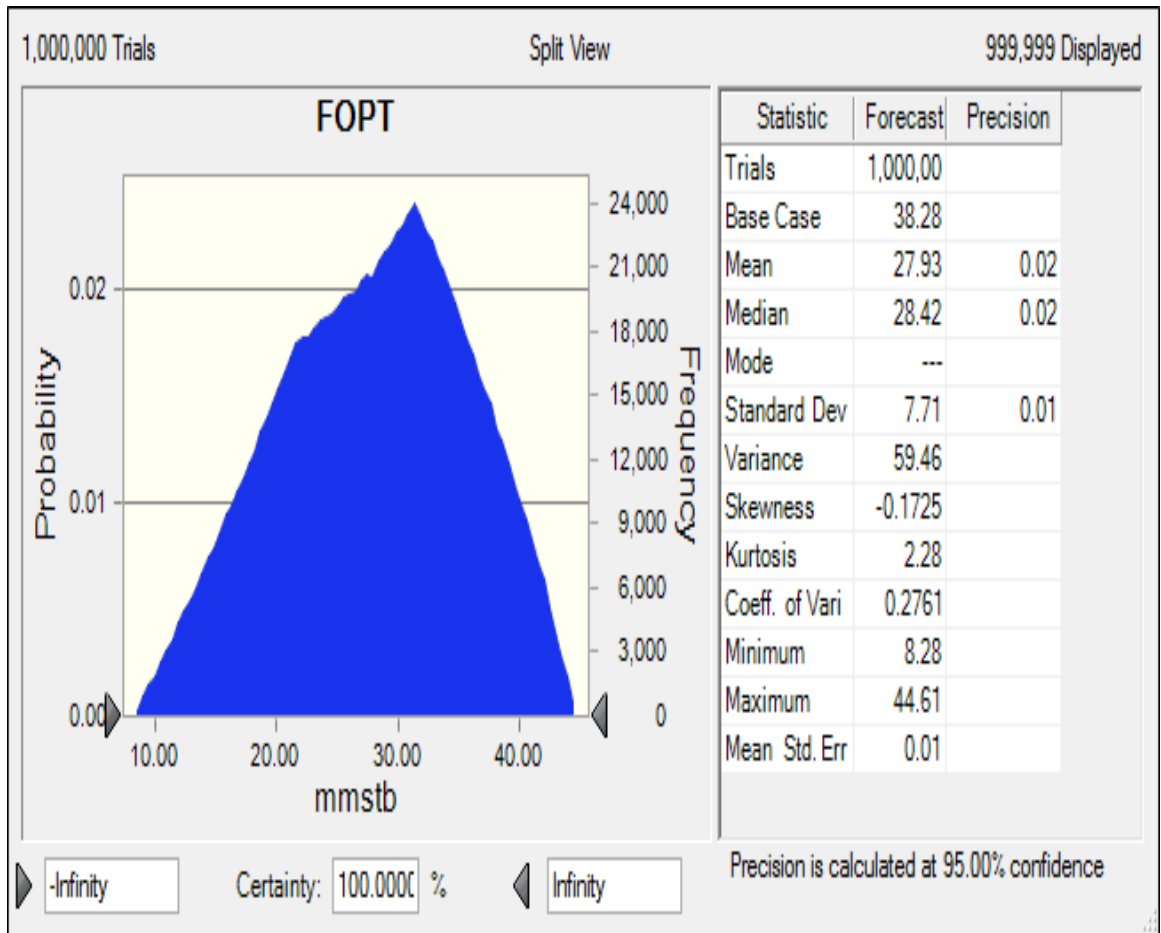
Figure 7. 11: Probability density function as area under the curve

Table 7. 2: Forecast distribution and corresponding percentiles

Percentiles	FOPT(MMSTB)	PERMX	SWI
P0	8.28	0.57	0.65
P5	14.67	0.61	0.66
P10	17.22	0.64	0.67
P15	19.16	0.68	0.69
P20	20.76	0.71	0.70
P25	22.17	0.75	0.71
P30	23.52	0.79	0.72
P35	24.81	0.82	0.74
P40	26.05	0.86	0.75
P45	27.26	0.89	0.76
P50	28.42	0.93	0.77
P55	29.53	0.97	0.79
P60	30.60	1.00	0.80
P65	31.62	1.04	0.81
P70	32.67	1.07	0.82
P75	33.79	1.11	0.84
P80	35.03	1.15	0.85
P85	36.40	1.18	0.86
P90	38.00	1.22	0.87
P95	40.03	1.25	0.89
P100	44.61	1.29	0.90

Uncertainty quantification using MCMC

In order to quantify the uncertainty on production forecast the Bayesian parameter estimation conditioned on historical information was performed using the software Winbugs (Spiegelhalter *et al*., 2000). This requires a prior distribution for the parameters and the likelihood function. Winbugs has a built-in likelihood function for uncensored and censored normal data that was used in these simulations.

Parameter estimation was made from updating with the prior distribution to compute the posterior distribution using Bayes' Theorem mathematically stated as:

$$p(\theta/D) = \frac{f(D/\theta)\varepsilon(\theta)}{\int f(D/\theta)\varepsilon(\theta)d\theta}$$

The stochastic parameters $\beta_0, \beta_1, \beta_2$ and τ are given proper prior distributions, while the logical expression for σ allows the standard deviation to be estimated.

To check the convergence of MCMC simulations, multiple chains with divergent starting points were run using derivative-free adaptive rejection sampling algorithm. Figure 7. 12 shows the trace plots for different parameters. The overlapping of the chains is an indication that reasonable convergence has been achieved after 11000 iterations. To obtain samples for posterior inference, Monte Carlo error was calculated for each parameter. A total of additional 10000 simulations were required to obtain Monte Carlo error less than 5% of the sample standard deviation for all parameters.

Table 7. 3 shows the posterior summaries of the parameters of the regression coefficients and the variance of the regression model. The posterior means and medians of the coefficients of PERMX and SWI indicated that they are important variables. Moreover, it was observed that the posterior means of β are slightly different from the ordinary least square estimates $[2.152, 52.58, -17.31]^T$ concluding that our prior was essentially a little bit informative implementing minor on the model parameters.
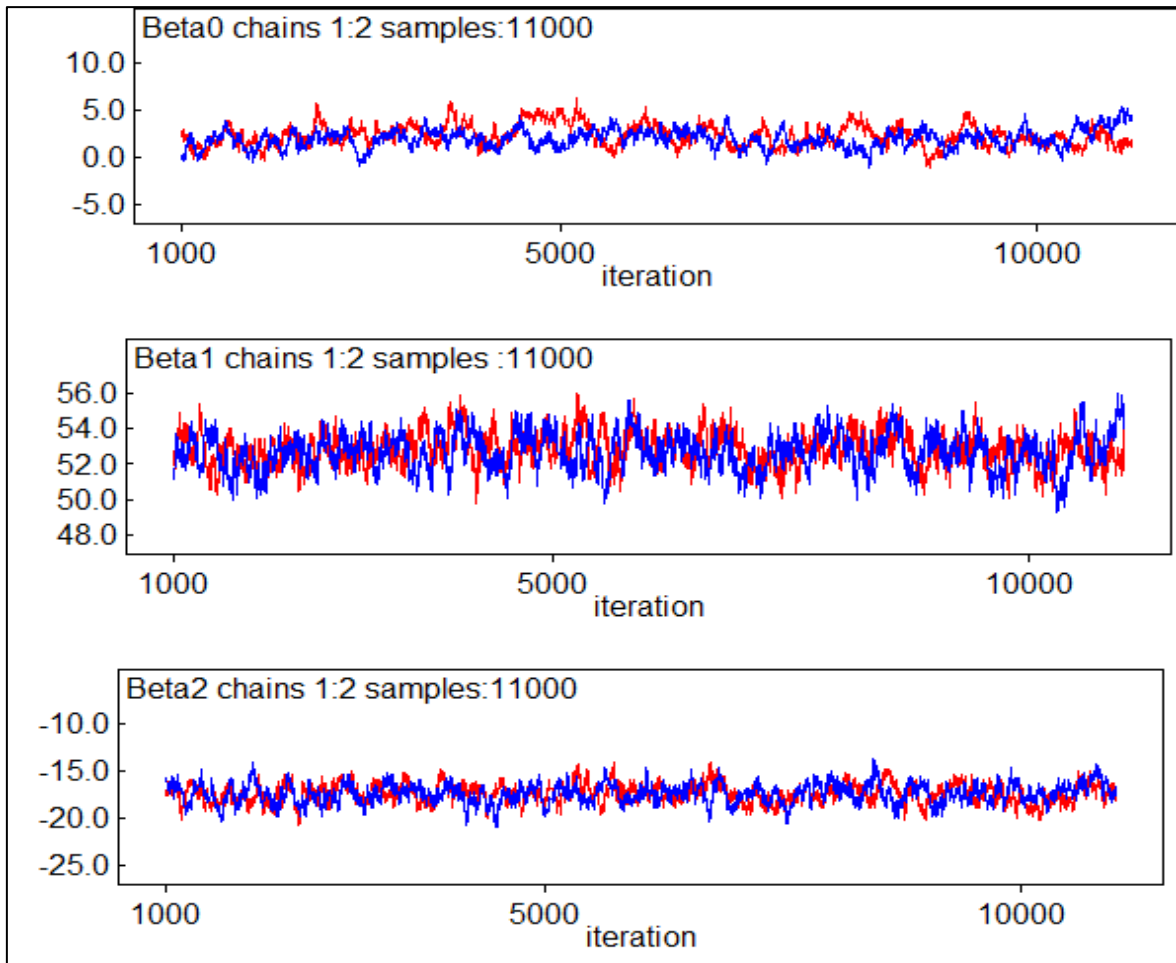
Figure 7. 12: History plots showing two chains that are overlapped, an indication of convergence

Table 7. 3: Posterior summaries of the indicator parameters included in the Bayesian model

node	mean	sd	MC error	2.5%	10%	50%	90%	97.5%	start	sample
beta0	2.152	1.020	0.0649	0.156	0.8411	2.164	3.43	4.098	12001	16000
beta1	52.580	1.041	0.0605	50.470	51.21	52.61	53.89	54.51	12001	16000
beta2	-17.310	0.993	0.0552	-19.36	-18.58	-17.29	-16.06	-15.4	12001	16000

Figure 7. **13** displays the posterior kernel density plots for model parameters βi. The posterior distributions of the coefficients are normal for all the variables. The posterior

median of the distribution and the posterior mean justify inclusion of the variables in the model.
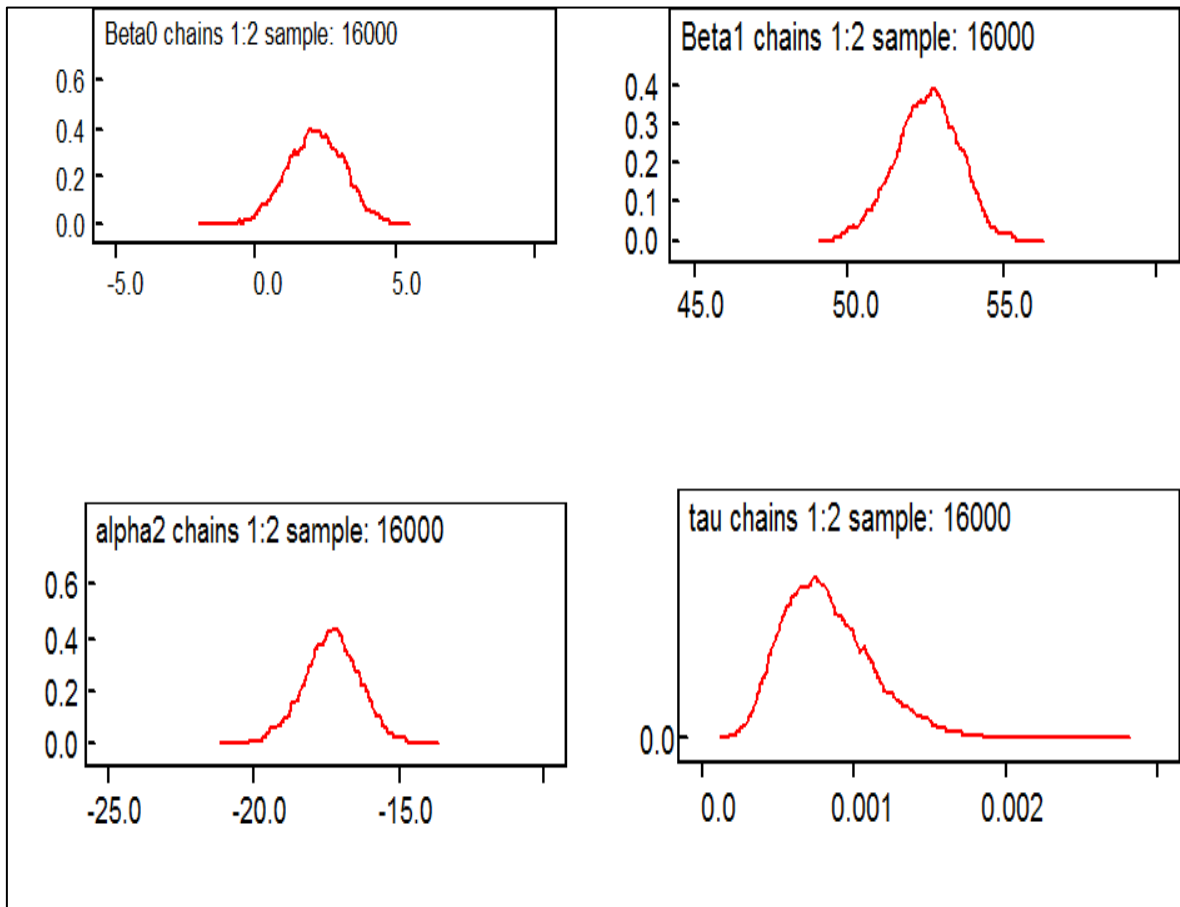
Figure 7. 13: Posterior densities of the regression coefficients

Figure 7. 14 shows the comparison of forecast uncertainty using ordinary and Markov Chain Monte Carlo simulations. The high uncertainty in the extreme forecast distributions (P10 – P90) associated with OMCS can be attributed to the assumption of parameter independency on the forecast. When parameters are not independent (iid) the MCMC procedure offers a flexible environment for fitting a multilevel Bayesian models. The procedure evaluates models, uses a self-tuning random walk Metropolis algorithm and generates samples from the target posterior distributions. It produced posterior estimates

and convergence diagnostics. The parameter obtained using MCMC procedures are:
P2.5%, P10%, P50% P97.5% and P90%.
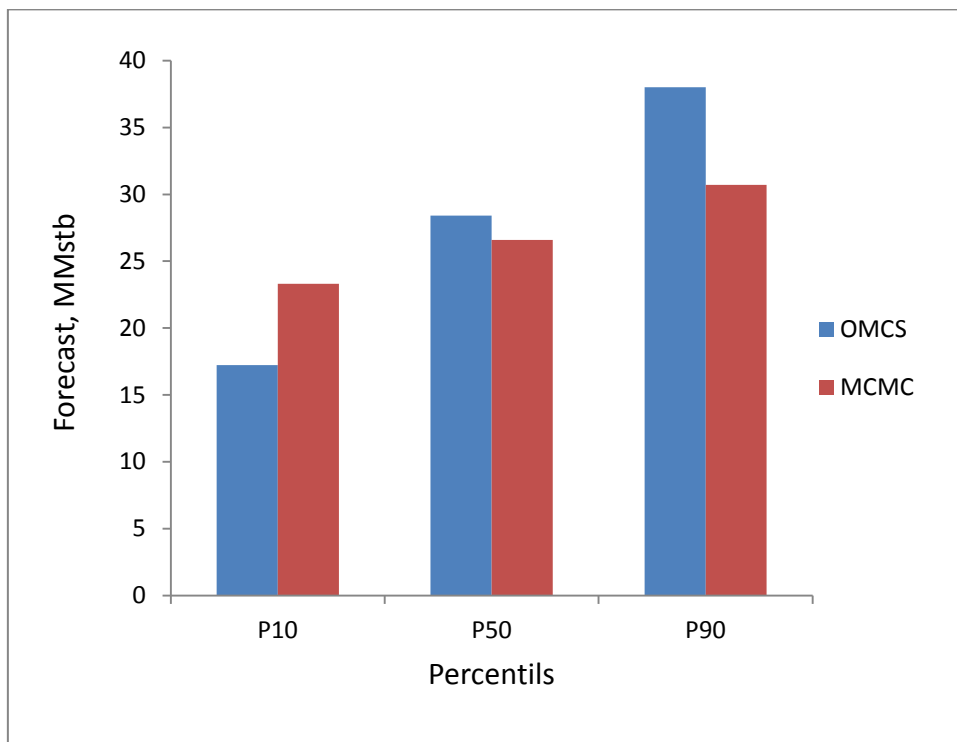
Figure 7. 14: Histogram showing comparison of forecast distribution using ordinary and Markov Chain Monte Carlo simulations.

Chapter 8

8. Contribution to Knowledge

8.1 Major contributions

This research has contributed in the following ways:

1. An integrated approach combining use of site characterization, experiment design, Monte Carlo simulation and oil/gas transport modeling is developed to address the model and parameter uncertainties. The integrated framework presented can be followed as a strategic procedure for assessing reservoir uncertainty.

2. Comparative study and what if analysis on implementation of different experimental designs and responses surface algorithms used for variable screening and response surface construction was presented. This is of high interests for practitioners involved in predicting production curves or water cut and has potential benefit for the community.

3. A simple framework for infill well placement and optimization is presented. The method is simple, easy, straight forward and reproducible in other fields for assessment of infill opportunity involving infill location, selection and placement.

4. Mathematical foundation that shows the differences and implications for wanton use of Monte Carlo approximations for uncertainty quantification is presented with example.

8.2 Published research articles

1. **Arinkoola, A.O** and Ogbe, D.O (2015): "Examination of experimental designs and response surface methods for uncertainty analysis of production forecast: A Niger Delta case study", *Journal of Petroleum Engineering*, Vol. 2015, ID 714541, http://dx.doi.org/10.1155/2015/714541.

2. **Arinkoola, A.O**., Haruna, M.O. and Ogbe, D.O (2015): "Quantifying uncertainty in infill well placement using numerical simulation and experimental design: case study", *Journal of petroleum exploration and production technology*, ISSN 2190-0558, DOI 10.1007/s13202-015-0180-z, http://paperity.org/p/73385638.

3. **Arinkoola, A.O**., Aladeitan, M.Y and Ogbe, D.O (2015): "Integration of structural uncertainty and experimental design for uncertainty quantification", *Journal of Petroleum and Gas Engineering*, Vol. 6 (7), pp. 74-89, DOI: 10.5897/JPGE2014.0209. http://www.academicjournals.org/JPGE

4. **Arinkoola, A.O**., Duru, U.I. and Onuh, H.M (2015): "Development of proxy model for production forecast using adaptive neuro-fuzzy inference system and experimental design", *Int. J. Petroleum Engineering*, Vol. 1, No. 3, pp.189-220.

http://www.inderscienceonline.com/doi/pdf/10.1504/IJPE.2015.071062

Chapter 9

9. Conclusion

This study addressed the issue of uncertainty identification, uncertainty quantification, infill optimization and selection of appropriate experimental design methods for building reservoir proxy model for reservoir management. These are problems areas being confronted in many oil fields management and are important elements to consider in planning the development of new concept for efficient recovery. In this research we built 3 stochastic models using structural map uncertainty. Majorly, well log data was used following developed geological framework for properties distribution. We examined various DoE methods, compared them and highlighted the implications of their arbitrary usage for practical applications. We presented mathematical foundations for Monte Carlo simulations and identified the implications of underlying assumptions in decision making. In line with the set objectives, the summary of the derivatives of this study is provided as follows:

9.1 Conclusions

1. Structural map uncertainty was successfully used as a basis for generating stochastic models for uncertainty forecast of the volumes of hydrocarbons in place in a case study of Niger Delta marginal field. A geological concept formulated proved adequate and allows for multiple property integration. The approach adopted saves considerable time, permits

handling of relatively small static realizations, reproducible and very useful when only limited data are available.

2. Optimization of infill location, selection and placement was successfully carried out using numerical simulation of a full field study. Recoveries were evaluated in 4 different fault blocks (A, B, C and D) and set of only vertical wells, only horizontal wells and combination of vertical and horizontal wells were drilled. The number and type of infill wells, horizontal well length, perforation intervals and inter-well spacing were considered as uncertainty parameters. Two horizontal wells of 1000 meters lateral length each was recommended for drilling and evaluation in the reservoir fault blocks B and D. The methodology is useful as a practical guide where project delivery time is a serious issue of concerns.

3. For uncertainty analysis, this study successfully examined three screening designs (Placket-Burman, fractional factorial, and one variable at-a-time) and four response surface methodologies (Box-Behnken, central composite, D-optimal, and full factorial) commonly used for uncertainty analysis. In all screening methods, years of production forecast played important role on associated number of "heavy-hitters." Relative variation method (one variable at-a-time) was identified with largest number of parameters and hence not economical in application due to the attendant large number of simulation runs. Unlike Placket-Burman, a low resolution fractional factorial in addition to main effects, considered significance of factor interactions, required more simulation runs, but can prevent exclusion of some factors with minimal main effect but significant interaction

effect. Nevertheless, the analysis performed in this study shows that there was no added advantage using fractional factorial in lieu of Placket-Burman for screening.

It was agreed that, the selection of "best" model for uncertainty quantification must be based on the reservoir management objectives. Box-Behnken method was adequate to determine P10/P50/P90 and associated models within the analysis domain. On the other hand, for future development strategies evaluation such as EOR, stimulation, and the needs for acquiring additional information, full factorial and central composite designs are more efficient predictors within acceptable margin of error. However, where full factorial 3-level design is not practicable (when uncertainty number greater than 4), a 2-level factorial or high resolution fractional factorial method was discovered to be adequate for the construction of response surfaces for uncertainty quantification.

4. Response surface models developed using classical experimental designs in (3) above are uneconomical and time consuming. The use of uniform design of experiment (UDoE) and associated polynomial averaging method was found to be more advantageous in terms of cost and time. Apart from accuracy, experimenter can decide on the number of simulations based on available time and resources. The ANFIS-based model fitting technique requires fewer parameters when compare with RSM based proxy-models and is more accurate especially if there is occurrence of non-linearity between the dependent and independent variables.

5. The application of Ordinary Monte Carlo analysis around a history match is not valid since parameters are not independent and identically distributed. A full Bayesian treatment is required, rather than a simple Monte Carlo approach.

Chapter 10

10. Future Works

10.1 Suggestions for Future Work

Several areas of applications of experimental design, response surface methodologies, Fuzzy logic and optimal control theory are suggested as potential areas for future research.

1. Application of the experimental design/response surface methodology for history matching and prediction of multi-response reservoir performance. It would be interesting to see if a response surface can predict many flow responses accurately.

2. RSM-based proxy models are purely statistical and have no consideration of the physics underlying the process, a proxy that can be calibrated and one that honors physics would be very useful for the purpose of optimization of petroleum reservoirs. For risk analysis, a method that integrates history matching and risk workflow is desirable.

3. The use of experimental design to investigate well interference and optimum number of wells within the reservoir.

4. Investigate adaptive control theory, Fuzzy logic and optimal control methodologies for history matching, uncertainty analysis and well placement optimization

5. Reservoir performance predictions and forecast using knowledge discovery in databases (KDD). This will involve taking the advantages of the advancements in hardware and software to analyze large amounts of production data using data science techniques.

6. Investigate the economic impact of decisions obtained from short-term production optimizations on long-term oil recovery.

Nomenclature

ANFIS	Adaptive Neuro-Fuzzy Inference System
M	Thousand
MM	Million
STB	Stock-Tank-Barrel
MULTFLT	Fault transmissibility multiplier
PV	Pore Volume
FVF	Oil Formation Volume Factor
F	Field
WCT	Water cut
OPT	Total oil production
WPT	Total water production
GOR	Gas-oil ratio
PERMX	Horizontal permeability
PERMZ	Vertical permeability
WBT	Water breakthrough time
SWI	Initial water saturation
PORO	Porosity
OVISC	Oil viscosity
P10	10 Ppercentile
P50	50 percentile
P90	90 percentile
mD	Millidarcy
PV	Pore volume
STOIIP	Stock tank oil initial in place

Symbol

β	formation volume factor
σ^2	variance
ϵ	subset
$\gamma\ (\ )$	variogram function
λ	kriging weight
φ	porosity
σ	standard deviation
$C\ (\ )$	covariance function
J	productivity index

Subscripts

a	aquifer
r	reservoir
t	total
min	minimum
max	maximum
i	coordinate, initial
j	coordinate
E	error
o, w, g	Oil, water, gas
c	criticalwater

Superscripts

D	dimension
T	transpose

Bibliography

Adams, S. J. (2005): "Quantifying Petrophysical Uncertainties" SPE 93125 paper

    presented at   the Asia Pacific Oil & Gas Conference and Exhibition held in Jakarta, Indonesia, 5 – 7 April

Ahmed, T. and Mckinney, D.P. (2005): Advanced Reservoir Engineering, 1st Edition,

    Elsevier, Gulf Professional Publishing, New York

Aigbodion, V.S., Hassan, S. B, Dauda, E. T and Mohammed, R. A (2010): The

    Development of Mathematical Model for the Prediction of Ageing Behavior for Al-Cu-Mg/Bagasse   Particulate Composite. J. of Minerals & Materials Characteristics &Engineering, (9):   907-917

Al-Shamma, B.R. and Teigland, R., (2006): History Matching of The Valhall Field Using a

    Global Optimization Method and Uncertainty Assessment, SPE 100946, presented

    at SPE Annual Technical Conference and Exhibition (Sept., 2006).

Alabert, F., (1987): The Practice of Fast Conditional Simulation Through the LU

    Decomposition of the Covariance Matrix; Math Geology, Vol. 19, No. 5, pp. 369-386, 1987

Alhuthali, A.H., Oyerinde, D. and Datta-Gupta, A., (2006): Optimal Waterflood

    Management Using Rate Control, SPE 102478, presented at SPE Annual Technical Conference and Exhibition (Sept., 2006).

Allen, T. T., Bernshteyn, M.A., and Kabiri- Bamoradian, K. (2003): Constructing

    metamodels   for computer experiments. Journal of Quality Technology, 35:264-274

Almeida Netto, Schiozer D.J., Ligero, E.L., Maschio, C. (2003): History matching Using
Uncertainty Analysis. SPE International Conference, Society of Petroleum
Engineers.   Calgary, Alberta, Canada

Amudo C., Graf T., Haris N.R., Dandecar R., Ben Amor F. and May R.S (2008): ''
Experimental Design and Response Surface Models as a Basis for Stochastic
History Match- A Niger   Delta   Experience'' IPTC 12665 presented at the
2008 International Petroleum Technology Conference, Kuala Lumpa, Malaysia,
Dec. 3-5

Apaydin, O.G., Iwere, F.O., Luneau, B., and Ma, Y (2005): "Critical Parameters in Static
and   Dynamic Modeling of Tight Fluvial Sandstones," SPE 95910 presented at
the SPE   Annual Technical Conference and Exhibition, Dallas, Texas, USA,
9-12 October,

2005

Artem ratchkovski, david O. Ogbe and Akanni S. Lawal (1999):''Application of
Geostatistics and   Conventional Methods to Derive Hydaulic Flow Units for
Improved Reservoir   description: A Case of Edicott Field, Alaska,'' paper SPE
54587 presented at 1999 SPE   Western Regional Meeting, Anchorage,
Alaska, May 26-23

Ates, H., Bahar, A., El-Abd, S., Charfeddine, M., Kelkar, M. and Datta- Gupta, A (2005):
Ranking and Upscaling of Geostatistical Reservoir Models by Use of Streamline
Simulation: A field Case Study, paper SPE 81497, SPE Reservoir Evaluation and
Engineering, Feb., 2005.

Azuka, C. A, Ali, S. S, and Tara La Force (2009): Uncertainty Evaluation in Field

Development and Export Planning. Paper SPE 121993 presented at the SPE EUROPEC/EAGE Annual   conference and exhibition held at Amsterdam, The Netherlands, 8-11 June, 2009

Ballin, P.R., Aziz, K., Journel, A.G (1993): "Quantifying the Impact of Geological Uncertainty   on Reservoir Performing Forecasts," paper SPE 25238 presented at the 12th SPE   Symposium on Reservoir Simulation, New Orleans, USA, 28 Feb – 3 March 1993.

Ballin, P.R., Clifford, P.J. and Christie, M.A., Cupiagua (2001): A Complex Full-Field Fractured   Reservoir Study Using Compositional Upscaling, paper SPE 66376, presented at SPE   Reservoir Simulation Symposium, Houston, Feb., 2001.

Bi Z, Oliver D S and Reynolds A C (2000): Conditioning 3D Stochastic Channels to Pressure Data. SPE Jounal 5 474 484

Box, G.E.P., Hunter, W. G., and Hunter, J.S. (2005): Statistics for experimenters: Design, Innovation, and Discovery, 2nd Edition, John Wiley & Sons, New York

Bustamante, D.S., Keller, D.R. and Monson, G.D. (2005): Understanding Reservoir Performance and Uncertainty using a Multiple History Matching Process, paper SPE 95401, presented   at Annual Technical Conference and Exhibition (Oct., 2005).

Carlson, M.R.: Practical Reservoir Simulation, PennWell, Tulsa, (2003): Chambers, R.L., Yarus, J.M. and Hird, K.B. (2000): "Petroleum Geostatistics for Nongeostatisticians – Part 1," The   Leading Edge (May 2000) 474-479.

Castellini, A., Yeten, B., Singh, U., Vahedi, A., Sawiris, R (2006): "History Matching and Uncertainty Quantification Assisted by Global Optimization Techniques," 10th

European   Conference on the Mathematics of Oil Recovery — Amsterdam, The Netherlands 4 – 7   September 2006

Castellini, A., Chawathe, A., Larue, D., Landa, J.L., Jian, F.X., and Toldi, J.L (2003):

"What is Relevant to Flow? A Comparative Study Using a Shallow Marine

Reservoir," SPE 79669   presented   at   the   SPE   Reservoir   Simulation Symposium, Houston, Texas, USA, 3-5   February, 2003

Chavent G, Dupuy M and Lemonnier P (1975): History matching by use of optimal theory,

SPE   4627, SPE Journal, 15(1) 74–86

Coates, G. R and Dumanoir, J. L (1974): "A New Approach To Improved Log – Derived Permeability.": The Log Analyst, Pp17. (January-February 1974).

Coates, G. R And Denoo, S. (1981): "The Producibility Answer Product" The Technical

Review,   Schlumberger Hauston (June 1981) 29 No. 2 P55-63

Corre, B., Thore, deFeraudy, V., Vincent, G. (2000): "Integrated Uncertainty Assessment

for   Project Evaluation and Risk Analysis," paper SPE 65205, presented at SPE European   Petroleum Conference, Paris, France, 24-25 Oct 2000.

Cotento, F.M, Godi A, Nicota G, and Pizzo A; " A Risk Analysis Approach: From

Subsurface to Siurface" IPTC 10493 presented at the International Petroleum Technology Conference,   Doha, Qatar, 21-23 November, 2005

Cullick, A. S., Johnson D., and Shi G., (2006):"Improved and More-Rapid History

Matching with a Nonlinear Proxy and Global Optimization". Paper SPE 101993 presented at the   SPE Annual Technical Conference and Exhibition, San Antonio, Texas, 24-27 Sept

Da Cruz, P.S., Horne, R.N., Deutsch, C.V. (2004): "The Quality Map: A Tool for

Reservoir Uncertainty Quantification and Decision Making," SPEREE (Feb 2004), 6

Dake, L.P. (1978): Fundamentals of Reservoir Engineering, Elsevier Scientific Publishing Company, Amsterdam (1978).

David O. Ogbe, Fabian O. Iwere, Ernie Gomez and Ekeng Henshaw (2009): "Conceptual

Model for Fast Tracking Decision Making in the Reservoir Management" SPE 121392 Paper presented at the SPE Western Regional Meeting held in San Jose, Califonia, USA, 24- 26 Mach

Dejean, J.P. and Blanc, G. (1999): "Managing Uncertainties on Production Predictions

Using Integrated Statistical Methods," paper SPE 56696 presented at the 1999 SPE Annual Technical Conference and Exhibition, Houston, 3–6 October.

De Waal, J. A. Smits, R.M.M, de Graaf, J.D, Schipper, B. A. (1991): Measurement and Evaluation of Resistivity- index Curves. The Log Analyst, September- October

1991, Pp583-595

Deutsch C. V, Srinivasan S. and Mo Y (1996): "Geostatistical Reservoir Modeling

Accounting for Precision and Scale of Seismic Data" Paper SPE 36497 presented at the 1996 SPE Annual Technical Conference and Exhibition held in Denver, Colorado, U S A, 6-9 October 1996.

Dong Y and Oliver D S (2005): Quantitative Use of time-lapse Seismic Data for Reservoir Description, SPE 84571, SPEJ, 10 91-99.

Dong Y and Oliver D S (2008): Reservoir Simulation Model Updates via Automatic

History Matching With Integration of Seismic Impedance Change and Production Data, SPE 12550, International Petroleum Technology Conference, Kuala Lumpur, Malaysia, December 3-5

Dunlop, K.N.B., Vossepoel, F.C., Xu, R., Sarma, P., Alhutali, A.H., Reynolds, A.C.

(2010): Results of   the Brugge benchmark study for flooding optimization and
history matching. SPE Reserv. Evalu. Eng. 13(3), 391–405 (2010)

Durlofsky, L.J. (2003): Upscaling of Geocellular Models for Reservoir Simulation: A

Review of Recent Progress, paper presented at 7th International Forum on
Reservoir Simulation,   Germany (June 2003).

Dykstra, H. and Parsons, R. L. (1950): "The Prediction of Oil Recovery in Waterflood."
Seconday Recovey of Oil in the United States, 2nd ed. American Petroleum

Institute (API), 1950, pp. 160-174.

Egbogah, E. O. (1994): "EOR Target Oil and Techniques of its Estimation," J. Petr. Sc.

and Eng., 10 (334)

Ekwere Peters (210): Advanced Petrophysics, African University of Science and

Technology,   Abuja, Course material for PE223, 2010

Eiben, A.E., Smith, J.E. (2003): "Introduction to Evolutionary Computing," Springer,

Berlin (2003)

Evensen G (2003): The Ensemble Kalman Filer: theoretical formulation and practical
implementation, Ocean Dynamics, 53 343–367.

Evensen, G. (2007): "Data Assimilation, The Ensemble Kalman Filter," Springer, Berlin

 (2007)

Evensen, G., Hove, J., Meisingset, H.C., Reiso, E., Seim, K.S., Espelid, O (2007): "Using

the   EnKF for Assisted History Matching of a North Sea Reservoir Model,"
paper 106184 presented at the 2007 Reservoir Simulation Symposium, The
Woodlands, USA, 2007

Fasanino G, Molinard J E, de Marsily G and Pelcé V (1986): Inverse Modeling in Gas
   Reservoirs, SPE 15592, 61st SPE Annual Technical Conference and Exhibition,
   New   Orleans, Texas, October 5-8.

Fatemeh Moeinikia and Nassar Alizadeh (2012): Experimental Design in Reservoir
    Simulation: An Integrated Solution for Uncertainty analysis, a case study. J.
   Petrol. Explor. Prod.   Technol., 2, 75-85

Femi V. Akinwumi, Elias C. Arochukwu, and Abiola S. Abdul-Kareem," Managing
   Uncertainties in Hydrocarbon-in-place Volumes in a Northern Depobelt Field,
Niger   Delta, Nigeri"a . SPE 88880 Paper presented at the 28th Annual SPE International
   Technical Conference and Exhibition in Abuja, Nigeria, August 2-4, 2004.

Friedmann, F. Chawathe, A. Larue D.K (2003): Assessing Uncertainty in Channelized
   Reservoirs Using Experimental Designs; SPE 85117, SPE Reservoir Evaluation &
   Engineering August 2003

Fuller, S.M., Sarem, A.M., and Gould, T.L (1992): Screening Waterfloods for Infill
   Drilling Opportunities, paper SPE 22333 presented at the SPE International
   Meeting on Petroleum   Engineering held in Beijing, China, 24-27 March,
   1992.

Gen, M., Cheng, R. (2000): "Genetic Algorithms & Engineering Optimization," John
   Wiley & Sons, Inc., New York (2000)

Gilks, W.R., Richardson, S. and D.J. Spiegelhalter. (1996). Markov chain Monte Carlo
   Methods in practice, Chapman & Hall

Gu Y, Oliver D S (2004): History Matching of the PUNQ-S3 Reservoir Model Using the
   Ensemble Kalman Filter, SPE 89942, SPE Annual Technical Conference and
    Exhibition,   Houston, USA, September 26-29.

Guohua G, Gaoming L and Reynolds A C (2004): A stochastic optimization algorithm for automatic history matching, SPE 90065, SPE Annual Technical Conference and Exhibition, Houston, Texas, September 26-29.

Hook, J. R (1983): The Precision of Core Analysis Data and Some Implications for Reservoir   Evaluation. SPWLA Twenty- Fourth Annual Logging Symposium June 27-30, 1983.   Paper Y.

Hudson, J.W., Jochen, J.E., and Jochen, V.A (2000): Practical Technique to Identify Infill Potential in Low- permeability Gas Reservoirs Applied to the Milk River

Formation in   Canada, paper SPE 59779 presented at the 2000 SPE/CERI Gas Symposium, Calgary, 3-   5 April.

Hui, M., Zhou, D., Wen, X. and Durlofsky, L.J (2004): Development and Application of a

New   Technique for Upscaling Miscible Processes, paper SPE 89435, presented at SPE/DOE   Symposium on Improved Oil Recovery, Tulsa (April 2004).

Idrobo, E.A., Choudhary, M., and Datta-Gupta, A (2000): "Swept Volume Calculations

and   Ranking of Geostatistical Reservoir Models Using Streamline Simulation," paper SPE   62557 presented at the 2000 SPE/AAPG Western Regional Meeting, Long Beach,   California, 19–23 June.

Jacquard P and Jain C (1965): Permeability distribution from field pressure data, Soc. Pet.

Eng.   Journal, 281-294.

Jafarpour B., and McLaughlin D.B. (2007): History matching with an Ensemble Kalman

filter   and discreate cosine parameterization. paper SPE 108761 presented at SPE Annual   Technical Conference and Exhibition, Anaheim, USA, 11-14 November.

Journel, A.G. and Alabert, F (1990): New Method for Reservoir Mapping; Journal of

Petroleum Technology, pp. 212-218, February 1990. June.doi: 10.2118/113498-MS

Kalla, S. and White, C. D. (2007): Efficient Design of Reservoir Simulation Studies for Development and Optimization, SPE-95456-PA, Res Eval & Eng 10 (6); 629-637.

Doi: 10.2118/95456-PA

Kelkar, M, Godofredo, P (2002): "Applied Geostatistics for Reservoir Characterization," published by SPE, 2002.

G. Kuczera & E. Parent (1998). Monte Carlo assessment of parameter inference in

Catchments models: The Metropolis algorithm. Journal of Hydrology, 211, pp.69 –

85

Lambers, J. and Gerritsen, M (2005): An Integration of Multilevel Local-Global Upscaling

with Grid Adaptivity, paper SPE 97250, presented at SPE Annual Technical Conference and Exhibition, Dallas (Oct. 2005).

Lamy, P., Swaby, P.A., Rowbotham, P.S., Dubrule, O. and Haas, A. (1998): From Seismic

to Reservoir Properties with Geostatistical Inversion, SPE 57476, Annual Technical Conference and Exhibition (1998)

Li R, Reynolds A C and Oliver D S (2003): History matching of three-phase flow

production data, SPE Journal, 8(4) 328–340, 2003.

Li, Y. and Johns, R.T (2005): Rapid Flash Calculations for Compositional Modeling, SPE 95732, Annual Technical Conference and Exhibition (Oct., 2005).

Little, A.J., Jutila, H.A., Fincham, A (2006): "History Matching With Production

Uncertainties Eases Transition Into Prediction," paper SPE100206 accepted for publication at the SPE Europec/EAGE Annual Conference and Exhibition held in Vienna, Austria, 12-15 June 2006

Linhua Guan, Yuqi Du, Zhiming Wang (2005): Infill Drilling-lessons Learnt In the Past 20 Years, 18th World Petroleum Congress, September 25 - 29, 2005, Johannesburg, South Africa Copyrigh t2005. World Petroleum Congress

Manceau, E., Mezghani, M., Mezghani, I. Z., Rogero, F (2001):"Combination of Experimental Design and Joint Modeling Methods for Quantifying the Risk Associated with   Deterministic and Stochastic Uncertainties – An Integrated Test Study; SPE 71620. SPE Annual Technical Conference and Exhibition, New Orleans, Louisiana, 30 September – 3   October 2001.

Mattax C. C. and Dalton R L (1991): Reservoir simulation, SPE 20399, Journal of Petroleum Technology, 42 692-695.

Mclennan, J and Deutsch, C (2005): Ranking Geostatistical Realizations by Measures of Connectivity; Society of Petroleum Engineers (SPE), Paper 98168, 2005.

Meisingset, K.K. (1999): "Uncertainties in Reservoir Fluid Description for Reservoir Modeling,"   SPEREE Oct 1999, 2 (5).

Mohaghegh, S.D., Hafez Hafez, Razi Gaskari and Masoud Haajizadeh (2006): Uncertainty Analysis of a giant Oil Field in the Middle East Using Surrogate Reservoir Model, SPE 101474, presented at SPE International Petroleum Exhibition and (Nov., 2006)

Mohaghegh, S (2000): Virtual-Intelligence Applications in Petroleum Engineering: Part 1—Artificial Neural Networks. Journal of Petroleum Technology [S.I.], v. 52, n. 9, p. 8, September

Montgomery, Douglas C (2005): Design and Analysis of Experiments: Response surface method and designs. New Jersey: John Wiley and Sons, Inc.

Morris, M.D. (2000): Three techno metrics experimental design classics. Techno metrics, 42(1): 26-27

Mu'azu. K., Mohammed-Dabo, I.A and Waziri, S.M (2012): "Development of Mathematical Model for the Prediction of Essential Oil Extraction from Eucalyptus Citriodora Leave" J. Basic. Appl. Sci. Res., 2(3)2298-2306

Ogbalor Cyril and Anthony Peacock (2010): "Using Experimental Design with Reservoir simulation to Manage Subsurface Uncertainties-A Niger Delta Case Study," paper SPE 140613 presented at the 34th Annual SPE international Conference and Exhibition,   Tinapa-Calabar, Nigeria, July 31-August 7, 2010

Ofoh, E.P (1992): Geological Heterogeneity in the Niger Delta: A Case for Additional Recovery   through a Combined Effort of Geologically Targeted infill Drilling, Stimulation, and   Gas-Lift Installation, paper SPE 24745 presented at the 67th, 1992

Olatunji, S.O, Selamat, A., Abdul Raheem, A. and Omatu, S (2011): "Modeling the Correlations   of Crude Oil Properties based on Sensitivity Based Linear Learning Method".   Engineering Applications of Artificial Intelligence, 24: 686-696

Olea, R.A (1991): "Geostatistical Glossary and Multilingual Dictionary," Oxford University Press, 1991.

Oliver D S, Chen Yan (2010): Recent progress in history matching, a review, journal of ComputGeosci, © Springer Science+Business Media B.V.2010

Pathak R, Ogbe, D. O and Jensen,J. L. (2000): Application of Geostatistical and Fluid Flow Simulations to Evaluate Options for Well Placement. Paper SPE 62554 presented at the 2000 SPE/AAPG Western Regional Meeting held in Long Beach, California, 19–23 June 2000.

Peaceman, D.W (2003): A New Method for Calculating Well Indexes for Multiple

  Wellblocks   with Arbitrary Rates in Numerical Reservoir Simulation, SPE
  79687, SPE Reservoir Simulation Symposium (Feb., 2003).

Peak W.T., Abadah M. and Skander L.:"Uncertainty Assessment Using Experimental

  Design: Minagish Oolite Reservoir," paper SPE 91820 presented at the 2005
  SPE Reservoir   Simulation Symposium, Houston, Texas, Jan. 31-Feb. 2

Peng, C.H., & Gupta, R (2003): Experimental Design in Deterministic Modeling:

  Assessing   Significant Uncertainties; SPE 80537. SPE Asia Pacific Oil and Gas
  Conference, Jakarta,   Indonesia, 9-11 September 2003.

Peters, L., Arts, R.J., Brouwer, G.K., Geel, C.R., Cullick, S., Lorentzen, R.J., Chen, Y.,

  Dunlop,   K.N.B., Vossepoel, F.C., Xu, R., Sarma, P., Alhutali, A.H.,
  Reynolds, A.C. (2010):   Results of   the Brugge benchmark study for
  flooding optimization and history   matching. SPE   Reserv. Evalu. Eng. 13(3),
  391–405 (2010)

Phan, V. and Horne, R.N (1999): Determining Depth-Dependent Reservoir Properties

  using   Integrated Data Analysis, paper SPE 56423, presented at Annual Technical

  Conference   and Exhibition (Oct., 1999).

Ph. Theys (1997): "accuracy- Essential Information for a Log measurement" SPWLA 38th
  Annual Logging Symposium, June 15-18, 1997 Paper V

Risso, F.V.A, Risso, V.F, and Schiozer, D.J. (2007):" Risk Assessment of Oil Field Using

  Proxy Models: A Caser Study" paper 2007-138 presented at the Petroleum
  Society's 8th Canadian International Petroleum Conference, Calgary, Alberta,
  Canada, June 12-14

Roger Jang, J. S. (1993): ''ANFIS: Adaptive-Network-Based Fuzzy Inference System''
Transactions on Systems, Man, and Cybernetics, Vol. 23, No. 3, pp665-685, 1993

Roggero, F., Hu, L.Y (1998): "Gradual Deformation of Continuous Geostatisticals Model
for   History Matching," paper SPE 49004 presented at the SPE 1998 Annual
Technical   Conference and Exhibition, New Orleans, USA.

Ruijian L, Reynolds A C, Oliver D S (2003): History Matching of Three-Phase Flow
Production   Data, SPE 87336, SPE Journal, 4 328-340.

Sablok, R. and Aziz, K (2005): Upscaling and Discretization Errors in Reservoir
Simulation,   paper SPE 93372, presented at SPE Reservoir Simulation
Symposium, Houston (Feb.   2005).

Salam, K.K, Araromi, D.O, Ikiensikimama, S.S. (2011): "Neuro-Fuzzy Modeling for the
Prediction of below-Bubble-Point Viscosity. Petroleum Science and Technology.
2011;29(17):1741-1752.

Sandsdalen, L., Barbieri, M., Tyler, K., and Aasen, J.O (1996) : "Applied Uncertainty
Analysis   Using Stochastic Modeling ", paper SPE 35533 presented at the
European 3-D Reservoir   Modeling Conference, Stavanger (norway), 16-17
April 1996.

Sampaio, T. P, Ferreira Filho, V. J. M, de Sa Neto, A. (2009): SPE 122148 presented at
The 2009 SPE Latin American and Caribbean Petroleum Engineering Conference
held in Cartagena, Colombia, 31May–3 June.

Schaaf, T., Coureaud, B., and Labat, N. (2008): Using Experimental Designs, Assisted
History   Matching Tools and Bayesian Framework to get Probabilistic
Production Production   Forecast. Paper SPE 113498 presented at the
Europe/EAGE Conference and Exhibition,   Rome, 9-12

Schiozer, D J, Sousa S H G (1997): Use of External Parallelization to Improve History

   Matching,   SPE 39062, Latin American and Caribbean Petroleum Engineering
   Conference, 1997,   Rio de Janeiro, Brazil, August 30 - September 3

Schiozer, D.J., Ligero, E.L., Suslick, S.B.;Costa, A.P.A., Santos, J.A.M.(2004): Use of

   Representative Models in the Integration of Risk Analysis and Production Strategy
   Definition, JPSE, n1- 2, v.44, pp.131-141, 2004

Schulze-Riegert, R., Haase, O., Nekrassov, A. (2003): "Combined Global and Local

   Optimization Techniques Applied to History Matching," paper SPE 79668 prepared

   for   presentation at the SPE Reservoir Simulation Symposium held in Houston,
   Texas, U.S.A., 3–5 February 2003

Schulze-Riegert, R., Krosche, M., Fahimuddin, A., Ghedan, S (2007): "Multi-Objective

   Optimization with Application to Model Validation and Uncertainty

   Quantification," paper SPE 105313 presented at the 15th SPE Middle East Oil &
   Gas Show and Conference, Kingdom of Bahrain, 11–14 March 2007.

Selberg, S., Schulze-Riegert, R., Stekolschikov, K (2007): "Event Targeting Model

    Calibration   Used for History Matching Large Simulation Cases," paper 106044
   was prepared for   presentation   at   the   2007   SPE   Reservoir   Simulation
   Symposium held in Houston, Texas, U.S.A., 26–28 February 2007

Smith, A. E M. and Roberts, G. O. (1993) Bayesian computation via the Gibbs sampler

   And related Markov chain Monte Carlo methods. J R. Statist. Soc. B, 55, 3-23.

Sprunt, E. S, Hensel, W. M., York, C. E, Honarpour, M. M (1988).: Compilation of

   Electrical   Resistivity Measurements Performed by Twenty- Five Laboratories.
   The Log Analyst,   January- February 1988, P.13-39

Steagall, D.E. and Schiozer, D.J (2001): Uncertainty Analysis in Reservoir Production

Forecasts   During Appraisal and Pilot Production Phases; paper SPE 66399
presented at the SPE   Reservoir   Simulation Symposium, Houston, TX, 11-14
February, 200

Stern, D (2005): "Practical Aspects of Scaleup of Simulation Models," SPE 89032, SPE

JPT (September, 2005)

Subbey, S., Christie, M. and Sambridge, M. (2003): A Strategy for Rapid Quantification of
Uncertainty in Reservoir Performance Prediction, paper SPE 79678, presented at

SPE   reservoir simulation symposium (Feb., 2003).

Thakur, G.C. and Satter, A. (1998): Integrated Waterflood Asset Management, PennWell,

1998.

Timur, A (1968): "An Integration Of Permeability, Porosity and Residual Saturation
Relationship For Sandstone Reservoirs".: The Log Analyst, Vol. 9 No. 4 Pp. 8 (
July-   August 1968).

Tyler, K., Sandsdalen, L., Maeland, J.O., Aasen, J.O., Siring, E., and Barbieri, M. (1996) :
"Integrated Stochastic Modeling in Reservoir Evaluation for Project Evaluation and

Risk   Assessment", paper SPE 36706 resented at the 1996 SPE Annual Technical
Conference   and Exhibition, Denver, 6-9 October

Vega, L., Rojas, D. and Datta-Gupta, A (2003): Scalability of the Deterministic and

Bayesian   Approaches to Production Data Integration into Field-Scale
Reservoir Models, paper SPE   79666, presented at SPE Reservoir Simulation
Symposium (Feb., 2003).

Vanegas, J.W, Cunha, J.C, and Cunha, L. B. (2006): "Uncertainty Assessment of

production   Performance for a Heavy Oil Offshore Field by using the
Experimental Design Technique", paper 2006-125 presented at the Petroleum

society's 7th Canadian International Petroleum Conference, Calgary, Alberta, Canada, June 13-15, 2006.

Verbruggen, R., Pannett, S., Stone, G. (2002): "Understanding Reserves Uncertainties in a Mature Field by Reservoir Modeling," paper SPE 77896, presented at the SPE Asia Pacific Oil and Gas Conference and Exhibition, Melbourne, Australia, 8-10 Oct 2002.

Vincent, G., Corre, B., Thore, P (1999): "Managing Structural Uncertainty in a Mature Field for Optimal Well Placement," SPEREE August 1999, 2(4).

Voneiff, G.W. and Cipolla, C. (1996): A New Approach to Large-Scale Infill Evaluations Applied to the Ozona (Canyon) Gas Field, paper SPE 35203 presented at the 1996 SPE Permian Oil and Gas Recovery Conference, Midland, Texas, 7-29 March.

Walstrom, J.E., Mueller, T.D., McFarlane, R. C. (1967): "Evaluating Uncertainty in Engineering Calculations," Journal of Petroleum Technology, Dec 1967, p 1595

Wen, X.H., Chen, W. (2005): "Real-Time Reservoir Model Updating Using Kalman Filter," paper 92991 presented at the 2005 Reservoir Simulation Symposium, The Woodlands, USA, 2005

Williams, G.J.J., Mansfield, M., MacDonald, D., Bush, M. D. (2004): "Top-Down Reservoir Modeling," paper SPE89974 presented at the ATCE 2004, Houston, Texas, 26-29. Sep. 2004

Yeten B., Castellini, A., Guyagular, B., and Chen, W. H. (2005): "A comparison Study on Experimental Design and Response Surface Methodologies". Paper SPE 93347 presented at the SPE Reservoir Simulation Symposium, Houston, Texas, USA, Jan. 31- Feb. 2

Zhang, D. (2002): Stochastic Methods for Flow in porous Media: Coping with Uncertainties.

San   Diego, California: Academic Press.

APPENDIX A

Correlations used for the Synthetic log Estimations

1. Volume of shale estimation

$$V_{sh} \; Steiber \; (1970) = \frac{GR \; Index}{1.5 - GR \; Index} \qquad\qquad A1$$

$$GR \; Index = \frac{[GR_{log} - GR_{min}]}{[GR_{max} - GR_{min}]} \qquad\qquad A2$$

2. Total and effective porosity estimation

Total porosity was obtained from the Formation Density (FDC) logs. A grain density of 2.65 *g/cc,* which is typical of the Niger Delta, and densities of 1.00 *g/cc* for water, 0.6 *g/cc* for oil and 0.20 *g/cc* for gas can be used.

$$PHIT = 0.67 * \frac{DT - DT_{max}}{DT} \qquad\qquad A3$$

$$PHIT = \frac{RHO_{matrix} - RHO_{log}}{RHO_{matrix} - RHO_{filtrate}} \qquad\qquad A4$$

$$PHIE = PHIT * (1 - V_{sh}) \qquad\qquad A5$$

3. Water saturation

Indonesian correlation for water saturation

This assumed m = 2, a = 1 and n = 2

$$S_w = \sqrt{\left(\frac{1}{R_t} - \frac{V_{sh}}{R_{sh}}\right) * \frac{R_w(1 - V_{sh})^2}{\emptyset^2}} \qquad A6$$

GR_{Index} = linear relationship between Gamma ray log and Volume of shale

GR_{min} = Gamma ray log reading in 100% clean zone in API unit

GR_{max} = Gamma ray log reading in 100% shale zone in API units

PHIT = Total porosity

DT_{ma} = interval travel transit time in matrix (sandstone) 55.5µft/s

DT = transit time log

RHOM = Density of matrix (2.60 - 2.65 g/cc)

RHOB = Bulk density (this is the density log)

RHOFL = Density of filtrate (1.0 – 1.1 g/cc)

APPENDIX B

Design Matrices of 3-Level Experimental Designs and ANOVA

B1 **Design Matrix for box-Behnken Design**

Run	A:PORO	B:PERMX	C:PERMZ	D:ISW	E:OVISC	FOPT (MMSTB)	Run	A:PORO	B:PERMX	C:PERMZ	D:ISW	E:OVISC	FOPT (MMSTB)
1	0	0	-1	-1	0	3.04E+07	24	-1	0	0	1	0	3.18E+07
2	1	0	0	-1	0	3.14E+07	25	-1	0	1	0	0	3.41E+07
3	0	0	-1	1	0	3.24E+07	26	-1	0	0	0	-1	3.49E+07
4	0	-1	-1	0	0	3.22E+07	27	1	0	0	0	-1	3.74E+07
5	0	0	0	1	-1	3.48E+07	28	-1	0	-1	0	0	3.27E+07
6	0	0	0	0	0	3.41E+07	29	0	1	0	0	1	3.39E+07
7	0	0	1	1	0	3.37E+07	30	0	-1	0	0	1	3.18E+07
8	-1	0	0	0	1	3.23E+07	31	0	-1	1	0	0	3.35E+07
9	-1	1	0	0	0	3.36E+07	32	0	1	0	1	0	3.33E+07
10	0	0	0	-1	1	2.99E+07	33	0	0	1	-1	0	3.14E+07
11	-1	0	0	-1	0	2.99E+07	34	0	-1	0	-1	0	2.94E+07
12	1	1	0	0	0	3.58E+07	35	0	0	1	0	-1	3.75E+07
13	0	0	0	1	1	3.20E+07	36	0	0	0	0	0	3.41E+07
14	1	0	-1	0	0	3.47E+07	37	0	0	-1	0	1	3.30E+07
15	0	-1	0	1	0	3.13E+07	38	0	0	0	-1	-1	3.24E+07
16	0	1	-1	0	0	3.44E+07	39	1	0	0	1	0	3.36E+07
17	0	0	0	0	0	3.41E+07	40	0	1	0	-1	0	3.12E+07
18	0	0	0	0	0	3.41E+07	41	0	0	1	0	1	3.43E+07
19	0	0	0	0	0	3.41E+07	42	0	1	0	0	-1	3.68E+07
20	1	0	1	0	0	3.63E+07	43	1	-1	0	0	0	3.34E+07
21	0	0	0	0	0	3.41E+07	44	-1	-1	0	0	0	3.17E+07
22	0	0	-1	0	-1	3.58E+07	45	0	1	1	0	0	3.58E+07
23	0	-1	0	0	-1	3.46E+07	46	1	0	0	0	1	3.43E+07

..

B2 Design Matrix for Central Composite Design

Run	A:PORO	B:PERMX	C:PERMZ	D:ISW	E:OVISC	FOPT (STB	Run	A:PORO	B:PERMX	C:PERMZ	D:ISW	E:OVISC	FOPT (STB
1	0	0	0	0	0	3.41E+07	17	0	0	0	-2	0	3.06E+07
2	0	0	0	0	2	3.33E+07	18	1	1	-1	1	-1	3.61E+07
3	-1	1	-1	-1	-1	3.19E+07	19	-1	1	1	-1	1	3.30E+07
4	-2	0	0	0	0	3.31E+07	20	0	0	0	0	0	3.41E+07
5	0	0	2	0	0	3.52E+07	21	1	-1	1	-1	1	3.01E+07
6	1	1	1	-1	-1	3.52E+07	22	-1	-1	1	-1	-1	3.11E+07
7	-1	-1	-1	1	-1	3.19E+07	23	0	0	0	0	0	3.41E+07
8	0	0	0	0	0	3.41E+07	24	-1	-1	1	1	1	3.05E+07
9	1	1	-1	-1	1	3.09E+07	25	0	0	0	0	0	3.41E+07
10	0	0	-2	0	0	3.38E+07	26	1	-1	-1	-1	-1	3.15E+07
11	1	1	1	1	1	3.43E+07	27	1	-1	-1	1	1	3.08E+07
12	0	-2	0	0	0	3.26E+07	28	2	0	0	0	0	3.51E+07
13	0	0	0	2	0	3.27E+07	29	0	0	0	0	-2	3.62E+07
14	0	2	0	0	0	3.47E+07	30	1	-1	1	1	-1	3.52E+07
15	-1	1	1	1	-1	3.52E+07	31	-1	1	-1	1	1	3.13E+07
16	0	0	0	0	0	3.41E+07	32	-1	-1	-1	-1	1	2.79E+07

B3 Design Matrix for Full Factorial Design

Run	A:PORO	B:PERMX	C:ISW	D:OVISC	FOPT (STB	Run	A:PORO	B:PERMX	C:ISW	D:OVISC	FOPT (STB
1	-1	0	0	-1	3.49E+07	45	-1	0	0	0	3.31E+07
2	-1	1	0	0	3.36E+07	46	0	1	1	1	3.25E+07
3	1	1	0	1	3.49E+07	47	-1	-1	-1	0	2.87E+07
4	1	-1	0	0	3.34E+07	48	-1	-1	0	0	3.17E+07
5	1	0	0	1	3.43E+07	49	0	-1	0	-1	3.46E+07
6	-1	0	0	1	3.23E+07	50	-1	0	1	-1	3.36E+07
7	0	0	0	0	3.41E+07	51	0	-1	1	1	3.04E+07
8	-1	-1	1	0	3.05E+07	52	0	1	1	0	3.33E+07
9	-1	1	-1	1	2.97E+07	53	0	0	0	0	3.41E+07
10	-1	1	0	-1	3.55E+07	54	0	-1	-1	1	2.88E+07
11	0	0	1	0	3.27E+07	55	0	0	0	0	3.41E+07
12	0	0	0	-1	3.62E+07	56	1	0	0	-1	3.74E+07
13	0	-1	0	0	3.26E+07	57	1	0	1	1	3.28E+07
14	1	1	1	-1	3.65E+07	58	0	0	-1	1	2.99E+07
15	-1	0	-1	-1	3.15E+07	59	0	-1	-1	-1	3.11E+07
16	1	0	0	0	3.51E+07	60	-1	-1	1	1	2.97E+07
17	1	1	1	1	3.34E+07	61	0	0	0	0	3.41E+07
18	0	0	-1	-1	3.24E+07	62	0	1	-1	0	3.12E+07
19	0	1	-1	-1	3.32E+07	63	1	0	-1	1	3.06E+07
20	-1	1	1	1	3.16E+07	64	1	-1	1	1	3.11E+07
21	-1	1	-1	-1	3.22E+07	65	0	1	0	1	3.39E+07
22	0	-1	1	0	3.13E+07	66	-1	-1	0	-1	3.35E+07
23	-1	0	-1	0	2.99E+07	67	0	0	1	-1	3.48E+07
24	-1	-1	1	-1	3.22E+07	68	0	-1	0	1	3.16E+07
25	0	0	0	1	3.33E+07	69	0	1	0	0	3.47E+07
26	1	-1	1	-1	3.41E+07	70	1	-1	-1	-1	3.18E+07
27	0	0	0	0	3.41E+07	71	-1	1	-1	0	3.04E+07
28	1	-1	0	1	3.26E+07	72	-1	-1	-1	-1	3.03E+07
29	1	-1	-1	1	2.94E+07	73	0	1	0	-1	3.68E+07
30	0	-1	-1	0	2.94E+07	74	1	0	1	-1	3.58E+07
31	1	1	0	0	3.58E+07	75	0	1	-1	1	3.04E+07
32	1	-1	-1	0	3.00E+07	76	-1	0	-1	1	2.92E+07
33	0	0	-1	0	3.06E+07	77	-1	1	1	-1	3.41E+07
34	0	1	1	-1	3.54E+07	78	1	-1	1	0	3.20E+07
35	0	0	0	0	3.41E+07	79	1	1	-1	1	3.12E+07
36	1	1	-1	0	3.20E+07	80	0	0	0	0	3.41E+07
37	-1	1	0	1	3.94E+07	81	1	1	0	-1	3.81E+07
38	-1	1	1	0	3.24E+07	82	0	-1	1	-1	3.32E+07
39	1	1	-1	-1	3.42E+07	83	-1	-1	-1	1	2.81E+07
40	1	0	-1	0	3.14E+07	84	1	0	1	0	3.36E+07
41	1	1	1	0	3.44E+07	85	1	-1	0	-1	3.56E+07
42	-1	0	1	0	3.18E+07	86	1	0	-1	-1	3.33E+07
43	-1	0	1	1	3.10E+07	87	0	0	1	1	3.20E+07
44	-1	-1	0	1	3.10E+07						

B4 Design Matrix for D-optima Design

Run	A:PORO	B:PERMX	C:PERMZ	D:ISW	E:OVISC	FOPT (STB	Run	A:PORO	B:PERMX	C:PERMZ	D:ISW	E:OVISC	FOPT (STB
1	-1	-1	0	1	1	2.97E+07	15	-1	1	1	-1	1	3.03E+07
2	-1	0	0	0	0	3.31E+07	16	0	1	-1	-1	1	3.02E+07
3	-1	-1	1	1	-1	3.32E+07	17	-1	1	0	-1	-1	3.22E+07
4	1	-1	-1	-1	-1	3.15E+07	18	1	-1	0	-1	1	2.94E+07
5	1	-1	1	1	-1	3.52E+07	19	0	0	0	1	0	3.27E+07
6	-1	-1	1	-1	-1	3.11E+07	20	1	1	-1	-1	0	3.16E+07
7	1	-1	-1	1	1	3.08E+07	21	-1	-1	-1	1	-1	3.19E+07
8	1	1	0	1	1	3.34E+07	22	-1	1	-1	1	-1	3.38E+07
9	1	-1	-1	1	-1	3.37E+07	23	-1	-1	-1	-1	0	2.85E+07
10	-1	1	1	1	-1	3.52E+07	24	1	1	1	1	-1	3.77E+07
11	0	-1	0	0	0	3.26E+07	25	1	1	-1	1	-1	3.61E+07
12	1	-1	1	1	1	3.19E+07	26	1	1	1	-1	-1	3.52E+07
13	0	0	0	1	0	3.27E+07	27	1	-1	1	-1	-1	3.28E+07
14	-1	1	-1	1	1	3.13E+07							

B5 ANOVA for Central Composite Method

Source	Sum of Squares	DF	Mean Square	F-Value	Prob > F	
Model	1.12E+14	6	1.87E+13	150.56	< 0.0001	significant
A-PORO	1.23E+13	1	1.23E+13	99.26	< 0.0001	
B-PERMX	1.56E+13	1	1.56E+13	125.51	< 0.0001	
C-PERMZ	6.64E+12	1	6.64E+12	53.48	< 0.0001	
D-ISW	1.49E+13	1	1.49E+13	119.8	< 0.0001	
E-OVISC	2.99E+13	1	2.99E+13	241.28	< 0.0001	
B^2	2.50E+13	1	2.50E+13	201.23	< 0.0001	
Residual	2.36E+12	19	1.24E+11			
Lack of Fit	2.36E+12	14	1.68E+11			
Pure Error	0.00E+00	5	0.00E+00			
Cor Total	1.14E+14	25				

B6 **ANOVA for Full Factorial Method**

Source	Sum of Squares	DF	Mean Square	F-Value	Prob > F	
Model	1.55E+14	7	2.22E+13	498.56	< 0.0001	significant
A-PORO	2.20E+13	1	2.20E+13	493.41	< 0.0001	
B-PERMX	3.04E+13	1	3.04E+13	682.51	< 0.0001	
C-PERMZ	1.03E+13	1	1.03E+13	231.32	< 0.0001	
D-ISW	3.07E+13	1	3.07E+13	689.69	< 0.0001	
E-OVISC	5.58E+13	1	5.58E+13	1252.1	< 0.0001	
AB	2.59E+11	1	2.59E+11	5.82	0.0246	
AE	4.76E+11	1	4.76E+11	10.69	0.0035	
Residual	9.80E+11	22	4.45E+10			
Cor Total	1.56E+14	29				

B7 **ANOVA for D-Optimal Method**

Source	Sum of Squares	DF	Mean Square	F-Value	Prob > F	
Model	1.19E+14	8	1.49E+13	298.02	< 0.0001	significant
A-PORO	1.57E+13	1	1.57E+13	313.94	< 0.0001	
B-PERMX	2.52E+13	1	2.52E+13	505.67	< 0.0001	
C-PERMZ	7.31E+12	1	7.31E+12	146.49	< 0.0001	
D-ISW	2.76E+13	1	2.76E+13	552.75	< 0.0001	
E-OVISC	3.98E+13	1	3.98E+13	798.23	< 0.0001	
D^2	5.46E+12	1	5.46E+12	109.38	< 0.0001	
E^2	2.86E+11	1	2.86E+11	5.73	0.0278	
AE	2.25E+11	1	2.25E+11	4.51	0.0478	
Residual	8.98E+11	18	4.99E+10			
Lack of Fit	8.98E+11	17	5.28E+10			
Pure Error	0	1	0			
Cor Total	1.20E+14	26				

APPENDIX C

C1: Sample **Data Collected using CCD for ANFIS Modelling**

Run	A:PERMX	B:PERMZ	C:SW	D:KRW@S	E:SWCR	F:SGCR	G:OVISC	FOPT (MMstb)
1	0.57	0.5	0.9	1.25	0.53	1.5	1.1	18.8122
2	1.29	0.5	0.65	0.36	0.53	1.5	1.1	18.8157
3	0.57	5	0.9	0.36	1.07	0.5	1.1	23.1352
4	1.29	5	0.9	1.25	0.53	1.5	0.9	22.0524
5	0.57	0.5	0.65	1.25	0.53	1.5	0.9	18.8203
6	1.29	5	0.65	0.36	1.07	1.5	1.1	22.3992
7	0.57	0.5	0.65	1.25	1.07	1.5	0.9	21.6266
8	1.29	0.5	0.9	0.36	0.53	1.5	1.1	20.3431
9	1.29	5	0.65	1.25	1.07	1.5	1.1	21.4155
10	2.14	2.75	0.78	0.8	0.8	1	1	21.7073
11	0.57	0.5	0.65	0.36	1.07	1.5	0.9	22.2557
12	1.29	5	0.65	1.25	0.53	1.5	0.9	25.2557
13	0.57	0.5	0.65	1.25	0.53	0.5	0.9	20.1382
14	0.57	0.5	0.65	0.36	0.53	0.5	1.1	19.5311
15	0.57	0.5	0.65	0.36	1.07	0.5	1.1	21.0733
16	1.29	0.5	0.65	0.36	1.07	1.5	1.1	22.1336
17	0.57	5	0.9	1.25	1.07	0.5	0.9	23.8764
18	1.29	5	0.65	0.36	1.07	1.5	0.9	24.751
19	1.29	0.5	0.9	0.36	0.53	1.5	0.9	23.3246
20	0.93	2.75	0.78	2.3	0.8	1	1	21.3688
21	1.29	5	0.9	0.36	0.53	0.5	1.1	20.5187
22	0.57	0.5	0.9	0.36	0.53	0.5	1.1	20.3436
23	1.29	5	0.9	1.25	1.07	1.5	0.9	24.6412
24	0.93	-4.82	0.78	0.8	0.8	1	1	21.4119
25	1.29	0.5	0.65	0.36	1.07	0.5	0.9	24.1527
26	1.29	0.5	0.9	0.36	0.53	0.5	1.1	20.6541
27	0.93	2.75	0.78	-0.69	0.8	1	1	23.0267
28	0.93	2.75	0.78	0.8	0.8	-0.68	1	21.8378
29	1.29	0.5	0.9	1.25	0.53	0.5	0.9	22.1298
30	0.57	5	0.65	1.25	1.07	0.5	0.9	22.6888
31	0.57	5	0.65	0.36	1.07	1.5	1.1	21.3166
32	0.57	5	0.9	1.25	1.07	1.5	1.1	21.812
33	0.57	0.5	0.9	0.36	0.53	1.5	0.9	22.6442
34	0.93	2.75	1.2	0.8	0.8	1	1	24.0267
35	1.29	5	0.9	0.36	0.53	0.5	0.9	21.8569
36	1.29	5	0.65	1.25	0.53	0.5	0.9	21.4757
37	0.93	2.75	0.78	0.8	0.8	1	1	21.5352
38	1.29	5	0.65	1.25	1.07	0.5	0.9	23.577
39	0.57	0.5	0.9	0.36	0.53	1.5	1.1	19.7099
40	1.29	5	0.9	1.25	0.53	0.5	1.1	21.1066

C1 Continued

Run	A:PERMX	B:PERMZ	C:SW	D:KRW@S	E:SWCR	F:SGCR	G:OVISC	FOPT (MMstb
41	1.29	0.5	0.9	1.25	1.07	1.5	1.1	21.907
42	1.29	5	0.65	0.36	0.53	1.5	0.9	20.7368
43	0.93	2.75	0.78	0.8	-0.11	1	1	19.0473
44	0.57	0.5	0.9	1.25	1.07	0.5	1.1	21.4696
45	0.57	0.5	0.65	1.25	1.07	0.5	1.1	20.7338
46	1.29	0.5	0.65	0.36	0.53	1.5	0.9	20.6415
47	1.29	0.5	0.65	0.36	0.53	0.5	1.1	19.8321
48	0.57	0.5	0.65	1.25	1.07	0.5	0.9	21.9283
49	0.57	5	0.9	0.36	0.53	1.5	1.1	19.8473
50	-0.28	2.75	0.78	0.8	0.8	1	1	20.667
51	0.57	5	0.65	1.25	1.07	1.5	0.9	22.6415
52	1.29	0.5	0.65	1.25	0.53	0.5	0.9	20.9744
53	1.29	5	0.65	1.25	0.53	0.5	1.1	20.3529
54	0.57	0.5	0.9	0.36	0.53	0.5	0.9	21.319
55	1.29	0.5	0.9	1.25	0.53	0.5	1.1	20.7658
56	1.29	5	0.65	0.36	0.53	0.5	1.1	20.3391
57	1.29	0.5	0.65	1.25	1.07	1.5	0.9	22.335
58	1.29	5	0.9	0.36	1.07	1.5	0.9	26.0848
59	1.29	5	0.9	1.25	1.07	0.5	1.1	22.5086
60	0.93	2.75	0.78	0.8	0.8	1	0.66	23.3181
61	0.57	5	0.65	0.36	0.53	0.5	0.9	20.7989
62	0.57	0.5	0.9	0.36	1.07	0.5	0.9	24.4832
63	0.57	5	0.9	0.36	0.53	1.5	0.9	20.9042
64	0.57	0.5	0.9	1.25	0.53	1.5	0.9	20.5857
65	1.29	5	0.65	0.36	0.53	1.5	1.1	19.4279
66	0.57	5	0.65	1.25	0.53	1.5	1.1	18.804
67	0.57	5	0.9	1.25	0.53	0.5	0.9	22.49
68	0.57	5	0.9	0.36	0.53	0.5	1.1	20.6541
69	0.57	5	0.9	0.36	1.07	1.5	1.1	22.6961
70	0.57	5	0.9	1.25	0.53	0.5	1.1	20.6307
71	0.57	5	0.65	1.25	0.53	0.5	0.9	20.1382
72	0.57	5	0.65	1.25	0.53	1.5	0.9	18.8273
73	1.29	0.5	0.9	1.25	0.53	1.5	1.1	20.4642
74	0.57	5	0.65	1.25	1.07	1.5	1.1	20.4327
75	0.57	0.5	0.9	0.36	1.07	0.5	1.1	22.501
76	1.29	5	0.9	0.36	1.07	0.5	0.9	26.5719
77	1.29	0.5	0.9	0.36	1.07	1.5	1.1	23.0481
78	1.29	5	0.9	0.36	1.07	0.5	1.1	23.7883
79	0.57	0.5	0.65	1.25	0.53	0.5	1.1	25.5719
80	0.57	5	0.9	1.25	1.07	0.5	1.1	22.0995
81	0.57	0.5	0.9	1.25	1.07	1.5	1.1	20.9552

C1 Continued

Run	A:PERMX	B:PERMZ	C:SW	D:KRW@S	E:SWCR	F:SGCR	G:OVISC	FOPT (MMstb
82	1.29	0.5	0.65	1.25	0.53	1.5	0.9	19.261
83	0.57	0.5	0.9	1.25	0.53	0.5	1.1	20.055
84	0.57	0.5	0.65	0.36	1.07	0.5	0.9	23.0715
85	1.29	0.5	0.65	1.25	0.53	0.5	1.1	19.6872
86	0.57	0.5	0.9	1.25	1.07	1.5	0.9	22.9086
87	0.57	5	0.9	1.25	0.53	1.5	0.9	21.1922
88	0.57	0.5	0.65	1.25	1.07	1.5	1.1	20.1214
89	0.57	0.5	0.65	1.25	0.53	1.5	1.1	18.7978
90	1.29	5	0.9	0.36	1.07	1.5	1.1	21.0455
91	1.29	5	0.65	0.36	0.53	0.5	0.9	20.9744
92	0.57	0.5	0.9	1.25	1.07	0.5	0.9	23.1701
93	0.57	0.5	0.9	0.36	1.07	1.5	1.1	21.7174
94	1.29	0.5	0.9	1.25	1.07	1.5	0.9	23.5204
95	1.29	5	0.65	1.25	1.07	1.5	0.9	23.0475
96	1.29	5	0.9	1.25	1.07	1.5	1.1	22.163
97	0.57	5	0.65	0.36	0.53	0.5	1.1	23.1204
98	0.57	0.5	0.9	1.25	0.53	0.5	0.9	21.6179
99	0.57	5	0.65	0.36	1.07	0.5	1.1	21.9125
100	1.29	0.5	0.9	0.36	0.53	0.5	0.9	22.3575
101	0.57	5	0.65	1.25	1.07	0.5	1.1	21.0749
102	1.29	5	0.9	0.36	0.53	1.5	1.1	20.3764
103	0.93	2.75	0.78	0.8	0.8	1	1.34	20.6197
104	0.93	10.32	0.78	0.8	0.8	1	1	21.9389
105	0.57	5	0.9	0.36	1.07	0.5	0.9	25.3627
106	1.29	5	0.65	0.36	1.07	0.5	1.1	22.653
107	0.57	5	0.65	0.36	1.07	1.5	0.9	23.6267
108	1.29	0.5	0.65	1.25	0.53	1.5	1.1	24.6016
109	1.29	0.5	0.9	0.36	1.07	0.5	0.9	25.3684
110	0.57	5	0.65	0.36	1.07	0.5	0.9	23.8358
111	1.29	5	0.65	1.25	0.53	1.5	1.1	19.1139
112	1.29	5	0.9	1.25	0.53	1.5	1.1	21.0455
113	1.29	5	0.9	0.36	0.53	1.5	0.9	24.3291
114	0.57	5	0.65	0.36	0.53	1.5	0.9	20.5364
115	0.57	5	0.65	1.25	0.53	0.5	1.1	19.9665
116	1.29	0.5	0.65	1.25	1.07	0.5	1.1	21.2923
117	1.29	5	0.9	1.25	1.07	0.5	0.9	24.5016
118	1.29	0.5	0.9	0.36	1.07	0.5	1.1	23.4522
119	0.57	0.5	0.65	0.36	0.53	1.5	0.9	19.9409
120	1.29	0.5	0.9	1.25	1.07	0.5	0.9	23.8764
121	0.57	0.5	0.65	0.36	1.07	1.5	1.1	19.1637
122	0.57	5	0.9	0.36	1.07	1.5	0.9	21.3127
123	1.29	0.5	0.9	1.25	1.07	0.5	1.1	21.8837
124	1.29	0.5	0.65	0.36	1.07	1.5	0.9	23.5699
125	1.29	0.5	0.65	1.25	1.07	1.5	1.1	20.9733
126	0.57	0.5	0.65	0.36	0.53	1.5	1.1	18.8003
127	0.93	2.75	0.78	0.8	0.8	2.68	1	21.4367
128	0.57	5	0.9	1.25	0.53	1.5	1.1	18.8205
129	1.29	5	0.65	1.25	1.07	0.5	1.1	21.4313
130	1.29	0.5	0.65	0.36	1.07	0.5	1.1	21.4347
131	1.29	0.5	0.65	0.36	0.53	0.5	0.9	20.9266
132	1.29	5	0.9	1.25	0.53	0.5	0.9	22.3127
133	1.29	5	0.65	0.36	1.07	0.5	0.9	23.7393
134	0.57	5	0.9	1.25	1.07	1.5	0.9	23.6727
135	0.57	0.5	0.9	0.36	1.07	1.5	0.9	23.3554
136	0.93	2.75	0.78	0.8	1.71	1	1	24.421
137	0.57	0.5	0.65	0.36	0.53	0.5	0.9	20.5845
138	0.57	5	0.9	0.36	0.53	0.5	0.9	23.5896
139	1.29	0.5	0.9	1.25	0.53	1.5	0.9	21.6737
140	1.29	0.5	0.9	0.36	1.07	1.5	0.9	25.2784
141	0.93	2.75	0.35	0.8	0.8	1	1	19.2872
142	0.57	5	0.65	0.36	0.53	1.5	1.1	18.8071
143	1.29	0.5	0.65	1.25	1.07	0.5	0.9	22.3605

C2: CCD Matrix for development of EQ. 3.1

Run	PHIE	SW	NTG	OWC	Thickness	STOIIP (MMSTB)	Run	PHIE	SW	NTG	OWC	Thickness	STOIIP (MMSTB)
1	1	-1	1	1	-1	54	26	1	1	-1	1	-1	61
2	-1	-1	1	-1	1	41	27	1	-1	1	-1	1	46
3	0	0	0	0	0	48	28	-1	1	-1	-1	1	50
4	0	0	0	0	0	47	29	0	0	2	0	0	54
5	2	0	0	0	0	54	30	0	0	0	0	0	65
6	1	1	-1	-1	-1	54	31	1	1	1	1	-1	41
7	-1	1	1	1	1	48	32	1	1	1	1	1	56
8	-2	0	0	0	0	59	33	-1	-1	-1	-1	-1	68
9	0	0	0	0	2	50	34	0	0	0	0	0	54
10	1	-1	-1	-1	-1	59	35	1	1	-1	-1	1	40
11	1	-1	1	1	1	44	36	1	1	-1	1	1	54
12	-1	-1	1	1	1	44	37	-1	1	-1	-1	-1	56
13	-1	1	-1	1	1	54	38	0	2	0	0	0	59
14	0	-2	0	0	0	45	39	0	0	0	0	-2	48
15	0	0	0	0	0	53	40	-1	1	-1	1	-1	54
16	0	0	0	0	0	54	41	-1	-1	-1	-1	1	54
17	-1	-1	-1	1	-1	54	42	1	-1	-1	1	-1	54
18	0	0	0	0	0	65	43	-1	-1	-1	1	1	48
19	-1	1	1	-1	-1	49	44	1	-1	-1	1	1	53
20	-1	-1	1	1	-1	54	45	1	1	1	-1	1	66
21	1	-1	1	-1	-1	54	46	1	-1	-1	-1	1	54
22	0	0	0	-2	0	62	47	0	0	0	2	0	48
23	1	1	1	-1	-1	53	48	-1	1	1	1	-1	56
24	0	0	0	0	0	55	49	-1	1	1	-1	1	54
25	-1	-1	1	-1	-1	40	50	0	0	-2	0	0	40

C3: Box-Behnken Design Matrix for development of EQ. 6.2 based on fractional screening

Run	A:PORO	B:PERMX	C:PERMZ	D:ISW	E:OVISC	STOIP (STB)
1	0	0	-1	-1	0	3.04E+07
2	1	0	0	-1	0	3.14E+07
3	0	0	-1	1	0	3.24E+07
4	0	-1	-1	0	0	3.22E+07
5	0	0	0	1	-1	3.48E+07
6	0	0	0	0	0	3.41E+07
7	0	0	1	1	0	3.37E+07
8	-1	0	0	0	1	3.23E+07
9	-1	1	0	0	0	3.36E+07
10	0	0	0	-1	1	2.99E+07
11	-1	0	0	-1	0	2.99E+07
12	1	1	0	0	0	3.58E+07
13	0	0	0	1	1	3.20E+07
14	1	0	-1	0	0	3.47E+07
15	0	-1	0	1	0	3.13E+07
16	0	1	-1	0	0	3.44E+07
17	0	0	0	0	0	3.41E+07
18	0	0	0	0	0	3.41E+07
19	0	0	0	0	0	3.41E+07
20	1	0	1	0	0	3.63E+07
21	0	0	0	0	0	3.41E+07
22	0	0	-1	0	-1	3.58E+07
23	0	-1	0	0	-1	3.46E+07
24	-1	0	0	1	0	3.18E+07
25	-1	0	1	0	0	3.41E+07
26	-1	0	0	0	-1	3.49E+07
27	1	0	0	0	-1	3.74E+07
28	-1	0	-1	0	0	3.27E+07
29	0	1	0	0	1	3.39E+07
30	0	-1	0	0	1	3.18E+07
31	0	-1	1	0	0	3.35E+07
32	0	1	0	1	0	3.33E+07
33	0	0	1	-1	0	3.14E+07
34	0	-1	0	-1	0	2.94E+07
35	0	0	1	0	-1	3.75E+07
36	0	0	0	0	0	3.41E+07
37	0	0	-1	0	1	3.30E+07
38	0	0	0	-1	-1	3.24E+07
39	1	0	0	1	0	3.36E+07
40	0	1	0	-1	0	3.12E+07
41	0	0	1	0	1	3.43E+07
42	0	1	0	0	-1	3.68E+07
43	1	-1	0	0	0	3.34E+07
44	-1	-1	0	0	0	3.17E+07
45	0	1	1	0	0	3.58E+07
46	1	0	0	0	1	3.43E+07

C4: CCD Matrix for development of EQ. 6.3 based on fractional factorial screening

Run	A:PORO	B:PERM	C:PERMZ	D:ISW	E:OVISC	STOIIP(STB)
1	0	0	0	0	0	3.41E+07
2	0	0	0	0	2	3.33E+07
3	-1	1	-1	-1	-1	3.19E+07
4	-2	0	0	0	0	3.31E+07
5	0	0	2	0	0	3.52E+07
6	1	1	1	-1	-1	3.52E+07
7	-1	-1	-1	1	-1	3.19E+07
8	0	0	0	0	0	3.41E+07
9	1	1	-1	-1	1	3.09E+07
10	0	0	-2	0	0	3.38E+07
11	1	1	1	1	1	3.43E+07
12	0	-2	0	0	0	3.26E+07
13	0	0	0	2	0	3.27E+07
14	0	2	0	0	0	3.47E+07
15	-1	1	1	1	-1	3.52E+07
16	0	0	0	0	0	3.41E+07
17	0	0	0	-2	0	3.06E+07
18	1	1	-1	1	-1	3.61E+07
19	-1	1	1	-1	1	3.30E+07
20	0	0	0	0	0	3.41E+07
21	1	-1	1	-1	1	3.01E+07
22	-1	-1	1	-1	-1	3.11E+07
23	0	0	0	0	0	3.41E+07
24	-1	-1	1	1	1	3.05E+07
25	0	0	0	0	0	3.41E+07
26	1	-1	-1	-1	-1	3.15E+07
27	1	-1	-1	1	1	3.08E+07
28	2	0	0	0	0	3.51E+07
29	0	0	0	0	-2	3.62E+07
30	1	-1	1	1	-1	3.52E+07
31	-1	1	-1	1	1	3.13E+07
32	-1	-1	-1	-1	1	2.79E+07

C5: D-Optimal Matrix for development of EQ. 6.4 based on fractional factorial screening

Run	A:PORO	B:PERMX	C:PERMZ	D:ISW	E:OVISC	STOIIP(STB)
1	-1	-1	0	1	1	2.97E+07
2	-1	0	0	0	0	3.31E+07
3	-1	-1	1	1	-1	3.32E+07
4	1	-1	-1	-1	-1	3.15E+07
5	1	-1	1	1	-1	3.52E+07
6	-1	-1	1	-1	-1	3.11E+07
7	1	-1	-1	1	1	3.08E+07
8	1	1	0	1	1	3.34E+07
9	1	-1	-1	1	-1	3.37E+07
10	-1	1	1	1	-1	3.52E+07
11	0	-1	0	0	0	3.26E+07
12	1	-1	1	1	1	3.19E+07
13	0	0	0	1	0	3.27E+07
14	-1	1	-1	1	1	3.13E+07
15	-1	1	1	-1	1	3.03E+07
16	0	1	-1	-1	1	3.02E+07
17	-1	1	0	-1	-1	3.22E+07
18	1	-1	0	-1	1	2.94E+07
19	0	0	0	1	0	3.27E+07
20	1	1	-1	-1	0	3.16E+07
21	-1	-1	-1	1	-1	3.19E+07
22	-1	1	-1	1	-1	3.38E+07
23	-1	-1	-1	-1	0	2.85E+07
24	1	1	1	1	-1	3.77E+07
25	1	1	-1	1	-1	3.61E+07
26	1	1	1	-1	-1	3.52E+07
27	1	-1	1	-1	-1	3.28E+07

C6: Factorial Design Matrix for development of EQ. 6.5 based on fractional factorial screening

Run	A:PORO	B:PERMX	C:PERMZ	D:ISW	E:OVISC	STOIIP(STB)
1	-1	-1	-1	1	1	3.00E+07
2	-1	1	-1	1	1	3.15E+07
3	-1	1	1	-1	-1	3.19E+07
4	-1	-1	1	-1	1	3.38E+07
5	-1	1	-1	-1	-1	3.11E+07
6	-1	-1	1	1	-1	3.28E+07
7	1	-1	-1	1	-1	3.30E+07
8	1	-1	-1	1	1	3.52E+07
9	1	-1	1	-1	-1	3.19E+07
10	1	-1	-1	-1	-1	3.37E+07
11	-1	1	-1	1	-1	3.38E+07
12	-1	-1	-1	1	-1	3.61E+07
13	-1	-1	1	-1	-1	3.32E+07
14	1	1	1	-1	1	3.52E+07
15	1	-1	1	-1	1	3.52E+07
16	1	1	1	-1	-1	3.77E+07
17	-1	1	-1	-1	1	2.79E+07
18	1	1	-1	-1	-1	2.91E+07
19	1	1	-1	1	1	2.94E+07
20	-1	1	1	1	1	3.09E+07
21	1	1	1	1	-1	2.88E+07
22	1	1	-1	-1	1	3.01E+07
23	1	-1	1	1	1	3.19E+07
24	-1	-1	1	1	1	2.94E+07
25	1	1	1	1	1	3.09E+07
26	-1	1	1	-1	1	3.13E+07
27	1	-1	1	1	-1	3.31E+07
28	1	-1	-1	-1	1	3.05E+07
29	-1	-1	-1	-1	1	3.19E+07
30	1	1	-1	1	-1	3.24E+07
31	-1	-1	-1	-1	-1	2.84E+07
32	-1	1	1	1	-1	3.14E+07

C7: Box-Behnken Design Matrix for development of EQ. 6.6 based on PB screening

Run	A:PORO	B:PERMX	C:ISW	D:OVISC	STOIIP (STB)
1	0	0	0	0	3.17E+07
2	1	0	1	0	3.34E+07
3	0	0	1	1	3.36E+07
4	-1	0	-1	0	3.58E+07
5	1	0	-1	0	3.24E+07
6	0	0	0	0	3.48E+07
7	0	-1	0	1	2.99E+07
8	0	0	0	0	3.20E+07
9	-1	-1	0	0	3.49E+07
10	0	-1	0	-1	3.74E+07
11	1	1	0	0	3.23E+07
12	0	1	0	-1	3.43E+07
13	0	1	0	1	2.94E+07
14	1	-1	0	0	3.12E+07
15	-1	1	0	0	3.13E+07
16	0	-1	-1	0	3.33E+07
17	0	0	0	0	2.99E+07
18	0	1	-1	0	3.14E+07
19	0	-1	1	0	3.18E+07
20	0	0	-1	-1	3.36E+07
21	0	0	0	0	3.46E+07
22	0	0	-1	1	3.68E+07
23	0	1	1	0	3.18E+07
24	-1	0	0	1	3.39E+07
25	1	0	0	1	3.41E+07
26	-1	0	0	-1	3.41E+07
27	1	0	0	-1	3.41E+07
28	-1	0	1	0	3.41E+07

C8: Full Factorial Design Matrix for development of EQ. 6.7 based on PB screening

Run	A:PORO	B:PERMX	C:ISW	D:OVISC	STOIIP (STB)
1	0	1	-1	1	3.03E+07
2	0	-1	-1	0	3.11E+07
3	0	1	-1	-1	3.18E+07
4	1	-1	1	1	3.15E+07
5	0	1	1	1	3.24E+07
6	1	1	-1	-1	3.33E+07
7	1	-1	1	-1	3.22E+07
8	-1	1	0	1	3.32E+07
9	-1	-1	-1	1	3.42E+07
10	1	0	0	1	3.35E+07
11	0	0	0	0	3.46E+07
12	-1	1	-1	1	3.56E+07
13	-1	0	0	0	3.49E+07
14	0	-1	0	0	3.62E+07
15	-1	0	1	1	3.74E+07
16	0	0	1	0	3.55E+07
17	1	1	0	0	3.68E+07
18	0	1	-1	0	3.81E+07
19	1	0	1	1	3.22E+07
20	1	0	0	-1	3.32E+07
21	0	1	0	1	3.41E+07
22	1	-1	-1	1	3.36E+07
23	-1	0	0	-1	3.48E+07
24	1	-1	0	1	3.58E+07
25	1	1	0	1	3.41E+07
26	1	0	1	-1	3.54E+07
27	-1	0	-1	1	3.65E+07
28	0	0	0	0	2.87E+07
29	0	0	-1	0	2.94E+07
30	1	1	1	0	3.00E+07
31	0	1	1	-1	2.99E+07
32	-1	1	1	1	3.06E+07
33	0	1	0	-1	3.14E+07
34	1	0	0	0	3.04E+07
35	1	1	1	1	3.12E+07
36	-1	0	1	-1	3.20E+07
37	-1	-1	1	0	3.17E+07
38	-1	0	-1	-1	3.26E+07
39	0	0	1	-1	3.34E+07
40	0	-1	0	-1	3.31E+07
41	0	-1	1	1	3.41E+07
42	0	0	0	-1	3.51E+07

C8: Continuation of FFD Matrix for EQ. 6.7

Run	A:PORO	B:PERMX	C:ISW	D:OVISC	STOIIP (STB)
43	0	-1	1	0	33620000
44	1	-1	-1	-1	34740000
45	0	1	1	0	35820000
46	1	0	1	0	30470000
47	0	0	0	1	31270000
48	-1	-1	-1	-1	32050000
49	1	1	0	-1	31790000
50	0	-1	0	1	32740000
51	-1	0	1	0	33620000
52	0	0	-1	1	32350000
53	-1	0	0	1	33340000
54	-1	1	0	0	28130000
55	1	-1	-1	0	28770000
56	0	0	0	0	29370000
57	1	1	-1	0	29190000
58	1	-1	0	-1	29920000
59	0	0	1	1	30610000
60	0	0	0	0	29670000
61	-1	-1	1	-1	30440000
62	-1	1	-1	0	31180000
63	-1	-1	0	1	30960000
64	1	-1	1	0	32650000
65	-1	-1	0	-1	32290000
66	1	0	-1	1	33320000
67	-1	0	-1	0	34270000
68	-1	1	1	-1	33900000
69	0	1	0	0	34920000
70	-1	-1	0	0	29670000
71	-1	1	0	-1	30440000
72	1	1	1	-1	31130000
73	0	0	-1	-1	31030000
74	0	-1	-1	1	31960000
75	0	0	0	0	32780000
76	-1	1	1	0	31570000
77	1	1	-1	1	32530000
78	1	0	-1	0	33410000
79	0	0	0	0	34140000
80	-1	-1	1	1	34140000
81	1	-1	0	0	34140000
82	1	0	-1	-1	34140000
83	0	-1	-1	-1	34140000
84	-1	-1	-1	0	34140000

C9: D-Optimal Design Matrix for development of EQ. 6.8 based on PB screening

Run	A:PORO	B:PERMX	C:ISW	D:OVISC	STOIIP (STB)
1	-1	-1	1	1	2.94E+07
2	-1	-1	1	1	3.32E+07
3	-1	-1	1	-1	3.56E+07
4	1	1	1	1	2.90E+07
5	0	1	0	0	3.16E+07
6	1	1	1	-1	3.42E+07
7	0	-1	-1	-1	3.55E+07
8	-1	1	1	0	3.10E+07
9	1	1	-1	0	3.36E+07
10	0	0	0	-0.5	3.03E+07
11	-1	-1	1	-1	3.05E+07
12	1	1	1	-1	3.65E+07
13	1	-1	0	-1	3.11E+07
14	0	-1	0	0	3.06E+07
15	-1	-1	-1	0	3.49E+07
16	-1	1	-1	1	3.31E+07
17	1	-1	-1	1	3.51E+07
18	1	0	0	0	3.26E+07
19	0	0	0	1	3.47E+07
20	-1	1	-1	-1	3.65E+07
21	1	-1	1	0	3.16E+07
22	1	0	-1	-1	3.11E+07
23	1	-1	-1	1	3.03E+07
24	-1	1	-1	-1	2.92E+07

C10: CCD Matrix for development of EQ. 6.9 based on PB screening

Run	A:PORO	B:PERMX	C:ISW	D:OVISC	STOIIP (STB)
1	-1	1	-1	1	3.03E+07
2	0	0	0	-1.68	3.22E+07
3	-1	-1	1	-1	3.42E+07
4	0	0	-1.68	0	3.22E+07
5	-1.68	0	0	0	3.41E+07
6	0	0	0	0	3.41E+07
7	0	1.68	0	0	3.65E+07
8	1	1	-1	-1	2.81E+07
9	1	-1	-1	1	2.94E+07
10	1	-1	1	1	2.97E+07
11	0	0	0	0	3.34E+07
12	1	1	1	-1	2.97E+07
13	-1	1	1	1	3.11E+07
14	0	0	1.68	0	3.16E+07
15	0	0	0	0	3.34E+07
16	0	0	0	1.68	3.31E+07
17	0	0	0	0	3.34E+07
18	0	0	0	0	3.34E+07
19	-1	-1	-1	-1	3.47E+07
20	1.68	0	0	0	3.62E+07
21	0	-1.68	0	0	3.41E+07

C11: D-Optimal Design Matrix for development of EQ. 6.10 based on OVAT screening

Run	A:PORO	B:PERMX	C:PERMZ	D:AQUIPV	E:SWI	F:KRW	G:OVISC	STOIIP(STB)
1	0	0	0	0	0	0	-1	34010000
2	0	0	0	0	0	0	-1	29680000
3	-1	-1	-1	-1	-1	-1	1	32430000
4	-1	1	-1	-1	-1	1	1	31740000
5	1	1	-1	-1	1	-1	1	33800000
6	1	-1	-1	-1	1	-1	-1	30650000
7	-1	-1	-1	1	1	1	-1	32740000
8	-1	1	-1	1	1	-1	1	32740000
9	-1	1	-1	-1	1	-1	-1	29760000
10	-1	1	1	-1	-1	-1	-1	31640000
11	1	-1	1	-1	-1	-1	1	28560000
12	1	0	0	0	0	0	0	32880000
13	-1	1	1	1	1	-1	-1	31730000
14	-1	1	1	-1	1	-1	1	33770000
15	1	-1	1	-1	1	1	-1	29850000
16	1	1	1	-1	-1	1	1	35090000
17	0	0	-1	0	0	0	0	34270000
18	-1	-1	1	-1	1	-1	-1	28650000
19	1	1	-1	-1	-1	-1	-1	29760000
20	0	0	0	0	-1	0	0	32540000
21	1	1	-1	1	1	-1	-1	29980000
22	-1	-1	1	1	-1	1	1	31310000
23	0	0	0	0	0	-1	0	33330000
24	-1	1	1	-1	1	1	-1	32200000
25	1	1	1	1	1	1	1	36050000
26	1	-1	-1	1	-1	1	1	36120000
27	0	0	0	-1	0	0	0	31680000
28	1	-1	1	1	-1	1	-1	30900000
29	1	1	1	-1	1	-1	-1	32270000
30	-1	1	-1	1	-1	1	-1	35650000
31	0	-1	0	0	0	0	0	32270000
32	-1	-1	-1	-1	-1	-1	-1	36510000
33	-1	-1	-1	-1	-1	1	-1	33180000
34	1	1	-1	-1	1	1	-1	31060000

C12: Box-Behnken Design Matrix for development of EQ. 6.11 based on OVAT screening

Run	A:PORO	B:PERMX	C:PERMZ	D:AQUIPV	E:SWI	F:KRW	G:OVISC	STOIIP(STB)
1	0	-1	0	0	1	0	-1	2.97E+07
2	0	0	0	0	0	0	0	3.41E+07
3	-1	0	1	0	1	0	0	3.17E+07
4	0	0	0	1	-1	-1	0	3.25E+07
5	0	0	1	-1	0	0	1	3.05E+07
6	0	1	-1	0	0	-1	0	3.14E+07
7	1	0	0	0	0	-1	1	3.25E+07
8	1	-1	0	-1	0	0	0	3.35E+07
9	0	0	0	0	0	0	0	3.57E+07
10	0	1	-1	0	0	1	0	3.69E+07
11	-1	0	0	0	0	-1	1	3.52E+07
12	0	1	0	0	1	0	1	3.78E+07
13	0	-1	-1	0	0	-1	0	3.19E+07
14	1	0	0	0	0	1	-1	3.38E+07
15	1	0	0	0	0	1	1	3.26E+07
16	1	0	-1	0	1	0	0	3.46E+07
17	0	0	-1	1	0	0	-1	3.03E+07
18	1	0	1	0	-1	0	0	3.32E+07
19	-1	-1	0	-1	0	0	0	3.32E+07
20	1	0	-1	0	-1	0	0	3.65E+07
21	-1	0	0	0	0	1	1	2.88E+07
22	0	0	0	1	1	-1	0	3.04E+07
23	0	-1	0	0	-1	0	1	2.98E+07
24	0	0	1	1	0	0	1	3.25E+07
25	-1	0	0	0	0	1	-1	3.12E+07
26	1	1	0	-1	0	0	0	3.20E+07
27	-1	0	-1	0	1	0	0	3.30E+07
28	0	-1	0	0	-1	0	-1	3.52E+07
29	-1	0	1	0	-1	0	0	3.19E+07
30	0	0	0	1	1	1	0	3.37E+07
31	0	1	0	0	-1	0	-1	3.40E+07
32	0	0	1	-1	0	0	-1	3.52E+07
33	0	-1	-1	0	0	1	0	3.51E+07
34	0	0	0	0	0	0	0	3.66E+07
35	1	0	1	0	1	0	0	3.62E+07
36	0	1	0	0	1	0	-1	3.79E+07
37	-1	0	-1	0	-1	0	0	3.23E+07
38	0	0	0	-1	1	1	0	3.33E+07
39	-1	-1	0	1	0	0	0	3.47E+07
40	0	0	0	-1	-1	-1	0	2.92E+07
41	0	0	0	-1	1	-1	0	3.11E+07
42	0	1	1	0	0	-1	0	3.06E+07
43	0	0	0	1	-1	1	0	3.22E+07
44	0	-1	1	0	0	1	0	3.15E+07
45	-1	1	0	1	0	0	0	3.33E+07
46	-1	0	0	0	0	-1	-1	3.27E+07
47	0	0	-1	-1	0	0	1	3.46E+07
48	0	0	1	1	0	0	-1	3.18E+07
49	0	0	0	0	0	0	0	3.39E+07
50	-1	1	0	-1	0	0	0	3.30E+07
51	0	-1	0	0	1	0	1	3.43E+07
52	0	1	1	0	0	1	0	3.26E+07
53	0	0	0	-1	-1	1	0	3.48E+07
54	1	-1	0	1	0	0	0	3.40E+07
55	1	1	0	1	0	0	0	3.63E+07
56	0	1	0	0	-1	0	1	3.21E+07
57	0	0	-1	-1	0	0	-1	3.51E+07
58	0	0	0	0	0	0	0	3.41E+07
59	0	-1	1	0	0	-1	0	3.31E+07
60	0	0	0	0	0	0	0	3.41E+07
61	1	0	0	0	0	-1	-1	3.61E+07